Secretogranin-2 complete gene knockouts in zebrafish reveal their stimulatory roles in female reproduction

Weththasingha Kankanamalage Erandani

A thesis submitted to the University of Ottawa in partial fulfillment
of the requirements for the Doctorate in Philosophy degree in Biology
Faculty of Science, University of Ottawa

Thèse soumise à l'Université d'Ottawa en réalisation partielle
des exigences du doctorat en philosophie en biologie
Faculté des sciences, Université d'Ottawa

Ottawa, Canada, 2025

Acknowledgements

First and foremost, I would like to express my deepest gratitude to my supervisor, Dr. Vance L. Trudeau, who allowed me to pursue my Ph.D. in Canada. I am immensely grateful to be a part of the Teamendo.ca lab and for the guidance and support I have received under your mentorship. You made us feel like a part of your family, invited us to your home, and enjoyed every celebration with the lab, and I truly feel lucky to learn from the best in the neuroendocrinology field. I would also like to thank my thesis committee, Dr. Mark Ekker, Dr. Jan Mennigen, and Dr. Alfonzo Abizaid, for the support and help they have provided on this project through their valuable feedback and suggestions. I also thank Dr. Rajendhran Rajakumar, who agreed to be on my thesis evaluation committee, and Dr. Adelino Canário, my external examiner. I want to express my heartfelt gratitude to all the current and past Teamendo members for their invaluable assistance during my time in the lab. From the past members, I must thank Dr. Peng Di, who helped me acclimate to the lab and taught me immunohistochemistry, and Victoria Spadicini, for supporting me with pituitary shape measurements. I want to extend a special thank you to Dr. Chunyu Lu for his expertise and assistance with all the mass spectrometry (MS) analyses, procedure development, and data processing, which were vital to several components of this work. Also, thank you for all the brainstorming discussions and for helping me in so many ways as a friend. I am also grateful to the honours students who worked diligently with me to analyze behaviour recordings: Kamryn Henderson, Sophie Wark and Majd Sabbah. Majd also contributed to the GVBD assessments in Appendix B. Special thanks go to the Berman lab for generously providing access to their digital PCR equipment and facilities, the uOttawa Histology core for their support and technical expertise in histological sample processing, and Dr. Zhibin Ning from the Proteomics Resource Center, University of Ottawa. I also wish to acknowledge the Ekker lab and Vishal Saxena for their contributions to the CRISPR design and microinjection procedures, as well as Animal Care and Veterinary Services for the zebrafish care. I would like to thank my mother, who encouraged me to follow my dreams, and her belief in me has been a constant source of strength. I express my deep gratitude to my husband, Geeth, for always being there for me, especially during late-night experiments in the lab throughout my academic journey. I also want to thank my son, Ayan, who blessed me with the title of “Mother” and patiently waited to play with me until I completed the thesis. This thesis could not have been accomplished without the support and contributions of everyone, even those not mentioned. Thank you all!

Abstract

Secretogranin-2 (Scg2) is a precursor protein in secretory vesicles of neuroendocrine neurons and pituitary hormone-secreting cells. Enzyme processing of Scg2 yields the bioactive peptide secretoneurin (SN) and others. Evidence links SN to reproductive control, enhancing gonadotroph function in several species. We employed CRISPR-Cas9 to excise both the *scg2a* and *scg2b* genes and generate single and double knockout (DKO) zebrafish. To confirm the success of gene deletion, the knockout lines were rigorously validated through sequencing, peptide mass spectrometry and immunohistochemistry. The *scg2a-/-* and *scg2b-/-* lines were crossed to establish a DKO model to investigate the role of the *scg2* genes in zebrafish reproduction. Morphometric assessments indicated that *scg2b-/-* and DKO females had increased weight but shorter body lengths. Behavioural analysis showed reduced quiver behaviour in male *scg2a-/-* and *scg2b-/-* fish, while significant delays in oviposition were observed for females in the *scg2b-/-* and DKO groups. Lower spawning rates were recorded for within-line crosses of *scg2a-/-, scg2b-/-* single KO, and DKO fish (28%, 24%, and 16.6%) compared to WT (64.5%), and all KO groups exhibited low fecundity. The unspawned DKO females could not spawn with WT males, evidencing female-specific spawning defects. Ovarian histology revealed a reduction in mature oocytes and increased atresia in the DKO ovary. The injection of synthetic SNa, SNb, or human chorionic gonadotropin did not restore spawning, highlighting severe reproductive dysfunction in DKO females. Molecular analysis using digital PCR for genes encoding neuropeptides and gonadotropins indicated that, at pre-ovulation, DKO females exhibited decreased *gnrh3* and increased *avp* levels in the hypothalamus, along with upregulated pituitary *lhb* and *fshb*, and downregulated *gnrhr2*. Expression of *oxt* was significantly reduced in both telencephalon and hypothalamus during ovulation, whereas *avp* was highly expressed only in the hypothalamus. Additionally, during ovulation, *gnrhr2* and *cga* were downregulated in the pituitary, while *lhb* and *fshb* levels remained elevated. Post-ovulation, *oxt* in the telencephalon was consistently downregulated, and levels of hypothalamic *gnrh2, avp*, and pituitary *cga* were also reduced compared to WT. Ovarian *lhcgr* and *star1* expression showed significant reduction throughout the ovulation cycle, indicating impaired hormonal signalling and disrupted reproductive regulation in the HPG axis. The shape of the pituitary in DKO fish was altered, having an abnormal elongated shape compared to the teardrop-like oval shape in the WT pituitary**.** Single-pituitary proteomics identified 3674 proteins and

revealed 51 significantly altered proteins between DKO and WT, indicating a major shift in pituitary function. These results demonstrate that *scg2a* and *scg2b* are crucial for reproduction in zebrafish, impacting spawning, oviposition timing, fecundity, oocyte maturation, and the regulation of reproductive hormones in the HPG axis. The secretograninergic system is, therefore, important for the regulation of fertility.

Résumé

La sécrétogranine-2 (Scg2) est une protéine précurseur des vésicules sécrétoires des neurones neuroendocriniens et des cellules hypophysaires sécrétrices d'hormones. La transformation enzymatique de la Scg2 produit le peptide bioactif sécrétoneurine (SN) et d'autres. Il est prouvé que la SN joue un rôle dans le contrôle de la reproduction, en améliorant la fonction gonadotrophique chez plusieurs espèces. Nous avons utilisé CRISPR-Cas9 pour exciser les gènes *scg2a* et *scg2b* et générer des poissons zèbres à simple et double knock-out (DKO). Pour confirmer le succès de la délétion des gènes, les lignées knockout ont été rigoureusement validées par séquençage, spectrométrie de masse des peptides et immunohistochimie. Les lignées *scg2a-/-* et *scg2b-/-* ont été croisées pour établir un modèle DKO afin d'étudier le rôle des gènes scg2 dans la reproduction du poisson zèbre. Les évaluations morphométriques ont indiqué que les femelles *scg2b-/-* et DKO avaient un poids plus élevé mais des longueurs de corps plus courtes. L'analyse comportementale a montré un comportement de frémissement réduit chez les poissons mâles *scg2a-/-* et *scg2b-/-*, tandis que des retards significatifs dans l'oviposition ont été observés chez les femelles des groupes *scg2b-/-* et DKO. Des taux de reproduction plus faibles ont été enregistrés pour les croisements intra-ligne des poissons *scg2a-/-, scg2b-/-* single KO, et DKO (28%, 24%, et 16,6%) par rapport au WT (64,5%), et tous les groupes KO ont présenté une faible fécondité. Les femelles DKO qui n'avaient pas frayé ne pouvaient pas frayer avec des mâles WT, ce qui démontre des défauts de frayage spécifiques aux femelles. L'histologie ovarienne a révélé une réduction des ovocytes matures et une augmentation de l'atrésie dans l'ovaire DKO. L'injection de SNa synthétique, de SNb ou de gonadotrophine chorionique humaine n'a pas rétabli la ponte, ce qui met en évidence un grave dysfonctionnement de la reproduction chez les femelles DKO. L'analyse moléculaire par PCR numérique des gènes codant pour les neuropeptides et les gonadotrophines a indiqué qu'avant l'ovulation, les femelles DKO présentaient une diminution de *gnrh3* et une augmentation des niveaux d'*avp* dans l'hypothalamus, ainsi qu'une augmentation des niveaux de *lhb* et de *fshb* dans l'hypophyse et une diminution des niveaux de *gnrhr2*. L'expression d'*oxt* était significativement réduite dans le télencéphale et l'hypothalamus pendant l'ovulation, alors qu'*avp* n'était fortement exprimé que dans l'hypothalamus. De plus, pendant l'ovulation, *gnrhr2* et *cga* ont été régulés à la baisse dans l'hypophyse, tandis que les niveaux de *lhb* et de *fshb* sont restés élevés. Après l'ovulation, *oxt* dans le télencéphale était constamment régulé à la baisse, et les niveaux de *gnrh2* et *avp*, hypothalamique, et *cga* hypophysaire étaient également réduits par rapport à la WT.

L'expression ovarienne de *lhcgr* et *star1* a montré une réduction significative tout au long du cycle d'ovulation, indiquant une signalisation hormonale altérée et une régulation reproductive perturbée dans l'axe HPG. La forme de l'hypophyse des poissons DKO était altérée et présentait une forme anormalement allongée par rapport à la forme ovale de l'hypophyse WT. La protéomique hypophysaire a identifié 3674 protéines et a révélé 51 protéines significativement modifiées entre DKO et WT, indiquant un changement majeur dans la fonction hypophysaire. Ces résultats démontrent que les gènes *scg2a* et *scg2b* sont essentiels à la reproduction chez le poisson zèbre, car ils ont un impact sur le frai, le moment de la ponte, la fécondité, la maturation des ovocytes et la régulation des hormones reproductrices dans l'axe HPG. Le système sécrétograninergique est donc important pour la régulation de la fertilité.

Table of Content

List of Figures

List of Tables

Abbreviations

AA	Apex area
AA metabolism	Arachidonic acid metabolism
AVP	Arginine vasotocin
BAC	Bicinchoninic Acid Protein assay
BLAST	Basic Local Alignment Search Tool
BP	Base peak
BPA	Bisphenol A
CaMKII	Calmodulin-dependent kinase II
cAMP	Cyclic AMP
CCK	Cholecystokinin
cDNA	Complementary DNA
CgA	Chromogranin A
CgB	Chromogranin b
COX	Cyclooxygenase
cPLA2	Cytosolic phospholipase A2
CRISPR	Clustered regularly interspaced short palindromic repeats
CYP-450	Cytochrome P450
DAPI	4′,6-diamidino-2-phenylindole
DHEA	Dehydroepiandrosterone
DHP	17α,20β-dihydroxy-4-pregnen-3-one
DKO	Double knockout
DNA	Deoxyribonucleic acid
dPCR	Digital PCR
ECM	Extracelular matrix
EDTA	Ethylenediaminetetraacetic acid
EGF	Epidermal growth factor
ELISA	Enzyme-linked immunosorbent assay
ERK	Extracellular signal-regulated kinases
EtOH	Ethanol
FDR	False discovery rate
FeSP	Female-specific sex steroid-responsive peptidergic
FSH	Follicle-stimulating hormone
GABA	Gamma-aminobutyric acid
GnRH	Gonadotropin-releasing hormone
GO	Gene Ontology
GPCR54	G protein-coupled receptor number 54
GRCZ11	Zebrafish genome annotation in Ensembl
gRNA	Guide RNA
GSI	Gonadosomatic index
GVBD	Germinal vesicle breakdown
hCG	Human chorionic gonadotropin
H & E	Hematoxylin and Eosin
HEPES	4-(2-hydroxyethyl)-1-piperazineethanesulfonic acid

HFD	High-fat diet
hpf	Hours post-fertilization
hpi	Hours post incubation
hpp	Hours post purging
HPG	Hypothalamic-pituitary-gonadal axis
HPLC	High-performance liquid chromatography
HSD	Tukey Honest Significant Difference
IF	Immunofluorescence
IHC	Immunohistochemistry
KCl	Potassium chloride
KO	Knockout
L	Liter
LC-MS/MS	Liquid chromatography-tandem mass spectrometry
LFQ	Label-free quantitation
LH	Luteinizing hormone
LOX	Lipoxygenase
MAPK	Mitogen-activated protein kinase
MgSO4	Magnesium sulphate
MIH	Maturation-inducing hormone
MPF	Maturation-promoting factor
MRI	Magnetic resonance imaging
mRNA	Messenger ribonucleic acid
MS-222	Tricaine methanesulfonate
NaCl	Sodium Chloride
NaOH	Sodium hydroxide
NHEJ	Non-homologous end joining
NPY	Neuropeptide Y
NTCs	No template controls
OXT	Oxytocin
PAM	Protospacer Adjacent Motifs
PBS	Phosphate buffered-saline
PCOS	Polycystic ovary syndrome
PCR	Polimerace chain reaction
PG	Primary growth stage oocytes
PGCs	Primordial germ cells
PI	Pars Intermedia
PN	Pars nervosa
POA	Preoptic area
POMC	Pro-opiomelanocortin
PPD	Proximal pars distalis
PRL	Prolactin
Prp	Prion protein
PTU	Propylthiouracil
RNA	Ribonucleic acid
ROS	Reactive oxygen species
RPD	Rostral pars distalis

RT-qPCR	Real-time RT polymerase chain reaction
SCG2	Secretogranin2
SN	Secretoneurin
TALEN	Transcription activator-like effector nucleases
TCA	The mitochondrial Krebs cycle
TGN	Trans-Golgi network
Tris-HCl	Tris hydrochloric acid
TSH	Thyroid-stimulating hormone
WT	Wildtype
ZFN	Zinc finger nuclease

Chapter 1: General Introduction

1.1 Rationale, Hypothesis and Objectives

Reproduction is intricately regulated by the endocrine system, which coordinates the production and release of hormones essential for reproductive function. Key endocrine glands, such as the hypothalamus, pituitary, and gonads, form the hypothalamic-pituitary-gonadal (HPG) axis, produce reproductive hormones, including gonadotropin-releasing hormone (GnRH), luteinizing hormone (LH), follicle-stimulating hormone (FSH), and sex steroids (estrogens and testosterone). These hormones are pivotal in orchestrating reproductive cycles, gametogenesis, and ovulation. Over the decades, extensive research in neuroendocrinology has elucidated the crucial roles of these hormones, both independently and in their integrated impact on the reproductive process. Zebrafish (*Danio rerio*) have emerged as an exceptional model organism for studying reproductive biology, owing to their genetic similarity to humans, rapid development, and amenability to advanced gene-editing technologies, such as CRISPR-Cas9. Thus, zebrafish have enabled groundbreaking gene knockout studies, providing critical insights into the molecular mechanisms governing reproduction and potential therapeutic avenues, and shedding light on the current understanding of the neuroendocrine control of reproduction.

Several such gene mutation and knockout studies have investigated the effects of GnRH gene knockout in zebrafish and medaka, revealing surprising findings that change the initial understanding of the role of GnRH in teleost fish reproduction and thereby suggesting that there could be other hormones and neuropeptides, that may also play critical roles in regulating the reproductive axis. In zebrafish, the knockout of both *gnrh2* and *gnrh3* genes resulted in no significant impact on reproduction, suggesting the existence of compensatory mechanisms outside the GnRH system (Marvel et al., 2018; Spicer et al., 2016). The double *gnrh* knockout zebrafish exhibited upregulation of several genes in the brain, including gonadotropin-inhibitory hormone *(gnih)*, secretogranin 2 *(scg2)*, tachykinin 3a *(tac3a)*, and pituitary adenylate cyclase-activating peptide 1 *(pacap1)*, indicating a potential network of alternative pathways influencing reproductive control (Marvel et al., 2018). In medaka, although *gnrh1* knockout in females prevents ovulation and reduces the expression of *lhb*, it does not affect *fshb* expression or follicle development (Takahashi et al., 2016). Moreover, single-cell RNA sequencing of pituitary cells in wild-type and *gnrh3-/-* adult female zebrafish revealed that the loss of the *gnrh3* gene did not significantly affect

gonadotrope gene expression profiles, reinforcing the hypothesis that alternative mechanisms may compensate for the loss of GnRH genes in teleosts (Tanaka et al., 2024).

One promising candidate is secretoneurin (SN), a 31–34 amino acid neuropeptide derived from the larger precursor protein secretogranin-2 (Scg2). Scg2 was initially identified as a granin protein from the bovine pituitary (Rosa & Zanini, 1981), and its immunoreactivity was detected in LH-positive granules in sheep and rats (Crawford & McNeilly, 2002; Watanabe et al., 1991). The first suggestion of its reproductive role was made in 1998 when the activation of GABAergic neurons upregulated *scg2a* mRNA, accompanied by a decrease in LH cell content in the goldfish pituitary gonadotroph cells (Blázquez et al., 1998). Further studies have demonstrated that SN plays a significant role in gonadotropin regulation. For instance, SN treatment significantly increases LH release and production in mouse LβT2 gonadotropin cells, which share characteristics with normal pituitary gonadotrophs (Zhao et al., 2011). Similarly, in goldfish, SN has been shown to stimulate LH secretion from gonadotrophs (Zhao et al., 2009; Zhao et al., 2010). Additionally, in mice, SN activates extracellular signal-regulated kinases (ERK) in LβT2 cells during acute and chronic treatments, suggesting its involvement in intracellular signalling pathways critical to reproductive hormone regulation.

Further studies from our lab indicated that *scg2a-/-; scg2b-/-* zebrafish TALEN frameshift mutants exhibit poor reproductive performance, including a reduction in spawning and *scg2a* mutation leads to significant impairments in ovulation (Mitchell et al., 2020). Injection of SN into wild-type female zebrafish could successfully stimulate ovulation without the presence of a male, and these fish showed a higher level of SNa peptides in the pituitary as well as the whole brain during the pre-ovulatory period (Peng et al., 2025). Immunohistochemistry studies revealed that SNa neurons in the preoptic area (POA) were progressively activated before ovulation, peaking at the time of presumptive ovulation. Intraperitoneal injection of SNa stimulated ovulation and Lh cell activation in the pituitary, suggesting that SN plays a stimulatory reproductive role in zebrafish (Spadacini, 2024).

Given this background and the lack of data on the impacts of complete SCG2 gene knockout in any vertebrate model, I set out to develop and characterize reproductive potential in novel *scg2a* and *scg2b* knockout zebrafish. The hypotheses and objectives of the research are presented below, followed by a review of relevant literature at the foundation of the thesis. Note that gene and protein

nomenclature follow conventions for humans when referring to mammals but follow conventions for zebrafish when referring to teleosts. (https://zfin.atlassian.net/wiki/spaces/general/pages/1818394635/ZFIN+Zebrafish+Nomenclature+Conventions#:~:text=References-,1.,named%20zebrafish%20mutants%20and%20genes).

Hypothesis

Complete deletion of the *scg2* genes will result in severe reproductive deficits because Scg2/SN is critical for normal pituitary and gonadal function.

Objectives

1. Creation of the *scg2a-/-, scg2b-/-* and *scg2a-/-; scg2b-/-* double knockout zebrafish and validation
2. Characterization of the *scg2a-/-, scg2b-/-* and *scg2a-/-; scg2b-/-* double knockout zebrafish ovarian morphology, reproductive behaviour and reproductive performances.
3. Assessment of the role of *scg2*/SN in the HPG axis by mRNA/protein level comparison of *scg2a-/-; scg2b-/-* double knockout and wildtype zebrafish.

1.2 The hypothalamic-pituitary-gonadal (HPG) axis

The hypothalamic-pituitary-gonadal (HPG) axis plays crucial and essential roles in regulating reproductive processes in mammals and teleosts, integrating internal and external cues to ensure reproductive success. Despite some species-specific differences, the fundamental architecture and function of the HPG axis are conserved across vertebrates, highlighting its evolutionary importance in reproductive biology. The first endocrine organ of this axis is the hypothalamus, which is situated in the ventral forebrain. The central region produces stimulating and inhibitory hormones to regulate hormones released from the pituitary gland. In vertebrates, the hypothalamus's preoptic area and arcuate nucleus produce and release GnRH, which stimulates the pituitary to release LH and FSH, essential for gonadal function (Casteel & Singh, 2023). In mammals and other tetrapods, the hypothalamus and pituitary connection is via the median eminence-portal blood system, which transports hypophysiotropic hormones to the pituitary (Trudeau, 2022). In contrast, in teleosts, including medaka and zebrafish, hypophysiotropic neurons, such as GnRH neurons, directly innervate the anterior lobe of the pituitary gland. Both

direct neural innervation and vascular delivery of signals have been observed in these species (Fontaine et al., 2020; Trudeau, 2022; Trudeau & Somoza, 2020). Under the control of the hypothalamus, the pituitary acts as a master endocrine controller in vertebrates. FSH and LH hormones that are secreted in the pituitary are released into the bloodstream, and when they reach the gonads, they help to modulate various reproductive processes. In females, FSH triggers the early stages of folliculogenesis, while pulsatile LH is crucial for the later stages, including final oocyte maturation and ovulation (Kaprara & Huhtaniemi, 2018; Tanaka et al., 2024). In males, FSH primarily targets Sertoli cells in the testes, which support spermatogenesis and maturation. At the same time, LH acts on Leydig cells to stimulate testosterone production; thereby, the synergetic action of FSH and testosterone supports spermatogenesis qualitatively and quantitatively (Oduwole et al., 2018). The balance of gonadotropins in circulation is carefully regulated by feedback from gonadal sex steroids, as well as nonsteroidal gonadal factors such as activin, which exert complex feedback effects at multiple levels of the HPG axis, fine-tuning its activity.

1.3 Teleost reproduction and its neuroendocrine regulation

Teleosts are the largest and most diverse group of bony fishes, comprising approximately 30,000 species with a wide range of morphological adaptations and ecological niches (Wootton & Smith, 2014). Teleost reproduction exhibits remarkable diversity, showcasing the most varied reproductive strategies in vertebrates (Mayer, 2019). Most teleosts are oviparous, where they release eggs and sperm into the water and externally fertilize. Teleost fish exhibit diverse sex determination mechanisms, including genetic sex determination, environmental sex determination, or a combination of both, which can vary among species (Mank et al., 2006; Rajendiran et al., 2021). While some species possess well-defined sex chromosomes (e.g., medaka with an XX/XY system), others, such as zebrafish, exhibit a polygenic sex determination system without a definitive sex chromosome. Environmental factors, including temperature, population density, and nutrition, can influence sex determination in some species, leading to plasticity in their reproductive roles (Baroiller et al., 2009). This flexibility in sex determination is advantageous in fluctuating environments, enabling teleosts to optimize reproductive success.

In addition to their diverse sex determination mechanisms, teleosts employ two primary reproductive strategies: semelparity and iteroparity. Semelparous species, such as Pacific salmon (Oncorhynchus spp.), invest all their energy into a single reproductive event before dying, a strategy

often associated with high juvenile mortality and unpredictable environments (Wootton,1993). In contrast, iteroparous species, which constitute the majority of teleosts, reproduce multiple times throughout their lifespan, allowing for greater reproductive assurance over time (Rajendiran et al., 2021). Some iteroparous species, which constitute most teleost species, can reproduce multiple times throughout their lives (Rajendiran et al., 2021).

Teleost reproduction is intricately controlled by a complex neuroendocrine system that shares similarities with other vertebrates while also possessing unique features. While the HPG axis forms the core of this system, recent research has revealed a complex network of neuropeptides and neurotransmitters involved in the neuroendocrine control of teleost reproduction beyond the classical HPG axis. The direct neuronal communication between the hypothalamus and pituitary of teleost allows for more precise and regionalized control of the hormone secretion system that involves a complex interplay of stimulatory and inhibitory factors, including over 20 stimulatory and 15 inhibitory neuropeptides, as well as various neurotransmitters. In some species like zebrafish and medaka, neuronal and vascular control has been identified between the hypothalamus and pituitary (Trudeau et al., 2023). Among the stimulatory neuropeptides, GnRH plays a central role by stimulating the release of gonadotropins from the pituitary, and kisspeptin acts on GnRH neurons to enhance gonadotropin release. However, its role appears species-specific and potentially dispensable in teleosts (Trudeau, 2018).

Studies using mammalian models have shown that reproductive function depends on the production of the GnRH decapeptide, thereby stimulating LH and FSH release from the anterior pituitary (Nicol et al., 2002). It has been confirmed in GnRH-null mice that having reduced FSH and LH concentrations leads to infertility (Cattanach et al., 1977). Multiple isoforms of Gnrh exist due to genome duplication throughout evolution. The mammalian form is Gnrh1, which is found in the hypothalamic preoptic region of the brain (Fernald & White, 1999; Neill, 2002). Another form, Gnrh2, is present in the midbrain tegmentum of teleosts. The Gnrh2 was initially found in the chicken midbrain (Miyamato et al., 1984) and reported in mammals and fish but not in rodents (Conlon et al., 1993; Sherwood et al., 1993; Kasten et al., 1996; White et al., 1998; Millar, 2004). The Gnrh3 neuropeptide, also known as salmon Gnrh, is the hypophysiotropic decapeptide of many teleosts (Lethimonier et al., 2004). Cyprinids and salmonids have Gnrh2 and Gnrh3 only. It is suggested that in these fish, Gnrh3 has taken over the stimulatory role of mammalian Gnrh1 (Tello et al., 2008; Roch et al., 2014; Trudeau, 2018). It has been reported that a naturally occurring

mutation in the Gnrh1 gene causes idiopathic hypogonadotropic hypogonadism in humans (Bouligand et al., 2009; Cattanach et al., 1977) and a TALEN frameshift mutant of Gnrh1 leads to female infertility in medaka fish while having no significant effect on the reproduction in males (Takahashi et al., 2016). Genetic mutations of Gnrh1 result in disrupted puberty and infertility in mice and humans (Bouligand et al., 2009). The Gnrh2 form is known to be involved in the regulation of feeding (Nishiguchi et al., 2012) and in regulating reproductive behaviour in female mammals such as shrews (*Suncus murinus*) (Hofmann, 2006; Desaulniers et al., 2017). In addition, laser ablation of Gnrh3 neurons at early developmental stages has reduced oocyte development and failed ovulation in zebrafish (Abraham et al., 2010). In marked contrast, gonadal development and reproduction are unaffected when the *gnrh3* gene is mutated in zebrafish via transcription activator-like effector nucleases (TALEN) genome editing technology (Spicer et al., 2016). The same group then created the Gnrh2 and Gnrh3 double knockout, which still did not affect the reproductive capacity of the mutated zebrafish (Marvel et al., 2018). Gnrh3 knockouts have male-biased sex ratios with a lower number of primordial germ cells compared to the wild type (Feng et al., 2020).

Kisspeptin is another crucial neuropeptide that plays a central role in regulating reproduction by stimulating GnRH secretion, mediating sex steroid feedback, and influencing various aspects of reproductive functions in mammals (Nejad et al., 2017). In addition, it was discovered that kisspeptin is the key upstream regulator, innervating mammalian GnRH neurons that express the receptor GPCR54 (G protein-coupled receptor 54). Mutations of GPCR54 result in hypogonadotropic hypogonadism in humans (de Roux et al., 2003; Seminara et al., 2003; de Roux, 2006). Studies in mammalian models have confirmed that kisspeptin is essential to activate GnRH neurons and thereby for the stimulation and release of LH (Irwig et al., 2004; Messager et al., 2005; Clarkson & Herbison, 2006; Fabre-Nys et al., 2017). In non-mammalian teleost, kisspeptin mutations do not result in infertility and impaired reproduction. In zebrafish, TALEN-mediated mutations of the kisspeptin-related genes kisspeptin1 and kisspeptin2 and their receptors (kiss/kissr) did not alter reproduction, and the fish displayed normal fertility, gonadal maturation and gonadotropin levels (Tang et al., 2015). Also, the kisspeptin administration (*in vitro*) in goldfish did not significantly influence Lh secretion from the pituitary cells in primary culture (Li et al., 2009). Even when kisspeptin 1 and 2 are disrupted along with the Gnrh3, the triple mutant zebrafish undergo normal puberty and gonadal development (Liu et al., 2017). Together with the Gnrh2 and Gnrh3 mutant observations in fish models, these results are in marked contrast to mammals.

Furthermore, mutations in the medaka kiss/kissr system suggest that the role of kisspeptin could be non-reproductive (Nakajo et al., 2018) and suggests having roles such as modulation of metabolism, immune system regulation, energy balance, as it influences feeding behaviour and metabolic processes in various species (Ogawa & Parhar, 2018).

There are other known stimulatory neuropeptides, such as orexin, that have been shown to stimulate GnRH neurons in some species. Neuropeptide Y (NPY) has emerged as another important player, with studies demonstrating its ability to increase plasma LH levels and stimulate GnRH release in various teleost species such as goldfish, common carp, rainbow trout, and the sea bass (Breton et al., 1991; Cerdá-Reverter et al., 1999; Peng et al., 1993). Emerging neuropeptides such as nesfatin-1, neurokinin B, and cholecystokinin (CCK) have also been implicated in the regulation of teleost reproduction (Trudeau, 2022). Recent research has revealed a novel and crucial role for cholecystokinin (CCK) in teleost reproduction by preferentially activating FSH cells and stimulating FSH secretion, thereby linking nutritional status to reproduction (Hollander-Cohen et al., 2024; Li et al., 2025). This intricate interplay of neuropeptides and neurotransmitters and the close connection between energy balance and reproduction highlights the complexity of the neuroendocrine control of teleost reproduction and underscores the need for further research to fully elucidate these mechanisms.

1.4 Overview of the Granin Family Proteins

The granin family of proteins, characterized by its acidic and heat-stable properties, plays a crucial role in the regulated secretory pathways of endocrine, neuroendocrine, and neuronal systems (Huttner et al., 1991). The granin family is divided into chromogranins and secretogranins. Chromogranins (CgA and CgB) are distinguished by a disulfide-bonded loop at the N-terminus. At the same time, secretogranins lack this feature and include seven members: (secretogranin 2 (SCG2), secretogranin 3 *(*SCG3 or 1B1075), secretogranin 4 (SCG4 or HISL-19), secretogranin 5 (SCG5), secretogranin 6 (SCG6) (Montero-Hadjadje et al., 2008), SCG7 (Helle, 2004) and pro-SAAS (Fricker et al., 2000; Zhao et al., 2009b). Granins serve as large precursor proteins that specific prohormone convertases can proteolytically process at multiple cleavage sites to produce a multitude of small bioactive peptides (Huttner & Natori, 1995). They are synthesized in the rough endoplasmic reticulum and transported to the trans-Golgi network (TGN), where conditions such as low pH and high calcium ion concentrations induce their aggregation and interaction with sorting

receptors, leading to secretory granule formation. Upon specific stimulation, these granules fuse with the cell membrane, releasing their contents into the bloodstream (Bartolomucci et al., 2011; Courel et al., 2010; Fischer-Colbrie et al., 1995; Ozawa & Takata, 1995). Chromogranins are conserved throughout vertebrates, and the secretogranin 2 (*Scg2*) precursor protein is mainly conserved as a short domain which produces a peptide known as SN that is located in the central core region of Scg2 (Blazquez et al., 1998). This SN domain contains a core sequence of YTPQ-X-L-X8-EL, which is highly conserved in evolution with a 90-100% sequence similarity between mammals (Mitchell et al., 2020; Zhao et al., 2009). Moreover, goldfish SN shares 59% identity with human SN and is more than 75% identical with some other vertebrate SN peptides (Blazquez et al., 1998).

1.5 Secretogranin 2 and biological functions of the derived SN peptides

The *SCG2* gene encodes the precursor protein SCG2, a large acidic, tyrosine-sulfated preproprotein found in the secretory vesicles of key neuroendocrine neurons and pituitary hormone-secreting cells. SCG2 has several proposed biological roles, including acting as a carrier protein for packaging peptide hormones and neuropeptides into secretory vesicles (Bassetti et al., 1990; Troger et al., 2017). SCG2 is targeted to the trans-Golgi network, where it facilitates the sorting and packaging of neuropeptides and hormones into secretory granules, also known as dense-core secretory granules or large dense-core vesicles (Fleming et al., 2023; Hotta et al., 2009). SCG2 was identified as a binding partner of SCG3 using a yeast two-hybrid system and confirmed through immunoprecipitation. This interaction is essential for forming secretory granules containing various appetite-related neuropeptides such as NPY, Orexin and POMC (Hotta et al., 2009). This precursor is cleaved to produce several bioactive peptides, including SN, each with unique and potentially overlapping biological functions. While many of these peptides remain inadequately studied, some, such as SN, EM66, and Manserin, have been identified and partially examined.

Even though it is not conserved in fish (Zhao et al.,2009) EM66, a 66-amino acid peptide derived from the SCG2 precursor, has been investigated in studies focusing on its distribution and possible roles in the nervous system, particularly its involvement in feeding behaviour and neuroendocrine regulation in rats (Boutahricht et al., 2007; Yamani et al., 2013; Yamani et al., 2010; Montero-Hadjadje et al., 2003; Trebak et al., 2017). It is highly expressed within hypothalamic neuroendocrine areas, specifically in the parvocellular aspect of specific nuclei and

has been identified in the hypothalamic paraventricular nucleus of rats (Yamani et al., 2013; Yamani et al., 2010; Trebak et al., 2017). Manserin, a 40-amino acid peptide, is linked to glucose homeostasis and neuroendocrine regulation; however, it remains understudied. First identified in rat brain tissue, this neuropeptide is widely distributed throughout the neuroendocrine system, including the hypothalamus, pituitary, adrenal glands, and inner ear of rats (Ida-Eto et al., 2012; Yajima et al., 2004; Yajima et al.,2008). Additionally, SCG2 processing fragments, which include N-terminal and C-terminal fragments as well as intermediate peptides, further expand the functional landscape of this gene (Troger et al., 2017).

The bioactive SN is a 31-34 amino acid short peptide resulting from the proteolytic processing of the central core region of the SCG2 precursor that has been studied in detail (Trudeau et al., 2012). SN has been implicated in various physiological processes, including regulating reproduction, modulation of neurotransmission, involvement in inflammatory responses, and potential roles in neuronal differentiation. SN has been reported to be acting as a cardiovascular regulator, reducing ventricular arrhythmia and heart failure progression through calmodulin-dependent kinase II (CaMKII) inhibition and modulating calcium handling (Ottesen et al., 2015; Plášek et al., 2022). Additionally, a few studies suggest its potential role in modulating local inflammatory responses and its involvement in regulating adrenergic neurotransmission and facilitating neuroimmune communication (Da Fonte et al., 2017; Liang et al., 1999; Pertl et al., 1998; Wiedermann, 2000). Moreover, SN shows potential as a prognostic biomarker in cardiovascular conditions (Ottesen et al., 2015; Plášek et al., 2022)

There are two Scg2 variants identified in teleosts, which are the result of a gene duplication event of an ancestral form (Peng et al., 2025). In zebrafish, these Scg2a and Scg2b precursor proteins are, respectively 539 and 583 amino acids long and generate the SNa1-34 and SNb1-31 bioactive peptides. Recently, it was shown that SNa and SNb are each further processed into many shorter fragments, the most abundant being SNa1-14, SNa19-34, SNb1-17 and SNb19-31 (Lu et al., 2023). The teleost scg2 shares relatively poor sequence identity with that of mammals (79-87%) except for a conserved sequence region representing SN peptides; that is identical to their mammalian counterpart (Samia et al., 2004; Zhao et al., 2010; Trudeau et al., 2012) (Table 1). This sequence conservation may be the determinant of the biological actions of SN (Zhao et al., 2009).

```
Homo                    TNEIVEEQYTPQSLATLESVFQELGKLTGPNNQ-
Danio SNa               TNENAEEQYTPQKLATLQSVFEELSGIASSKTNT
Oryzias SNa             TKENVEEKYTPQNLATLQSVFDELEKMTAAKGIR
Danio SNb               ATEDLDEQYTPQSLANMRSIFEELGKLSAAQ---
Oryzias SNb             TTEDLDEQYTPQSLANLRSIFEELERMPGLQ---
CONSENSUS               :.*  :*:****.**.: *:*:**  :.. :
```

Table 1: Shown are the genus names for the following organisms included in the sequence alignments: *Danio rerio* (zebrafish), *Oryzias latipe*s (medaka), and *Homo sapiens* (human). The consensus YTPQ-XL-X8-EL signature that defines this vertebrate peptide family is underlined in *H. sapiens* SN and *D. rerio* SNa and SNb for reference. CLUSTAL multiple sequence alignment by MUSCLE 3.8 (https://www.ebi.ac.uk/jdispatcher/msa/muscle?stype=protein).

A receptor for SN has yet to be identified despite numerous attempts by various research groups, including ours, yielding no success. Some studies suggest that SN may interact with a G-protein-coupled receptor (GPCR) found on gonadotrophs, increasing cyclic AMP and MAPK/MEK signalling pathways (Zhao et al., 2011), as well as potentially an AKT-dependent pathway (Tao et al., 2018). It is important to note that AKT signalling is not exclusive to GPCRs and can be activated by mechanisms that do not depend on GPCR signalling, making the concept of SN signalling through a GPCR still hypothetical.

Evidence accumulating suggests that the SN has a vital role in controlling reproduction. Mahata et al. (1993) provided some early suggestions for a reproductive role for Scg2 and SN peptides. In the pituitary of ovariectomized female rats, the *Scg2* mRNA level increased alongside *Lhb* mRNA levels, suggesting a regulatory mechanism involving the *SCG2* gene during the sexual maturation of rats (Anouar & Duval, 1991; Anouar & Duval, 1992; Kakar et al., 2004). After discovering more about the reproductive role of Scg2/SN, the potential endocrine roles of the SN were reviewed by Trudeau et al. (2012), where it was suggested that SN may be a new hormone. Using a polyclonal antibody against goldfish SNa, Canosa et al., (2011) showed that neuronal cell bodies in the preoptic region contained the highest immunoreactivity, co-localizing with isotocin (fish oxytocin) in the magnocellular cells projecting to posterior and anterior regions of the pituitary. In the rat hypothalamus, SN and oxytocin are also co-stored in magnocellular neurons, and the mRNA levels are co-regulated (Mahata et al., 1993), providing further evidence for a relationship between these neuropeptides. In the highly regionalized teleost pituitary, lactotroph

cells in the rostral pars distalis express SNa, whereas adjacent gonadotrophs or somatotrophs do not (Zaho et al., 2009; Trudeau et al., 2012).

These studies indicate that SN could be delivered to Lh cells through direct innervation of the pituitary or via paracrine diffusion from the lactotrophs to the gonadotrophs in goldfish. Both *in vitro* and *in vivo* experimental evidence demonstrate that SN can stimulate Lh release from goldfish pituitary cells (Blazquez et al., 1998; Zhao et al., 2006; Zhao et al., 2009a; Zhao et al., 2010; Zhao et al., 2011). The stimulatory effects of mammalian SN on pituitary luteinizing hormone release from mouse LβT2 gonadotroph cells provide additional *in vitro* evidence for SN's significance in regulating reproduction (Zhao et al., 2011). In catfish (*Heteropneustes fossilis*), *scg2b* was abundant in various brain regions and pituitary, and it was localized in the ovarian granulosa cell layer. Recent data from our lab provides compelling evidence for a reproductive role of SN, where TALEN-mediated frameshift mutations in *scg2a* and *scg2b* in zebrafish result in a phenotype of partially reduced reproductive capacity, characterized by diminished spawning and male courtship behaviour (Mitchell et al., 2020).

1.6 Thesis Presentation

This doctoral thesis consists of six chapters. Chapter 1 provides a general introduction, delivering essential background information to set the context for the study. Chapters 2, 3, 4, and 5 detail the research findings, with Chapter 2 focusing on Objective 1, Chapter 3 exploring Objective 2, and Chapters 4 and 5 investigating Objective 3. Chapter 6 concludes the thesis by summarizing the key findings and suggesting possible directions for future research. Each of the four data chapters can stand alone as an independent manuscript. Additionally, there are two appendix chapters. While there is some overlap in content among these chapters, efforts were made to minimize redundancy.

1.7 Ethics Statement

All experiments were approved by the University of Ottawa's Animal Care Protocol Review Committee and complied with the guidelines established and approved by the Canadian Council on Animal Care for the use of animals in research.

Based on these previous data, I hypothesized that Scg2/SN neurons stimulate LH production, and the complete deletion would result in severe reproductive deficits. To address this,

we created a *scg2* complete gene knockout (KO) in zebrafish using the CRISPR-Cas9 gene editing system and validated it with several molecular methods, such as gene sequencing, immunocytochemistry, and mass spectrometry analysis of SN peptides.

Chapter 2: Creation and validation of the *scg2a-/-, scg2b-/-* and *scg2a-/-; scg2b-/-* double knockout lines

2.1 Abstract

Previous analysis of TALEN-mediated frameshift mutations from our lab indicated impaired spawning in zebrafish. Building upon this gene editing effort, we employed CRISPR-Cas9 to achieve more extensive and complete excision of the *scg2* genes. This study describes the creation and comprehensive validation of a complete double knockout (DKO) of the *scg2a* and *scg2b* genes in zebrafish, created using CRISPR-Cas9 technology. To construct this DKO model, we first developed several single KO lines of *scg2a* and *scg2b*. These lines were validated with a multi-faceted approach that combined genetic, histological, and peptidomic techniques to ensure the accuracy and completeness of the knockout. Initial screening involved genotyping and DNA sequencing to identify potential founder fish. Mass spectrometry analysis confirmed the complete absence of the Scg2a and Scg2b products and SNa and SNb in some of the KO lines. Three out of 8 KO lines failed to pass all validation steps, so were eliminated from the study. Two selected *scg2a-/-* and *scg2b-/-* single KO lines were crossed to produce the DKO line. Immunohistochemistry (IHC) for the SNa and SNb peptides in the brain and pituitary tissues confirmed the successful gene deletion of the single KO and DKO fish, which were obtained. This thoroughly validated *scg2a-/-; scg2b-/-* DKO model represents a significant advancement in our ability to study the reproductive functions of these genes. The comprehensive validation employed here sets a rigorous standard for gene knockout studies, ensuring reliable and reproducible results for future functional and phenotypic analyses.

2.2 Introduction

The advent of genome editing technologies has transformed the landscape of genetic research, enabling the precise manipulation of specific genes to elucidate their functions. Genome editing technologies have revolutionized the use of zebrafish as a model organism in many fields of biological research. There are several methods, including morpholinos, zinc finger nuclease (ZFN), transcription activator-like effector nuclease (TALEN) and CRISPR-Cas9 (clustered regularly interspaced palindromic repeats), each of them has its unique advantages and disadvantages. These tools allow researchers to create targeted gene knockouts, knock-ins, and

other modifications, providing valuable insights into vertebrate biology and potential therapeutic targets for human diseases. Among them, the CRISPR-Cas9 genome editing system utilizes a programmable guide RNA (gRNA) to direct the Cas9 endonuclease to a specific DNA sequence for cleavage, enabling precise, economical and efficient genetic modifications, facilitating the study of gene function, disease modelling, and developmental processes (Li et al., 2021). This method offers several advantages over previous gene editing techniques. One key advantage of the CRISPR-Cas9 system is its simplicity in design and implementation, as it does not require complex protein engineering steps (Li et al., 2020). Additionally, the CRISPR-Cas9 system has been shown to have high targeting efficiency and a relatively low rate of off-target effects, making it a highly precise tool for gene editing (Newman & Ausubel, 2016; Li et al., 2020). Leveraging these advantages, the CRISPR-Cas9 system can be employed to generate a complete knockout of specific genes, which is instrumental in investigating impacts on reproductive processes. Here, I describe the creation and validation of a complete DKO of the *scg2*a and *scg2b* genes in zebrafish using CRISPR-Cas9.

Previous research from our lab employed TALEN-mediated gene editing to generate frameshift mutants of *scg2a* and *scg2b* lines (Tao et al., 2018; Mitchell et al., 2020). In those mutant fish, spawning success, reproductive behaviour and overall spawning were significantly reduced compared to the control wild-type fish (Mitchell et al., 2020). However, while useful for gene disruption, the TALEN system presents limitations. It can sometimes result in an incomplete knockout, where some functional domains of the target gene remain intact. Furthermore, some TALEN mutants might initiate translation from an alternative start codon, leading to the production of truncated but partially functional proteins that were intended to be disrupted. For example, Lee et al. (2020) found that nonsense-mediated decay was unable to remove the mutant mRNAs in twelve out of sixteen homozygous mutant mice with frameshift mutations generated using engineered nucleases. Also, some publications providing guidelines to create loss-of-function mutants in TALEN acknowledge the potential for alternative start codons and the need to target crucial functional domains to ensure complete loss of function (Ma et al., 2016).

In contrast, CRISPR-Cas9 technology offers a more comprehensive approach to gene editing by introducing double-strand breaks at specific loci, potentially leading to more extensive disruptions of the target gene through non-homologous end joining (NHEJ) or homology-directed

repair. The primary objective of this chapter is to detail the methodology and extensive validation of the complete knockout of both *scg2a* and *scg2b* genes using CRISPR-Cas9 technology.

Validating a gene knockout model, whether in mice, zebrafish, or other systems, typically involves a multi-step process to confirm the successful elimination of the target gene and its protein product (Dalvie et al., 2022). Where PCR-based methods such as genotyping are used to amplify the region of interest and detect the presence of the engineered mutation or deletion is common among most studies, it is often followed by DNA sequencing of the targeted locus to verify the exact genetic modification and ensure no unintended mutations occur during the editing process. However, additional verification at the protein level, such as Western blotting, immunohistochemistry (IHC) or immunofluorescence (IF) techniques are also valuable for visualizing the lack of protein expression in specific tissues or cellular compartments (Tong et al., 2023).

In our study, we validated our knockout models using a comprehensive array of techniques to ensure the accuracy and reliability of our genetic manipulations. Genotyping and sequencing were initially performed to identify fish that were successfully gene-edited. To assess the impact of the knockout at the protein level, we employed immunohistochemistry (IHC) to visualize the absence of the target protein in the brain and pituitary tissues, providing spatial information about the effectiveness of the knockout across different cell types. Furthermore, we utilized mass spectrometry analysis, a highly sensitive and specific technique, to definitively confirm the absence of the target protein and any potential truncated products. This multi-faceted validation approach provides robust evidence for the successful generation of the *scg2a-/-, scg2b-/-* DKO model and establishes a solid foundation for subsequent functional studies and phenotypic analysis.

2.3 Materials and Methods

2.3.1 Experimental animals

Wildtype (WT) zebrafish were sourced from an in-house stock at the University of Ottawa (uOttawa Wild type), bred and raised according to standard husbandry procedures. Fish were maintained in 10-L tanks of dechlorinated City of Ottawa tap water at a density of 5fish/L in a recirculating system (Techniplast, Montréal, QC, Canada) at a temperature of 28^{o}C on a 14:10 light-dark cycle. Fish were fed once or twice daily with GEMMA zebrafish diets (Skretting, Vancouver, BC, Canada) according to embryonic larval and adult life stages. All experiments were

conducted in accordance with animal care guidelines provided by the Canadian Council on Animal Care and with prior approval from the University of Ottawa Animal Care Committee.

2.3.2 Generation of the *scg2a* and *scg2b* knockout lines

The *scg2*a and *scg2b* knockout zebrafish have been created using the CRISPR-Cas9 gene-editing technique. The zebrafish genome annotation (GRCZ11) in Ensembl was accessed and the *scg2a* (Chromosome 15 - NC_007126.7) and *scg2b* genes sequences (Chromosome 2 - NC_007113.7) and gene structures were mapped using Snap Gene (Dotmatics, Boston, MA, USA). To identify CRISPR-Cas9 target sites, 5 kb sequence flanking translation start (5') and stop site (3') were used in CHOPCHOP software (Montague et al., 2014). The single guide RNA (sgRNA) templates were created by annealing gene-specific oligonucleotides containing the T7 promoter sequence, the 20 base pairs (bp) target site (Figure 1) followed by the Protospacer Adjacent Motifs (PAM) sequence, and a complementary region of 80 bp constant oligonucleotide (Gagnon et al., 2014). All sgRNAs were transcribed using the HighScribe™ T7 Quick High Yield RNA synthesis kit (New England BioLabs, Ipswich, MA, USA) and purified using 5M ammonium acetate and ethanol precipitation. RNA bands were detected by electrophoresis on a 1% agarose gel, and RNA purity and concentration were measured using a Nanodrop 1000 spectrophotometer (Thermo Fisher Scientific, Waltham, MA, USA). Microinjections were performed in 1-cell stage embryos for both *scg2a* and *scg2b* gene deletions. The injection solution comprised of the following: 40 ng/µl for each sgRNA, 20 ng/µl Cas9 protein (New England BioLabs, Ipswich, MA, USA), and 0.1% Phenol Red ($(C_6H_4OH)_2C_7H_4SO_3$) (Sigma, Burlington, MA, USA) suspended Danieau buffer (in mmol/L: 58 NaCl, 0.7 KCl, 0.4 $MgSO_4$ 0.6 $Ca(NO_3)_2$, and 5.0 HEPES ($C_8H_{18}N_2O_4S$); pH 7.6). At 1-day post fertilization (dpf), 20 embryos from each injection were genotyped. Following confirmation of whole gene deletions, the rest of the embryos were reared to sexual maturity (90 pdf). At maturity, each fish developed from an injected embryo had its fins clipped and was genotyped (Founder fish- F0). The selected male and female fish were individually mated with WT fish. Twenty embryos were collected from each clutch and genotyped to confirm the successful heritability of the gene knockout. Five F0 fish (4A, 7A, 13A, 16A, 18A) for the *scg2a-/-* KO line and 4 four F0 fish (4B, 6B, 12B, 20B) for the *scg2b-/-* KO line were selected. Offspring from each F0 mating were housed separately, and when they reached maturity, genomic DNA was extracted from fin clippings. This genomic DNA was used for PCR and genotyping. Selected heterozygous

F1 fish were in-crossed within the line to generate the F2 generation, where the population consisted of 25% of homozygous KO fish. Each homozygous KO fish was in-crossed again to generate the F3 generation of single *scg2a-/-* and *scg2b-/-* KO lines.

From the *scg2a-/-* (Line 7A) and *scg2b-/-* (Line 4B) lineages homozygous KO fish were in-crossed to create the *scg2a-/+* and *scg2b-/+* heterozygous fish and finally, they were in-crossed at their mature age, to genotype for selection of the *scg2a-/-, scg2b-/-* DKO fish (Figure 2). The validity of these single and DKO lines was primarily confirmed by genotyping (Figure 3), sequencing (Figure 4), mass spectroscopy and immunohistochemistry methods (Figure 5, Figure 6). For each single KO and DKO line, fish were used for experimentation only after the F3 generation.

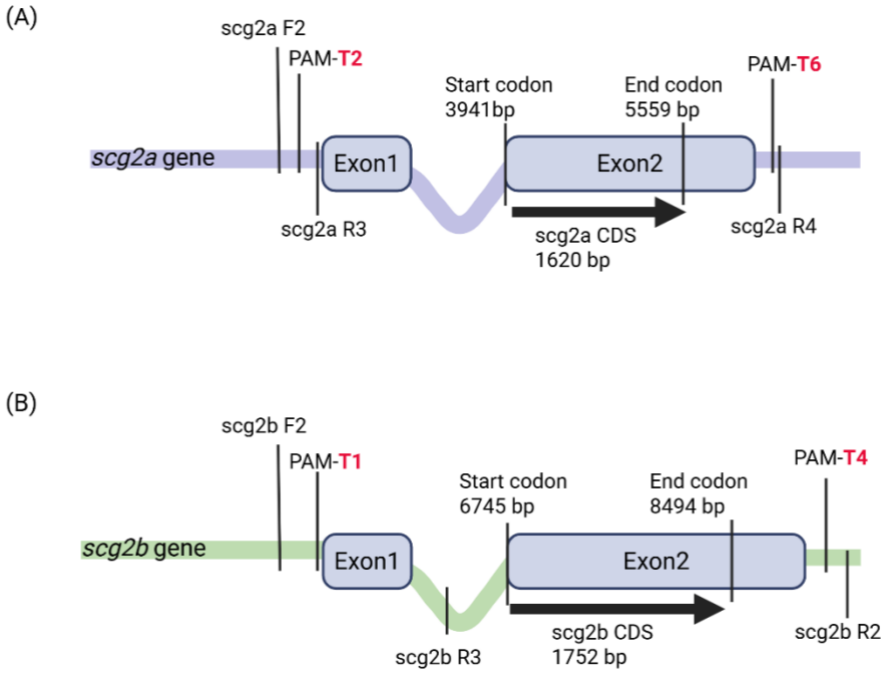

Figure 1. Schematic representation of the *scg2a* (A) and *scg2b* (B) gene structures in zebrafish. (A) The coding sequence (CDS) for *scg2a* spans 1620 base pairs (bp). Site 2 (T2) and site 6 (T6) were targeted using CRISPR-Cas 9 guide RNA to remove the Scg2a coding sequence. (B) The *scg2b* CDS extends for 1752 bp. Site1 (T1) and site 4 (T4) were targeted by the guide RNA. The positions of the Protospacer Adjacent Motifs (PAM) used in CRISPR-Cas9 gene editing are marked adjacent to the target sites, and the binding locations of the *scg2a* F2, R3 and R4, *scg2b* F2, R2 and R4 oligonucleotide primers used for genotyping are marked on the map.
.

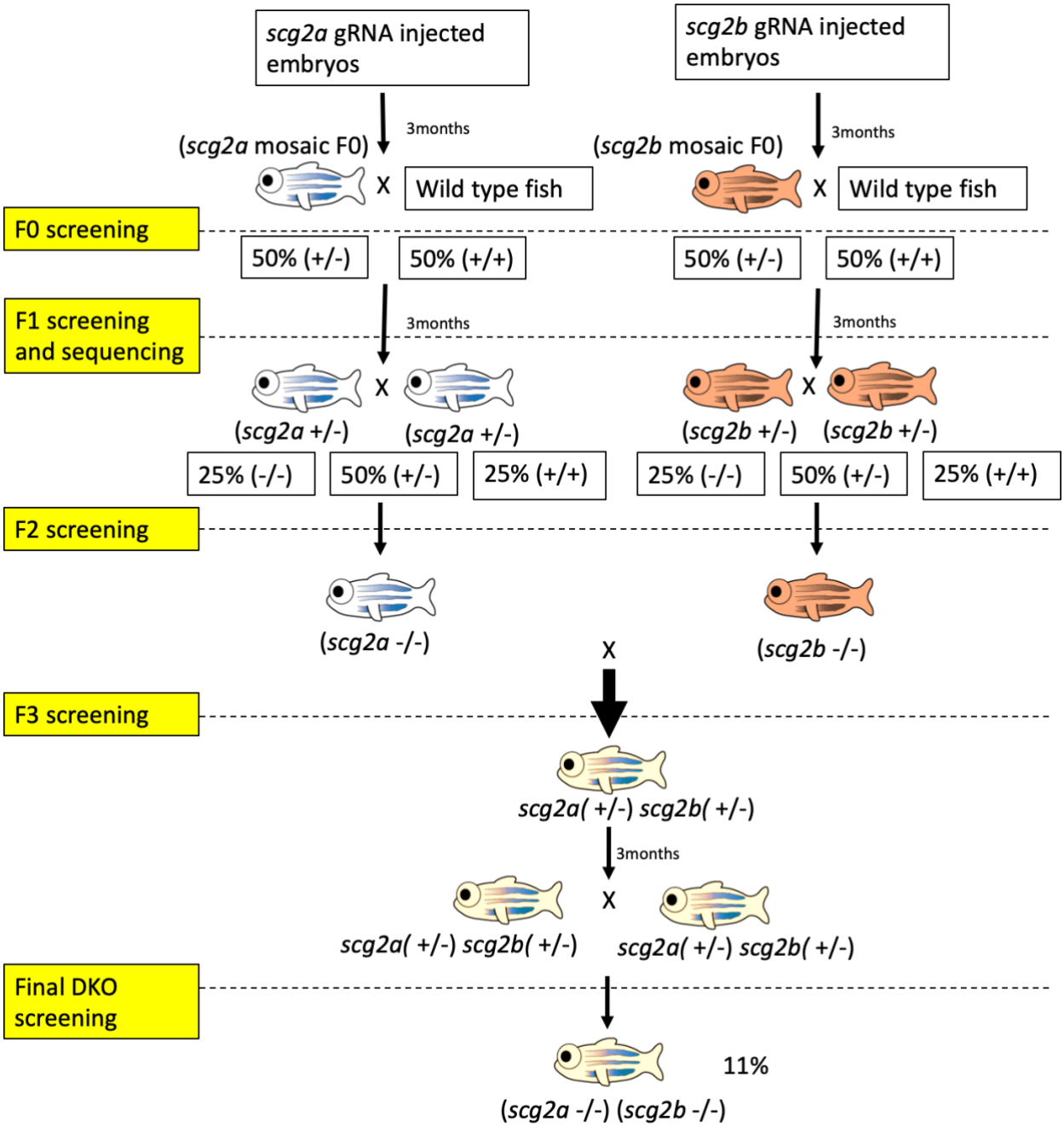

Figure 2. Schematic representation of the stepwise process of establishing *scg2a-/-, scg2b-/-* single knockouts and the *scg2a-/-, scg2b-/-* DKO model. F0 screening: CRISPR-Cas9 with *scg2a* and *scg2b* guide RNA (gRNA) injected zebrafish embryos were raised until mature age (3 months), fin clip genotyping for F0 fish and embryo genotyping for the embryos resulted from WT cross, were conducted to confirm successful gene deletion in founder (F0) fish. F1 screening and sequencing: Heterozygous mutant fish were identified through genotyping in the first generation and after the F2 generation homozygous KO fish identification, the genomic DNA extracted from the mutant band was Sanger sequenced. F2 screening: Genotyping was used to segregate wild-type, heterozygous, and homozygous knockout fish for each gene. F3 screening: Subsequent generations

were screened to establish homozygous lines. Final DKO screening: The final step involved genotyping to identify and confirm the true homozygous DKO (*scg2a-/-, scg2b-/-*) fish.

2.3.3 Validation of the *scg2a-/-*, *scg2b-/-*, and *scg2*a*-/-, scg2b-/-* DKO fish

2.3.3.1 Genomic DNA amplification, gel electrophoresis and sequencing

Gel electrophoresis was used as the first-level screening method to distinguish the heterozygous and homozygous KO fish from WT. Each fish was lightly anesthetized with 0.128 mg/mL buffered tricaine (MS-222; Syndel Laboratories, Nanaimo, BC, Canada) and a small caudal fin clipping was collected. The collected tissue was dissolved, and the genomic DNA was extracted by 100 mg/l in 50 µl of 50 mmol/l NaOH at 98°C for 10 minutes (min) followed by neutralization with 5 µl of 1 mol/l Tris–HCl (pH 8). The extracted gDNA was used for PCR amplification using *scg2a* and *scg2b* gene target site-specific primers (Table 2), and gel electrophoresis using a 2% Agarose gel containing SYBR-safe DNA gel stain (ThermoFisher Scientific, San José, CA) run for 25 min at 120 V was used to visualize amplicons (figure 3). Based on the amplicon size, each gel band was detected, and the fish were separated based on their genotypes. Genomic DNA extracted from the fin clips was submitted for Sanger sequencing (Genome Québec, McGill University, Montréal, Canada).

Gene name	**Gene symbol**	**Forward Primer (5'3')**	**Reverse Primer (3'5')**	**Annealing Temp (°C)**
Secretogranin 2a	*scg2a*	F2: TCATTCCACTGTGGTGAAACC	R3: GCGTCATCGTTTTCGAAAGAC R4: AGATTTCATGTCGTGCATGCC	57
Secretogranin 2b	*scg2b*	F2: GTGAATGATTACCGTCGGTAG	R2: CTCACACTTCAGAACACGTAC R3: ATAAGCCCGAGATGAGATAGG	57

Table 2: Genotyping primer sequences (F2: Forward primers, R3- Reverse primer3, R4-Reverse primer 4) and annealing temperatures for *scg2a* and *scg2b* genes.

2.3.3.2 Mass spectroscopy

Brain and pituitary samples were dissected from F2 and F3 generation single and DKO and their sibling female WT fish. Peptide extraction was carried out for individual samples according to our previously described protocol for liquid chromatography-tandem mass spectrometry (LC-MS/MS) analysis (Lu et al., 2023). A Dionex Ultimate RS3000 was connected to an Exploris 480

mass spectrometer (ThermoFisher Scientific, San Jose, CA) and operated with a nano-electrospray interface in positive ion mode. The solvent system consisted of buffer A (0.1% FA in water) and buffer B (0.1% FA in 80% acetonitrile). Reconstituted peptides were loaded on a 75 μm I.D. × 150 mm fused silica analytical column packed in-house with 3 μm ReproSil-Pur C18 beads (100 Å; Dr. Maisch GmbH, Ammerbuch, Germany). The flow rate was set to 300 nL/min, and the gradient was set as 5–35% buffer B in 30 min. The spray voltage was set to 2.2 kV, and the temperature of the heated capillary was 275°C. One full MS scan from 350 to 1200 m/z was followed by a data-dependent MS/MS scan of the 15 most intense ions with a dynamic exclusion repeat count of 1 in 20 seconds. The mass resolution was 60,000 for MS1 and 15,000 for MS2. Real-time internal calibration by the lock mass of background ion 445.120025 was used. All data were recorded using Xcalibur software (ThermoFisher Scientific, San Jose, CA). Data acquisition and analysis were performed using Thermo Xcalibur software, version 2.2. For the identification of SNa and SNb peptides, m/z values of 933.2098 (M+4H+) and 1152.8936 (M+3H+) were used in the full MS scan, respectively, with a mass tolerance of 10 ppm within a 60-second identification time window. A chromatogram peak was defined by a minimum of five continuous data points.

2.3.3.3 Immunohistochemistry

Heads from sibling WT and *scg2a-/-, scg2b-/-* DKO fish were fixed in 4% paraformaldehyde, decalcified in 0.5 M EDTA for 5-7 days, then washed in PBS (3x15 min). Samples were dehydrated in ethanol (30–99%), cleared in xylene (2x30 min), and transferred to paraffin at 60°C for 1 hour, followed by overnight incubation in fresh paraffin. The next day, samples were embedded, sectioned (8 μm) using a Microm HM350 micrometer (Heidelberg, Germany), and mounted on Superfrost™ Plus slides (Fisherbrand, cat#12-550-15). For immunofluorescence, sections were deparaffinized in xylene (2x20 min), rehydrated in ethanol (99% to 70%), and placed in PBS. Antigen retrieval was performed in 0.01 M sodium citrate at 85°C for 30 minutes, followed by blocking with 1% skim milk and 0.3% Triton X-100 for 30 minutes.

The sections were then incubated overnight at 4 °C with our specific polyclonal rabbit-anti-goldfish SNa antiserum (1:600). The SNa antiserum has been extensively validated in our laboratory (Canosa et al., 2011; Zhao et al., 2006; Peng et al., 2025). It has been shown using Western blotting that the SNa antibody may recognize the precursor and any processed fragment

containing the SNa epitope (Zhao et al., 2006). Therefore, we refer to this as Scg2a/SNa immunoreactivity (ir). The epitope (YTPQKLATLQSVFEE) recognized by the goldfish SNa antibody is identical to the central 15 amino acids in zebrafish SNa (Table1). Tao et al., 2018 also demonstrated that this antibody recognizes synthetic zebrafish SNa, exhibiting no SNb cross-reaction on dot blots (Tao et al., 2018). Immunoreactivity of SNa in the preoptic area and pituitary of WT zebrafish was documented by Peng et al. (2025), thus it was used here to confirm and validate the *scg2a-/-,scg2b-/-* DKO fish line. Guinea pig-anti-Oxt antiserum (Abcam, cat#ab228508) in 1:800 dilution was used as a control (Altmieme et al., 2019; Canosa et al., 2011). It specifically recognizes fish Oxt (also known as isotocin) and SNa is expressed in Oxt neurons (Canosa et al., 2011) in the preoptic area (POA) and pituitary. The specificity of the guinea pig-anti-Oxt antiserum in goldfish (Canosa et al., 2011) and zebrafish (Altmieme et al., 2019) has been previously validated.

On the next day, after being washed 2 X 10 min each in PBS solution, sections were incubated at room temperature for 2 hours in goat anti-rabbit IgG (H+L) secondary antibody, Alexa Fluor™ Plus 488 (ThermoFisher Scientific, San Jose, CA, cat#A32731) diluted to 1:500 for SNa and goat anti-guinea pig IgG (H+L), Alexa Fluor™ 594 (ThermoFisher Scientific, San Jose, CA, cat#A11076) diluted to 1:500 for Oxt. Finally, coverslips were mounted on the slides with 60 µl of ProLong™ diamond antifade mountant with DAPI nuclear staining (ThermoFisher Scientific, San Jose, CA, cat#P36962). Images were captured on Zeiss axio imager Z2 upright fluorescence microscope with apoTome.2. All images were captured as Z-stacks and processed using the extended depth of focus function in ZEN 3.2.0. Post-processing adjustments, including brightness, contrast, and color balance, were made using FIJI in ImageJ 1.54f.

Before this study, there were no specific SNb antibodies available, and attempts to develop a polyclonal antibody specific to SNb failed. Therefore, we developed a mouse monoclonal anti-zebrafish SNb antibody in collaboration with ABclonal Inc. (Woburn, MA, USA). Briefly, the development of monoclonal antibodies (mAbs) followed a multi-phase process. First, an antigenic peptide (C-RSIFEELGKLSAAQ: Scg2b198-211) was synthesized and used to immunize five Balb/c mice over a 63-day schedule to elicit an immune response. Following immunization, the antiserum of the immunized mice was tested against both SNb and SNa peptides. According to the titer data, a mouse with good immune response against SNb while having a very low titer against SNa was selected, and splenocytes from that mouse were fused with myeloma cells (SP2/0). The

resulting hybridomas were screened using enzyme-linked immunosorbent assay (ELISA) to identify positive clones. Forty positive clones were identified and tested for the reaction with 2 peptides (SNa: C-QSVFEELSGIASSK-BSA, SNb: C-RSIFEELGKLSAAQ-BSA). The top candidates showing a preference for the SNb antigen were subcloned, and monoclonality was confirmed through limiting dilution. After screening, 10 subcloned hybridomas were selected and screened again for immunoreactivity. After observing the immunoreactivity in the zebrafish brain and pituitary sections, clones CMC0539-02-A and CMC0532-02-A were selected, and their mAbs were purified. Finally, each mAb (1 mg each) was produced from each clone, and the antibodies were validated through ELISA. Hybridoma cell lines are stored in liquid nitrogen. For the validation of the SNb antibody (clone CMC0539-02-A) immunoreactivity was confirmed through a pre-adsorption assay and a dilution series assay assessed from 1:100 to 1:700. It was determined that the 1:200 and 1:300 dilutions were the best for the zebrafish pituitary. The specificity of the antibody was confirmed with a pre-adsorption assay and using *scg2b-/-* single KO brain and pituitary sections (Appendix A- Figure A3). After confirmation of the specificity, SNb-ir was observed in brain and pituitary sections in WT and *scg2a-/-, scg2b-/-* DKO zebrafish and co-localization was observed against Oxt-ir and SNa-ir, separately.

Further antibody assessments were performed with the *scg2b-/-* 4B KO, and WT brain/pituitary sections were incubated with SNa (1:600) and SNb (1:200) primary antibody, without antigen pre-adsorption. For the observation of SNb-ir and co-localization with SNa-ir, WT sections were separately incubated with SNa rabbit-anti-goldfish SNa antiserum (1:600) with SNb mouse monoclonal anti-zebrafish antibody (1:200). To assess any potential co-localization of Oxt-ir and SNb-ir and to confirm the absence of both SNa and SNb-ir in the DKO, control WT and DKO brain and pituitary sections were incubated with the newly developed SNb mouse monoclonal anti-zebrafish antibody (1:200) and guinea pig anti-Oxt antiserum (1:800).

After each primary antibody incubation at 4^0C overnight, sections were washed with PBS solution and incubated at room temperature for 2 hours with their respective secondary antibodies. For SNa and SNb co-localizations, we respectively used goat anti-rabbit IgG (H+L) secondary antibody, Alexa Fluor™ Plus 488 (ThermoFisher Scientific, San Jose, CA, cat#A32731) and goat anti-mouse IgG1 Cross-Adsorbed Secondary Antibody, Alexa Fluor™ 594 (ThermoFisher Scientific, San Jose, CA, cat # A-21125) diluted to 1:500.

To perform colocalization of Scg2b/SNb-ir and Oxt-ir, we used donkey anti-mouse IgG (H+L), Alexa Fluor Plus 488 (ThermoFisher Scientific, San Jose, CA, cat#21202) diluted in 1:500 for SNb and goat anti-guinea pig IgG (H+L), Alexa Fluor 594 (ThermoFisher Scientific, San Jose, CA, cat#A11076) diluted in 1:500 for Oxt. After mounting coverslips with 60 µl of ProLong™ diamond antifade mountant with DAPI nuclear staining (ThermoFisher Scientific, San Jose, CA, cat#P36962), imaging and image processing were conducted like the previously described process.

2.4 Results

2.4.1 Gel electrophoresis confirm the *scg2* deletion

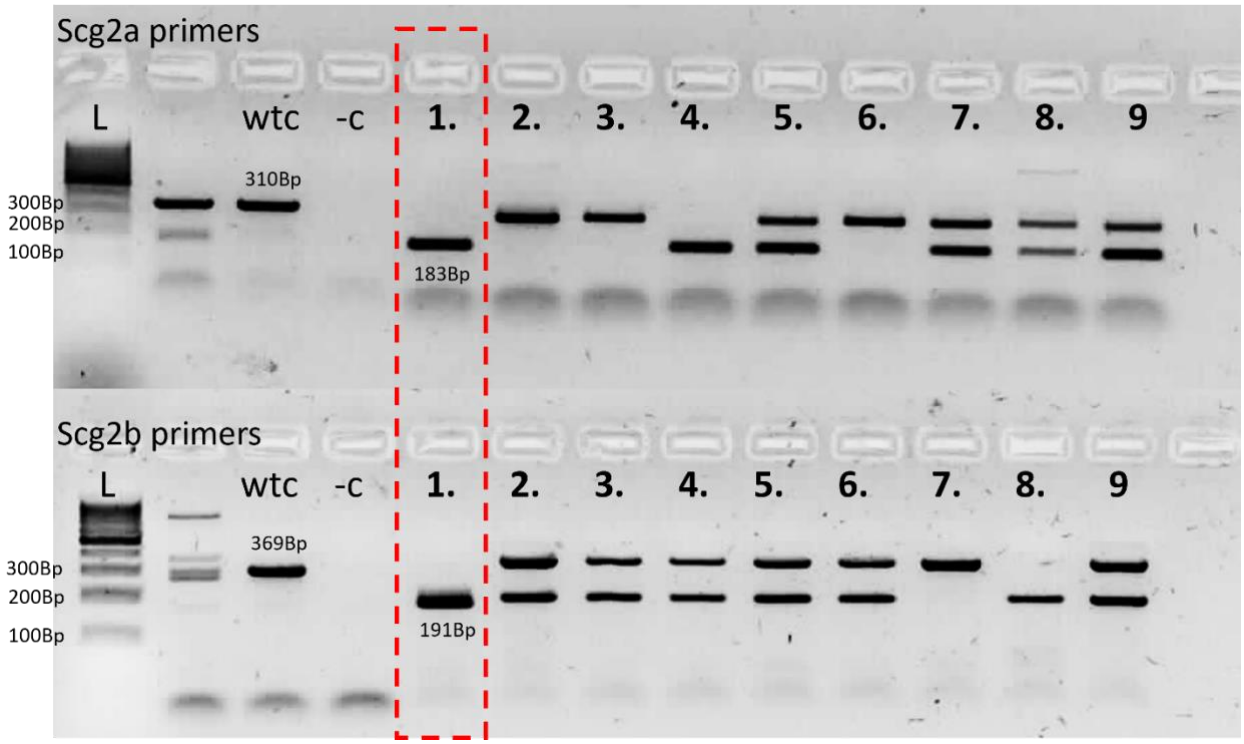

Figure 3. Validation of *scg2a-/-; scg2b-/-* (7AX4B) DKO zebrafish through genotyping.
The gel shows PCR products amplified using primers specific for *scg2a* (top panel) and *scg2b* (bottom panel). Lane L represents the molecular weight ladder, with band sizes indicated. Lanes labeled wtc show the wild-type control, with *scg2a* (310 bp) and *scg2b* (369 bp) products. The negative control (-c) displays no amplification. Lanes 1 to 9 represent DNA from individual zebrafish samples, where bands at 183 bp for *scg2a* and 191 bp for *scg2b* confirm the successful knockout genotypes. The red dashed box highlights sample 1, showing correct band sizes for both *scg2a* and *scg2b* DKO alleles.

2.4.2 Sanger sequencing confirmation

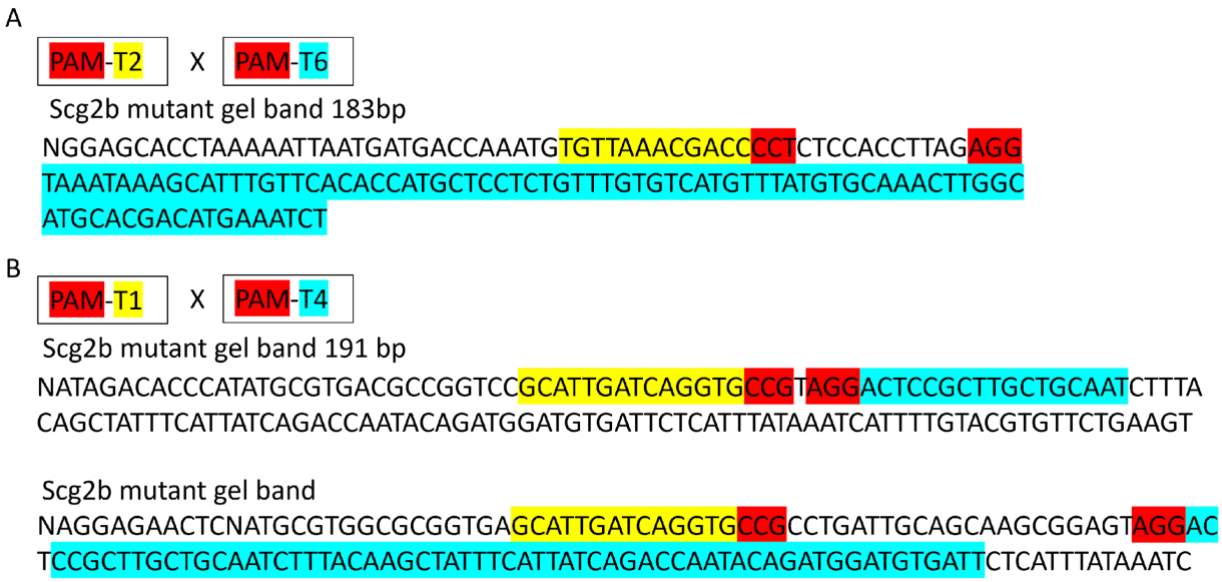

Figure 4. Sequence alignment of *scg2a-/-* and *scg2b-/-* KO gel bands showing CRISPR-Cas9 target sites. The sequences represent the mutant bands for *scg2a* (183 bp, top) and *scg2b* (191bp, bottom), displaying the CRISPR-Cas9 edited regions. In each sequence, the PAM sites are shown in red, while the target sequences upstream of the coding sequence are highlighted in yellow (T2 for *scg2a* and T1 for *scg2b*). The regions marked in blue indicate the target sequences downstream of the coding sequence (T6 for *scg2a* and T4 for *scg2b*). These sequences correspond to the gel bands observed during genotyping and the successful deletion when the target sites are close by, confirming the successful introduction of gene deletion at the respective target sites for *scg2a* and *scg2b*.

This sequencing data confirmed that the CRISPR-Cas9-based gene edition completely deleted the *scg2a-/-* gene locus (NCBI Gene ID: 793796, genomic region NC_007126.7 (43142897.43144757), and *scg2b-/-* gene locus (NCBI Gene ID: 777641, genomic regionNC_007113.7 (47582041.47585197), removing a region of 4112 base pairs and 3061 base pairs, respectively.

2.4.3 Mass spectroscopy confirmation of the absence of SNa and SNb peptides

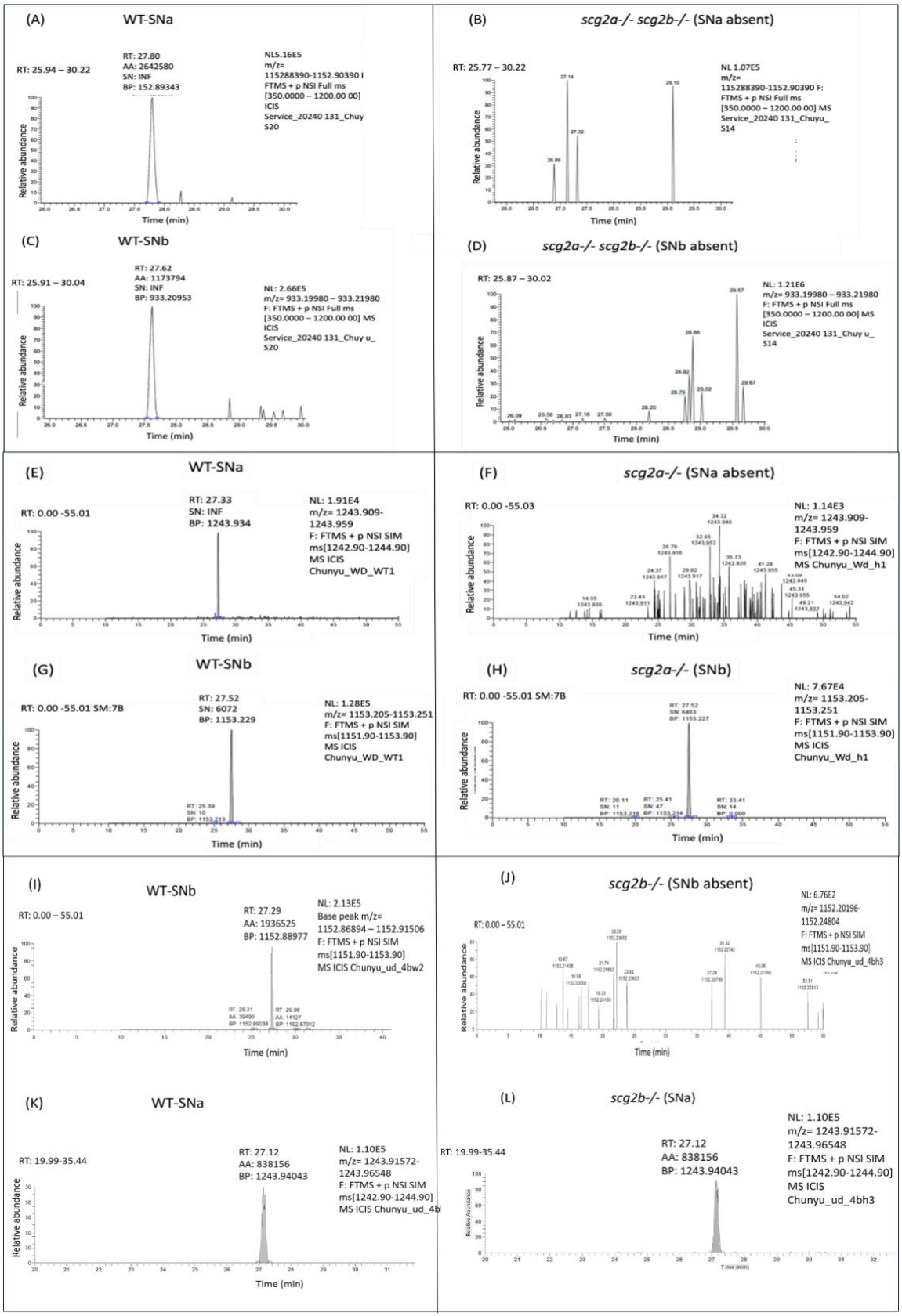

Figure 5. Chromatograms showing the detection of SNa and SNb peptides in female wild-type (WT), *scg2a-/-* (7A) *scg2b-/-* (4B) *scg2a-/-, scg2b-/-* (7Ax4B) double KO (DKO) zebrafish brain and pituitary explants. Panels (A) and (C) display the chromatograms for SNa and SNb peptides, respectively, in WT zebrafish. Both peptides show distinct retention times (RT) and peak intensities, confirming their presence. Panels (B) and (D) show chromatograms of *scg2a-/- scg2b-/-* DKO where SNa and SNb are absent, indicated by a lack of corresponding peaks at expected RTs. Panels (E) and (G) provide mass spectrometry data confirming the presence of SNa and SNb peptides in WT samples. Panels (F) show the absence of the SNa peptide in *scg2a-/-* (7A) single KO, reinforcing the complete knockout. In panel H, the SNb peptide is intact in the *scg2a-/-* (7A) KO. Panels (I) and (K) provide mass spectrometry data confirming the presence of SNb and SNa peptides in control WT samples. Panel (J) shows the absence of the SNb peptide in *scg2b-/-* (4B) single KO, and in panel (H), SNa peptide is intact in the *scg2b-/-* (4B) KO.

Mass spectroscopy analysis confirmed the absence of SNa and SNb peptides in the brain and pituitary of *scg2a-/-* and *scg2b-/-* KO fish lines (Figure 5). Wild-type fish have normal levels of SNa and SNb, whilst the *scg2a* and *scg2b* KO fish do not produce SNa or SNb, respectively. The *scg2a* KO fish express normal SNb levels, and *scg2b* fish have normal SNa levels. Moreover, both peptides are completely lacking in the *scg2a*-/-, *scg2b*-/- DKO fish. It is important to note that 3/8 KO lines failed to pass the mass spectroscopy analysis and were eliminated. The selected KO lines for the DKO line development (*scg2a-/-* 7A KO line and *scg2b-/-* 4B KO line) were confirmed and passed the mass spectroscopy analysis. An explanation for these failed lines was not investigated. From the successful KO lines *scg2a-/-* 13A and 7A KO and the *scg2b* -/-12B, 4B KO lines were maintained and were further characterized.

2.4.4 Immunohistochemistry

Immunohistochemical studies further validated the success of complete *scg2a-/-* and *scg2b-/-* gene KO. Wild-type female zebrafish exhibit a significant amount of SNa-ir (green, Figure 6B) and Oxt-ir (red; Figure 6C) in neuronal cell bodies (blue; Figure 6A) in the preoptic area (POA), with clear co-expression (Figure 6D). No SNa-ir was found in the DKO fish (Figure 6E, F), but Oxt-ir in the POA remained normal (Figure 6G, H). Similarly, WT females exhibit a significant amount of SNa-ir (green; Fig 7B) and Oxt (red; Figure 7C) in neuronal fibres innervating the neural lobe of the pituitary, with clear co-expression (Figure 7D). No SNa-ir was found in the pituitary of DKO fish (Fig 7E, F), but Oxt-ir in the pituitary remained normal (Figure 7G, H). This anatomical data also confirms the successful KO of Scg2a and the SNa peptide.

After generating the mouse anti-zebrafish SNb monoclonal antibody, dilution series and pre-adsorption assays were conducted (Appendix A- Figure A 3) to verify specificity. Immunohistochemical analyses on *scg2a-/-, scg2b-/-* DKO fish and their WT sibling controls confirmed the complete KO of the *scg2b* gene, as shown by the absence of SNb-ir in DKO and *scg2b-/-* 4B K fish.

In WT female zebrafish, we observed prominent SNb-ir (green, Figure 8B) and Oxt-ir, (red; Figure 8C) within neuronal cell bodies (blue; Figure 8A) in the pituitary, with clear co-expression of these markers (Figure 8D). However, in DKO fish, SNb-ir was absent in the pituitary (Figure 9F, H), while the Oxt-ir remained unchanged (Figure 8G, H). Similarly, in WT females, substantial SNb-ir (red; Figure 9B) and SNa-ir (green; Figure 9C) were present in neuronal fibers innervating the neural lobe of the pituitary, with evident co-expression (Figure 9D). In *scg2b-/-* 4B knockout fish, no SNb-ir was detected in the pituitary (Figure 9F, H), although SNa-ir was unaffected (Figure 9G, H). These findings further validate the successful KO of both Scg2a, Scg2b, and the SNa and SNb peptides in zebrafish.

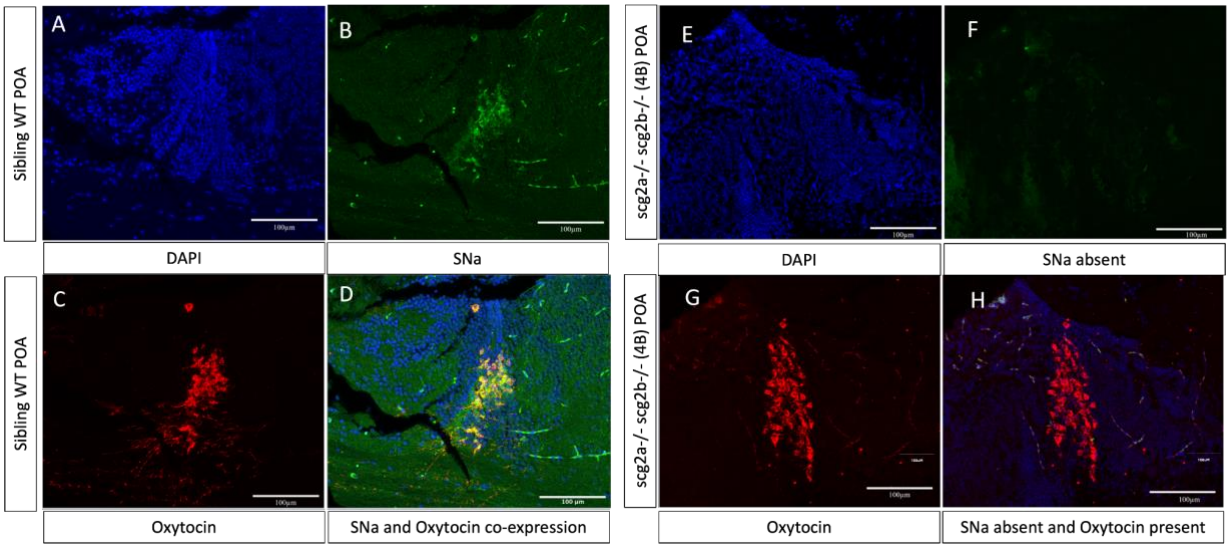

Figure 6. Secretoneurin a (SNa) and oxytocin (Oxt) immunoreactivity (ir) in the pre-optic area (POA) of female wild-type (WT) and *scg2a-/-, scg2b-/-* DKO zebrafish. (A-D) WT POA. (A) DAPI nuclear staining, (B) SNa-ir, (C) Oxt-ir, (D) Merge of SNa and Oxt images demonstrating colocalization (yellow). (E-H) *scg2a-/-; scg2b-/-* DKO POA. (E) DAPI nuclear staining, (F) No evidence of SNa-ir, (G) Oxt-ir, (H) Merge of SNa and Oxt images demonstrating an absence of SNa-ir in Oxt neurons of *scg2a-/-, scg2b-/-* DKO fish. Scale bar: 100 µm.

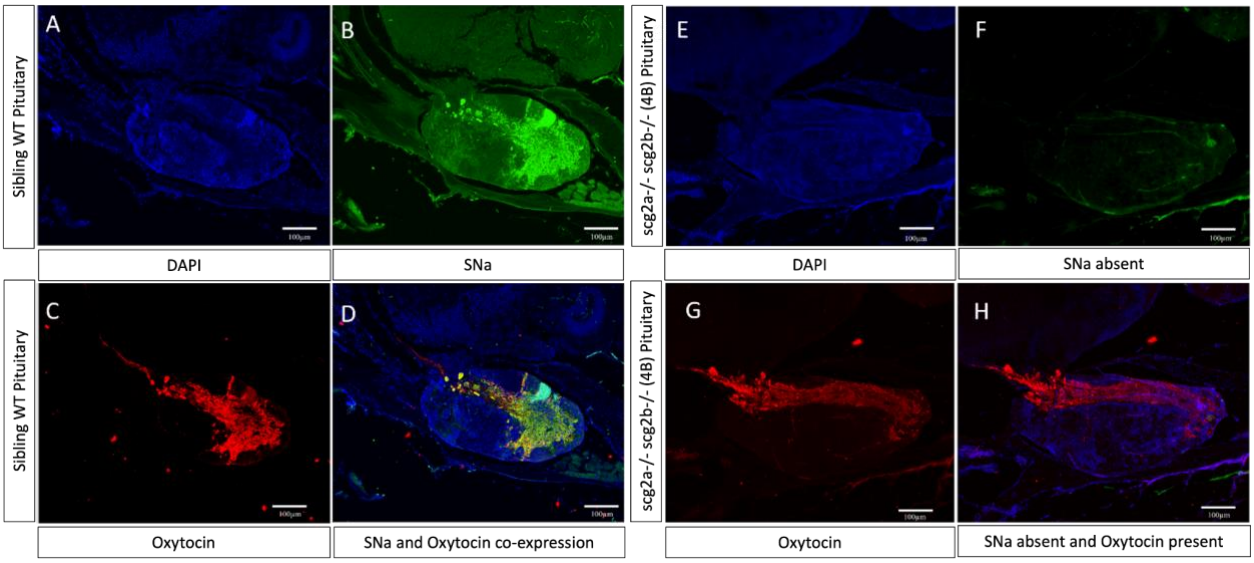

Figure 7. Secretoneurin a (SNa) and oxytocin (Oxt) immunoreactivity in the pituitary of female wild-type (WT) and *scg2a-/-, scg2b-/-* DKO zebrafish. (A-D) WT pituitary. (A) DAPI nuclear staining, (B) SNa-ir, (C) Oxt-ir, (D) Merge of SNa and Oxt images demonstrating colocalization (yellow). (E-H) *scg2a-/-, scg2b-/-* DKO pituitary. (E) DAPI nuclear staining, (F) No evidence of SNa-ir, (G) Oxt-ir, (H) Merge of SNa and Oxt images demonstrating an absence of SNa-ir in Oxt neuronal fibers in the pituitary of *scg2a-/-, scg2b-/-* DKO fish. Scale bar: 100 µm.

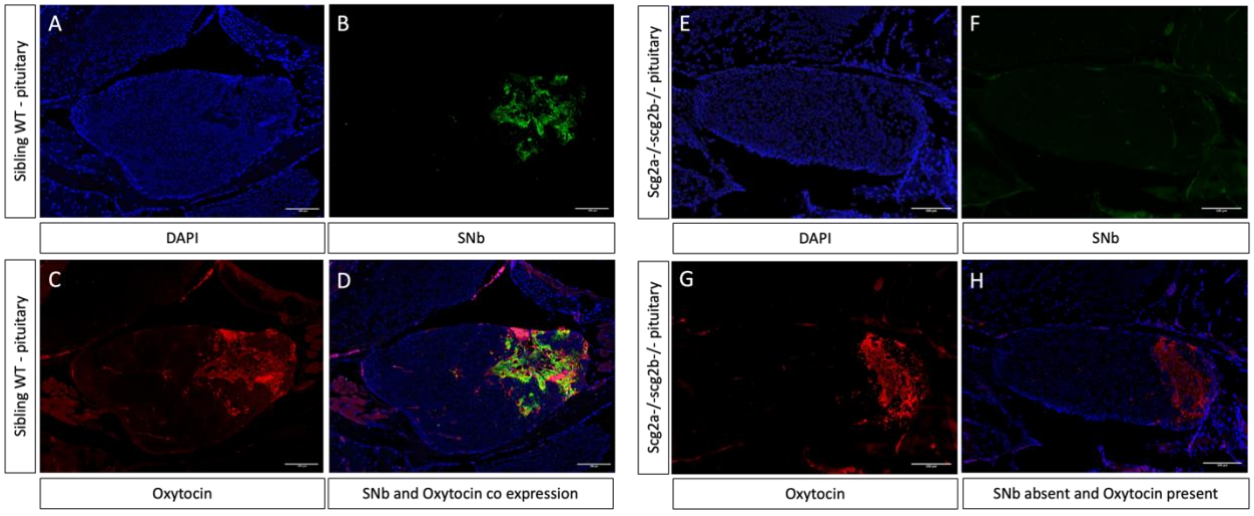

Figure 8. Comparison of SNb immunoreactivity (ir) in the pituitary of wild-type (WT) and *scg2a-/-, scg2b-/-* DKO) zebrafish. (A-D) WT Pituitary, DAPI nuclear staining, (A), SNb-ir (B), Oxt-ir (C), and SNb with Oxt-ir co-expression (E-H) *scg2a-/-, scg2b-/-* DKO Pituitary. DAPI nuclear staining, (E), SNb-ir is absent (F) Oxt-ir (G), and SNb absent in the Oxt neurons of *scg2a-/-, scg2b-/-* DKO fish (H). (scale bar: 100µm).

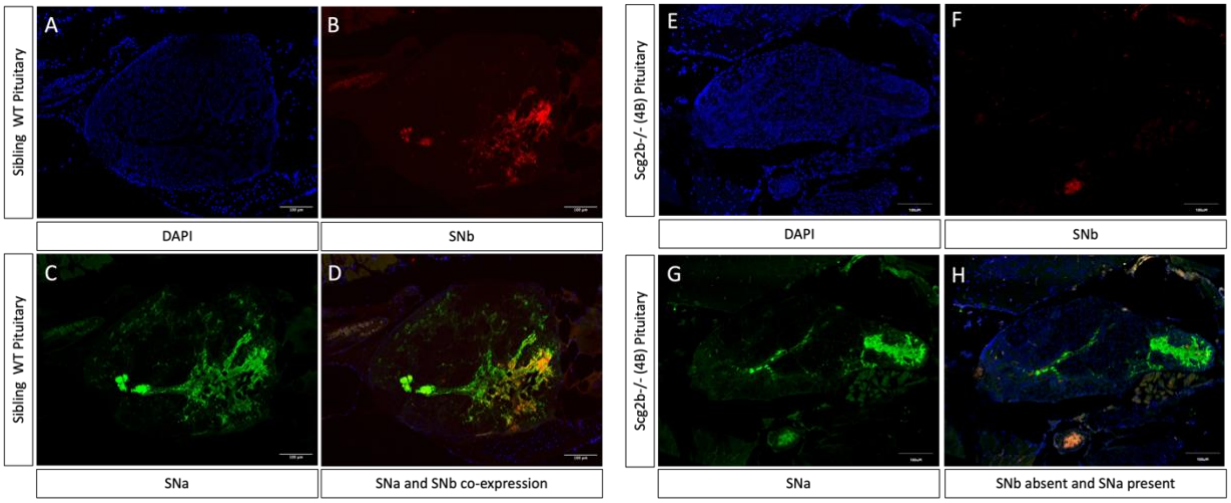

Figure 9. Comparison of SNb immunoreactivity (ir) in the pituitary of wild-type (WT) and *scg2b-/-* 4B KO) zebrafish. (A-D) WT Pituitary, DAPI nuclear staining, (A), SNb-ir (B), SNa-ir (C), and SNb with SNa-ir colocalization (E-H) *scg2b-/-* 4B KO Pituitary. DAPI nuclear staining, (E), SNb-ir is absent (F) SNa-ir (G), SNb absent and the SNa-ir present in the *scg2b-/-* 4BKO fish (H). (scale bar: 100µm).

2.5 Discussion

The *scg2a-/-; scg2b-/-* complete DKO line (*scg2-/-* 7 A KO line crossed with *scg2b-/-* 4 B KO line) was established. Precise mutations and excision of both *scg2a* and *scg2b* genes were achieved using CRISPR-Cas9 gene editing technology. The CRISPR-Cas9 method involves designing a guide RNA (gRNA) that targets specific sequences within the target gene, leading to double-strand breaks from the target sites of the coding sequence. The repair of these breaks often results in insertions or deletions (indels) that disrupt the coding sequence (Hwang et al., 2013). However, the indel knockouts are not complete gene knockouts because the gene function is only disrupted but not completely deleted. For instance, the TALEN frameshift mutation model for *scg2a* and *scg2b* in zebrafish disrupted gene function using a few base pair deletions (Mitchell et al., 2020) differs significantly from the complete gene deletion of the current *scg2a-/-; scg2b-/-* DKO model. The CRISPR-Cas9-based DKO line achieves a complete gene knockout, where the entire genes encoding the Scg2a and Scg2b precursor proteins are fully deleted from the zebrafish genome. This complete deletion eliminates the possibility of residual gene activity, distinguishing it from the frameshift mutation approach.

In this study, the complete *scg2a-/-, scg2b-/-* gene KO was generated using two gRNAs that break the coding sequence from two targeted locations in each gene. We were able to delete

the whole coding sequence of the *scg2a* and *scg2b* genes. The main advantage of this method is that it efficiently deletes the whole coding sequence of the gene, ensuring that the gene function is erased (Komori et al., 2023). However, this is a large chromosomal deletion that invariably will remove all peptides arising from Scg2a and Scg2b precursor processing, which could affect the studied system.

To ensure the proper deletion of the *scg2a* and *scg2b* genes, it is important to validate each step. As the first step, embryo genotyping was performed after the injection of the CRISPR-Cas9 constructs to ensure that the gene was deleted as intended. Zebrafish embryos were collected post-injection, and genomic DNA was extracted. Using PCR amplification and subsequent gel electrophoresis, we detected indels at the targeted *scg2* locus. This initial screening helped identify individuals with potential knockouts. After rearing them to adulthood, fish were fin-clipped, genotyped, and confirmed for the presence of a mutant band through gel electrophoresis. At the F1 generation level, Sanger sequencing of the PCR products from genotyped embryos provided precise information on the mutations introduced by CRISPR-Cas9, confirming the disruption of both *scg2a* and *scg2b* genes.

This is a similar validation approach that has been reported in other zebrafish CRISPR-Cas9 studies. For example, in the creation of a vasotocin complete gene knockout model using CRISPR-Cas9, the knockout was primarily validated through genotyping and DNA sequencing (Ramachandran et al., 2023). Similar CRISPR-Cas9 mutation models as well as TALEN mutants have been created for other reproductively important genes in zebrafish and medaka and validated using genotyping, sequencing, and immunohistochemistry methods (Marvel et al., 2018; Spicer et al., 2016; Yeh et al., 2017). Fleming et al., 2023 also generated a *scg2a* knockout in medaka, but the validation methods were limited to genotyping sequencing and immunohistochemistry.

While these studies provided a comprehensive analysis at the genetic and phenotypic levels, they lacked deeper validation through proteomics, which could have offered additional insights into protein-level disruption. Protein level validations are important because, despite attempts to disrupt gene function, cells may produce unexpected protein products introduced as the non-homologous end joining repairs at the deletion sites, which retain some functionality of the original protein. This could also occur through mechanisms such as alternative translation start sites or exon skipping, which can circumvent the intended frame-shift mutations caused by indels. Researchers have observed this adverse outcome across diverse organisms, including cultured

mammalian cells (Kapahnke et al., 2016; Mou et al., 2017), zebrafish (Prykhozhij et al., 2017) and butterflies (Connahs et al., 2019), highlighting the complexity of genetic manipulation and the adaptability of biological systems.

Thus, protein-level validation, especially mass spectrometry, has been recently utilized for confirming the absence or modification of a target protein, as seen in only a few other studies. For example, a study on CRISPR-Cas9-based KO of prion protein (PrP) used mass spectrometry to compare the proteomic profiles of WT and knockout in immortalized mesenchymal stem cells, revealing significant differences in protein expression (Gross et al., 2021). Lin et al. (2019) indicates that any modification to coding sequences requires confirmation at the protein level and confirmed several genome-edited animal models including zebrafish, mouse and butterfly using mass spectrometry methodologies. The in-depth validation we undertook is often missed in other zebrafish gene mutation studies, where they focus most on genetic and phenotypic validation alone. Without proteomic analysis confirmation, changes in protein expression or some unexpected function of a residual or truncated protein can go undetected, leading to incomplete validation of the genetically modified organisms.

By incorporating mass spectrometry in the validation process, our study confirms knockouts at both the DNA and protein levels. Peptides were extracted from the KO fish brain and pituitary explants to confirm the absence of SNa and SNb peptides. However, not all knockout lines passed the mass spectrometry step. Unexpectedly, some *scg2a-/-* (4A, 16A) and *scg2b-/-* (6B) lines still expressed some level of the SN peptides, despite earlier DNA-level confirmation (Appendix A- Figure A1, A2). This discrepancy highlights the importance of validating at multiple levels to ensure accurate findings, much like the comprehensive validation strategies seen in other CRISPR-Cas9 knockout studies.

Additionally, immunohistochemistry analysis was conducted to confirm the complete absence of the immunoreactivity of the SNa and SNb peptides in the DKO fish brain and pituitary. We confirmed the results of Peng et al. (2025), demonstrating Scg2a/SNa-ir in the preoptic magnocellular, gigantocellular neurons and fibers, as well as throughout the pituitary in WT female zebrafish. Both Scg2a/SNa-ir and Oxt-ir can be seen in neuronal fibers, entering the pituitary via the infundibular stalk and neural lobe, PPD and RPD regions of WT zebrafish (Peng et al., 2025). This Scg2a/SNa-ir is completely absent in the *scg2a-/-; scg2b-/-* DKO brain and pituitary. Moreover, we specifically developed the first mouse monoclonal antibody against SNb. After

ensuring specificity, we visualized SNb immunoreactivity in brain and pituitary sections. We used Oxt-ir as a positive control in this study, and as expected, only the SNa-ir and SNb-ir were absent in the *scg2a-/-; scg2b-/-* DKO animals, where the Oxt-ir remained intact.

2.6 Implications and Future Directions

The creation and validation of the complete *scg2* gene knockout line in zebrafish provides a powerful tool for advancing research on endocrine regulation of reproduction. Our multi-step approach aligns with other studies that combine CRISPR-Cas9 with molecular and phenotypic assays for thorough validation, though our application of mass spectrometry provides an additional layer of precision in confirming protein-level changes.

With this model, future studies can focus on dissecting the distinct roles of the Scg2a and Scg2b paralogs, shedding light on their specific contributions to reproductive processes and potential implications for reproductive health disorders. The single KO and DKO lines not only open avenues for investigating the molecular mechanisms underlying the roles of the SN peptides but also offer opportunities for exploring the connection between SN and other important neuropeptides such as Gnrh and Oxt.

To further elucidate these connections, in Chapter 3, we explored the morphological and phenotypic differences between the single KO and DKO, particularly regarding their reproductive performance and behaviour. In Chapter 4, we investigated the gene expression differences in the HPG axis of DKO and WT fish across three critical time points in their ovulation cycle while also examining ovarian development. Chapter 5 compares the proteomics differences in single pituitary samples between WT and DKO lines, thereby providing a comprehensive view of the biochemical alterations associated with the loss of Scg2 function. This systematic exploration underscores the utility of the Scg2 KO model but also enhances our understanding of the intricate endocrine mechanisms regulating reproduction. Chapter 6 presents a summary and outlines several possible areas for future investigation of the Scg2//SN hormonal system.

Chapter 3: Targeted excision of the *scg2a* and *scg2b* genes impairs spawning and ovulation in zebrafish

3.1 Abstract

Following the successful development and validation of the *scg2a-/-; scg2b-/-* DKO zebrafish line, we assessed the morphological and reproductive behaviour phenotypes that result from the complete loss of Scg2. Body weight and length measurements revealed that *scg2b-/-* single KO females and DKO females were generally heavier and shorter to moderately sized in length compared to the other groups, while *scg2a-/-* single KO fish were longer in fork length. Fulton's condition factor confirmed that all fish were within normal size ranges, indicating overall good health. Behavioural analysis of within-line crosses demonstrated that both *scg2a-/-* ($p=0.0103$) and *scg2b-/-* single KO males ($p=0.0434$) exhibited decreased quiver behaviour, while *scg2b-/-* KO ($p<0.0001$) and DKO fish ($p=0.0027$) showed significant delays in their initial time of spawning. All *scg2a* and *scg2b* single KO and DKO fish demonstrated reduced spawning rates of 28%, 24%, and 16.6%, respectively, compared to the 64.5% spawning rate observed in WT siblings ($p<0.05$). Further assessment of KO fish indicated reduced fecundity ($p<0.0001$) but no differences in the 24-hour embryo survival. A second breeding attempt, where unspawned DKO females (N=18) were paired with naïve WT males, did not result in any successful spawning. Ovarian histological analysis suggested a defect in oocyte maturation from the vitellogenesis stage to mature oocytes in DKO females, accompanied by significantly higher quantities of late-stage atretic oocytes. Finally, *in vivo* injections of synthetic SNa and SNb peptides or human chorionic gonadotropin were insufficient to rescue spawning, highlighting severe reproductive impairment in *scg2a-/-; scg2b-/-* DKO zebrafish. Our data indicate that the *scg2a* and *scg2b* genes are essential for normal zebrafish reproduction, affecting both spawning behaviour and oocyte maturation

3.2 Introduction

Vertebrate reproduction entails a complex series of meticulously coordinated events, such as gamete production, effective fertilization, and the initial stages of embryonic development (Kornbluth & Fissore, 2015). In zebrafish, as in many other vertebrates, reproduction is governed by a complex interplay of hormonal signals, environmental cues, and genetic factors which control these events. Evaluating reproductive parameters in zebrafish requires a comprehensive assessment

of various factors that contribute to their reproductive success. These parameters typically include aspects of reproductive performance, such as mating behaviour, spawning frequency and the effectiveness of fertilization, indicated by clutch size, fertilization rate, and embryo viability. Furthermore, assessing the quality of gonads and their gamete production is crucial for identifying factors that contribute to successful fertilization. In this chapter, we evaluated the reproductive morphology, behaviour and performance of zebrafish with complete deletion of the *scg2a* and *scg2b* genes.

Zebrafish are photoperiodic breeders, usually spawning with the environmental cue of light onset (Abdollahpour et al., 2020). They exhibit complex reproductive behaviour that involves a series of stereotyped actions. Male zebrafish display characteristic courtship behaviour towards females, encompassing chasing, tail-nose contact, circling, zig-zag movement, and quivering (Darrow & Harris, 2004). However, with emerging technology and cutting-edge video recording equipment, it was described in detail with a series of new steps added and identified in the process as undulate, chase, escort, encircle, quivering, freezing, and wrap-around (Kalueff et al., 2013). During quivering, males oscillate their bodies close to the female, turning their heads by approximately 49 degrees to stimulate the female. In response, the female freezes and bends her body. The wrap-around occurs when the male contorts his trunk and wraps around the female's trunk, followed by the hooking behaviour, where the male adjusts until his trunk compresses the female's dorsal fin. After hooking, the male's trunk slides away from the female's dorsal fin while simultaneously sliding his pectoral fin across the female's gravid belly, stimulating egg release (Zempo et al., 2021). Mating episodes in zebrafish are defined as quivering, hooking, and spawning, with quivering being the initiator of the spawning. These behaviours are tightly linked, and failing to have a successful quiver has been shown to influence subsequent steps, leading to reduced or failed oviposition (Zempo et al., 2021). Reproductive performance assessment includes analyzing these mating behaviours, spawning outcomes, and the quality and survival of the embryos. Reproductive behaviour analysis focuses on the intricate courtship rituals and mating interactions between male and female zebrafish.

Moreover, analyzing spawning outcomes such as the number of spawning, timing of oviposition, fecundity, and survival rates of the embryos is important and has proven effective in identifying potential reproductive issues. Female zebrafish are known to spawn frequently with the onset of light and the presence of a male, producing several hundred eggs in one mating session

(Nasiadka & Clark, 2012). Sexually mature zebrafish can spawn in the laboratory continuously all year (Eaton & Farley, 1974). When observed in both wild and laboratory conditions, zebrafish spawning occurred just after dawn and lasted only for a 30-minute period. Their spawning behaviour was very rapid during this time, whereas they were less active toward the end and reproductive behaviour was never observed later in the day (Hutter S. et al., 2010). Reduced fecundity or late oviposition in zebrafish may stem from impaired ovulation or reduced oocyte quality, potentially leading to decreased fertilization rates and compromised embryonic development.

Both ovulation and oviposition are influenced by various factors, such as environmental cues like the light cycle, behavioural and pheromonal signals from the presence of a male, physiological aspects like oocyte development and maturation, and several neuroendocrine regulators (Spence et al., 2008; Tang et al., 2016; Zempo et al., 2021). Zebrafish ovaries contain oocytes at various developmental stages, ranging from oogonia to mature oocytes. The oogenesis process is divided into five stages based on morphological and physiological criteria (Li & Ge, 2020; Selman et al., 1993). Oocyte maturation in zebrafish occurs prior to the onset of light, with ovulation closely following (Wu et al., 2020). During maturation, oocytes exhibit a slight increase in size, become translucent, and their yolk transitions to a non-crystalline form as they undergo final meiotic maturation (Selman et al., 1993). This process facilitates the release of mature eggs into the ovarian lumen, which is known as ovulation. A recent study identified the role of pyroptosis—a form of programmed cell death that contributes to the weakening of the ovarian follicle wall (Liu et al., 2021) during ovulation.

Ovarian follicles that fail to mature are reabsorbed, degenerated, and considered atretic oocytes (Corriero et al., 2021). In teleost fishes, the atretic process involves three distinct mechanisms: autophagy, heterophagy, and apoptosis (Santos et al., 2008). Autophagy is the self-digestion of oocyte and follicular cells; heterophagy is the phagocytosis of egg components by granulosa cells that act as macrophages and the cell death process by apoptosis (Corriero et al., 2021). Atresia can serve as both a cause and a consequence of failed ovulation, depending on physiological and environmental factors. When environmental conditions or stress factors, captive conditions make reproduction unfavourable, teleosts may actively initiate atresia to reabsorb vitellogenic oocytes, effectively skipping spawning for that season (Yang et al., 2022). For example, in *Microstomus pacificus* (Pacific Dover sole), tilapia, and *Solea senegalensis* (flat fish),

significant follicular atresia results in reproductive inactivity despite the presence of advanced yoked oocytes (Rideout & Tomkiewicz, 2011; Sales et al., 2019; Yang et al., 2022). However, this phenomenon primarily affects fishes with determinate fecundity, where the recruitment of oocytes to secondary growth ceases prior to spawning. High levels of atresia, along with other histological indicators of reproductive status, can be interpreted quite differently for fishes with indeterminate fecundity (Rideout & Tomkiewicz, 2011), such as zebrafish. Furthermore, atresia can also be viewed as a consequence of failed ovulation. Several factors can contribute to failed ovulation and an increased rate of follicular atresia beyond physiological levels, as a degenerative response (Corriero et al., 2021). These could be environmental factors and toxic chemicals, metabolic dysregulation, stress and hormonal disruptions in the HPG axis. Exposure to endocrine-disrupting chemicals such as bisphenol A (BPA) in zebrafish induces follicular atresia by accelerating the previtellogenic and vitellogenic phases, which leads to abnormal follicular swelling and the recruitment of enlarged atretic follicles (Migliaccio et al., 2018). Follicular atresia is induced rapidly following the removal of gonadotropins in mammals (Hirshfield, 1991) and *in vitro* incubation of previtellogenic oocytes in gonadotropins (mainly Lh), epidermal growth factor (EGF), and 17β-estradiol function suppressed apoptosis and improved follicles survival in rainbow trout (Wood & Van Der Kraak, 2002). Stressors and stress-like concentrations of cortisol interfere with follicular phase endocrine events of the ewe by disrupting gonadotropin signalling, compromising timely expression of the preovulatory estradiol rise (Breen et al., 2005), which could promote apoptosis or autophagy in granulosa cells, eventually leading to atresia (Corriero et al., 2021). Atresia has been reported in several gene knockout and mutation lines. In zebrafish with leptin receptor knockout (*leper),* impaired leptin signalling dysregulates the HPG axis, delaying oocyte maturation and increasing levels of follicular atresia (Lakshminarasimha et al., 2022). Glucocorticoid receptor (*gr-/-*) knockout in zebrafish led to premature ovarian aging, including a high frequency of typical and atypical follicular atresia in vitellogenic oocytes (Faught et al., 2020).

3.3 Materials and Methods.

3.3.1 Experimental animals

Sibling WT zebrafish, *scg2a-/-* (7A) *and scg2a-/-* (13A)*, scg2b-/-* (4B), *scg2b-/-* (12B) single KO lines, along with the *scg2a-/-; scg2b-/-* DKO (7AX4B), were maintained in 3 L tanks at a density of 5 fish/L in a recirculating system at a temperature of 28°C, under a 14:10 light-dark

cycle (Techniplast, Montréal, QC, Canada). The fish were fed once or twice daily with GEMMA zebrafish diets (Skretting, Vancouver, BC, Canada) according to their embryonic, larval, and adult life stages. All experiments followed animal care guidelines provided by the Canadian Council on Animal Care and received prior approval from the University of Ottawa Animal Care Committee.

3.3.2 Morphological assessments

Morphological characteristics were evaluated by measuring the wet weight and fork length of *scg2a-/-, scg2b-/-* single KO and *scg2a-/-; scg2b-/-* DKO zebrafish, along with their age-matched WT siblings. The fish were raised to adulthood, and between 6 and 8 months of age, they were imaged and weighed after each breeding trial following light anesthesia with Tricaine (MS222), as per standard zebrafish husbandry protocols (Westerfield, 2000). Image analysis for fork length measurement was conducted using FIJI in ImageJ version 1.54f. Fulton's condition factor (K) was calculated from the weight and length data. Calculation was as follow; $K = 100 \times M/L^3$, where K = condition factor, M = body weight, and L = body length. It is considered a weight-length relationship used as a health status indicator in fish (Froese, 2006). A two-way ANOVA was conducted to examine the effects of sex (male/female) and genotype on these morphological characteristics.

3.3.3 Mating behaviour assessment

Reproduction was assessed via mating crosses between fish pairs within the same KO lines and WT zebrafish. All sibling WT, *scg2a-/-, scg2b-/-* single KO and DKO fish were raised to adulthood and maintained in single-sex groups at 5/L density 2 weeks before the spawning trials. Experiments were designed using a four-pair randomized block design (Figure 10), and each pair was from the within-line crosses of the single KO, DKO, and WT. For the behaviour trials, *scg2a-/-* (13A), *scg2b-/-* (4B) and *scg2a-/-; scg2b-/-* DKO (7A x 4B) pairs and sibling WT pairs (N= 20) were tested. The night before each breeding trial assessment, individual males and females were moved into 1 L static breeding tanks with a perforated base insert and separated overnight with a transparent, removable divider. The following morning, the physical barrier was removed at the beginning of the light cycle, and fish were allowed to breed for 90 minutes. Eggs were collected after each spawning.

During this time, fish were video recorded from the top and the side for 90 minutes. After each breeding assessment, the percentage of spawning was calculated. The number of eggs from each spawning was counted and kept in the incubator for 24 hours, and the 24-hour survival rate was calculated the next day. This behavioural assessment was repeated 3 times in the same manner over 3 years. Video files were analyzed for the time to first oviposition and quiver behaviour in the first 10 minutes by independent, unbiased observers trained to analyze and interpret the videos.

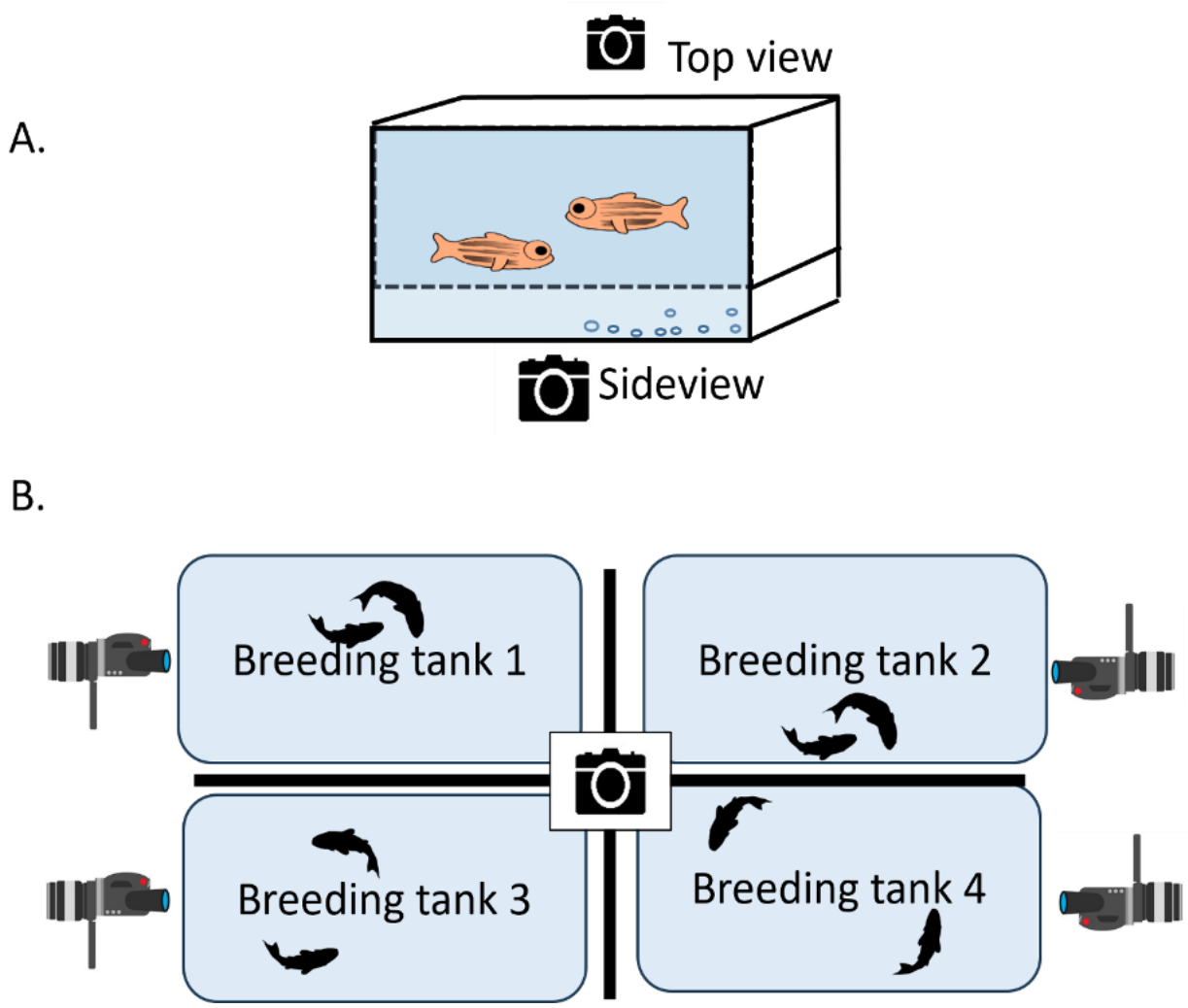

Figure 10. Breeding tank setup for mating behavioural recordings using a randomized block design. (A) Side view of the breeding tank, illustrating the recording area. (B) The top view of the setup shows the arrangement of five camcorder cameras positioned to capture both side and top views of the fish in four breeding tanks. This configuration allows for comprehensive monitoring of fish behaviour during breeding trials from multiple angles.

3.3.4 Assessment of the spawning ability of DKO females with naïve WT males

A second spawning attempt was made by mating of the unspawned DKO and WT females with naïve, sexually mature WT males. This experiment aimed to determine whether the unsuccessful within-line crossed DKO females could spawn with a naïve WT male. If they are unable to breed with normal WT males, it would demonstrate that the reproductive failure of the DKO females is not dependent on the males.

Before the experiment, WT and DKO fish were maintained in single-sex groups (5/L) for 2 weeks. First, within-line spawning was conducted according to the standard protocol, and unspawned DKO and WT females were noted and separated. A week following the first assessment, unspawned WT (N=16) and DKO female fish (N=18) were given a second spawning opportunity with a naïve WT male fish, and the percentage of spawning was calculated from the results (Figure 11).

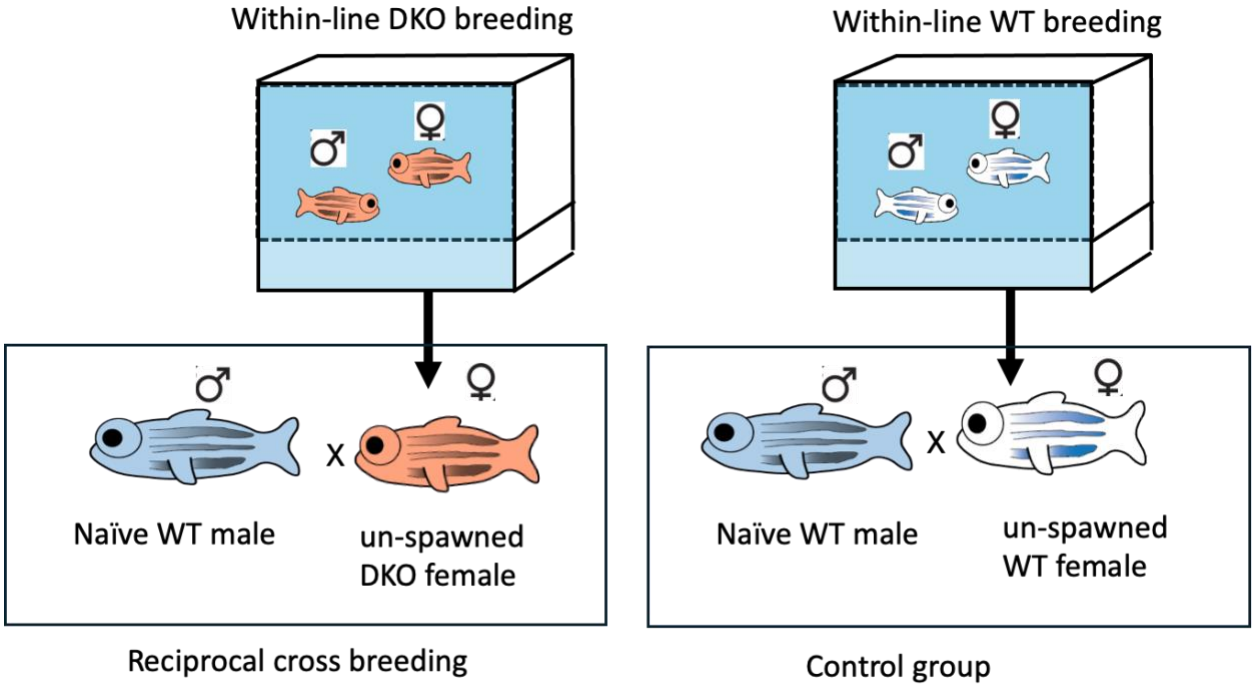

Figure 11. The second spawning attempt of unspawned DKO and WT female zebrafish with naive WT zebrafish males. Within the DKO line and WT siblings, the mating opportunity was provided for 90 min, and the unspawned DKO and WT females were isolated from this. After one week from the first breeding attempt, a second breeding attempt was made by pairing unspawned DKO females with naïve WT males (reciprocal crossbreeding) and unspawned WT females with naïve WT males (control group); N=18 pairs.

3.3.5 Ovarian Morphology

3.3.5.1 Ovarian GSI calculation

Fifteen sibling WT and *scg2a-/-; scg2b-/-* DKO female fish were euthanized at 7-8 months of age and weighed using an analytical balance. Ovaries were dissected and carefully removed to a small petri dish containing 0.6% saline. After removing the ovary, the fish carcasses were weighed again to determine the weight of the ovary. The gonadosomatic index (GSI; gonadal weight/body weight x 100) was calculated using the recorded measurements.

3.3.5.2 Ovarian histology

First, to observe the ovaries of the zebrafish non-invasively, WT and *scg2a-/-; scg2b-/-* DKO females (N=3) were lightly anesthetized using MS-222 according to standard zebrafish husbandry procedures described above. They were subsequently placed on a soft sponge immersed in MS-222, ventral side facing upward. The abdomens were observed and imaged using an ultrasound machine (Vevo MD Clinical High-Frequency Ultrasound with UHF70 29-71 MHz transducer). Images of the left ovary were assessed for length, width and area. After imaging, the fish were immediately returned to a freshwater tank for recovery.

Ovaries of sibling WT and *scg2a-/-; scg2b-/-* DKO females (N=5) were dissected and assessed histologically following a modified protocol from Lakshminarasimha et al., (2022). To synchronize oocyte development, all females were mated with males in a regular breeding protocol set up so that they were given a chance to release ovulated oocytes. After this 'purging,' ovarian samples were collected the same day, 6.5 hrs post-purging. Briefly, on the day of sample collection, female fish were euthanized in an ice bath, and the fish head and tail were amputated. The trunk of the fish was immediately fixed in 10% neutral buffered formalin (Sigma Aldrich, HT501128) for 72hours on a shaker. The samples were subsequently washed with PBS 3X, transferred to a 0.5 M EDTA solution, and incubated for a week. These samples were paraffin-embedded at the Louise Pelletier Histology Core, University of Ottawa (https://www.uottawa.ca/research-innovation/histology).

After embedding, the paraffin blocks were sectioned transversely to facilitate simultaneous observation of the paired ovaries. Serial 5 µm sections were obtained using the MICROM HM350 microtome (Heidelberg, Germany). To stage and quantify oocytes, 10 slides per ovarian pair were

collected 60 µm apart from each other, from the mid-region of the sample. Each slide contained four serial sections, covering a total of 740 µm of both ovaries. Following standard protocols, the collected ovarian sections were prepared for hematoxylin and eosin (H&E) staining. Images were captured using a stereo microscope (Olympus SZ2) equipped with Infinity Capture software (version 6.5.6). Based on their morphological and cellular characteristics, oocyte staging was conducted as described by Selman et al. (1993) and Li & Ge (2020). Briefly, primary growth follicles at stage 1 (stage 1A :7-20 µm, and stage 1B:20-140 µm), where oocytes are enclosed in cysts with multiple nucleoli and the primary oocytes characterized by nucleoli moving to the periphery of the nucleus, surrounded by a single layer of follicular cells. At the primary growth stage, the cytoplasm stains intensely basophilic (blue) with H&E staining (Deniz Koç et al., 2008). Stage 2 is identified as the cortical alveolus stage (140-340 µm), where the oocytes measure approximately 140-340 µm, and the cytoplasm remains basophilic but begins to show some clearing during staining. Stage 3 marks vitellogenesis (340-690 µm) with yolk accumulation, and the cytoplasm displays a spotted clearing pattern with yolk proteins staining pink to red with eosin. The nucleus remains visible and basophilic at this stage. Mature oocytes are counted as Stage 4 (690-730 µm), where the cytoplasm is filled with pink to red yolk bodies (Deniz Koç et al., 2008). Stage 5 was identified by the dissolution of the nucleus; the ooplasm consists primarily of yolk bodies, giving the oocyte a predominantly pink to red appearance at maximum size (730-750 µm). Atretic oocytes were identified and counted, separated from normal oocytes by histological features and classified into three distinct stages as described in Corriero et al., 2022. Early atresia ($\boldsymbol{\alpha}$) is marked by zona radiata fragmentation, presence of fused or expanded vitellus, and nucleus envelope fragmentation and disappearance. The mid or progressive atresia ($\boldsymbol{\beta}$) was identified by the presence of a large number of lipid vesicles and complete reabsorption of yolk granules. The advanced to late stage of atresia ($\boldsymbol{\gamma}$) was characterized by an irregular shape with a shrunken and gray colour appearance. They were smaller than the $\boldsymbol{\beta}$ stage and drastically reduced in the number of granulosa cells (Corriero et al., 2021; Migliaccio et al., 2018; Mohamedien et al., 2023). The delta stage ($\boldsymbol{\delta}$) as described in Corriero et al., 2022, could not be assessed in zebrafish, as in their examples of bluefin tuna (Thunnus thynnus) and swordfish (Xiphias gladius) showed species-specific characteristics at the final stage of atresia. Thus, all the advanced and late-stage atresia were counted as gamma stage in this study.

3.3.6 Rescue experiment

Sibling WT and *scg2a-/-; scg2b-/-* DKO fish were separated by sex two weeks prior to the experiment. The WT were compared to DKO injected with saline control and the SNa and SNb peptides. The randomized block design, video recording setup, and experimental groups are shown in Figure 12.

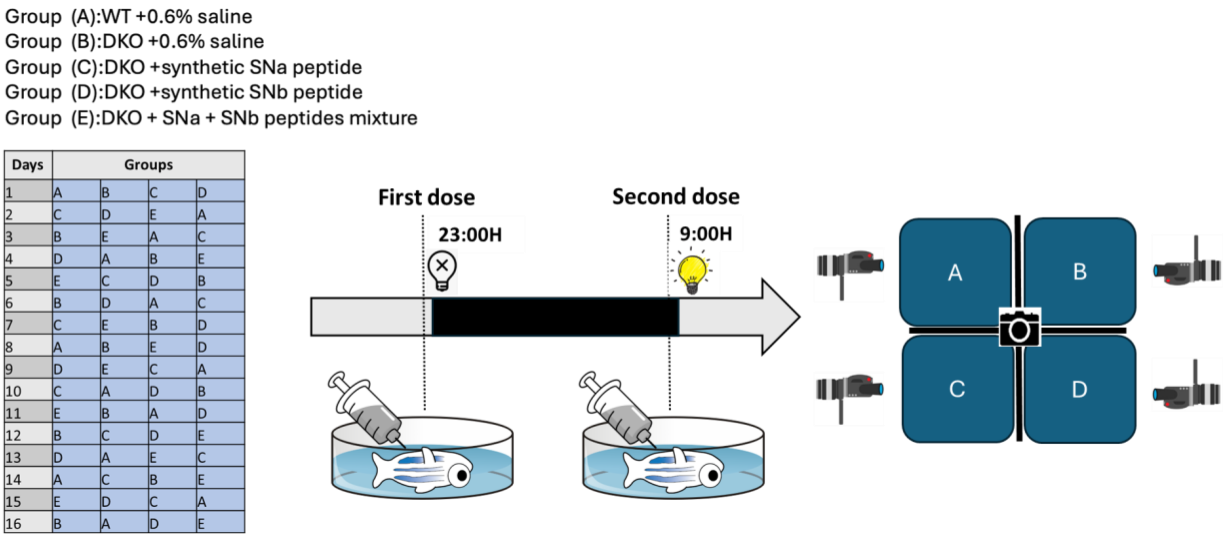

Figure 12. Peptide injection setup for rescue experiment. Both male and female fish were intraperitoneally injected 10 minutes before the 23:00H light off time at night with a first lower dose (0.25 nmol/g body weight) of the corresponding peptide for each experimental group (C-E) or control groups with saline (A-B). Fish were injected with a second higher dose (2.5 nmol/g body weight) 10 minutes before the 9:00H light at the time point. Spawning behaviour was recorded for 90 minutes.

The night before each breeding trial assessment, individual males and females were moved into a 1 L static breeding tank with a perforated base insert and separated overnight with a removable divider. Ten minutes before the lights went off in the experimental room (between 22:50-23:00h), fish were lightly anesthetized with tricaine methanesulfonate (MS-222) according to standard zebrafish husbandry procedures (Westerfield, 2000) and then weighed using an analytical balance. We employed a low-dose priming protocol. Intraperitoneal injections were performed on male and female fish using a 32-gauge Hamilton syringe with 0.6% saline solution (10 µl/g body weight), zebrafish SNa peptide (0.25 nmol/g body weight) or zebrafish SNb peptide (0.25 nmol/g body weight) or a mixture of both SNa and SNb peptides (0.125 nmol/g each). The SNa and SNb synthetic peptides were synthesized (ABclonal Inc. Woburn, MA, USA) and confirmed with mass

spectrometry to ensure their purity and quality. The doses of peptides were determined from several trials and previous studies from our lab by Di (2022) and Spadacini (2024), indicating that 2.5 nmol/g body weight SNa could induce ovulation. Several trials using WT fish determined the time points of the injections to ensure that the fish were not adversely affected by the dose or two separate rounds of injections.

After injection, the fish were immediately returned to clean water containing breeding cages, with a physical barrier separating the males and females. The following morning at 08:50 (10 minutes before the lights on at 09:00h), the fish were again anesthetized and injected with either saline solution (0.6%), zebrafish SNa peptide (2.5 nmol/g body weight) or zebrafish SNb peptide (2.5 nmol/g body weight) or a mixture of both SNa and SNb peptides (0.125 nmol/g each). Fish were immediately returned to clean water containing breeding cages, with a physical barrier separating the males and females. At 09:00h, the physical barrier was removed, and fish were allowed to interact for 90 minutes while recording their behaviour from the top and the side. Embryos were collected after 90 minutes of spawning. The pairs were allowed to continue spawning for another 5 hr (6.5 hours total) without recording. The eggs were collected at the end of the trial, counted and incubated at 28^0C for 24 hours for survival rate assessment.

After the first rescue experiment, saline-injected WT and *scg2a-/-; scg2b-/-* DKO females were mixed with their counterpart males for a week. After that, the fish were separated by sex for two weeks, and another experiment was conducted. This time, both spawned and unspawned males and females were injected 2 times with human chorionic gonadotropin (hCG). By injecting the Lh analog hCG, we attempted to rescue the spawning defects, as hCG can stimulate ovulation (Tang et al., 2016) and has been used previously to rescue *scg2* TALEN mutants (Mitchell et al., 2020). Ten minutes before lights off (between 22:50-23:00H), both males and females were injected i.p. with 5 IU/g hCG and, the following morning (between 8:50- 09:00H), injected with 50 IU/g hCG, a dose that effectively stimulates spawning in other zebrafish studies (Mitchell et al., 2020; Peng et al., 2025). The injected male and female fish pairs were allowed to interact for 90 minutes while recording from the top and the side. The eggs were collected after 90 minutes of spawning. The fish were thereafter allowed to continue spawning for another 5 hours (6.5 hours total) without recording, and eggs were subsequently collected and handled as described above.

3.3.7 Data analysis and statistics

GraphPad Prism v10 was used to analyze the data from the weight and length calculations, percentage of spawning, number of quivers, time to first oviposition, GSI and oocyte staging. The wet weight, fork length, Fulton's K factor data, and percentage of spawning success were analyzed by 2-way ANOVA followed by Tukey's multiple comparison test with a single pooled variance. Multiplicity-adjusted p-values are reported. Pooled data from the behavioural trials (time to first spawning, quiver behaviour, fecundity and 24-hour embryo survival) were nonparametric and not normally distributed from the Shapiro-Wilk test. They were analyzed using Kruskal-Wallis tests (for multiple groups) followed by Dunn's post-hoc test. All the reproductive behaviour data were pooled from the three behavioural trials. Reciprocal crossbreeding of DKO females with WT males and hCG injection rescue was analyzed by Fisher's exact test. The proportion of spawning data from the rescue experiment with i.p injections was analyzed by Z-score calculator for two population proportions with Bonferroni adjustment for multiple comparisons (https://www.socscistatistics.com/tests/ztest/default.aspx). The number of embryos per clutch after spawning from the rescue experiment was nonparametric. Thus, it was analyzed by one-way ANOVA (Kruskal-Wallis test) followed by Dunn's multiple comparisons. The number of embryos per clutch from spawning after hCG injected fish couples was analyzed using the nonparametric Mann-Whitney U test. Ovarian GSI was calculated and analyzed by Students' t-test. Ovarian histology were analyzed by Holm-Šídák test for multiple comparisons.

3.4 Results

3.4.1 Complete gene deletion of *scg2a* and *scg2b* moderately impacted the weight and length of zebrafish.

Morphological characteristics were evaluated by measuring the wet weight and fork length of *scg2a-/-, scg2b-/-* single KO and *scg2a-/-; scg2b-/-* DKO zebrafish, along with their age-matched WT siblings. Fulton's K condition factor was calculated from the length and weight measurements as described in the methods.

There was a female-biased sex difference (Figure 13A-13B) in body weight ($F(1, 280) = 48.77$, $p<0.001$. The main effect of genotype was also significant ($F(3, 280) = 6.467$, $p=0.0003$). The significant sex by genotype interaction ($F(3, 280) = 2.922$, $p= 0.0344$) indicates that the impact of genotype on weight differed between males and females. Post-hoc analysis revealed differences

in weight among several groups. Within genotypes, there were no significant differences between WT males and females (p=0.0959), and *scg2a-/-* single KO males and females (p= 0.4648). However, the *scg2b-/-* females were heavier than their male counterparts (p=0.0358), and DKO females also weighed heavier than their males as well (p= <0.0001). Across genotypes, and within females, DKO females were high in weight than WT females (p=0.0011) and *scg2b-/-* KO females (p=0.0449). All other female group comparisons were not significantly different (female WT vs female *scg2a-/-* (p=0.4489) or female *scg2b-/-* (p=0.9745). Across genotypes, no significant difference was found between the male zebrafish (Male WT vs *scg2a-/-* (p=0.0827), male *scg2b-/-* (p=0.9993), male DKO (p=0.9668). Comparison of weight across male and female groups in all genotypes revealed that all the KO females had a higher weight than the male WT zebrafish (WT male vs female *scg2a-/-* (p<0.0001), WT male vs female *scg2b-/-* (p=0.0049), WT male vs DKO female (p< 0.0001). Interestingly, female DKO appeared to be heavier than all other single KO male groups as well (p= 0.0011).

The fork length measurements (Figure 13-C) showed that the main effect of genotype was significant (F (3, 390) = 35.15, p<0.0001), indicating that the fish fork length depended on the genotype. Interestingly, the main effect of sex was not significant, (F (1, 390) = 1.393, p= 0.2387) and there was no significant interaction effect between sex and genotype (F (3, 390) = 0.02755, p=0.9938) suggesting that the impact of genotype on fork length was consistent across both sexes. Both male and female *scg2a-/-* zebrafish had significantly longer fork lengths compared to WT and *scg2b-/-* fish of both sexes (p<0.05 for all comparisons). For instance, female WT vs. female *scg2a-/-* showed a significant difference (p=0.0167), as did male WT vs. male *scg2a-/-* (p=0.0108). Conversely, *scg2b-/-* zebrafish tended to have shorter fork lengths than WT and *scg2a-/-* fish (p< 0.05 for most comparisons), with female WT vs. female *scg2b-/-* showing a significant difference (p=0.0065), and male WT vs. male *scg2b-/-* also differing significantly (p=0.0123). The DKO fish showed intermediate fork lengths, often not significantly different from WT fish. These results demonstrate that while sex plays a minimal role in determining fork length, the genetic modifications have a pronounced and consistent effect across both males and females.

For Fulton's factor (K) (Figure 13-D), the main effect of sex was significant (F (1, 370) = 53.38, p<0.0001), indicating that female zebrafish generally had higher K than males, probably due to their higher weight. Similarly, the main effect of genotype was also significant (F (3, 370) =18.07, p<0.0001), resulting in high K generally in the KO groups. Moreover, there is a significant

interaction effect between sex and genotype (F (3, 370) =3.774, p= 0.0108), suggesting that the effect of genotype on K varied between males and females.

Post-hoc analysis revealed that across genotypes within males, the *scg2b-/-* males had higher K compared to WT males (p=0.0489). Within females, a significantly high K was observed in *scg2b-/-* (p=0.0040) and DKO (p<0.0001) females compared to WT females. Notably, *scg2a-/-* and *scg2b-/-* (p=0.0001), *scg2a-/-* and DKO (p<0.0001) females were significantly different as well, where the *scg2a-/-* females K was generally low in comparison.

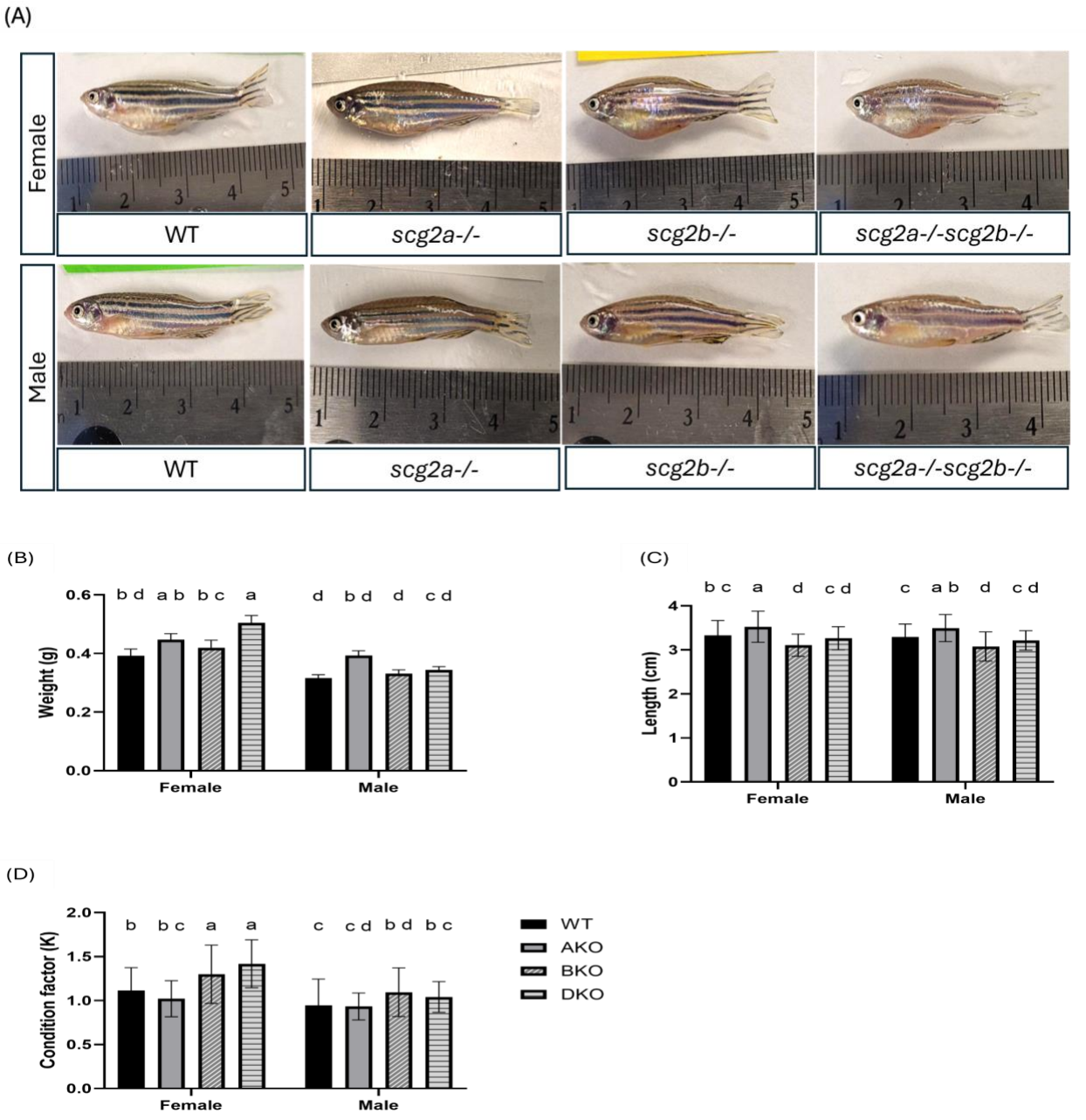

Figure 13. Morphometric parameters of sibling wildtype (WT), *scg2a -/-*(7 A) (AKO), *scg2b-/-* (4B) (BKO) and *scg2a-/-; scg2b-/-* (7Ax4B) (DKO) knockout fish at 6-8 months of age. (A) Morphology of WT, single KO, and DKO fish. (B) Body weight (g) (C) Fork length (cm). (D) Fulton's condition factor (K = 100 x body weight/length^3. Data are presented as the mean ± SEM (N=34- 37). Data were analyzed using a two-way ANOVA followed by Tukey's multiple comparison test. ^{a,b,c,d} Different superscripts indicate significant differences between groups ($p<0.05$).

3.4.2 Complete deletion of *scg2a* and *scg2b* genes in zebrafish reduces reproductive outcomes.

Data on spawning success, male quiver behaviour, time to first oviposition, fecundity, and 24-hour embryo survival were analyzed from the mating behaviour assays.

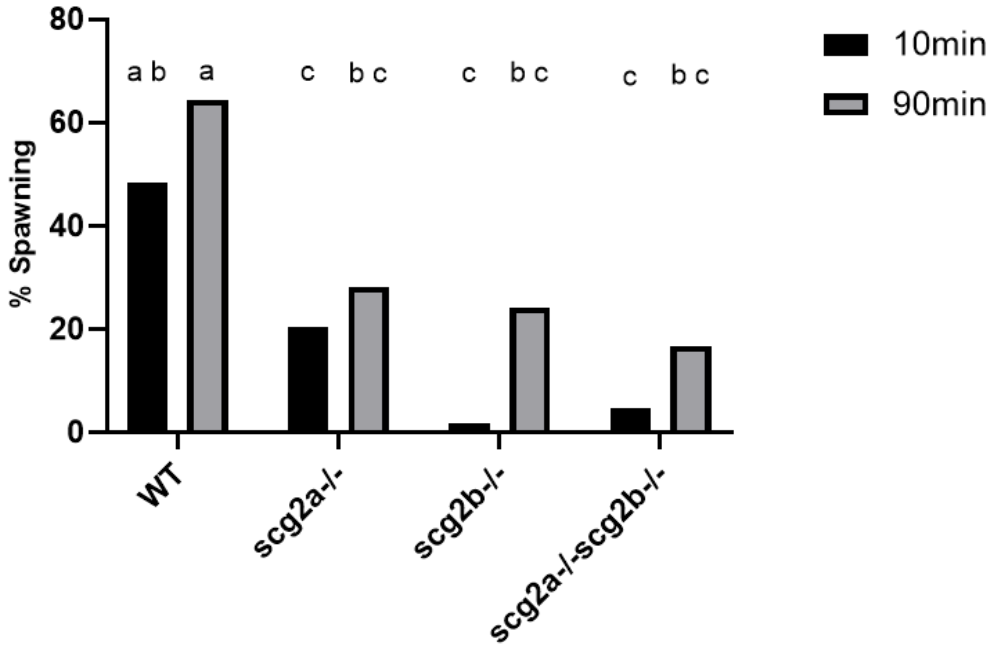

Figure 14. Spawning success of within-line pairwise mating of the sibling wildtype (WT), *scg2a* and *scg2b* KO zebrafish. Percentage of spawning success within the first 10 minutes (black) and 90 minutes (gray). Analysis was performed using two-way ANOVA (main effects only) followed by Tukey's multiple comparisons ($p<0.05$). ^{a,b,c,d} Different superscripts indicate significant differences between groups (*$p<0.05$*). Sample numbers: WT (N=62), *scg2a-/-* (N=39)*, scg2b (-/-)* (N=58) *scg2a-/-; scg2b-/-* DKO zebrafish (N=42),

Genotype had a significant ($F(3, 3) = 45.10$, $p= 0.0054$) effect on spawning (Figure 14). Time was also significant ($F(1, 3) = 21.42$, $p= 0.0190$), showing a moderate increase in the number of couples spawning by 90 min, irrespective of genotype. During the first 10 minutes of spawning,

48% of sibling WT couples spawned, while this was only 20.5% for *scg2a-/-* KO, 1.7% for *scg2b-/-* KO and 4.7% for *scg2a-/-*, *scg2b-/-* fish. Within 90 minutes, 64.5% of WT successfully bred, yet spawning only increased slightly to 28%, 24% and 16% for the scg*2a-/-*, *scg2b -/-* and *scg2a-/-; scg2b-/-* DKO lines. Post-hoc analysis revealed that WT fish have a significantly higher rate of spawning compared to the single and DKO genotypes at both time points ($p < 0.05$; $q > 10.22$ for all comparisons between KO and WT). Among the KO genotypes, *scg2a-/-* showed the highest spawning percentages (28%), followed by *scg2b-/-* (24%) and then *scg2a-/-; scg2b-/-* DKO (16.6%), which exhibited the lowest spawning rates. The biggest difference was between WT and DKO at 90 minutes of spawning ($q = 14.56$, $p < 0.05$).

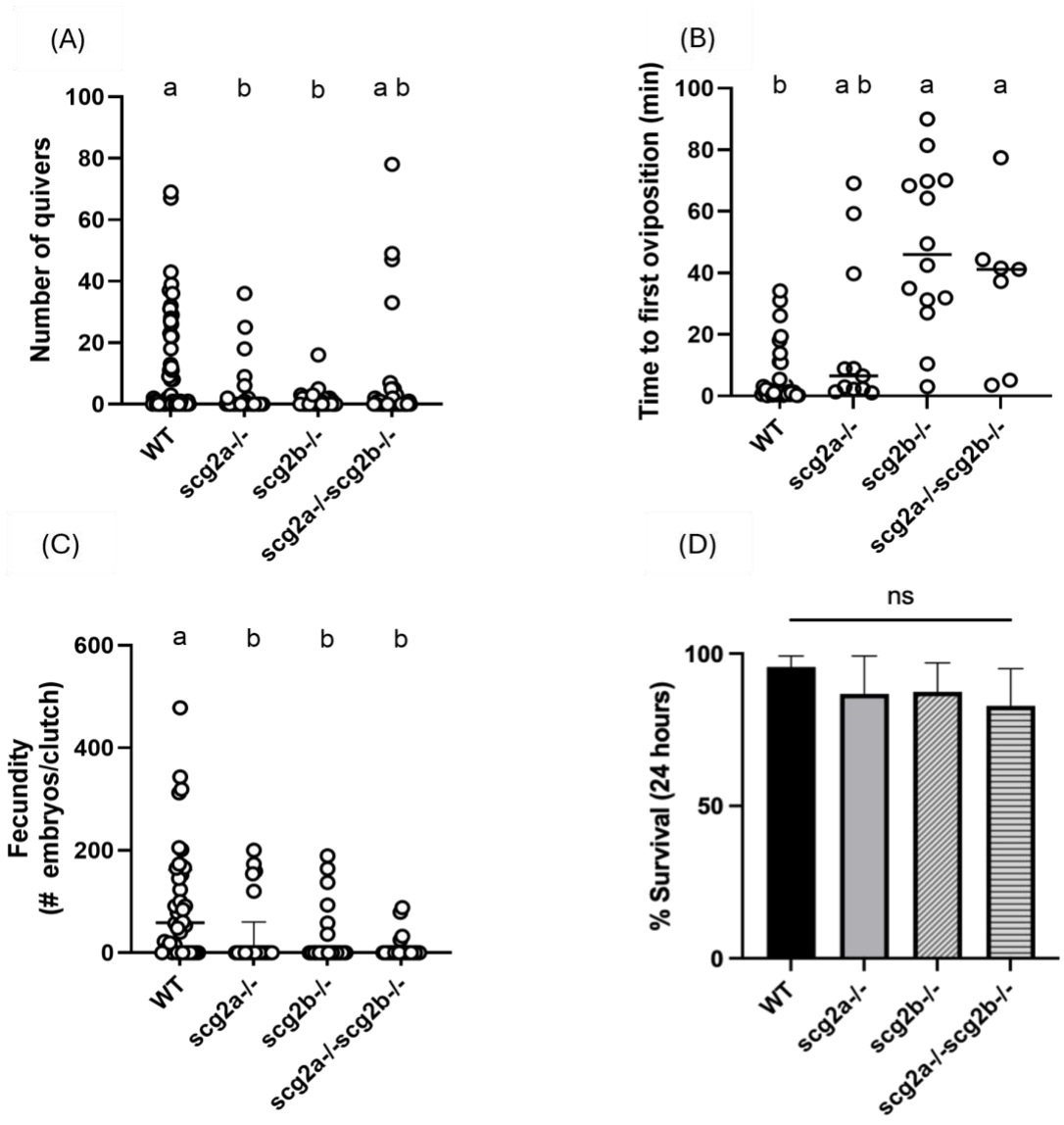

Figure 15. Quiver behaviour, time to first oviposition, fecundity and survival of embryos produced during within line pairwise mating of the sibling WT (N=62), *scg2a-/-* single KO (N=39), *scg2b-/-* single KO (N=58), *scg2a-/-; scg2b-/-* DKO zebrafish (N=42). (A) The number of quivers within the first 10 minutes of spawning. (B) Time to first oviposition. Dots represent individual data points, lines in the middle represent median values. (C) Number of embryos per clutch. If there was no spawning, then the clutch size was assigned to zero. Dots represent individual data points, horizontal dark lines represent median values, and whiskers represent interquartile ranges. (D) Percentage of embryo survival within 24 hours. Each bar represents the median value, and whiskers represent interquartile ranges. Statistical analysis was done using the nonparametric one-way ANOVA (Kruskal-Wallis test) followed by Dunn's multiple comparisons test with Bonferroni's correction. [a,b,c,d] Different superscripts indicate significant differences between groups ($p<0.0001$) and ns indicates data that are not different ($p>0.05$).

In the first 10 min of spawning, the number of quivers was different ($H(3) = 12.46$, $p< 0.05$) between WT and the single KO groups (Figure 15-A). The WT males exhibited more quivers than *scg2a-/-* ($p=0.0103$) and *scg2b-/-* males ($p=0.0434$). Both WT and s*cg2a-/-; scg2b-/-* DKO males exhibited highly variable levels of quiver activity. While most s*cg2a-/-; scg2b-/-* DKO males exhibited very low quiver activity, 4/42 males nevertheless showed normal activity. Thus, quiver activity was similar in WT and DKO males ($p=0.254$).

Time to first oviposition (Figure 15 -B) differed among the genotypes ($H(3) = 34.64$, $p< 0.0001$). The *scg2b-/-* single KO and *scg2a-/-; scg2b-/-* DKO lines were significantly delayed in their first oviposition compared to the sibling WT group (*scg2b-/-* and WT $p< 0.0001$; *scg2a-/-; scg2b-/-* DKO and WT $p= 0.0027$, median 1.25 minutes). While the *scg2b-/-* single KO group and DKO were delayed in spawning (median 45.96 minutes and 41.18 minutes, respectively), the few spawning couples in the *scg2a-/-* single KO were able to spawn early (median 6.52 minutes). But due to the variability, *scg2a-/-* was showing an intermediate effect, not different from *scg2b-/-* or DKO (*scg2b-/-* and *scg2a-/-* $p= 0.1699$; DKO and *scg2a-/-* $p= 0.9971$). No significant differences were observed between *scg2a-/-* and WT ($p= 0.1428$) or between DKO and *scg2b-/-* ($p> 0.9999$).

Fecundity was estimated by determining the number of embryos per clutch (Figure 15-D) and varied in a genotype-dependent manner ($H(3) = 33.33$, $p< 0.0001$). Spawned WT pairs exhibited a significantly higher fecundity (Figure 15-C) compared to *scg2a-/-* ($p= 0.0043$), *scg2b-/-* ($p< 0.0001$), and *scg2a-/-; scg2b-/-* DKO ($p< 0.0001$). Interestingly, for those animals that spawned, no significant differences ($p= 0.2933$) were observed between the WT and the three KO groups regarding the 24-hour survival of the embryos (Figure 15-D).

3.4.3 The *scg2a-/-; scg2b-/-* DKO female fish do not spawn with naïve WT males.

Females that had not spawned in the first breeding trial were subjected to a second spawning attempt with new naïve WT males (Figure 16-A). Accordingly, 9 of the 16 WT females that had not spawned in the first trial, spawned successfully (56.25%). However, none of the 18 *scg2a-/-; scg2b-/-* DKO females spawned when presented with the new males. Thus, spawning success in WT and DKO groups differed significantly (p=0.0002), demonstrating that naïve WT males could not induce spawning in DKO females during a second trial. The quiver counts between the two groups were not significantly different (Figure 16-B, p=0.2691).

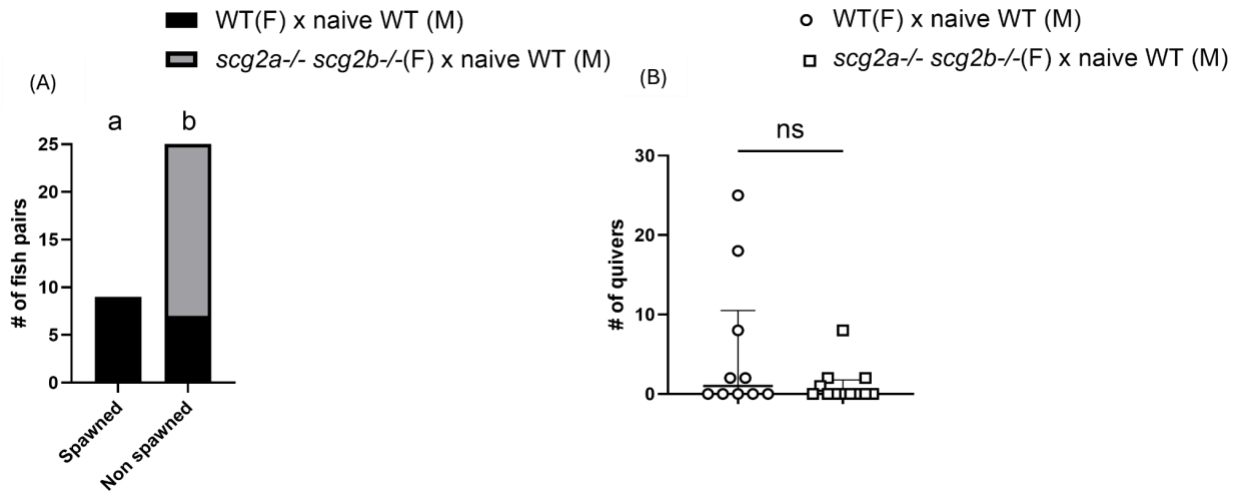

Figure 16. Assessment of the second spawning event and male quiver behaviour of previously unspawned WT females with naïve WT males (N=16) and previously unspawned *scg2a-/-; scg2b-/-* DKO females with naïve WT males (N=18) within 90 minutes of the breeding. (A) Number of fish pairs spawned within 90 minutes. The statistical analysis was performed using Fisher's one-tailed exact test, and [a,b,c,d] different superscripts indicate significant differences between groups ($p<0.0001$). (B) The number of quivers within the first 10 minutes of spawning. The statistical analysis was done using the Mann-Whitney U test. ns, not significantly different ($p>0.05$). Dots represent individual data points, horizontal dark lines represent median values, and whiskers represent interquartile ranges.

3.4.4. Complete gene deletion of *scg2a* and *scg2b* leads to follicular atresia and reduced numbers of mature oocytes.

Previous data indicated that the complete deletion of the *scg2a* and *scg2b* genes resulted in impaired spawning and various other indicators of reproductive performance, including delayed ovulation and reduced fecundity in zebrafish. The second spawning assessment of the previously

unspawned DKO fish indicated that the female DKO was unable to spawn despite being presented with a healthy, genotypically normal WT male counterpart. Therefore, we compared the GSI and ovarian morphology of the WT and DKO females.

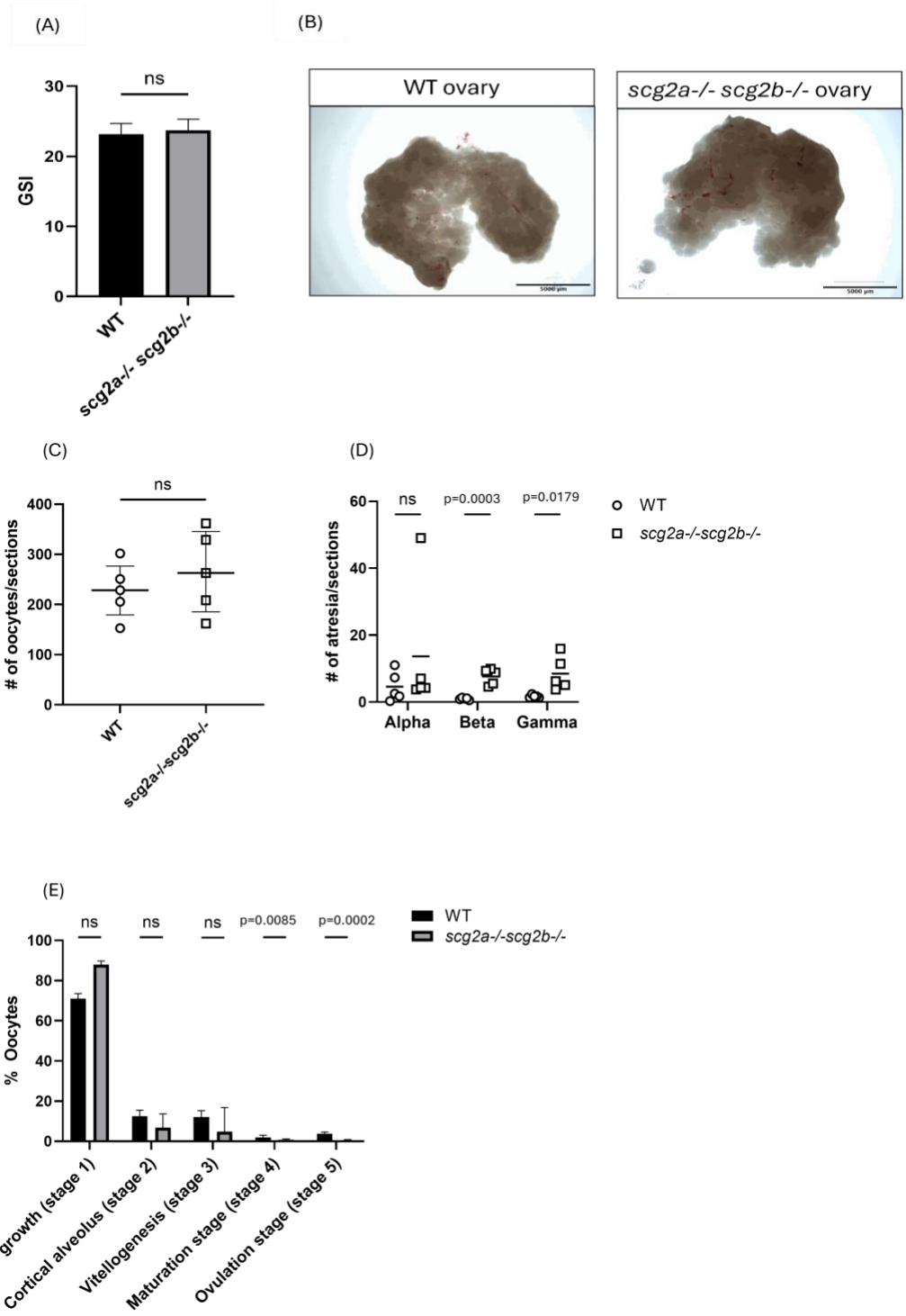

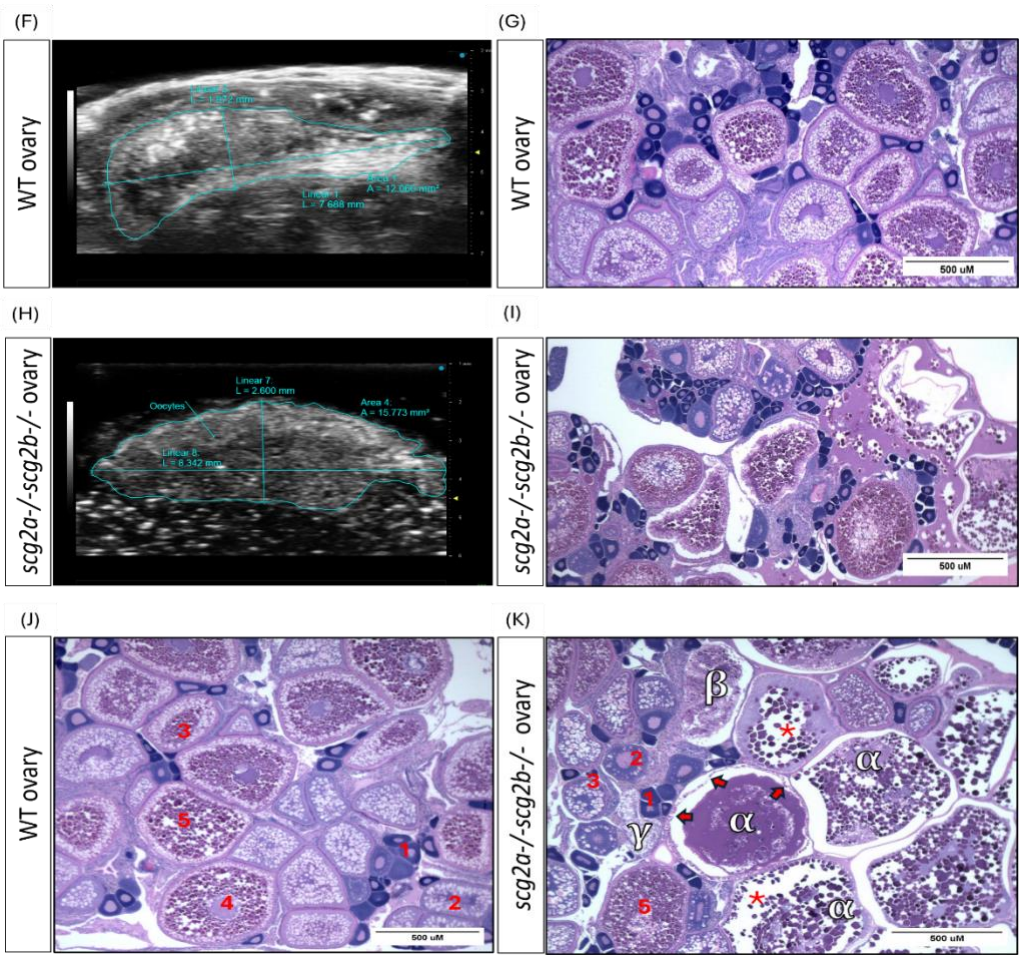

Figure 17. Morphology, gonadosomatic index (GSI), and the histological analysis of the WT and *scg2a-/-; scg2b-/-* DKO ovaries. (A) GSI of sibling WT and *scg2a-/-*; *scg2b-/-* DKO zebrafish. Data are presented as mean ± S.E.M (N=15, unpaired t-test; *p<0.05). (B) Morphology of the dissected ovaries of WT and *scg2a-/-; scg2b-/-* DKO zebrafish. The scale bar indicates 5000 µm. (C) Total number of oocytes per paired ovaries (N=5, unpaired t-test; n.s., p>0.05). (D) Number of alpha, beta and gamma stage atretic oocytes per paired ovaries per each fish (N=5, unpaired t-test; p<0.05) (E) Comparison of ovarian follicular stages in WT and DKO fish as a percentage of total normal oocytes. Ovaries were fixed in neutral buffered formalin (10% NBF), underwent standard histological procedures, and five µm-thick sections were stained with H & E (N=5) 6.5 hrs post purging, unpaired T-test with the Holm-Šídák method for multiple comparisons. The significant p values are noted above the bars; ns, not significantly different (p>0.05). Live, non-invasive visualization of the WT (F) and DKO ovaries (H) using ultrasound (N=3). The images indicate the length, width, and area of the ovaries. Sections of WT ovaries (G, J) and DKO ovaries (I, K) stained with H & E. Scale bar indicates 500 µM. The ovarian follicular stages are labelled as follows: 1-primary growth follicle. 2 – cortical alveolus; 3 – vitellogenesis stage; 4 - maturation stage follicle; and 5 – fully grown follicle at ovulation. Alpha (**α**) is the early stage atretic follicle, Beta (***β***) is the secondary stage atresia, and Gamma (***γ***) is advanced and late-stage atresia. Asterisk shows the empty area resulted from the absorption of the vitellus. Arrows show the fragmentation of zona radiata**.**

There was no difference (p=0.8035) in GSI (Figure 17- A) of the WT and *scg2a-/-; scg2b-/-* DKO females, and they appeared normal after dissection and observation (Figure 17- B). Paraffin fixed ovaries of WT and DKO at 6.5 hours post purging were observed after H & E staining, and each follicular stage was counted, averaged per pair of ovaries. The average total number of oocytes per pair of ovaries in each fish (Figure 17-C) was not different between the two groups (df=8, t=0.8333, p=0.4288). There was no significant difference (df=8, t=1.003, p=0.3453) in the average number of early-stage ($\boldsymbol{\alpha}$) atretic follicles (Figure 17-D). This contrasts the significant difference between WT and DKO females in mid or progressive stage ($\boldsymbol{\beta}$) atresia (df=8,t=6.176, p=0.0002) and late stage ($\boldsymbol{\gamma}$) atresia (df=8,t=2.967, p=0.0179). Assessment of the percentage of oocytes at each stage revealed an impact of *scg2* KO on mature oocytes (Figure 17-E). Firstly, there was no change in the percentages of stage 1 (df=-12.92, t=1.496, p=0.1729), stage 2 (df=3.796, t=1.253, p=0.2455) and stage 3 (df=3.757, t=0.7642, p=0.4667) oocytes. In marked contrast, there were fewer stage 4 (df=1.330, t=3.467, p=0.0084) and stage 5 oocytes (df=3.030, t=6.287, p=0.0002) in DKO females.

3.4.5 *scg2a-/-; scg2b-/-* DKO fish are poor spawners that do not respond to SNa, SNb or hCG injections.

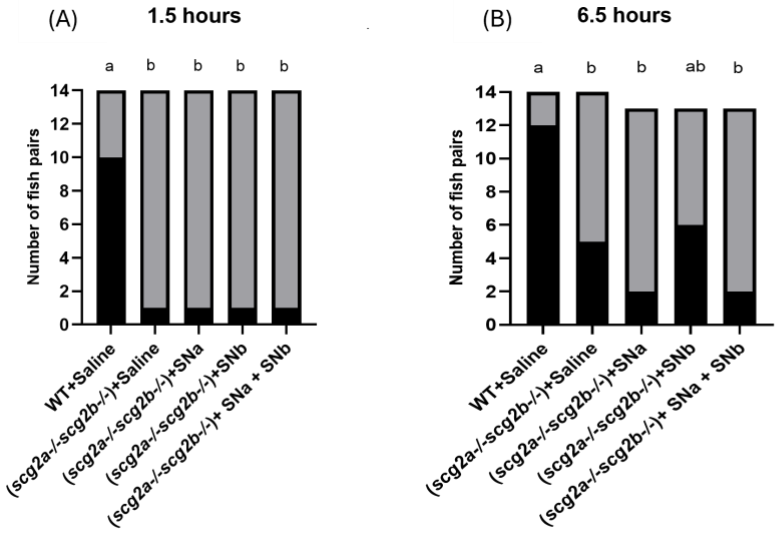

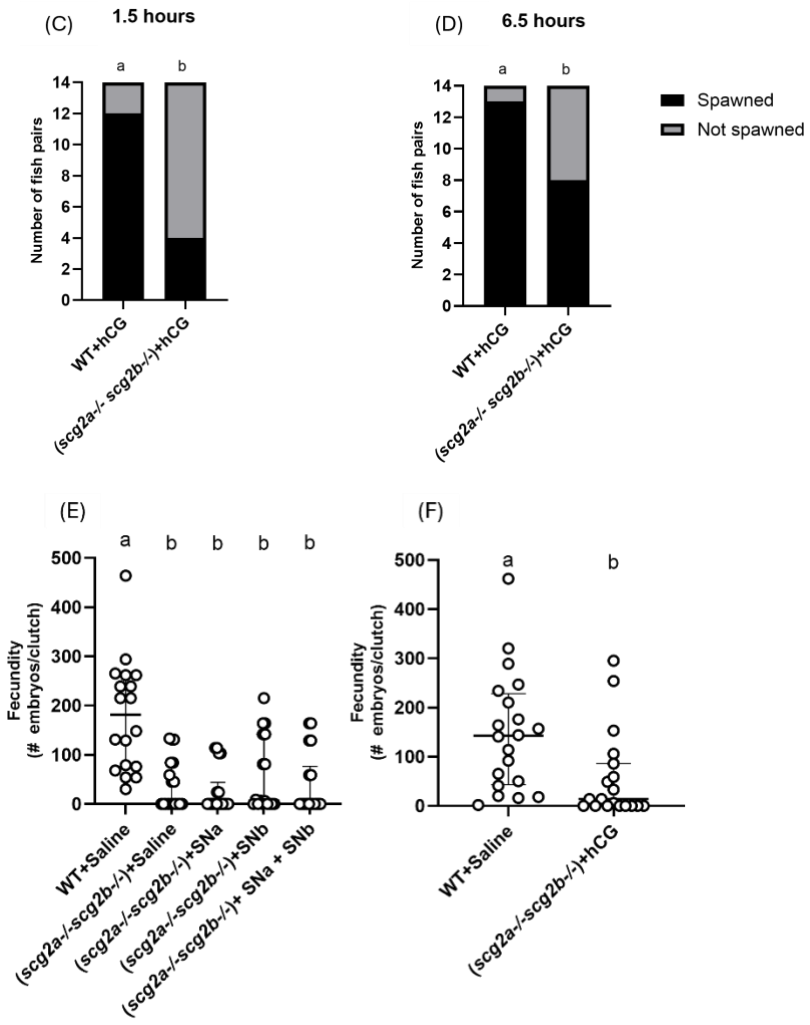

Figure 18. Comparison of the number of fish pairs spawned and fecundity of the WT females injected with saline control (N=14) and *scg2a-/-; scg2b-/-* DKO females injected with saline (N=14), SNa (N=13), SNb (N=13) and SNa+SNb (N=13) and hCG (N=14). Number of fish pairs spawning within the first (A) 1.5 hr and (B) 6.5 hr following injections. Data analysis was performed using one-tailed z score proportion test with Bonferroni's adjustment. Number of fish pairs spawning within the first (C) 1.5 hours and (D) 6.5 hours following injections. Data analysis was performed using one-tailed z score proportion test with Bonferroni's adjustment. (E) Number of embryos per clutch after 6.5 hr spawning in SNa, SNb and SNa+SNb injected fish couples. The value of zero is given for non-spawning pairs. Statistical analysis was done using the Kruskal-Wallis nonparametric one-way ANOVA followed by Dunn's multiple comparisons. (F) Number of embryos per clutch after 6.5 hr spawning in hCG-injected fish couples. Statistical analysis was done using the nonparametric Mann-Whitney U test. Dots represent individual data points, lines in the middle represent median values, and whiskers represent interquartile changes. The results are significant at $p < 0.05$ (N= 13-14). ^{a,b,c,d} Different superscripts indicate significant differences ($p < 0.05$, N= 13-14) between groups.

We next attempted to rescue reproductive deficits in the *scg2a-/-; scg2b-/-* DKO fish by i.p. hormone injections (Figure 18-A, B). At 1.5 hours, 10/14 (71.4%) WT saline-injected couples spawned and by 6.5 hours of breeding, 12/14 couples spawned (81.7%). In comparison, only 1/14 (7.1%) and 5/14 (35.7 %) saline-injected DKO pairs spawned in the same time periods, and they were significantly different at 1.5 hours (WT+Saline vs DKO+Saline ($z=3.4826$, $p=0.00175$) as well as 6.5 hours (WT+Saline vs DKO+ Saline $z= 2.7087$, $p= 0.02352$). Similarly, all SNa, SNb and SNa+SNb injected DKO groups exhibited significantly lower spawning rates than the saline injected WT fish at 1.5 hours of breeding, where 1/13 (7.69%) spawned in each peptide injected DKO group ($z=3.3678$, $p=0.00266$). Although spawning rates increased somewhat over time by 6.5 hours, none of the peptide injections significantly improved spawning. The percentage of spawning at 6.5 hours for DKO+SNb was 6/13 (46.15%), where it showed an intermediate response to the SNb peptide and not different from the WT+ Saline group ($z= 2.1788$ $p= 0.10241$). However, DKO+ Saline vs DKO+ SNb was not different either ($z= -.05516$ $p= 2.03812$). The other 2 groups of DKO+SNa and DKO+SNa+SNb were spawning 2/13 (15.38%) by the 6.5 hours and were still not spawning well compared to WT+Saline ($z= 3.6544$, $p= 0.00091$). In comparison, the DKO+Saline group vs the DKO+SNa and DKO+SNa+SNb was not significantly different ($z= 1.2044$, $p=0.80549$). Thus, according to the results, injections of SNa and SNb alone and in combination failed to improve spawning success.

Comparison between the fecundity of the spawned fish couples between each group revealed that the significant reduction in fecundity in the DKO females was not rescued by either of the injections (Figure 18-E), ($H (5) = 29.35$, $p< 0.0001$). Spawned WT pairs exhibited a significantly higher fecundity compared to DKO+Saline ($p=0.0005$), DKO+SNa ($p<0.0001$), DKO+SNb ($p= 0.0164$), and SNa+SNb injected DKO ($p=0.0001$) fish. Expectedly, no significant differences were observed between the fecundity of the DKO+ Saline vs DKO+ SNa ($p= 0.9999$) or DKO+ Saline vs DKO+ SNb ($p=0.9999$) and the DKO+ Saline vs DKO+ SNa+SNb ($p=0.9999$).

Since the DKO fish could not be rescued with the SNa, SNb, or SNa+SNb injections, we attempted to rescue this phenotype using two injections of hCG (5 IU/g body weight and 50 IU/g body weight) in both male and female zebrafish (Figure 18- C, D). In WT pairs injected with hCG 12/14 couples spawned (86%) at 1.5 hours, reaching 13/14 (93%) at 6.5 hours. Spawning success was higher in WT+hCG fish than in the DKO+hCG group, both at 1.5 hours (Figure 18-C) ($z=3.0551$, $p= 0.00111$) and 6.5 hours ($z=2.1822$, $p= 0.01463$) (Figure 18-D). Even though the

hCG-injected DKO fish increased their spawning by 6.5 hours, suggesting that at least a few DKO females were responsive to hCG, the rescue attempt with hCG was not completely successful. The fecundity of the spawned DKO couples was not improved by hCG (Figure 18- F), remaining different from WT (p=0.0013).

3.5 Discussion

We report that the complete deletion of the *scg2a* and *scg2b* genes in zebrafish led to significant anatomical, behavioural and fertility consequences, highlighting their importance for normal reproduction. These *scg2a/scg2b* single KO and DKO had lower spawning rates and fecundity compared to WT fish. The *scg2a-/-* and *scg2b-/-* single KO showed a reduction in male quiver behaviour, and *scg2b-/-* KO and DKO displayed delayed oviposition. While the ovaries of mutant females had a macroscopically normal appearance, detailed histological analysis revealed that the DKO females had reduced numbers of mature oocytes with significantly elevated numbers of atretic oocytes. While the DKO females weighed more, having a higher Fulton's K factor, they were within normal ranges for healthy fish. The DKO females were poor spawners, whether presented with either DKO or normal WT males, and could not be rescued by hormone injections.

The *scg2a* and *scg2b* deletions significantly impacted the reproductive performance of within-line crosses by reducing spawning capability and fecundity in both single KO and DKO. These results support some aspects of our previous study of zebrafish harbouring TALEN-mediated frameshift mutation of both genes (Mitchell et al., 2020). In the previous TALEN *scg2* mutants, spawning was recorded during the first 10 minutes of breeding and in the current study, we recorded spawning couples for up to 90 minutes, in order to document any delayed spawning. In TALEN *scg2* mutant spawning analysis, non-sibling WT, 62% (62/101) couples spawned, and this dropped significantly to 37%, 44%, and 6% for the *scg2a-/-, scg2b-/-,* and double frameshift mutant within-line crosses, respectively (Mitchell et al., 2020). As a percentage of WT spawning rate, the TALEN *scg2a-/-, scg2b-/-,* and double frameshift mutants exhibited 59.7% (37/62) 71% (44/62), and 96% (6/62) spawning ratios.

For direct comparison to Mitchell et al. (2020) we also quantified spawning rates in the first 10 minutes in the new CRISPR/Cas9 complete gene knockout lines (Table 3). In WT, 48% of couples spawned, and this dropped significantly to 20.5%, 1.7%, and 4.7% for the sibling *scg2a-/-, scg2b-/-,* and DKO within-line crosses, respectively. The full gene deletion KO was somewhat

similar but reduced regarding the *scg2a-/-* KO, where the spawning rates between KO and sibling WT is 45%, while the *scg2a-/-;scg2b-/-* DKO spawning rates is 9.8%. However, a significant difference in spawning was observed in the *scg2b-/-* single KO, where the spawning rate was reduced to just 3.5 %. Thus, compared to WT controls, less than 10% of DKO couples spawn in the first 10 minutes for both the TALEN and CRISPR/Cas9 models, demonstrating severe spawning impairment.

Genotype	Percentage spawning in 10 minutes		Percentage of spawning relative to WT	
	TALEN mutants	CRISPR/Cas9 KO	TALEN mutants	CRISPR/Cas9 KO
WT controls	62% (62/101)	48% (30/62)	n.a.	n.a.
scg2a-/-	37% (35/95)	20.5% (8/39)	59% (37/62)	45% (20.5/48)
scg2b-/-	44% (36/82)	1.7% (1/58) *	70% (44/62)	3.5% (1.7/48)
scg2a-/-;scg2b-/-	6% (5/88)	4.7% (2/42)	9.6% (6/62)	9.8% (4.7/48)

Table 3: Comparison of spawning activity in TALEN-mediated frame-shift *scg2* mutants (Mitchell et al., 2020) and the CRISPR/Cas9 full gene knockout mutant zebrafish (present study). Asterisk represents a significant difference ($p<0.0001$, $z=5.5751$, T-test, two-tailed) between the two mutant models. All other comparisons of spawning at 10 min were not significantly different.

These current results indicate that the DKO fish demonstrate the lowest spawning rate compared to their WT siblings, having a four-fold reduction even after 90 min of spawning time. Compared to the initial 10 minutes, there was an overall increase in spawning success in all genotypes, but the suppressed spawning in the single and DKO within-line crosses was still evident. This decline in spawning rates clearly demonstrates that the complete deletion of either *scg2a* or *scg2b* or both genes highly impacts spawning behaviour. The *scg2b* gene appears to have a pronounced impact on spawning success. When given a second opportunity to mate with a naïve WT male, the previously unspawned DKO females failed to spawn entirely. These findings indicate that DKO females have reproductive deficits, rendering them unable to spawn normally with either DKO or normal WT males.

Some other gene mutations affecting pituitary hormones impair reproduction, showing both similarities and important differences from our findings. For instance, *lhb* and *fshb* mutations in teleosts cause reduced spawning. Zebrafish and medaka *lhb-/-* females were infertile when paired with WT males (Chu et al., 2014; Takahashi et al., 2016; Zhang et al., 2014) and in contrast, homozygous or heterozygous *lhb* receptor (*lhr*) knockout zebrafish females were fertile (Chu et al., 2014). In all these KO lines, males were fertile, having normal testicular development and spawning. Both male and female *fshb-/-* zebrafish also remain fertile (Zhang et al., 2014). In contrast, while *fshb-/-* male medaka are fertile, the females are infertile (Takahashi et al., 2016). When the *fsh* receptor (*fshr*) is mutated in zebrafish, follicular activation fails at all growth stages, and they are sex-reversed to fertile males (Zhang et al., 2015).

In contrast to the pituitary hormone KO, neuropeptide deletions until recently yielded controversial results. For example, *gnrh2-/-; gnrh3-/-* DKO zebrafish showed no major reproductive effects except *gnrh 1* KO in medaka (Marvel et al., 2018; Spicer et al., 2016; Takahashi et al., 2016). This provides evidence that there are species-specific isoform effects for the *fshb* and *gnrh* on the reproduction between medaka and zebrafish. When compared with the current study, the *scg2a-/-* and *scg2b-/-,* as well as the DKO, within line mated couples, exhibit low spawning rates, and unspawned DKO females were infertile when crossed with WT males. These preceding knockout studies question the established notions regarding the essentiality of *gnrh*2 and *gnrh3* for reproduction in teleosts. Instead, they support the previous literature of diverse multifactorial control over reproduction in zebrafish.

The first neuropeptide gene mutation model that showed a reproductive deficit was the *scg2* TALEN mutants generated from our lab (Mitchell et al., 2020). This current study of complete gene deletion supports the concept that the *scg2a* and *scg2b* genes or gene products are involved in reproductive control. Emerging from this is the indication of different roles for these paralogues. Despite expression of *scg2a* in behaviorally relevant neurons, *scg2a-/-* KO in female medaka showed no significant alterations in mating behaviour (Fleming et al., 2023), in contrast to our work in zebrafish. In medaka, Scg2a neurons function in a manner dependent on estrogen/Esr2b signaling in neurons associated with female sexual receptivity (Fleming et al., 2023). This could be either species-specific differences between medaka and zebrafish, as observed in *fshb-/-* and *gnrh1-/-* medaka mutants, or the methodology differences of the KO line creations. The medaka *scg2a-/-* KO was generated using CRISPR-Cas 9; however, they have a nucleotide deletion in the *scg2a*

coding sequence, in comparison to our full coding sequence deletion. Moreover, their group did not create a medaka *scg2b* paralogue deletion. Thus, the full *scg2/scg2b* effect was not studied. Recent studies have also revealed that mutating the type A cholecystokinin (CCK) leads to severe reproductive defects in zebrafish. These mutants exhibit a complete shutdown of both Lh and Fsh secretion, resulting in underdeveloped testes in males and a lack of females in the population (Hollander-Cohen et al., 2024; Li et al., 2025).

We explored whether behavioural defects were part of the mechanism underlying failed reproduction. While all within-line crosses produced some fertilized eggs, fecundity was much reduced in single and DKO pairs. For those fish that did spawn, there was considerable variability in the time to oviposition. In WT, median time was rapid at ~1.3 minutes. A few *scg2a-/-* single KO pairs similarly began oviposition rapidly, but 3 couples were delayed, so median time was ~6.5 minutes. In marked contrast, both *scg2b*-/- single KO and DKO pairs exhibited very significantly delayed initiation of oviposition, with median times of ~46 and 41 minutes. This difference in impact on ovposition times is the first clear indication of differentiated function of the *scg2a* versus *scg2b* genes. By comparing oviposition times of all mutants, there was no evidence of additive effects, indicating that *scg2b* KO is the primary determinant of this delay. Our previously reported TALEN *scg2* mutants had reduced ovulation, and the DKO exhibited the most severe phenotype (Table 3). However, Mitchell et al. (2020) did not examine time to oviposition and only recorded behaviours for 10 minutes. On the other hand, mutation of the brain type aromatase revealed specific effects on time to oviposition in female zebrafish (Shaw et al., 2023). These *cyp19a1b*-/- females have normal gonadal E2, and ~50% reduction in brain E2 levels, and a higher latency to the first oviposition (Shaw et al., 2023). This effect was linked to lower *avp* expression in the hypohtalamus; Avp peptide injection rescued the defect in oviposition time (Shaw, Lu, et al., 2023). The *cyp19a1b*-/- females differ significantly from *scg2* mutants, because they had increased number of eggs spawned and significantly more larvae died during early development resulting in change female fecundity compared to WT.

The analysis of the mating behaviour videos from the first 10 minutes revealed a significant decrease in male quiver behaviour in the *scg2a -/-* and *scg2b -/-* single KOs, but not in the DKO. While we observed a decline in quivering in the DKO fish, variability was high, and the data were not different compared to WT. This finding somewhat contradicts the previously observed reduction in quiver behaviour in the *scg2* TALEN mutants, where all the mutants exhibited

deficiencies in their quivers (Mitchell et al., 2020). Quivering behaviour in zebrafish has been noted and quantified in a few previous studies. Yong et al. (2017) report that an androgen receptor KO resulted in impaired male courtship behaviours during mating trials, exhibiting fewer chases, tail-noses, zigzags, and quivers, as well as a slower initiation of reproductive behaviour. Additionally, vasotocin KO zebrafish demonstrate reduced quiver behaviour due to this gene deletion (Ramachandran et al., 2023). These findings indicate that individual gene deletions of *scg2a* and *scg2b* in single knockouts affected male quiver behaviour, with *scg2b* being particularly responsible for the delay in spawning. Although the double deletion does not significantly impact quiver, the spawning delay caused by the *scg2b* deletion was sufficient for the DKO fish, especially females, to perform poorly in spawning. As a result of these upstream defects, both the single KO lines and DKO experienced a significant reduction in their spawning.

We next considered the morphological and anatomical basis for impaired reproduction. Body weight, fork length, and overall health (Fulton's K factor) were genotype dependent. Additionally, sex played a significant role in determining both weight and the K factor. The most pronounced difference was observed between WT and DKO females, with DKO females exhibiting the highest weight and K value. Across all groups, body weight ranged from 0.3 to 0.5 g, and length ranged from 3.0 to 3.4 cm. Fulton's K was 1.1 for WT females and 0.96 for WT males. In single KO and DKO groups, average K values ranged from 0.93 to 1.4, with the lowest in *scg2a-/-* KO males and the highest in DKO females. Consistent with these results, previous studies have reported higher K factors in female zebrafish due to a deeper abdomen, especially when gravid (Grigg et al., 2023). This increased body depth, which contributes to a higher K value, is sensitive to changes in body shape (Grigg et al., 2023). The elevated K value in DKO females compared to WT and single KO fish may indicate thicker bodies or higher fat content, as observed in skipjack tuna (*Katsuwonus pelamis*) (Jin et al., 2015). However, further studies are needed to assess fat content. Notably, the calculated K values fell within the previously reported normal range for adult zebrafish (0.8 to 3) (Clark et al., 2018), indicating that both WT and KO fish were healthy and in good condition. These morphometric data from WT, *scg2a-/-*, *scg2b-/-*, and DKO fish suggest that reduced spawning rates were not due to poor health or underweight conditions but rather to other physiological factors, such as gonadal development, maturation, or alterations in reproduction-related neuroendocrine factors. Given that the spawning defect was female-dependent and most significant in DKO females

compared to WT, we further analyzed and compared the ovarian morphology of *scg2a-/-; scg2b-/-* DKO females and their WT siblings.

Macroscopic observations indicated that the ovaries from all adult single KO and DKO lines are fully developed and appear normal compared to WT. Although reproductive impairments were noted, the gonadosomatic index (GSI) was not significantly altered in *scg2a-/-; scg2b-/-* DKO zebrafish. Histological analysis revealed that the ovaries from all adult single KO and DKO lines, along with the WT, contained a complete range of developing follicles, from primary growth stage to fully grown and mature oocytes. When oocyte development was assessed from fish randomly selected from the static tanks, no differences were noted. Thus, we analyzed their ovaries after synchronizing oocyte development following the purging of existing oocytes through spawning. Oocyte staging from the H & E staining of the ovarian sections after purging revealed a significant reduction in mature oocytes at stages 4 and 5, indicating that the deletion of *scg2a* and *scg2b* disrupts oocyte maturation rather than ovarian growth. It is worth noting that although not significantly different from WT, the *scg2a-/-; scg2b-/-* DKO exhibits a higher percentage of primary growth stage oocytes, with slight decreases at the cortical alveolus and vitellogenesis stages.

Surprisingly, we observed increased numbers of advanced (beta) and late-stage (gamma) atretic follicles in DKO ovaries. Similarly, *lhr* mutants in zebrafish exhibit significantly higher numbers of mature degenerating oocytes, and both oocyte maturation and ovulation were affected in the *lhb* mutants, whereas only ovulation but not maturation was affected in *lhr* mutants (Chu et al., 2014). This latter study did not report on ovarian purging or different stages of atresia. Lakshminarasimha et al. (2022) observed disrupted oocyte maturation and increased oocyte atresia in leptin receptor KO zebrafish, particularly following purging and synchronization of oocyte development. Loss-of-function mutations of the leptin receptor result in low fecundity, low fertility rates, and impairments in oocyte maturation and ovulation without much impact on folliculogenesis in zebrafish (Tsakoumis et al., 2022). In glucocorticoid receptor KO (*gr-/-),* zebrafish, decreased fecundity with low spawning was observed in adult females, with increased follicular atresia and premature ovarian aging (Faught et al., 2020). Additionally, *avp-/-* KO zebrafish also display altered follicular stages with an overall reduction in oocytes without any reports of atresia. In these *avp-/-* females, even though the alterations were observed in the primary growth stage and ovulation stage oocyte count, the GSI was not impacted. (Ramachandran et al., 2023). The *scg2a-/-; scg2b-/-* DKO

females show a relatively similar ovarian GSI to WT. This could be explained by the increased and accumulated atretic oocytes that failed to ovulate, and the similarity in total oocyte counts in the *scg2a-/-;scg2b-/-* DKO females. Low spawning and fecundity are likely linked to these defects in oocyte maturation and increased atresia. This data suggests an upstream regulatory role of *scg2a* and *scg2b* in managing the transition from vitellogenin stage to full maturation and ovulation. Investigation of mechanisms underlying the role of Scg2 in oocyte maturation is required.

The spawning defects that we observed in the *scg2a-/-; scg2b-/-* DKO females were not rescued by SNa and SNb alone or in combination, or by hCG injections. Since single injections of these hormones were unable to modify impaired reproduction (data not shown), we injected fish with a lower priming dose of SNa or SNb (0.25 nmol/g body weight) the previous night prior to spawning and followed with a higher dose (2.5 nmol/g body weight) 10 minutes before the morning spawning experiment. Surprisingly, the double injections were also not effective. Previous studies from our lab reported that a single injection of 1 nmol/g SNa could induce ovulation within 6 hours in WT females in the absence of males outside the normal ovulatory period (Peng et al., 2025). Similarly, Spadacini (2024) confirmed the results in WT females and tested the 2.5 nmol/g SNa injections, which effectively stimulated ovulation in WT females. Moreover, injection of 1 nmol/g SNa in TALEN mutant fish (Mitchell et al., 2020) significantly increased spawning from 11 to 30 %, whereas SNb was ineffective. We reasoned that perhaps a longer period of female-male interactions were required to increase spawning rates in the *scg2a-/-; scg2b-/-* DKO pairs. Within 6.5 hours, ~86% of saline-injected WT pairs spawned, whereas ~36% saline-injected DKO pairs spawned over the same experimental period. After SNa alone or in combination with SNb, only 15 % of couples spawned. Even though the SNb injection alone showed an intermediate effect and the spawning rate improved to 48%, all DKO groups, irrespective of hormone injection, exhibited significantly lower spawning compared to the WT. This indicates that the DKO fish are not sensitive to SNa or SNb under the conditions described. The presence of the full range of follicular stages, albeit, lower levels of mature follicles in DKO suggested that perhaps these animals were deficient in surge Lh release, and could be responsive to the Lh agonist hCG, since is an effective stimulator of oocyte maturation, ovulation, and spawning in several fish species (Fernandes et al., 2013; Mollah & Tan, 1983; Palstra et al., 2023; Zidan et al., 2020).

A maximum of 93% of WT couples spawned within 6.5 hours of hCG injections. We observed that 57% of the hCG-injected DKO fish spawned, remaining significantly lower than WT.

This level of spawning was comparable to uninjected DKO pairs permitted to spawn for 6.5 hours. This indicates that the DKO mutants do not respond well to hCG *in vivo*. According to Corriero et al., 2022, fish undergoing marked ovarian atresia lose responsiveness due to disrupted somatic-germ cell communication and downregulated signalling pathways critical to gonadotropin responsiveness. In silver pomfret (*Pampus argenteus*), early atresia involves downregulation of cytokine-cytokine receptor interaction in the early atretic ovary, suggesting disrupted cellular communication, and this disruption prevents Fsh and Lh from maintaining oocyte viability, leading to irreversible degeneration (Yang et al., 2022). This ineffectiveness in restoring spawning or fecundity in *scg2* KO fish indicates that the reproductive defect is not merely a result of hormonal insufficiency but may involve structural or cellular abnormalities within the ovary or reproductive tract, which require further investigation. Similarly, in *lhb-/-* mutant (Chu et al., 2014) and leptin receptor KO (Tsakoumis et al., 2022) zebrafish, hCG is unable to fully rescue ovulation. Moreover, in *npr* (nuclear progesterone receptor) null zebrafish hCG could not rescue ovulatory defects (Tang et al., 2016). The maturation-inducing steroid DHP (17α,20β-dihydroxy-4-pregnen-3-one) could partially rescue the decreased fecundity observed in *lhb-/-* or *star-/-* KO zebrafish which could not be rescued by hCG (Shang et al., 2019), therefore, the effect of DHP on *scg2a-/-; scg2b-/-* DKO fish will be important to investigate in the future. The combined results of the failed rescue attempts indicate that the complete deletion of the *scg2a* and *scg2b* genes disrupts reproduction in zebrafish. This directed us toward the possibility of molecular level defects, which is presented in Chapter 4 and 5.

In conclusion, the *scg2a-/-; scg2b-/-* DKO zebrafish model provides valuable insights into the complex role of *scg2a* and *scg2b* in teleost reproduction. The inability to rescue the reproductive phenotype with hormonal treatments underscores the requirement for the Scg2 precursor proteins and/or derived peptides for ovarian function. This model offers a unique opportunity to further elucidate the molecular mechanisms underlying oocyte maturation, ovulation, and fertility in teleosts.

Chapter 4: Complete gene deletion of *scg2a* and *scg2b* modulates expression of key genes in the HPG axis

4.1 Abstract

To investigate the reproductive defects resulting from the complete gene deletion of *scg2a* and *scg2b*, we measured the spatiotemporal expression patterns of key reproduction-related transcripts in *scg2a-/-; scg2b-/-* DKO zebrafish females compared to wild-type (WT) controls using digital PCR (dPCR) across four different tissues. No significant differences between WT and DKO females were found in the telencephalon at pre-ovulation (05:00 a.m.) in *gnrh2*, *gnrh3, avp*, or *oxt* expression. In the hypothalamus, *gnrh3* was significantly lower (p=0.0183) and *avp* higher (p=0.0001) in DKO females. The pituitary exhibited elevated *lhb* and *fshb* in DKO females, while *cga* was unchanged. Ovarian *lhcgr* and *star1* remained significantly downregulated in DKO females at all time, with *npr* and *pgmrc1* unaffected. At ovulation (8:30 a.m.), gene expression patterns shifted. The *oxt* mRNA levels in the telencephalon were significantly lower in DKO females (p=0.0010), while other genes showed no differences from WT. In the hypothalamus, *gnrh3* and *gnrh2* levels were similar in DKO and WT females. Levels of *avp* were elevated in DKO females, while *oxt* was significantly lower. At the ovulation time point, pituitary *lhb* and *fshb* remained elevated, but *cga* expression was reduced. At post-ovulation (10:00 a.m.), *oxt* in the telencephalon remained lower in DKO, while other genes were unchanged. In the hypothalamus, *gnrh2* and *avp* were lower in DKO females. Hypothalamic *oxt* expression was comparable between genotypes. In the pituitary, *lhb* and *fshb* were similar in DKO and WT, while *cga* was decreased in DKO. Levels of *gnrhr2* were consistently lower in DKO females in the pre-ovulatory and ovulatory time points but showed no difference at post-ovulation. The disruptions in hypothalamic, pituitary, and ovarian gene expression indicate that the absence of *scg2a* and *scg2b* alters normal reproductive signalling.

4.2 Introduction

We hypothesized that reproductive defects resulting from the complete gene deletion of *scg2a* and *scg2b* may be due to altered expression of key genes within the HPG axis. We therefore targeted key players using digital PCR to assess mRNA levels. Hypothalamic Gnrh is considered the primary neuroendocrine regulator of reproduction in mammals, but only one of the factors involved in the multifactorial control of teleost reproduction (Trudeau, 2022). Gnrh2 is expressed

in the midbrain and functions as a neurotransmitter that influences sexual behaviour in vertebrates (Canosa et al., 2007; Ogawa et al., 2022; Somoza et al., 2002). Moreover, in zebrafish, Gnrh2 may have a specific role in regulating reproduction during fasting (Marvel et al., 2021). The Gnrh3 isoform plays a crucial role in early sex differentiation by regulating the proliferation of primordial germ cells (PGCs) through a MAPK-dependent pathway, as evidenced by the male-biased sex ratio observed in *gnrh3* null zebrafish (Feng et al., 2020). Both Gnrh2 and Gnrh3 neurons directly project to the teleost pituitary (Carolsfeld et al., 2000; White & Fernald, 1993), and upon secretion, they bind to multiple pituitary Gnrh receptors to differentially regulate Lh release (Chang and Pemberton, 2018). In zebrafish, for example, there are four functional G-protein-coupled Gnrh receptor subtypes with differential distributions and activation, implying that these receptor subtypes have novel functions in addition to the phylogenetically conserved regulation of the pituitary. Zebrafish Gnrhr2 is equally sensitive to Gnrh2 and Gnrh3 (Tello et al., 2008). In a recent study using single-cell RNA sequencing, it was shown that *gnrhr2* is uniquely expressed in Lh gonado-tropes in zebrafish pituitary, but not in FSH gonadotropes, suggesting that Gnrh3 mainly acts through Gnrhr2 on LH cells (Sakura et al., 2024).

Isotocin (Oxt) and vasotocin (Avp) are the teleost homologs of oxytocin and vasopressin, produced in preoptic and hypothalamic neurons. In rainbow trout, the nonapeptide neurons are activated upon Gnrh2 and Gnrh3 application (Saito et al., 2003). Oxt and Avp are linked to numerous reproductive functions, including oviposition (Banerjee et al., 2017). Additionally, Oxt has a stimulatory role in the Lh surge and ovulation in mammals (Evans et al., 2003) and robustly enhances Lh in the rice field eel (Yang et al., 2021). Normal *oxt* gene function is required for mate choice based on familiarity recognition in medaka (Yokoi et al. 2020). Female zebrafish lacking *avp* exhibit significantly reduced reproductive success (Ramachandran et al., 2023), and intraperitoneal injections of Avp rescue delayed oviposition in *cyp19a1b* mutants (Shaw et al., 2023). It is reported that SNa is also colocalized with Oxt and Avp in cells and fibers of the POA in weakly pulse-type electric fish, goldfish and zebrafish (Canosa et al., 2011; Peng et al., 2025; Pouso et al., 2015).

Gonadotroph cells release Lh and Fsh from the pituitary under the influence of Gnrh and other stimulatory and inhibitory peptides. Lh and Fsh belong to the glycoprotein hormone family, consisting of one common alpha subunit (Cga) and one hormone-specific beta subunit, Fshb and Lhb. Both subunits are essential for the full biological function of the gonadotropin hormones

(Gharib et al., 1990). Upon secretion, Fsh primarily binds to the Fsh receptor (Fshr) in granulosa cells in the ovarian follicles, stimulating their proliferation and promoting follicular growth (Kwok et al., 2005; Zhang et al., 2015). The Lh acts on the Lh receptor (Lhcgr) in theca cells and, later on, granulosa cells to induce ovulation by triggering proteolytic enzyme activity that facilitates follicular rupture. Functional characterization of zebrafish gonadotropin receptors revealed that both Lhcgr and Fshr are activated by Lh and Fsh, with overlapping signals between Lh and Fsh (Xie et al., 2017). Oocyte development and the early stages of development are under the control of Fsh, while maturation and ovulation are controlled by Lh (Clelland & Peng, 2009; Patiño et al., 2001). The expression of Lhcgr is low at the early stages of folliculogenesis but increases and peaks just before oocyte maturation (Kwok et al., 2005). When Lhcgr is activated, it initiates a cascade of events crucial for steroidogenesis, oocyte maturation, and ovulation. Steroidogenesis starts in the theca cells when cholesterol is converted into pregnenolone through the action of Cyp11a1, which is the rate-limiting step in steroidogenesis (Nagahama et al., 1995). The steroidogenic acute regulatory protein (Star) is an enzyme that transports cholesterol into the inner mitochondrial membrane where Cyp11a1 is located (Ings & Van Der Kraak, 2006; Nagahama & Yamashita, 2008). It has been recognized as a downstream target of Lh during zebrafish oocyte maturation (Shi et al., 2024). Pregnenolone is the precursor of all steroid hormones, and it undergoes a series of enzymatic conversions to yield various intermediates, including progesterone,17α-hydroxyprogesterone, dehydroepiandrosterone (DHEA), and androstenedione, which is subsequently converted into testosterone. Testosterone converts into estradiol, primarily in granulosa cells, where the enzyme aromatase (Cyp19a1) facilitates this transformation (Chakraborty et al., 2021). During oocyte maturation, hydration occurs through the uptake of water and the processing of yolk proteins, leading to an increase in oocyte volume and preparation for fertilization. Moreover, vitellogenesis plays a crucial role, as it transforms primary growth stage oocytes (PG) into secondary growth stage oocytes (Deniz Koç et al., 2008). Estradiol (E2) production in the ovary, which, in turn, promotes vitellogenesis (Clelland & Peng, 2009). Additionally, 17α-hydroxyprogesterone in the theca cell is converted to DHP in granulosa cells by the action of 20β-hydroxysteroid dehydrogenase (20β-HSD) (Nagahama, 1997). The DHP acts as the maturation-inducing hormone (MIH) in many teleost species, including zebrafish, and is crucial for oocyte maturation and ovulation by triggering germinal vesicle breakdown (GVBD) (Jéhannet et al., 2023; Tokumoto et al., 2011). Nuclear progesterone receptor (*npr*) mutant female

zebrafish were infertile despite the normal development of the oocytes but failed to ovulate even after treatment with hCG or DHP (Zhu et al., 2015).

Ovulation is the process by which the mature egg is released from the ovary. In zebrafish, this typically occurs before the onset of daylight, with spawning following within an hour after light exposure (Wu et al., 2018). The initial Lh surge signal on Lhcgr is amplified by the progestin synthesis in the preovulatory follicles and activates the Npr (Wu et al., 2021). Npr is essential in ovulation as *npr* - null zebrafish, mice, and rats are unable to ovulate (Conneely et al., 2001; Lydon et al., 1995; Tang et al., 2016; Zhu et al., 2015). Moreover, progestin receptor membrane component 1 (Ppgrmc1) and Pgrmc2 have been shown to regulate Npr and, thereby, ovulation, as *pgrmc1/2* null zebrafish exhibit reduced ovulation (Wu et al., 2021)

4.3 Materials and Methods

4.3.1 Tissue collection

The *scg2a-/-; scg2b-/-* DKO females and their age-matched sibling WT females at 8-9 months (N=10) were used for the experiment. Individual tissues of the telencephalon, hypothalamus, pituitary, and ovary were dissected at three different important time points over the natural ovulatory cycle (5 a.m. - pre-ovulation, 8.30 a.m. - ovulation and 10 a.m. - post-ovulation). During the 2:00 a.m. - 5:00 am, the *lhb* was to be highest (So et al., 2005), and 5:00 a.m. is considered to be the time of the preovulatory Lh surge. At 8:30 a.m., just before light on, was considered to be the ovulation time point (Peng et al., 2025; Zhou et al., 2011). We considered 10:00 a.m. as the post-ovulatory time point outside the spawning window of a normal fish. Ten female fish from each group were dissected at specific time points to collect the tissues. For all the time points, zebrafish were anesthetized in an ice bath, and extraction of the tissues was completed within 15 minutes. Extracted tissues were transferred to 1.5 ml Eppendorf tubes, immediately frozen in dry ice, and stored at -80 ^{0}C until RNA extraction.

4.3.2 RNA extraction

For the extraction of mRNA from the telencephalon, hypothalamus, and pituitary, the PureLink mini-RNA extraction kit (Thermo Fisher, Cat # 12183018A) was employed. The samples were homogenized using a homogenizer column (Thermo Fisher, Cat # 12183026) following the given protocol. Following extraction, RNA quality was assessed using the Agilent

TapeStation system according to manufacturer guidelines, based on the RNA integrity number (RIN number) and Nanodrop quantification. Confirmed quality RNA was stored at -80°C until complementary DNA (cDNA) synthesis was performed.

Total mRNA was extracted from the ovary following the manufacturer's protocols using Trizol™ (Thermo Scientific, Cat # 15596026), with minor adjustments. In summary, 500 µl of Trizol™ was added to each tube, and the tissues were homogenized with a homogenizer stick. The samples were centrifuged for 5 minutes at 12000 g and 4°C; afterward, the supernatant was transferred to Phasemaker™ tubes and incubated at room temperature for 5 minutes. Chloroform (200 µl per 1 ml of Trizol) was then added, followed by vigorous shaking for 15 seconds. The samples were allowed to sit at room temperature for 5 minutes before being centrifuged again at 12000 xg, 4°C for 15 minutes. The supernatant was moved to a new tube, and isopropanol (500 µl per 1 ml of Trizol) along with 1 µl of GlucoBlue™ (Invitrogen, Cat# AM9515) were added. The tubes were inverted 5 times, incubated at -20°C for 30 minutes, and then centrifuged at 12000 xg, 4°C for 10 minutes. The isopropanol was removed, and the samples were rinsed with 500 µl of 75% ethanol, followed by centrifugation at 7500 g, 4°C for 5 minutes. After removing the ethanol, the samples were washed again with 0.5 ml of 75% ethanol and centrifuged at 7500 g, 4°C for 5 minutes. The residual ethanol was removed, and the samples were left open to dry for 5 minutes in a fume hood. Depending on the RNA yield, samples were suspended in 15-25 µl of ddH2O and then heated at 60°C for 10 minutes. The total RNA concentrations and the absorbance ratios of 260/280 and 260/230 were measured using a spectrophotometer (NanoDrop 2000, Thermo Scientific).

4.3.3 cDNA synthesis

cDNA was synthesized using BioRad iScript™ cDNA Synthesis Kit (BioRad Cat # 1708891) for RT-qPCR according to the manufacturer's protocol and stored at -20°C. For the telencephalon, hypothalamus and pituitary samples, 100 ng of mRNA was used for the cDNA synthesis, while 300 ng of total RNA was used for the ovary samples. A two-step SYBR green-based, semi-quantitative, real-time RT polymerase chain reaction (RT-qPCR) determined cDNA quality and dilution factor. To determine the quality, single product amplification was confirmed by the melting curve method, and the best dilution was selected through running a dilution series

in both RT-qPCR and dPCR. All the cDNA for both control WT and DKO in one time point were extracted at the same time and stored at -20°C.

4.3.4 Primers

Primer design followed Mitchell et al. (Mitchell, Zhang et al., 2019) and (Peng et al., 2025) and was performed online (http://bisearch.enzim.hu/). Primers were synthesized by Integrated DNA Technologies. The annealing temperature of all the primers was 58°C. The primers were validated by RT-PCR, single product amplification was confirmed by the melting curve methods and the sequences were verified. The PCR products were sequenced, and the specificity was confirmed by the Basic Local Alignment Search Tool (BLAST). The primer information is shown in Table 4.

Gene(abbreviation)	Detected tissue	Sequence (5`-3`)	Accession number
Isotocin (*ist*)	Telencephalon, hypothalamus	Fw: GATCTGCTGCTGAAGCTCCT	NM_178291.2
		Rv: TACAAAAGTGGGTGGCGAGT	
Arginine vasotocin (*avp*)	Telencephalon, hypothalamus	Fw: AGGTCTGCATGGAAGAGGAG	NM_178293.2
		Rv: CTGCCTTCAGGACAGTCTGG	
Gonadotropin-releasing hormone 2 (*gnrh2*)	Telencephalon, hypothalamus	Fw: CAGAGGTTTCAGAGGAAGTGAAGC	NM_181439.4
		Rv: TGAGGGCATCCAGCAGTATTG	
Gonadotropin-releasing hormone 3 (*gnrh3*)	Telencephalon, hypothalamus	Fw: ATGGAGGCAACATTCAGGATGT	NM_182887.2
		Rv: CCTTTCAGAGGCAAACCTTCA	
Gonadotropin-releasing hormone receptor 2 (*gnrhr2*)	Pituitary	Fw: TCCTCAACCCTCTGTCCATC	NM_001144979.1
		Rv: TGCTTTGGGGAATCAATCTC	
Glycoprotein alpha (*cga*)	Pituitary	Fw: CTGCTGCTTTTCGAGAGCTT	AY424306.1
		Rv: AGTGGCAGTCTGTGTGGTTG	
Luteinizing hormone beta (*lhb*)	Pituitary	Fw: AATGCCTGGTGTTTCAGACC	NM_205622.2
		Rv: AACAGTCGGGCAGGTTAATG	
Follicle stimulating hormone beta (*fshb*)	Pituitary	Fw: TGTGGAGAGCGAAGAATGTG	AY714131.1
		Rv: AGACCTTCTGGGTGTGCTGT	
Luteinizing hormone receptor (*lhcgr*)	Ovary	Fw: TGAAAGAGCAGCCAGGTACT	AY714133.1
		Rv: TGCTAAATTTCCTTTCGCCG	
Nuclear Progesterone Receptor (*npr*)	Ovary	Fw: GGGCCACTCATGTCTCGTCTA	NM_001166335.1
		Rv: TCTCCACTCTGAAAATATGTGGACTTT	
Steroidogenic acute regulatory protein 1 (*star1*)	Ovary	Fw: GGTCTGAGGAAGAATGCAATGAT	BC075967.1
		Rv: CCAGGTCCGGAGAGCTTGT	
Progesterone receptor membrane component 1 (*pgmrc1*)	Ovary	Fw:CCTGGCTACGTTCTGTTTGG	NM_001007392.1
		RW: GGGTCCGCTCTAATCCTTCT	
Elongation factor alpha (*ef1α*)	Telencephalon, hypothalamus, pituitary, ovary	Fw: CAAGGAAGTCAGCGCATACA	L23807.1
		Rv: ACCGCTAGCATTACCCTCCT	

Table 4. Profiled transcripts, primer sequences and accession numbers used to quantify gene expression in WT and s*cg2-/-; scg2b-/-* DKO telencephalon, hypothalamus, pituitary and ovary.

4.3.5 Digital PCR assessment

Absolute quantification of the mRNA was performed using QIAcuity digital PCR reactions. All assays were validated using the QIAcuity Four 5-plex digital PCR System (Qiagen, Hilden, Germany). Digital PCR reactions consisted of 15 µL reaction mixture per well containing 10 µL QIAcuity 3x evergreen master mix (Qiagen), 1.2 µL mix of forward and reverse primer, 5 µL of cDNA and PCR-grade water. Assembled reactions were transferred into QIAcuity 8.5k 24-well Nanoplates (Qiagen) for partitioning using the Qiagen Standard priming Profile, and cDNAs were amplified under the following conditions: enzyme activation for 2 min at 95 °C and 40 cycles of 15 s at 95 °C and 15 s at 58 °C 15s at 72°C and then 2min in 72 °C. Partitions were imaged with 500 ms (EVA green) exposure time, with gain set to 6. The QIAcuity Software Suite (Qiagen, version 2.5) was used to determine sample thresholds using positive, negative, and no-template control wells (NTCs).

Gonadotropin-releasing hormone 2 (*gnrh2*), gonadotropin-releasing hormone 3 (*gnrh3*), isotocin (*oxt*), and vasotocin (*avp)* in the telencephalon and hypothalamus were quantified. In the pituitary, *lhb* and *fshb*, *cga* and gnrh receptor 2 (*gnrhr2*) were measured, followed by *lhcgr*, *star1*, *npr* and *pgmrc1* in the ovary.

4.3.6 Data analysis and statistics

The data for each tissue were normalized by Norma-Gene (Heckmann et al., 2011) and presented as individual values (N=9-10) with medians indicated. The levels of elongation factor 1 alpha (*ef1a)*, a commonly expressed gene, were used in the normalization procedures. All the results were statistically analyzed using GraphPad Prism 10 software. Normality and homoscedasticity were tested, followed by the Shapiro-Wilk test. If the data was normally distributed, a 2-tailed unpaired T-test was used, and if the data was not normally distributed, a 2-tailed Mann-Whitney U-test was used

4.4 Results

4.4.1 Telencephalon and Hypothalamic gene expression altered in the *scg2a-/-; scg2b-/-* DKO females

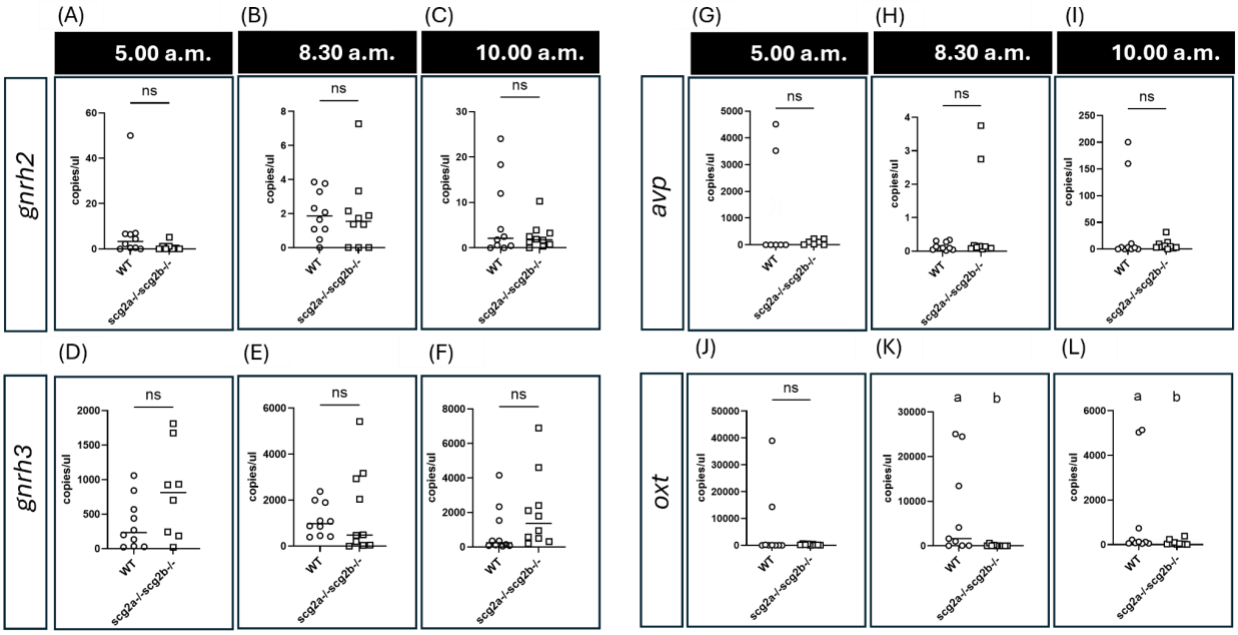

Figure 19. Telencephalon mRNA levels for neuropeptidergic genes in adult wild-type (WT) and *scg2a-/-;scg2b-/-* DKO females at three different time points. Shown are levels of *gnrh3* (A, B, C), *gnrh2* (D, E, F), *avp* (G, H, I), *oxt* (J, K, L) at the 5.00 a.m. (pre-ovulatory), 8.30 a.m. (ovulation) and 10.00 a.m. (post-ovulatory) time points. Dots represent individual data points (N=10), and horizontal lines represent median values. Note the differences in the scales of the Y-axes. Since the data were not normally distributed, statistical analysis was performed using the Mann-Whitney U test. [a,b]Different superscripts indicate significant differences; 'ns' denotes not significant ($p>0.05$).

In the telencephalon, *gnrh2* (Figure 19- A, B, C), *gnrh3* (Figure 19- D, E, F) and *avp* (Figure 19- G, H, I) levels were similar between WT and *scg2a-/-; scg2b-/-* DKO females across time (*gnrh3*: 5 a.m. p=0.0854, 8.30 a.m. p=0.7394. 10 a.m. p=0.0524; *gnrh2*: 5 a.m. p=0.7350, 8.30 a.m. p=0.6409, 5 a.m. p=0.07389; *avp:* 5 a.m. p=0.3980, 8.30 a.m. p=0.4813, 5 a.m. p=0.2247. In contrast, *oxt* mRNA copy number is lower in *scg2a-/-; scg2b-/-* DKO females compared to the WT at the ovulation time (Figure 19- K, p= 0.0010) and post-ovulation (Figure 19- L, p= 0.0185).

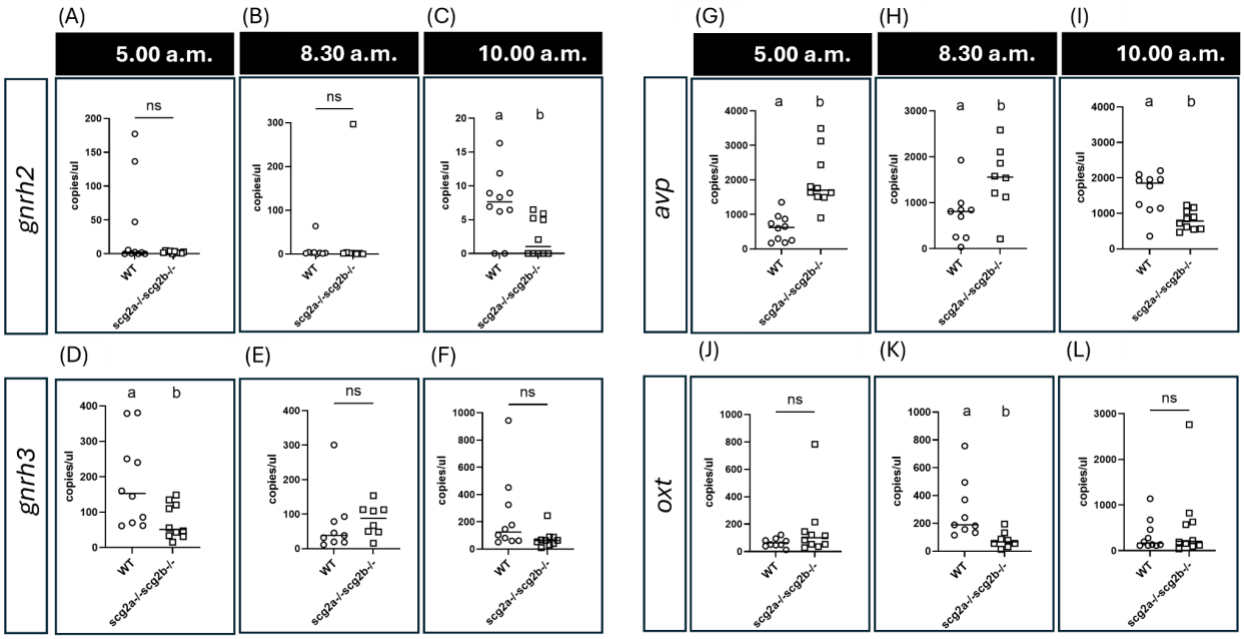

Figure 20. Hypothalamic mRNA levels of neuropeptidergic genes in adult wild-type (WT) and *scg2a-/-;scg2b-/-* DKO females at three different time points. Gene expression of *gnrh3* (A, B, C), *gnrh2* (D, E, F), *avp* (G, H, I) and *oxt* (J, K, L) at the 5.00 a.m (pre-ovulatory), 8.30 a.m. (ovulation time point) and 10.00 a.m. (post-ovulatory) timepoints. Dots represent individual data points (N=9-10), and horizontal lines represent median values. Note the differences in the scales of the Y-axes. Statistical analysis was performed for normally distributed data by 2-tailed unpaired T-test (panels A, G, H, I) or when not normally distributed by Mann-Whitney U-test). [a,b]Different superscripts indicate significant differences; 'ns' denotes not significant ($p>0.05$).

In the hypothalamus, *gnrh2*, *gnrh3*, *avp,* and *oxt* levels varied between genotypes at several time points. Hypothalamic *gnrh3* was higher in WT than DKO before ovulation at 5 a.m. (Figure 20-A, p= 0.0183) but was similar to WT levels at 8.30 a.m. (Figure 20- B, p=0.1672) and 10 a.m. (Figure 20- C, p=0.0630). In contrast, levels of *gnrh2* were not different between groups at the pre-ovulatory (Figure 20-D, p=0.8649) and ovulation times (Figure 20-E, p=0.4221). However, *gnrh2* was lower in the DKO hypothalamus compared to WT post-ovulation (Figure 20-F, p=0.0100). The level of *avp* in the hypothalamus was higher in DKO than WT at pre-ovulation (Figure 20- G, p= 0.0001) and ovulation (Figure 20- H, p= 0.0219), but was significantly lower post-ovulation (Figure 20- I, p= 0.0015). In contrast to *avp*, *oxt* levels in WT and DKO hypothalamus are similar at pre-ovulation (Figure 20- J, p=0.3930) and post-ovulation (Figure 20-L, p=0.7959), but were lower in the DKO at ovulation time at 8.30 a.m. (Figure 20- K, p=0.0025).

4.4.2 Pituitary gene expression is altered in the *scg2a-/-; scg2b-/-* DKO females

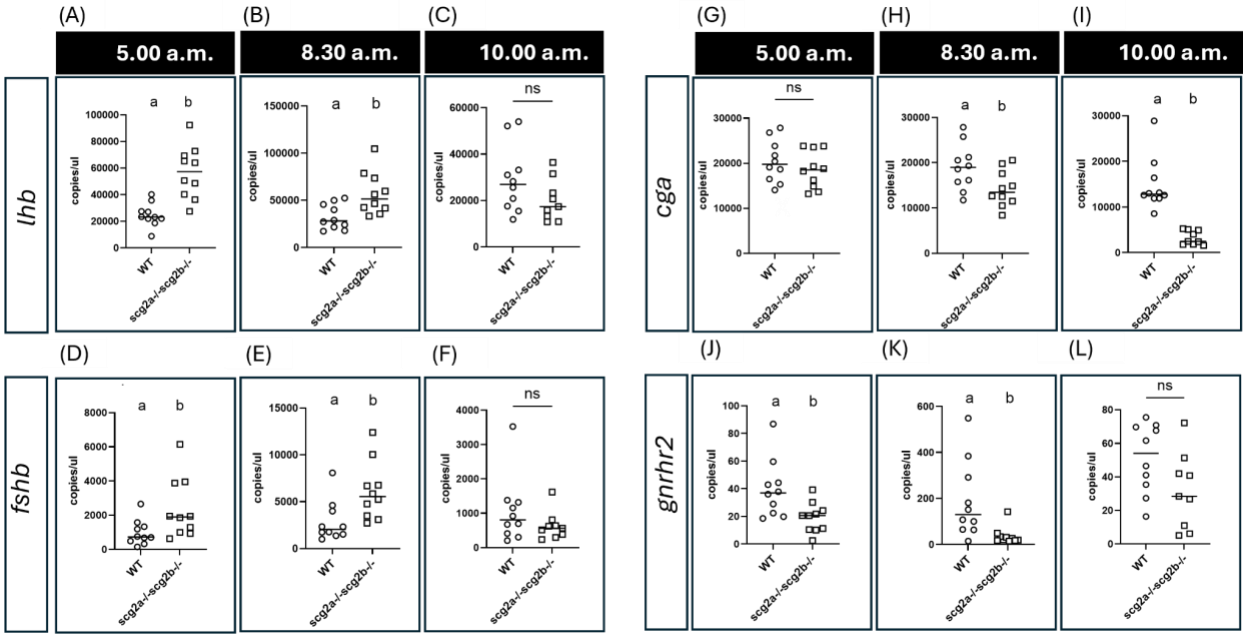

Figure 21. Pituitary mRNA levels of reproduction-related genes in adult wild-type (WT) and *scg2a-/-;scg2b-/-* DKO females at three different time points. Gene expression of *lhb* (A, B, C), *fshb* (D, E, F), *cga* (G, H, I) and *gnrhr2* (J, K, L) at the 5.00 a.m. (pre-ovulatory), 8.30 a.m. (ovulation time point) and 10.00 a.m. (post-ovulatory) timepoints. Dots represent individual data points (N=9-10), and horizontal lines represent median values. Note the differences in the Y-axis. Statistical analysis was performed when not normally distributed by the Mann-Whitney U-test (panels E, K, F, I) or by a 2-tailed unpaired T-test. [a,b]Different superscripts indicate significant differences; 'ns' denotes not significant ($p>0.05$).

Levels *lhb* and *fshb* in the pituitary were both significantly higher in DKO at the pre-ovulation (*lhb*: Figure 21-A, p=0.0002, *fshb*: Figure 21-D, p=0.0355) and ovulation (*lhb*: Figure 21-B, p=0.0080, *fshb*: Figure 21-E, p=0.0052) compared to WT. Post-ovulation levels of both *lhb* (Figure 21 -C, p=0.1261) and *fshb* (Figure 21 -F, p=0.2428) were similar in Wt and DKO groups. In marked contrast, *cga* mRNA levels were similar in WT and DKO pituitary at the pre-ovulatory time (Figure 21 -G, p=0.3547), but reduced in DKO at the ovulation (Figure 21 -H, p=0.0316) and post-ovulation (Figure 21 -I, p<0.0001) compared to WT. Levels of *gnrhr2* were in the DKO pituitary at the pre-ovulation time (Figure 21-J, p= 0.0126) and at ovulation (Figure 21-K, p= 0.0039), but were not different at the post-ovulatory time point (Figure 21-L, p= 0.0632).

4.4.3 Ovarian gene expression altered in the *scg2a-/-; scg2b-/-* DKO females

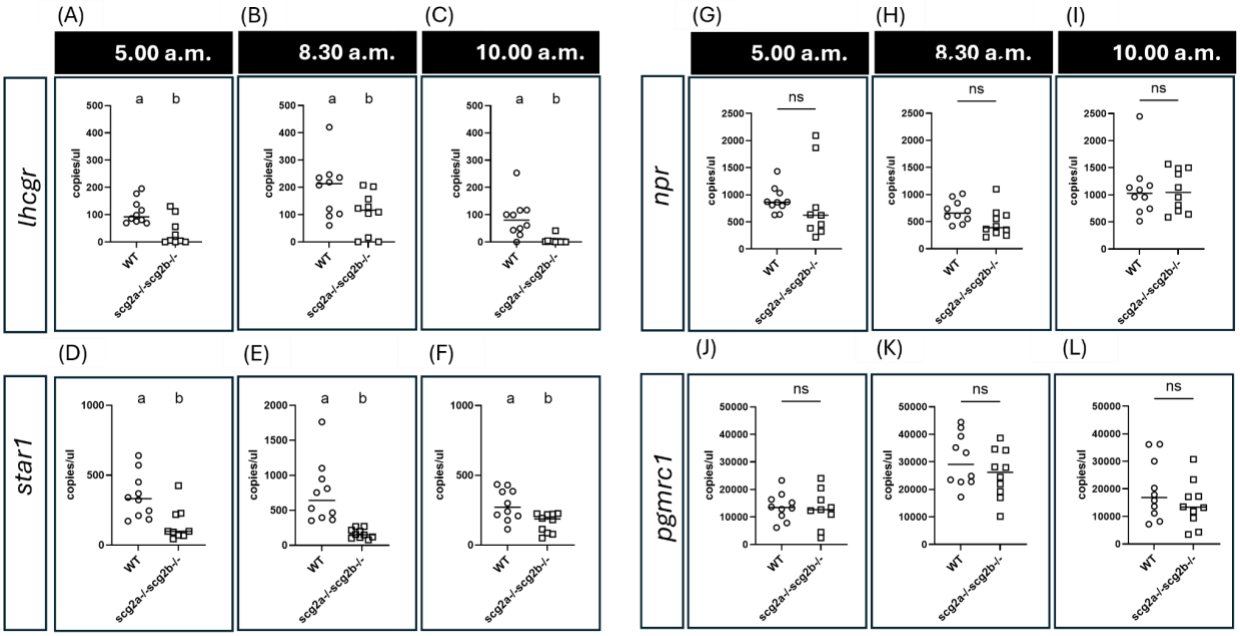

Figure 22. Ovarian mRNA levels of reproduction-related genes in adult wild-type (WT) and *scg2a-/-; scg2b-/-* DKO females at three different time points. Gene expression of *lhcgr* (A, B, C), *star1* (D, E, F), *npr* (G, H, I) and *pgmrc1* (J, K, L) at the 5.00 a.m. (pre-ovulatory), 8.30 a.m. (ovulation time point) and 10.00 a.m. (post-ovulatory) timepoints. Dots represent individual data points (N=9-10), and horizontal lines represent median values. Note the differences in the Y-axis. Statistical analysis was performed when not normally distributed by the Mann-Whitney U-test (panels E, K, F, I) or for normally distributed data by a 2-tailed unpaired T-test. [a,b]Different superscripts indicate significant differences; 'ns' denotes not significant ($p>0.05$). Note the different Y-axis scales.

Important effects of *scg2a-/-; scg2b-/-* DKO were evident in the ovaries. Levels of *lhcgr* were consistently low and significantly different at all the time points in DKO compared to WT (Figure 22 A, p=0.0076, Figure 22 B, p=0.0432, Figure 22 C, p=0.0011). Moreover, *star1* levels followed the same patterns, being consistently lower in DKO ovaries at all time points (Figure 22-D, p=0.0076, Figure 22-E, p=0.0006, Figure 22-F, p=0.0288). Both *npr* and *pgmrc1* were similarly expressed in the ovaries of WT and DKO females (*npr*: Figure 22-G, p=0.0789, Figure 22-H, p=0.0660, Figure 22-I, p=0.8534 and *pgrmc1*: Figure 22-J, p=0.7955, Figure 22-K, p=0.2469, Figure 22-L, p=0.2430).

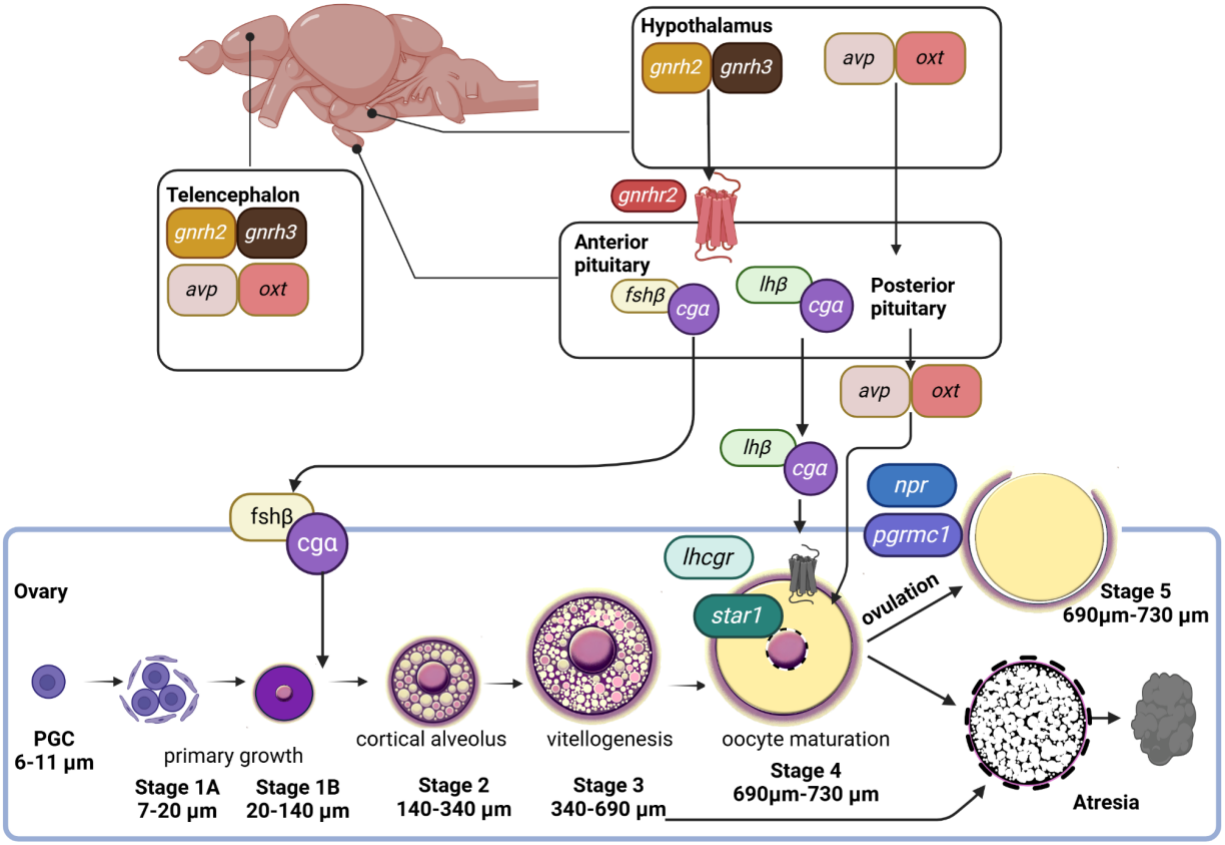

Figure 23. Schematic representation of the genes analyzed by dPCR. The oocyte development and maturation diagram is modified from Li and Ge 2020. (Created in Biorender.com)

4.5 Discussion

We measured the expression of key genes associated with reproductive regulation to investigate the potential mechanisms underlying disrupted spawning in DKO fish. Gnrh3 is considered the hypophysiotropic decapeptide of many teleosts, functioning similarly to Gnrh1 in mammals (Tello et al., 2008; Roch et al., 2014; Trudeau, 2018). In our study, we found that hypothalamic *gnrh3* expression is significantly reduced in the *scg2a-/-; scg2b-/-* DKO females at 5 a.m., the time of the presumptive pre-ovulatory Lh surge, Levels of hypothalamic *gnrh3* are also very low in *scg2* TALEN mutants (Mitchell et al., 2020). In normal WT zebrafish, the *gnrh3* expression may be expected to be high in the brain at some point before the preovulatory Lh surge, Peng et al. (2025) report that whole brain Gnrh3 levels in WT zebrafish females display a distinct pattern, increasing 1.6-fold concurrently with SNa1-34 between 2 a.m. and 5 a.m., at the expected

time of the Lh surge, before decreasing again at 8:30 a.m. at the time of ovulation. Post-ovulation, *gnrh3* was not significantly different between the groups. Previously, our lab showed that a single i.p. injection of SNa1-34 robustly upregulates *gnrh3* in the telencephalon and hypothalamus of WT zebrafish (Peng et al., 2025), and another lab reports that SNa1-34 stimulates *gnrh3* in hypothalamic fragments of orange-spotted grouper *in vitro* (Shu et al., 2018). Together, data from mutants and WT fish indicates a positive relationship between Scg2, SN and Gnrh neurons.

Along with the *gnrh3* in the hypothalamus, *gnrhr2* is also downregulated in the pituitary during preovulation and ovulation. With the reduction of both *gnrh3* and *gnrhr2*, we anticipated that the *fshb* and *lhb* subunits would similarly be downregulated; however, to our surprise, they were upregulated during pre-ovulation and ovulation. Furthermore, at the pituitary level, *cga* was downregulated during both ovulation and post-ovulation in the *scg2a-/-; scg2b-/-* DKO female pituitaries. These gene expression results stand in contrast to those from the previously generated *scg2* TALEN mutants, where no differences were observed in the *gnrhr2*, yet significantly low levels of *lhb* were noted, with *fshb* remaining unaffected (Mitchell et al., 2020). Nevertheless, the downregulation of *cga* is consistent between the *scg2* TALEN mutants (Mitchell et al., 2020) and the *scg2a-/-; scg2b-/-* complete gene KO animals reported here. Note that we analyzed gene expression across three different time points, while the previous TALEN mutants were evaluated only at a basal level at 10.00 a.m. The surprising upregulation of the *lhb* and *fshb* subunits in the pituitary, and yet the downregulation of *cga* suggests a possible limitation in the availability of the Cga subunit protein, and thus functional Lh and Fsh proteins may be reduced. Alternatively, the upregulation of *lhb* and *fshb* subunits in the pituitary could be indicative of altered ovarian steroid feedback. Both proposals remain speculative until tested experimentally.

Expression of *oxt* was downregulated in the telencephalon and hypothalamus of the *scg2a-/-; scg2b-/-* DKO fish compared to their WT siblings at ovulation, and this downregulation was consistent in the post-ovulation period in the telencephalon. The expression of *avp* was upregulated in the hypothalamus at pre- and ovulatory time points but downregulated at the post-ovulatory time point. Compared to previous work, *scg2a/2b* TALEN double mutants did not exhibit significant differences in *oxt* and *avp* gene expression in the telencephalon or hypothalamus. However, the single mutant females of *scg2a* and *scg2b* showed a significant decrease in *oxt* mRNA at a post-ovulatory time in telencephalon and reduction in *avp* only in the *scg2b* single mutants in telencephalon (Mitchell et al., 2020). Peng et al. (2025) demonstrated that SNa1-34

injections in WT zebrafish females increase telencephalon and hypothalamic *oxt* at 3 hours post-injection, but *avp* was not affected (Peng et al.,2025). The nonapeptide OXT and AVP are well-known regulators of sociosexual behaviours (Godwin & Thompson, 2012), and disrupted *oxt* and *avp* expression in our DKO females may contribute to reduced spawning, sexual behaviour and delayed oviposition, as described in Chapter 3.

In the ovary, *star1* and *lhcgr* were downregulated during pre-ovulation, ovulation, and post-ovulation, indicating a defect in ovarian tissue in DKO females. Star and Lhcgr play important roles in steroidogenesis. Significant downregulation of *star1* and *lhcgr* receptors in DKO females may contribute to disrupted ovulation, impairing steroidogenesis and crucial signalling pathways necessary for follicle maturation and rupture. Female zebrafish with a frameshift mutation of *star1* were reported to be infertile when crossed with WT males, and oocytes arrested at stage 4 (Shang et al., 2019). The same lab created a *lhb* null mutant zebrafish where similar oocyte maturation and ovulation defects were observed, and *star1* was low at the pre-ovulatory period (Shang et al., 2019). Moreover, *npr* gene mutation blocks ovulation entirely despite normal DHP levels, emphasizing its non-redundant role in follicle rupture (Liu et al., 2018; Wu & Zhu, 2021; Zhu et al., 2015). In zebrafish, *pgrmc1* and *pgrmc2* DKO leads to delayed oocyte maturation and lower female fertility, significantly decreasing ovulation rates (Wu & Zhu, 2021). Similarly, estrogen receptor *esr1* mutants initially show enhanced fertility but develop premature ovarian failure by 180 days post-fertilization (dpf), characterized by degenerated ovaries and downregulated vitellogenin (*vtg*) genes critical for yolk formation (Chen et al., 2018). Mutations of the *lhcgr* alone did not affect the reproduction in zebrafish, likely because Fshr can be activated by both Fsh and Lh in the zebrafish (Zhang et al., 2015).

In comparison, the previously generated *scg2* TALEN mutant fish had impaired ovulation; however, gene expression analysis was not performed on the ovary. Highlighting the importance of SNa in ovulation, synthetic SNa injections in WT fish induced ovulation and increased *lhcgr* and *npr* mRNA levels 3 hours post-injection (Peng et al., 2025). In contrast, *npr* and *pgrmc1* were not affected in *scg2a-/-; scg2b-/-* DKO at any of the time points. A possible explanation for this observation might be an activation of a compensatory mechanism preserving *npr* and *pgrmc1* expression in response to *star1* downregulation. Another possibility is that cell-specific effects might have been masked because we assessed whole-ovary expression levels. However, *avp* KO in zebrafish also reports that ovarian *npr* expression was not affected despite having mature oocyte

retention and low spawning rates (Ramachandran et al., 2023). Given the gene expression data in the ovary, *fshr* and other steroidogenesis-related genes such as cyp*11a1*, *hsd3b*, *cyp17a1, cyp19a1,* and androgen and estrogen levels are potentially important and should be assessed in these KO lines in the future.

In summary, targeted deletion of the *scg2a* and *scg2b* genes modulates reproduction-related gene expression in the brain, pituitary, and ovarian tissues during three time points in the ovulatory cycle in zebrafish. The significant decreases in sexual behaviour, spawning, fecundity, and oocyte maturation and increased atresia observed in *scg2* complete gene KO lines (Chapter 3) are therefore linked to the disruption of hormones and signalling pathways in the hypothalamo-pituitary-ovarian axis.

Chapter 5: Proteomic analysis reveals major differences and defects in the pituitary of *scg2a-/-;scg2b-/-* DKO zebrafish

5.1 Abstract

We observed an abnormal elongation and bump-like structure in the *scg2a-/-; scg2b-/-* DKO female pituitaries compared to smooth and oval-shaped pituitaries in the WT siblings. We used proteomic analysis to understand the basis of this disrupted morphology. A total of 3674 proteins were identified, with 51 being significantly different between the *scg2a-/-; scg2b-/-* DKO and WT samples at 2.00 p.m. Among these, 27 proteins were downregulated, and 24 were upregulated. As expected, Scg2a and Scg2b are not detected in the *scg2a-/-; scg2b-/-* DKO samples. There were no significant changes in the Lhb, Fshb, Cga, Tshb, Gh1, Avp and Oxt proteins. The gene ontology (GO) enrichment analysis (using the human genome) revealed that both the mitochondrial inner membrane (GO:0005743) and respiratory chain complex 1 (GO:0051604) have the highest downregulation, with five proteins related to each. Additionally, mitochondrial respiratory chain complex one assembly (GO:0032981) and mitochondrial electron transport from NADH to ubiquinone (GO:0006120) showed a downregulation, involving two proteins each. Additionally, the significantly dysregulated proteins were mapped with the KEGG mapper tool to visualize the proteins in zebrafish cellular pathways, and 21 different pathways were identified. The lack of Scg2a and Scg2b in the DKO pituitary disrupts essential cellular processes related to hormone biosynthesis, peptide processing, and signalling. It also impacts oxidative stress-related enzymes and decreases the expression of proteins crucial for extracellular matrix (ECM) stability and structural integrity, potentially leading to a structural adaptation.

5.2 Introduction

The pituitary glands of *scg2a-/-; scg2b-/-* DKO females were abnormal in shape compared to WT siblings. Therefore, we conducted a mass spectrometry (MS) based proteomics analysis to investigate and identify the protein level differences between the DKO and WT single pituitaries. The pituitary gland is a critical component of the endocrine system, regulating various physiological processes, including growth, reproduction, and homeostasis. In adult zebrafish, the pituitary gland is in a bony hollow beneath the hypothalamus, just behind the optic chiasm, like mammals (Pogoda & Hammerschmidt, 2007). The pituitary gland in vertebrates generally consists

of 2 main regions: the anterior lobe (adenohypophysis- AH) and the posterior lobe (neurohypophysis -NH), and an intermediate lobe in between. The NH differentiates from the infundibular floor of the third brain ventricle, whereas the AH originates from Rathke's pouch in mammals (Sage & Bern, 1971). Teleosts do not form a Rathke's pouch or an infundibulum; instead, the anterior neural ridge of the pre-placodal ectoderm develops into AH, and the neural ectoderm of the ventral diencephalon becomes NH (Chapman et al., 2005). The zebrafish pituitary reaches its maximum volume at approximately 24 hours post-fertilization (hpf), and the adenohypophysis becomes morphologically distinct, whereas the neurohypophysis remains indistinct until around 72 hpf (Chapman et al., 2005). The shape of the zebrafish pituitary is generally oval from the sagittal view, and this shape and structure can be altered for several reasons. Stress, inflammation and other factors can be influential on altered pituitary shape, and studies on hypothalamic-pituitary-thyroid axis alterations report changes in pituitary surface areas of zebrafish, indicating morphological adaptations to endocrine disruption by propylthiouracil (PTU) (Schmidt & Braunbeck, 2011). Some clinical reports in humans suggest that pituitary volume increases in puberty, in pregnancy, or with the administration of exogenous estrogens (Wong et al., 2014). Moreover, pituitary gland volume is significantly larger in polycystic ovary syndrome (PCOS) patients, depending on the LH/FSH ratio, according to the magnetic resonance imaging (MRI) of the human pituitary (Unlu et al., 2015). A comprehensive screening of 209 lethal and sub-viable knockout mouse lines identified 51 lines exhibiting embryonic pituitary malformations. These included absent, hypoplastic, or dysmorphic anterior and posterior lobes, often linked to deficiencies in signalling pathways such as cilia formation, epithelial-to-mesenchymal transition, or ventral diencephalon signalling (Martinez-Mayer et al., 2024). Mice deficient in Wnt5a (Wingless-Type MMTV Integration Site Family, Member 5A) signalling display abnormal morphology in the dorsal part of the developing pituitary (Cha et al., 2004).

Unlike mammals, the teleost pituitary is directly innervated by hypothalamic neurons, and six different hormone-secreting cell types are highly regionalized (Figure 24). While the rostral pars distalis (RPD) contains thyrotrophs and lactotroph cells that secrete thyroid-stimulating hormone (TSH) and prolactin (PRL), the proximal pars distalis (PPD) is where gonadotrophs and somatotrophs are located, secreting LH, FSH and growth hormone. (Trudeau, 2022). The posterior pituitary comprises neurosecretory nerve endings projecting from the cell bodies in the

hypothalamus, secreting two different nonapeptide hormones: arginine vasotocin (AVP) and isotocin (mammalian oxytocin) (Murphy et al., 1998).

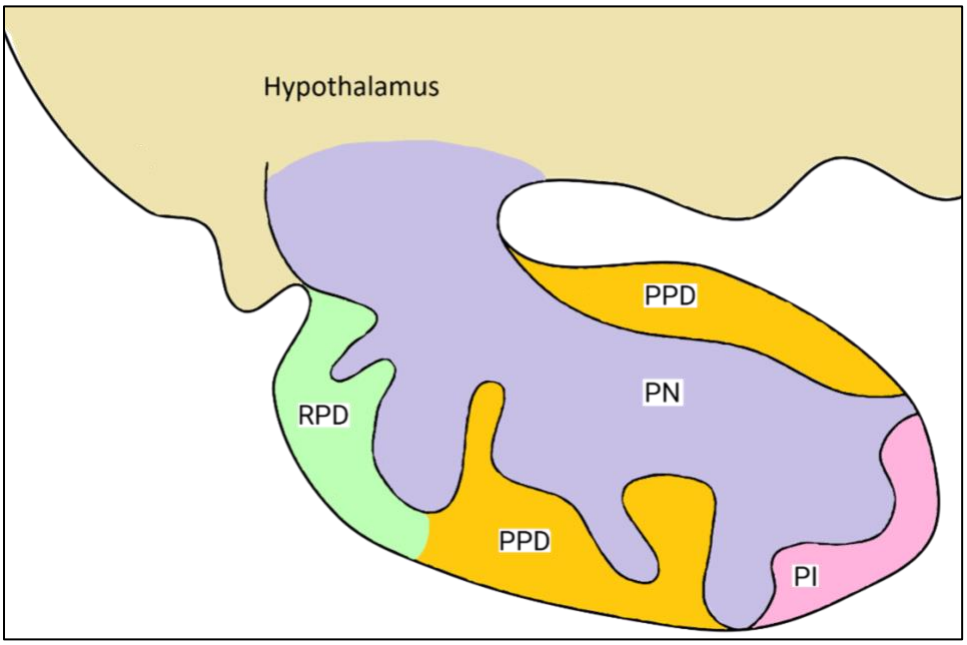

Figure 24. Schematic representation of teleost pituitary structure. PN- Pars nervosa, PI – Pars intermedia, PPD- Proximal pars distalis, RPD- Rostral pars distalis. (Created in Biorender.com)

These pituitary hormones are proteins and neuropeptides that travel through the bloodstream to various tissues and endocrine organs, where they regulate a wide variety of physiological processes. Measuring and profiling these proteins are crucial to identifying the regulatory processes and diagnosing the pituitary condition in the absence of the *scg2* genes. Several proteomics and peptidomics studies have been conducted on human and other mammalian pituitary glands; however, no studies on the zebrafish pituitary proteome have been performed except one from our lab (Lu et al., 2023). One study of a lobe-specific pituitary proteome in humans documented 4090 proteins with isoforms, mostly mapped into chromosomes 1, 2, and 11. About 1446 differentially expressed significant proteins were identified from human pituitaries (Banerjee et al., 2022). Single-cell RNA sequencing (scRNA-seq) has been employed to map the cellular diversity of the adult mouse pituitary, and there are few reports of mouse pituitary proteomics as well (Tsukada et al., 2019; Yang et al., 2024; De Vriendt et al., 2025; Ho et al., 2020).

In small teleost models such as zebrafish and medaka, pituitary size is minute, and researchers often have to pool multiple glands to obtain adequate material for molecular analyses

(Rahmad Royan et al., 2021; Teixeira et al., 2019). Even though there are not many proteome reports, there are several RNA-seq datasets for the zebrafish pituitary. The RNA-seq data for *gnrh3* null zebrafish pituitaries revealed a total number of 2194 cells in the WT sample, 4794 cells in the *gnrh3-/-* samples and 25,432 genes were detected in total (Tanaka et al., 2024). In medaka, gene expression profiles were generated through scRNA-seq, and 2,592 female, 3,804 male adult pituitary cells (*Oryzias latipes*) were profiled (Siddique et al., 2021).

Currently, the comprehensive analysis conducted by our lab is the only report of single-pituitary proteomics in zebrafish (Lu et al., 2023). The high-quality, high-performance liquid chromatography (HPLC) sorbents and LC-MS/MS technique used in that study permitted the simultaneous extraction of proteins and peptides from a single pituitary gland (Lu et al., 2023). Analysis of the data revealed a total of 1758 proteins in the WT zebrafish single pituitary samples, including Lhb, Oxt, Avp, Gh1, Pomc and several other key proteins and peptides (Lu et al., 2023). Here, we utilized the above method with a few improvements and modifications to characterize and compare proteins in the *scg2a-/-; scg2b-/-* DKO female and sibling WT female pituitaries.

5.3 Materials and Methods

5.3.1 Experimental animals

Wildtype (WT) zebrafish were sourced from an in-house stock at the University of Ottawa (uOttawa Wild type), bred and raised according to standard husbandry procedures. Fish were maintained in 10-L tanks of dechlorinated City of Ottawa tap water at a density of 5fish/L in a recirculating system (Techniplast, Montréal, QC, Canada) at 28 ° C on a 14:10 light-dark cycle. Fish were fed once or twice daily with GEMMA zebrafish diets (Skretting, Vancouver, BC, Canada) according to embryonic larval and adult life stages. All experiments were conducted following animal care guidelines provided by the Canadian Council on Animal Care and with prior approval from the University of Ottawa Animal Care Committee.

5.3.2 Pituitary structure observations

Previously sectioned and observed WT pituitaries were compared visually with the *scg2a-/-; scg2b* DKO female pituitary sections under DAPI nuclear staining. For the H&E staining, 9-month-old sibling WT and DKO female heads were fixed in 4% paraformaldehyde, decalcified in 0.5 M EDTA for 5-7 days, and embedded in paraffin following standard protocols. The next day, samples were embedded, sectioned (8 μm) using a Microm HM350 micrometer (Heidelberg,

Germany), and mounted on Superfrost™ Plus slides (Fisherbrand, cat#12-550-15). The H & E staining and scanning were performed by the Louise Pelletier Histology Core, University of Ottawa (https://www.uottawa.ca/research-innovation/histology).

5.3.3 Tissue collection and protein/peptide extraction

Single pituitaries of WT and *scg2a-/-; scg2b-/-* DKO female fish at 8-month age were dissected at 2:00 p.m. This time point is outside the ovulation time, targeting the assessment of the general protein status of the pituitaries. Proteins were extracted using a method developed by Dr. Chunyu Lu from our lab (Lu et al., 2023). After the extraction of the proteins, each sample was quantified for its total protein content using the Bicinchoninic Acid Protein assay (BAC) with Pierce BCA Protein Assay Kit (Thermo-fisher). Dried protein pellets and the peptides from the tissue homogenates were solubilized in 200 µL digestion buffer. Dithiothreitol was added to a final concentration of 10 mM and incubated at room temperature for 1 hr for reduction. Iodoacetamide was added to a final concentration of 20 mM and incubated at room temperature for 40 min in dark for alkylation. In the end, the protein sample was diluted 5-fold by 50 mM ammonium bicarbonate and digested by 1 µg trypsin (Worthington-biochemical, cat. no. LS02120) per 20 µg of protein overnight at room temperature, followed by a Solid Phase extraction (Lu et al., 2023).

For untargeted proteomics, a nano-flow HPLC system coupled with a Thermofisher LTQ-Orbitrap mass spectrometer was used. Briefly, a Dionex Ultimate RS3000 was connected to an Exploris 480 mass spectrometer (ThermoFisher Scientific, San Jose, CA) and operated with a nano-electrospray interface in positive ion mode. The solvent system consisted of buffer A (0.1% FA in water) and buffer B (0.1% FA in 80% acetonitrile). Reconstituted peptides resulting from enzymatic digestion were loaded on a 75 µm I.D. × 150 mm fused silica analytical column packed in-house with 3 µm ReproSil-Pur C18 beads (100 Å; Dr. Maisch GmbH, Ammerbuch, Germany). The flow rate was set to 300 nL/min, and the gradient was set as 5–35% buffer B in 30 min. The spray voltage was set to 2.2 kV, and the temperature of the heated capillary was 275°C. One full MS scan from 350 to 1200 m/z was followed by a data-dependent MS/MS scan of the 15 most intense ions with a dynamic exclusion repeat count of 1 in 20 seconds. The mass resolution was 60,000 for MS1 and 15,000 for MS2. Real-time internal calibration by the lock mass of background ion 445.120025 was used. All data were recorded using Xcalibur software (ThermoFisher Scientific, San Jose, CA).

Quantification was performed using normalized LFQ intensity. The peak lists of the raw files were processed and analyzed using MaxQuant software (Version 1.6.17.0) (ref: PMID: 19029910) against the zebrafish fasta downloaded from Uniprot (uniprot-taxonomy_7955), along with the built-in contaminant sequences. Cysteine carbamidomethylation was selected as a fixed modification; the methionine oxidation, protein N-terminal acetylation and ubiquitination were set for variable modification. Enzyme specificity was set to trypsin, not allowing for cleavage N-terminal to proline. Other parameters were used as default. The maxLFQ algorithm was used for quantification. The acquired MS/MS spectra were searched against the zebrafish protein database using MaxQuant with the label-free quantitation (LFQ) option. The false discovery rate (FDR) was set to ≤ 1% on both protein and peptide levels.

5.3.4 Data analysis and statistics

Data analysis was performed in collaboration with Dr. Chunyu Lu using an in-house Python script. Pandas' library (https://pandas.pydata.org/) was employed for basic functions. Data cleanup started with grouping the three *scg2a-/-; scg2b-/-* DKO samples as treatment, and the three WT samples as control. The LFQ intensity columns were employed to represent the relative protein levels. Protein entries with MS/MS count zero and one or machine-only identifications were marked with a value of zero to reduce false positives. Proteins were retained only if they contained at least two non-zero values in at least one group, followed by imputation of missing values by zero to maintain dataset integrity. The LFQ intensity values were log2-transformed to stabilize variance and approximate normality, while zero values were unchanged.

To assess the normality of the proteomics data observed between the DKO and WT groups, the Shapiro-Wilk test was used, and based on that, if the data were normally distributed, t-tests were applied, and if the data were not normally distributed, Mann-Whitney U tests were used. Differentially expressed proteins were identified by raw p-values indicating statistical significance, and where the absolute log2 fold change is more than 1.5 (a likely biologically relevant cutoff).

The volcano plots (Figure 26) are generated using the identified differentially expressed proteins and their fold changes. This statistical approach enables the identification of proteins with significant changes in abundance between the female DKO pituitary at 2.00 p.m. (KO_1400) and female WT pituitary at 2.00 p.m. (WT_1400) samples, providing insights into the biological impact of the conditions studied.

Functional enrichment and Gene Ontology (GO) Analysis were performed using Fisher's exact test. It was evaluated against a background set of detected proteins, and significance was determined based on the overrepresentation of GO terms among differentially expressed proteins. GO annotations were sourced from the official Gene Ontology database of human genes and loaded using custom functions. The KEGG pathway enrichment was performed by mapping identified proteins to KEGG zebrafish gene IDs using local mapping files such as ZFIN. Gene name variants were generated to improve match accuracy. Fisher's exact test was used to identify enriched pathways among the compared proteins. The significantly dysregulated protein IDs in the *scg2a-/-; scg2b-/-* DKO female pituitaries were converted to KEGG ID for the KEGG mapper tool to visualize these proteins on zebrafish pathway maps (https://www.genome.jp/kegg/mapper/color.html). five downregulated proteins for oxidative phosphorylation - respiratory chain complex 1 (map ID: dre00190- Figure 29), and two downregulated proteins in Arachidonic acid (AA) metabolism (map ID: dre00590- Figure 30) in zebrafish, are included here.

5.4 Results

5.4.1 Pituitary shape altered in the *scg2a-/-; scg2b-/-* DKO females

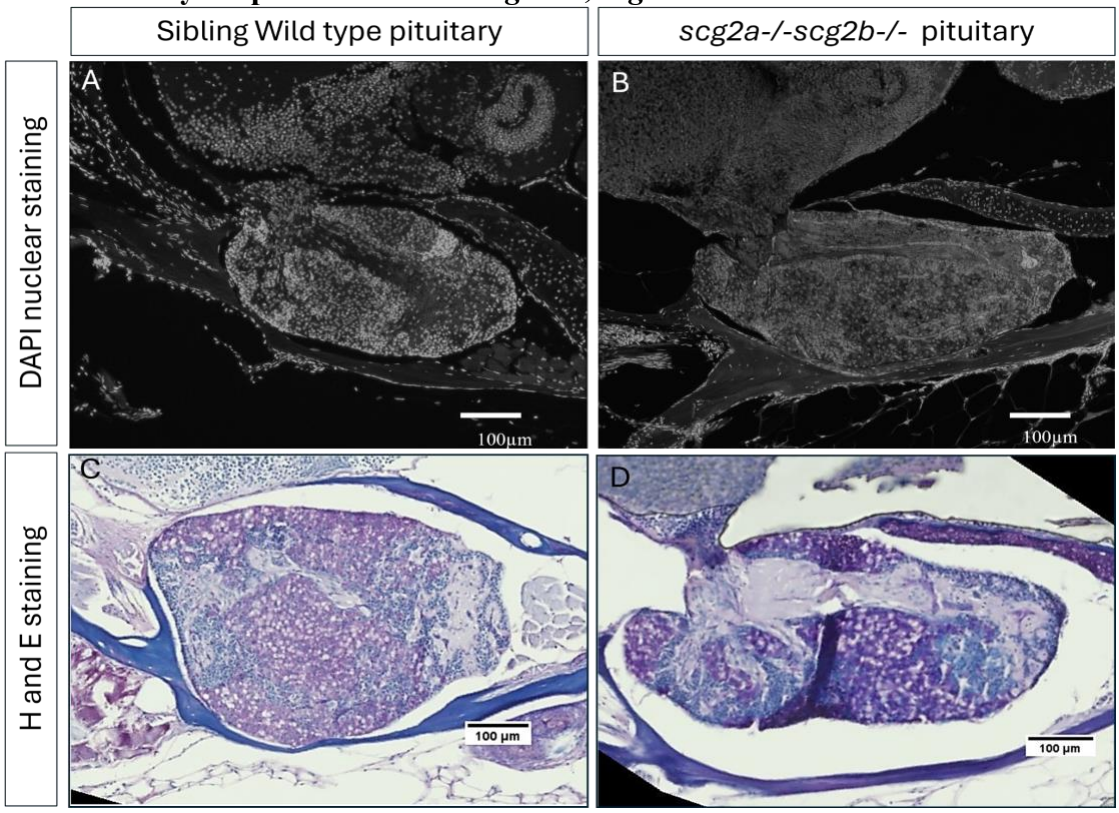

Figure 25. Comparison of pituitaries of WT and *scg2a-/-; scg2b-/-* DKO specimens. The top row shows DAPI nuclear staining of 8 µm paraffin sections of zebrafish pituitary tissue. (A) wild-type pituitary with normal cellular distribution, (B) *scg2a-/-; scg2b-/-* DKO pituitary, revealing altered architecture and a bump-like structure. The bottom row displays corresponding H and E-stained sections, (C) with the WT pituitary, (D) DKO pituitary, highlighting the histological changes induced by *sscg2a-/-,scg2b-/* deletions. Scale bars = 100 µm

5.4.2 Pituitary protein expression altered in the *scg2a-/-; scg2b-/-* DKO females

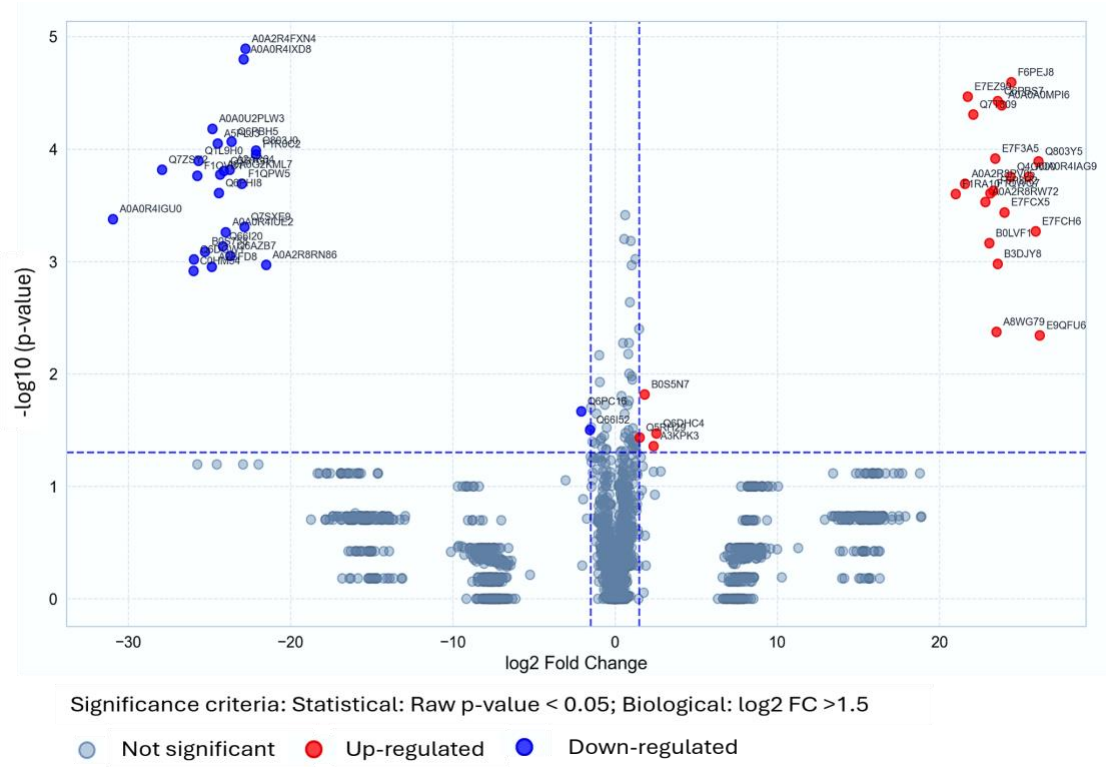

Figure 26: The volcano plot of the proteomics data comparison between WT siblings and *scg2a-/-; scg2b-/-* DKO female single pituitaries at 2.00 p.m. The horizontal coordinate is the difference multiple (logarithmic transformation at the base of 2), and the vertical coordinate is the significant difference p-value (logarithmic transformation at the base of 10). Red dots represent the expression profiles of 24 significantly upregulated proteins showing an absolute fold change > 1.5 in their relative abundance in *scg2a-/-; scg2b-/-* DKO female pituitaries. Blue dots represent the expression profiles of 27 significantly down-regulated proteins showing an absolute fold change > 1.5 in their relative abundance in *scg2a-/-; scg2b-/-* DKO female pituitaries. Gray dots represent non-dysregulated proteins between the groups. Comparison of pituitary proteins of WT and *scg2a-/-; scg2b-/-* DKO at 2.00 p.m. (FDR p<0.05), N=3.

	Protein ID	Gene name	Fold change	Raw P value	Functional annotation	Pathway/process
1	A0A0R4IGU0	Cnn1b	-30.9	0.0004	Thin filament-associated protein	Regulation and modulation of smooth muscle contraction. Predicted to enable actin filament binding activity and organization.
2	Q7ZSY2	mdh1ab	-27.9	0.0002	Malate dehydrogenase enzyme involved in the TCA cycle for energy production.	TCA cycle and cellular energy metabolism pathways.
3	C0HM54	Scg2a	-26.0	0.0012	Neuroendocrine protein of the granin family	Required for normal courting behavior and spawning in zebrafish
4	Q6DGW1	26-29kD-proteinase	-26.0	0.0010	Protease enzyme	Proteasome-mediated protein degradation pathways.
5	F1QVB1	ptgr1	-25.7	0.0002	Prostaglandin reductase involved in lipid metabolism and inflammation regulation.	Lipid metabolism and inflammatory response pathways.
6	Q1L9H0	cd9b	-25.7	0.0001	CD9 antigen, a tetraspanin.	Cell adhesion, migration, and immune signaling pathways.
7	B0S758	ttna	-25.3	0.0008	Titin, a giant muscle protein	Muscle contraction and sarcomere organization pathways.
8	A2BFD8	thy1	-24.9	0.0011	Cell surface glycoprotein	Neuronal signaling and immune response pathways
9	A0A0U2PLW3	ND5;mt-nd5	-24.8	0.0001	NADH dehydrogenase subunit 5	Mitochondrial electron transport chain, Oxidative phosphorylation pathway
10	A5PLJ3	zgc:165653	-24.5	0.0001	unknown	unknown
11	Q6PHI8	tktb	-24.4	0.0002	Transketolase enzyme involved in the pentose phosphate pathway for nucleotide biosynthesis.	Pentose phosphate pathway and carbohydrate metabolism pathways.
12	A0A0G2KML7	Unknown	-24.3	0.0002	Unknown	Unknown
13	Q66I20	serpinf1	-24.2	0.0007	Serpin family protein	Angiogenesis inhibition, tissue remodeling, fatty inflammation
14	Q3B7G1	ndufb5	-24.1	0.0002	NADH Dehydrogenase [Ubiquinone] 1 Beta Subcomplex Subunit 5. essential for mitochondrial electron transport chain function.	Oxidative phosphorylation pathway.
15	A0A0R4IUE2	unknown	-24.0	0.0005	Unknown	Unknown
16	A2AR64	rca2.1	-23.8	0.0002	Regulator of complement activation group 2 gene 1	Complement System Regulation and Immune Response
17	Q6AZB7	fhl2a	-23.7	0.0009	Fumarate hydratase enzyme	TCA cycle and cellular energy metabolism pathways.
18	Q6PBH5	ndufa4	-23.6	0.0001	NADH dehydrogenase subunit 4, part of mitochondrial complex I for ATP production.	Oxidative phosphorylation pathway.
19	F1QPW5	si:ch211-214p13.3	-23.0	0.0002	nectin-3-like protein	cell adhesion molecule, cell movement, proliferation, differentiation, polarization and survival
20	A0A0R4IXD8	dync1i2b	-22.9	0.0000	Dynein, cytoplasmic 1, intermediate chain 2a-like isoform X2	Critical for neurogenesis and homeostasis. Autosomal-recessive microcephaly syndrome
21	Q7SXE9	ndufa11	-22.8	0.0005	NADH dehydrogenase [ubiquinone] 1 alpha subcomplex subunit 11	NADH-ubiquinol reductase of the mitochondrial electron transport chain.
22	A0A2R4FXN4	elna	-22.8	0.0000	Elastin a	Extracellular matrix structural constituent
23	Q803J0	cyp2p6	-22.1	0.0001	Cytochrome P450 enzyme	Xenobiotic metabolism and steroid biosynthesis pathways.
24	F1R0C2	si:ch211-127i16.2	-22.1	0.0001	Unknown	Unknown
25	A0A2R8RN86	hspa12a	-21.5	0.0011	Heat shock protein family member	Protein folding and cellular stress response, adipocyte differentiation
26	Q6PC16	ndufb10	-2.1	0.0215	NADH dehydrogenase subunit B10, essential for mitochondrial electron transport chain function.	Oxidative phosphorylation pathway.
27	Q66I52	ndufs6	-1.6	0.0314	NADH Dehydrogenase (Ubiquinone) Fe-S Protein 6	The first enzyme complex in the electron transport chain of mitochondria. Oxidative phosphorylation pathway.

Table 5: List of significantly downregulated proteins (P<0.05, absolute Log2 fold change >1.5), their gene names, functional annotation and pathways in the WT siblings and *scg2a-/-; scg2b-/-* DKO female pituitaries at 2.00 p.m. N=3

	Protein ID	Gene name	Fold change	Raw P value	Functional annotation	Pathway/process
1	E9QFU6	histh1l3	26.2	0.0045	Histone H1-like	Predicted to enable double-stranded DNA binding activity and chromosome condensation
2	Q803Y5	krt15	26.1	0.0001	Keratin 15 a structural protein of epithelial cells involved in skin integrity	Cytoskeletal organization and epithelial tissue development pathways
3	E7FCH6	itih3a.2	25.9	0.0005	Inter-alpha-trypsin inhibitor heavy chain H3	May act as a carrier of hyaluronan in serum or as a binding protein between hyaluronan and other matrix protein, which are essential to cells undergoing biological processes
4	A0A0R4IAG9	unknown	25.5	0.0002	unknown	unknown
5	F6PEJ8	si:ch211-74m13.1	24.4	0.0000	Intercellular adhesion molecule 1 isoform X2. A cell surface glycoprotein and an adhesion receptor	Regulate leukocyte recruitment from circulation to sites of inflammation, driving inflammatory response.
6	Q4G000	ubqln4	24.4	0.0002	Ataxin-1 ubiquitin-like interacting protein	May function in the formation and regulation of multimeric protein complexes within the nucleus
7	E7FCX5	dmtn	24.0	0.0004	Dematin isoform X1	Cytoskeletal dynamics and adhesion pathways
8	A0A0A0MPI6	c1ql1	23.8	0.0000	complement C1q like 1. An ortholog of human *C1QL3* (complement C1q like 3) comes from the same gene family as *C1Q* (complement C1q).	*C1Q* expression in macrophages has been implicated in the functional process of eliminating apoptotic cells
9	Q6PBS7	pcmtl	23.6	0.0000	Protein-L-isoaspartate O-methyltransferase. Protein repair enzyme involved in methylation of damaged proteins	Protein repair and cellular stress response pathways
10	B3DJY8	ifi44fl	23.6	0.0010	Interferon-induced protein 44fl	play a significant role in the immune response to autoimmune disease
11	A8WG79	jac7	23.5	0.0042	Jacalin 7	Jacalin-related lectins are a type of carbohydrate-binding proteins
12	E7F3A5	cd68	23.4	0.0001	Macrosialin	Inflammation and immunity.
13	F6P8R2	osbp	23.3	0.0002	Oxysterol-binding protein	Present at membrane contact sites and act as either lipid transporters or sensors controlling lipid metabolism, cell signaling, and vesicle transport.
14	B1H1I1	cbln13	23.1	0.0002	cerebellin 13, synaptic organization protein involved in neuronal signaling	Synapse formation and neuronal morphogenesis pathways
15	B0LVF1	hspg2	23.1	0.0007	Heparan sulfate proteoglycan involved in extracellular matrix organization	Extracellular matrix regulation, cartilage development, and cell signaling pathways
16	F1QJT6	stau2	22.8	0.0003	RNA-binding protein involved in mRNA transport and localization	mRNA processing, localization, and cell cycle regulation pathways
17	Q7T309	serpinb1l3	22.1	0.0000	Serpin family protein involved in chaperone activity during stress response	Protein folding and stress response pathways
18	E7EZ90	thop1	21.7	0.0000	Thimet oligopeptidase is involved in peptide metabolism	Proteasome-mediated peptide processing pathways
19	A0A2R8PV05	si:dkey-78l4.6;si:dkey-78l4.11	21.6	0.0002	Potentially linked to embryogenesis based on zebrafish transcriptomic analysis	Embryogenesis and organ development pathways
20	F1RA10	glsb	21.0	0.0003	Novel glutaminase	Unknown
21	Q6DHC4	bfb	2.5	0.0338	Complement component bfb	Immune response
22	A3KPK3	si:dkey-21e2.10	2.4	0.0438	si:dkey-21e2.10	Predicted to be involved in protein maturation.
23	Q08CI5	blvra	1.8	0.0152	Biliverdin reductase A associated with antioxidant defense mechanisms	Predicted to be involved in heme catabolic processes and oxidative stress response pathways
24	Q5RH29	itih2	1.5	0.0368	Inter-alpha-trypsin inhibitor heavy chain 2, involved in extracellular matrix stability	Extracellular matrix stability and inflammatory response pathways

Table 6: List of significantly upregulated proteins (P<0.05, absolute Log2 fold change >1.5), their gene names, functional annotation and pathways in the WT siblings and *scg2a-/-; scg2b-/-* DKO female pituitaries at 2.00 p.m. N=3

According to the analysis, 51 proteins were differentially expressed in the *scg2a-/-; scg2b-/-* DKO female pituitary, out of 3674 total identified proteins (Figure 26). Out of these 51 proteins, 27 were downregulated (Table 5). There were 24 significantly upregulated proteins (Table 6) in DKO pituitaries compared to WT.

Protein IDs	Gene names	Protein names	Mean DKO	Mean WT	log2 Fold Change	Test Used	Raw p-value
H2A0A0	lhb	Lutenizing hormone subunit beta	30.61	30.70	-0.0832	t-test	0.9457
Q6QMG0	fshb	Follicle stimulating hormone subunit beta	15.74	14.91	0.8227	t-test	0.9435
Q6QX43	cga	gonadotropin alpha subunit	30.45	30.91	-0.4665	t-test	0.7526
Q801K4	tshba	Thyroid stimulating hormone subunit beta a	26.04	26.27	-0.2258	t-test	0.8811
A3KQQ9	scg3	Secretogranin-3	28.13	28.53	-0.3984	Mann-Whitney U	1.0000
Q5XJX1	scgn	Secretagogin	14.90	15.69	-0.7932	Mann-Whitney U	0.5066
Q8AV79	avp	Arginine vasopressin	15.66	8.13	7.5323	Mann-Whitney U	1.0000
F1QC27	oxt	Oxitocin	17.99	16.54	1.4546	Mann-Whitney U	0.5066
Q8UUT8	oxt	Oxitocin	27.11	26.15	0.9631	t-test	0.3959
Q1JQ34	gh1	Growth hormone 1	29.13	29.66	-0.5305	t-test	0.7471
F1R0Y2	prl	Prolactin	27.84	27.93	-0.0874	t-test	0.9448

Table 7: List of proteins, their gene names, mean intensity, absolute log2 fold change and p values for the WT siblings and *scg2a-/-; scg2b-/-* DKO female pituitaries at 2.00 p.m. N=3

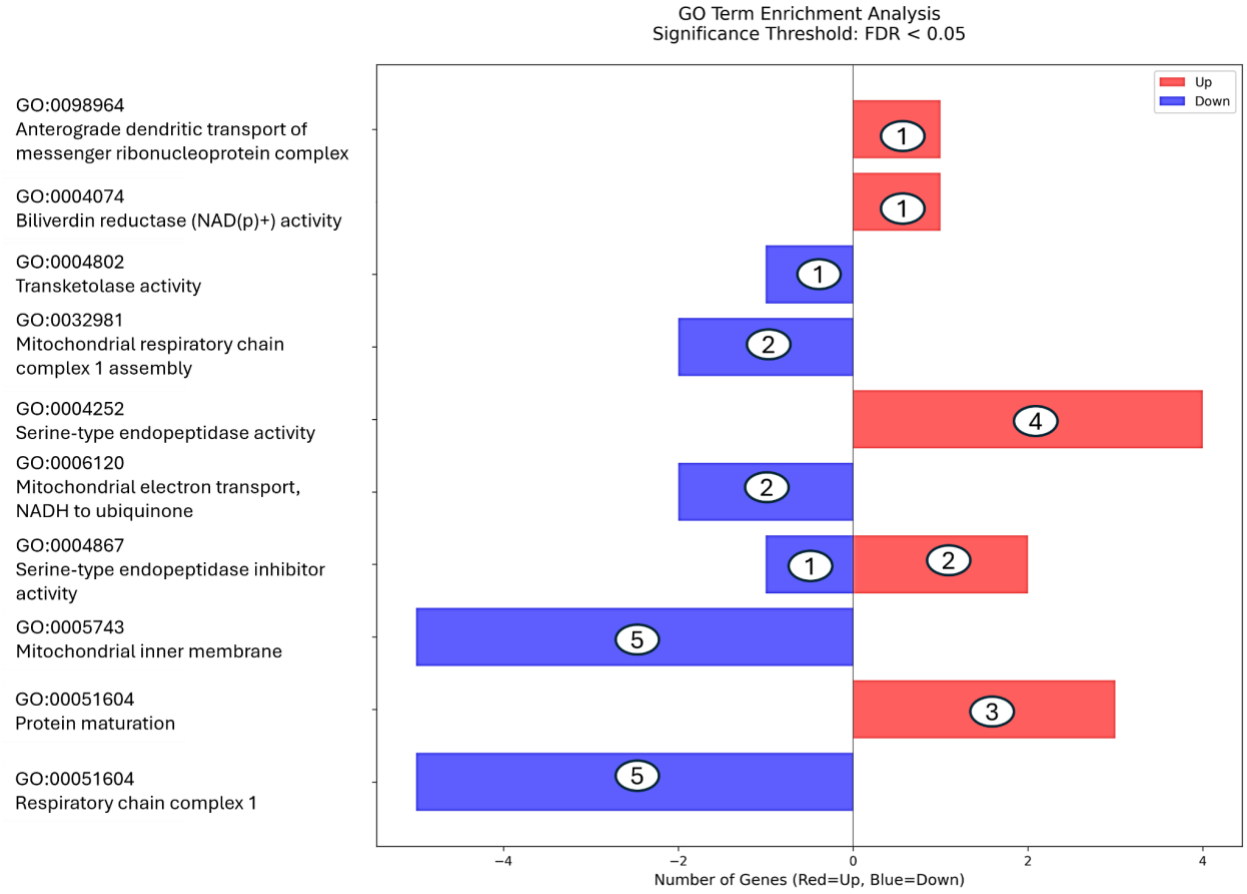

Figure 27: Gene ontology (GO) enrichment analysis of the corresponding differentially expressed proteins and GO enriched terms with FDR<0.05 in the *scg2a-/-; scg2b-/-* DKO female single pituitaries at 2.00 p.m. Red bars represent the upregulated, and blue bars represent the downregulated GO terms in each pathway. The number on each bar represents the number of differentially expressed proteins in each pathway. N=3

According to the GO enrichment analysis (Figure 27), mitochondrial inner membrane (GO:0005743) and respiratory chain complex 1 (GO:0051604) are significantly downregulated, with five proteins each. Mitochondrial respiratory chain complex 1 assembly (GO:0032981) and mitochondrial electron transport from NADH to ubiquinone (GO:0006120) are downregulated by two proteins each. Transketolase activity (GO:0004802) and serine-type endopeptidase inhibitor activity (GO:0004867) are also downregulated with one protein each. The most significantly upregulated GO term is serine-type endopeptidase (GO:0004252) activity, with four proteins. Also, protein maturation (GO:0051604) is upregulated, with three significantly upregulated proteins. Anterograde dendritic transport of messenger ribonucleoprotein complex (GO:0098964) and biliverdin reductase activity (GO:0004074) are significantly upregulated, each with one

protein. Interestingly, serine-type endopeptidase inhibitor activity shows both up and downregulation, suggesting complex regulatory changes in protease activity. The *scg2* DKO in zebrafish pituitary glands leads to a significant disruption of mitochondrial function, particularly affecting respiratory chain complex I and related processes.

KEGG mapper identified 41 proteins out of the 51 dysregulated proteins (both up and downregulated) in zebrafish, and they were associated with 21 different pathways in zebrafish (Figure 28).

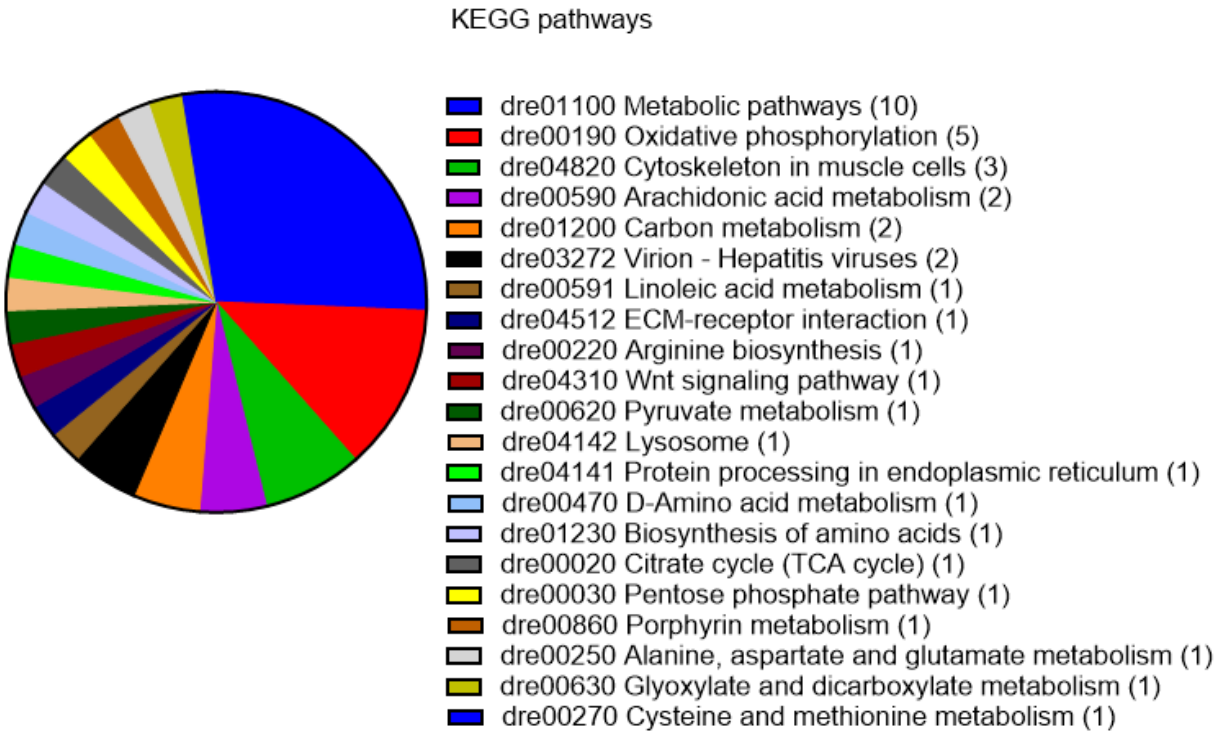

Figure 28: KEGG mapper-color tool visualization of the corresponding differentially expressed proteins with FDR<0.05 in the *scg2a-/-; scg2b-/-* DKO female single pituitaries at 2.00 p.m. The number on each bar represents the number of differentially expressed proteins in each pathway. N=3

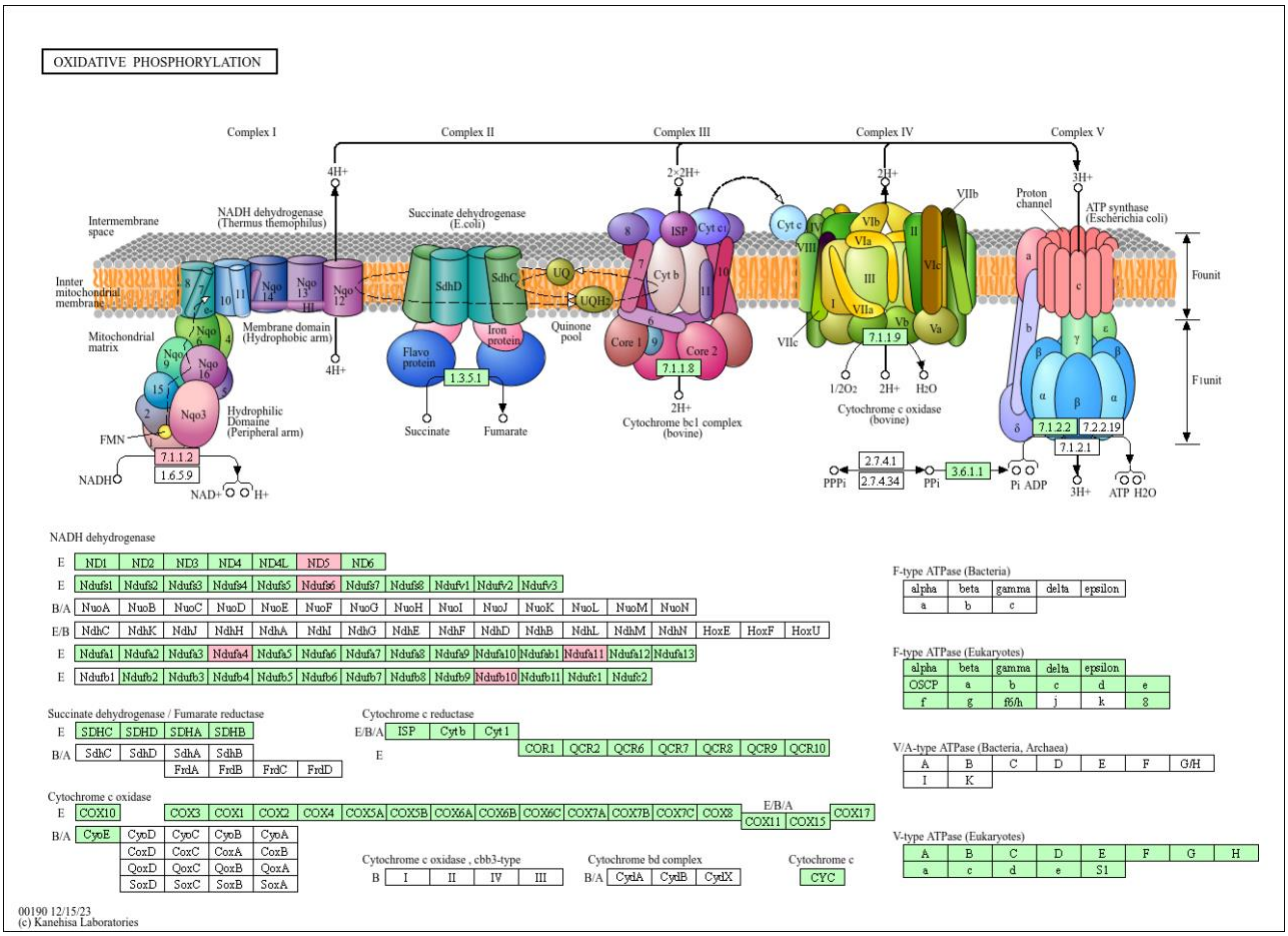

Figure 29: Oxidative phosphorylation pathway in zebrafish visualized using KEGG Mapper (map ID: dre00190). This pathway map illustrates the mitochondrial electron transport chain, encompassing Complexes I–V involved in oxidative phosphorylation. The diagram includes NADH dehydrogenase (Complex I), succinate dehydrogenase (Complex II), cytochrome bc1 complex (Complex III), cytochrome c oxidase (Complex IV), and ATP synthase (Complex V), along with associated subunits and cofactors. Five downregulated proteins (Ndufs6, Ndufa4, Ndufa11, Ndufb10, Nd5) identified in the present study are highlighted on the map in pink. The proteins commonly in the oxidative phosphorylation pathway in zebrafish are highlighted in green, and proteins that are in the pathway but non-orthologous to zebrafish are depicted in white. This map was generated using KEGG Mapper's "Color" tool, with zebrafish-specific proteins of interest mapped and colour-coded according to functional relevance.

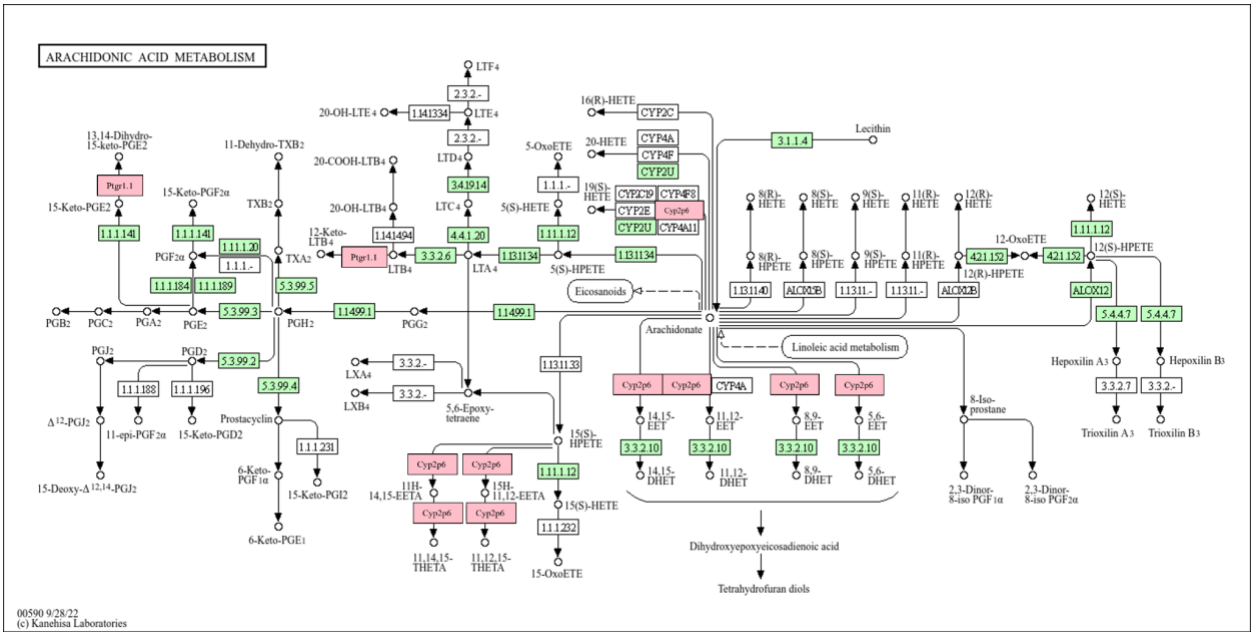

Figure 30. Arachidonic acid metabolism pathway in zebrafish visualized using KEGG Mapper (Map ID: dre00590). This map depicts the enzymatic conversion of arachidonic acid into various bioactive lipid mediators, including prostaglandins. Two downregulated proteins (prostaglandin reductase 1: Ptgr1.1, and cytochrome P450 2P6: Cyp2p6) are highlighted on the map in pink. The proteins commonly in the arachidonic acid metabolism pathway in zebrafish are highlighted in green, and proteins that are in the pathway but non-orthologous to zebrafish are depicted in white. This map was generated using KEGG Mapper's "Color" tool, with zebrafish-specific proteins of interest mapped and colour-coded according to functional relevance.

5.5 Discussion

To understand the molecular basis of structural abnormality of the pituitary in *scg2a -/-; scg2b -/-* double knockout (DKO) females, we performed a comparative proteomics study. Of the 3,674 proteins identified, 51 showed differential expression, with 27 proteins significantly downregulated and 24 upregulated in the DKO group. As anticipated, Scg2a and Scg2b were not present in DKO pituitaries, thus confirming the knockout. Interestingly, despite the observed structural alterations, there were no significant differences in reproductive hormone proteins such as Lhb, Fshb, Cga, Tshb, Gh1, Avp, and Oxt at 2.00 p.m.

According to the GO term analysis, five corresponding proteins were downregulated in the respiratory chain complex, and five more were downregulated in the mitochondrial inner membrane, suggesting a potential reduction in energy homeostasis. Moreover, mitochondrial electron transport and mitochondrial respiratory chain complex pathways were also

downregulated, each represented by two proteins. Mitochondrial complex I dysfunction is known to increase oxidative stress through elevated reactive oxygen species (ROS) production, which can trigger apoptotic pathways and disrupt calcium signalling, both critical for proper pituitary function (Sharma et al., 2009). Mitochondrial dynamics are strongly linked to mitochondrial dysfunction and are involved in numerous biological processes. Multi-omics research has demonstrated that signalling pathways associated with mitochondrial dysfunction, oxidative stress, and cell cycle dysregulation are present in human pituitary adenomas (Li & Zhan, 2019).

In addition, the serine-type endopeptidase activity pathway was enriched with four proteins, while within the serine-type endopeptidase inhibitor pathway, two proteins were upregulated and one was downregulated. The protein maturation pathway was also enriched by three proteins. Serine-type endopeptidases are a class of enzymes that utilize a serine residue in their active site to hydrolyze peptide bonds. In the pituitary gland, these enzymes are essential for processing prohormones into active hormones, a process necessary for proper endocrine function (Hill et al., 2002; Hook et al., 2008). Together, these findings suggest that protein processing and regulatory mechanisms are active in the pituitary gland under the analyzed condition. However, it is important to note that GO annotations were derived by mapping zebrafish proteins to their corresponding human orthologs using the official GO database, and therefore, functional interpretations should be made cautiously, acknowledging potential species-specific differences.

Among the significantly downregulated proteins, prostaglandin reductase 1 (protein ID: F1QVB1, gene: *ptgr1*) is involved in prostaglandin metabolism, catalyzing the reduction of keto-prostaglandins (Lee et al., 2018). Prostaglandin reductase 1 is an enzyme that inactivates prostaglandin E2 (PGE2) and prostaglandin F2α (PGF2α) (Wang et al., 2021). Downregulation of Ptgr1 could cause a buildup of PGE2, leading to increased prostaglandin signalling in the pituitary. Prostaglandins can selectively influence the synthesis and secretion of various pituitary hormones, acting directly at the pituitary and through hypothalamic mediation (Shewchuk, 2014). Expression of *ptgr1* is elevated in zebrafish female brains compared to males, and 17α-methyltestoterone (anabolic steroid- MT) treatment downregulates the expression of the prostaglandin genes PGE2 in zebrafish (Lee et al., 2018). They strongly suggest that prostaglandins are crucial for the activation of female spawning behaviour and that they can be produced locally in the brain. Estrogens are reported to upregulate the expression of PGE2 synthase (Frasor et al., 2003; Frasor

et al., 2008). During ovulation, PGF2α is transported to the brain via the bloodstream, where it triggers the female oviposition in goldfish (Stacey & Peter, 1979).

Cytochrome P450 (Cyp2p6) proteins are monooxygenases and catalyze many reactions involved in drug metabolism and synthesis of cholesterol, steroids and other lipids (Bertilsson et al., 2002). Cyp2p6 is downregulated in the *scg2a-/-; scg2b-/-* DKO female pituitary, suggesting defects in arachidonic acid metabolism pathways, cholesterol metabolism and possibly the steroidogenesis pathway. Additionally, studies of human genetic variants in Cyp2p6 indicate a role in pituitary function through its influence on dopaminergic and serotonergic signalling, which regulates prolactin secretion (Ozdemir et al., 2007; Peñas-Lledó et al., 2014). Note that a decrease in Cyp2p6 could lead to increased dopamine, which in many teleosts, including zebrafish, is a potent inhibitor of Lh release (Trudeau, 2022).

The KEGG mapper color tool identified Cyp2p6 and Pge2 proteins in the AA metabolism pathway. Arachidonic acid is released from cell membrane phospholipids by cytosolic phospholipase A2 (cPLA2) and is metabolized into various compounds mainly through the cyclooxygenase (COX), lipoxygenase (LOX), and cytochrome P450 (CYP-450) pathways. The metabolites of arachidonic acid are reported to be crucial for determining cell fates like proliferation, differentiation, and apoptosis. Some suggest that AA and its metabolites play significant roles in organ development and various diseases, including cardiovascular, kidney, liver, and skeletal development, as well as diabetes, obesity, and cancers in humans (Zhang et al., 2023).

Heat shock protein Hspa12a (Protein ID: A0A2R8RN86, gene: *hspa12A*) is also significantly downregulated in *scg2a-/-; scg2b-/-* DKO females. The specific role of Hspa12a in pituitary gland function is not directly addressed in the available research. However, Hspa12a belongs to the heat shock protein 70 (HSP70) family and is involved in cellular stress responses, ATP binding, and lactate metabolism (Wang et al., 2023). These mechanisms are critical for maintaining cellular homeostasis, which could indirectly support pituitary hormone synthesis or secretion. It is also required for adipocyte differentiation and diet-induced obesity in mice (Zhang et al., 2019). The knockout of HSPA12A (Hspa12a-/-) in mice reduced weight gain, adiposity, hyperlipidemia, and hyperglycemia from a high-fat diet (HFD) compared to their WT counterparts. Hspa12a-/- mice also exhibited improved insulin sensitivity relative to WT mice (Zhang et al.,

2019). However, further studies are needed to confirm the disruption in steroidogenesis and lipid metabolism, including steroid profiling and comparison of these DKO fish.

Most of the proteins are significantly downregulated in the mitochondrial Krebs cycle (TCA) and related to energy metabolism. For example, the malate dehydrogenase (Protein ID: Q 7ZSY2, gene: *mdh1tab*) enzyme reversibly catalyzes the oxidation of malate to oxaloacetate using the reduction of nicotinamide adenine dinucleotide **(**NAD+) to NADH and is an essential protein in the oxidative pathway. Also, they are involved in various metabolic processes such as gluconeogenesis and lipogenesis (Labrou & Clonis, 1997; Takahashi-Íñiguez et al., 2016). This protein ID was mapped in the carbon metabolism pathway, in KEGG mapper (dre01200), Glyoxylate and dicarboxylate metabolism (dre00630) and Cysteine and methionine metabolism (dre00270). Other key proteins were downregulated as well, such as fumarate hydratase (protein ID: Q6AZB7, gene: *fhl2a*) and NADH dehydrogenase subunits (Ndufb5, Ndufa4, Ndufa11, Ndufb10, Nd5; Mt-nd5), which are integral components of the mitochondrial electron transport chain (Figure 29), affecting oxidative phosphorylation and energy metabolism. They were identified in the zebrafish KEGG maps related to metabolic pathways (dre01100) as well. This downregulation suggests a reduction in the energy metabolism of the pituitary gland in the DKO females, which needs further investigation.

Moreover, there are few proteins related to cell adhesion, migration, and immune cell signalling that are downregulated (Protein ID: Q1L9H0, gene: *cd9b*) (Reyes et al., 2018), and neuronal signaling, cell differentiation, regeneration and immune responses (Protein ID: A2BFD8, gene: *thy1*) (Yang et al., 2020). Angiogenesis inhibition and tissue remodelling related Serpin family protein F1 (Protein ID: Q66I20, gene: *serpinf1*) is downregulated as well, which could be an indication of issues in pituitary blood vessel formation. In vivo experiments showed that *scg2b* TALEN mutants exhibit transiently impaired central artery development, and *scg2b* is crucial for neurovascular modelling in the larval zebrafish hindbrain (Tao et al., 2018). Serpins are among the most widely studied protease inhibitors (Chen et al., 2019; Yang et al., 2017). The biological function of Serpinf1 in fatty inflammation has been studied and reported in grass carp (Yang et al., 2017). Also, Serpin1 was identified in the Wnt signalling pathway (dre04310) in KEGG mapper.

Among the upregulated proteins, Keratin 15 (Protein ID: Q803Y5, gene: *krt15*) and Dematin isoform X1 (Protein ID: E7FCX5, gene: *dmtn*) are associated with cytoskeletal organization and cellular architecture. The specific function of dematin isoform X1 protein in the

pituitary has not been reported yet in zebrafish. Keratins, or cytokeratins, represent the primary epithelial-specific subgroup of intermediate filament proteins (Ku et al., 2016). Keratin-15 is also an epidermal biomarker in stem cells (Bose et al., 2013). Dematin is an actin-binding protein with a core domain and a headpiece domain (Chen et al., 2009). It functions upstream of RhoA (Ras homolog family member A), which is known to participate in cytoskeletal remodelling and regulates its activation. Dematin headpiece KO mouse models revealed a defect in stress fibre formation, membrane protrusions, cell motility, and cell adhesion (Mohseni & Chishti, 2008). Heparin sulfate proteoglycan is related to extracellular matrix and tissue remodelling (Protein ID: B0LVF1, gene: *hspg2*). Two inter-alpha-trypsin inhibitor proteins are upregulated in the *scg2a-/-;scg2b-/-* DKO female pituitaries. One is inter-alpha-trypsin inhibitor heavy chain 2 (Protein ID: Q5RH29, gene: *itih2*) heavy chain H3 (Protein ID: E7FCH6, gene: *itih3a.2*). Ithih2 is involved in extracellular matrix stability, and Ithih3a.2 is orthologous to human ITIH1, which is a protease inhibitor and predicted to enable serine-type endopeptidase inhibitor activity (Zhang et al., 2024). Inter-alpha-trypsin inhibitor family members interact with extracellular matrix molecules (ECM) and, most notably, hyaluronan, inhibit complement, and provide cell regulatory functions (Lord et al., 2020). One of the many functions of ITIH1 in mammals is that it binds directly to hyaluronic acid on skeletal muscle and adipose tissue surface, causing ECM stability and subsequent insulin resistance. Another report suggests that the increased ITIH1 may impact β-cell activity in mice, with a liver-specific deletion of the Gna13 gene (G protein α-13) (Zhang et al., 2024). With these proteins significantly upregulated, it is tempting to suggest that this contributed to structural remodelling or cell-type composition changes in the pituitary, potentially affecting hormone secretion and cell-to-cell communication. This could be a possible explanation for the structural abnormalities observed in the *scg2a-/-; scg2b-/-* DKO female pituitaries.

Some of the protein repair, folding, and stress response-related proteins are upregulated in the KO pituitaries. For example, protein L-isoaspartate O-methyltransferase (protein repair) (Protein ID: Q6PBS7, gene: *pcmtl*) is an enzyme that repairs by converting abnormal L-isoaspartyl residues back into normal L-aspartyl residues in proteins (Soliman et al., 2021). Zebrafish *pcmt* and *pcmtl* gene knockdown larvae exhibited morphological defects, reduced survival rates, and elevated isoaspartyl levels. There is significant disruption in brain calcium balance in these morphants (Soliman et al., 2021). Serpin family chaperone serpinb1l3 (Protein ID: Q7T309, gene: *serpinb1l3*) is another upregulated protein that regulates a programmed death pathway of NETosis

(neutrophil extracellular trap generation), initiated in mature neutrophils by pathogens and inflammatory mediators (Hou et al., 2015). Increased *SERPINB1* expression is frequently observed in tissues undergoing stress-induced remodelling or damage repair, including in the pancreas, lungs, and immune tissues in mice (Benarafa et al., 2011; Farley et al., 2012; Hou et al., 2015). Upregulated expression of Serpinb1l3 in the pituitary gland could be interpreted as an attempt to limit protease-mediated cell damage due to remodelling or structural reorganization, or a compensatory mechanism activation in the pituitary. Thimet oligopeptidase (Protein ID: E7EZ90, gene: *thop1*) is a zinc metalloendopeptidase involved in peptide metabolism. It hydrolyzes several key neuroendocrine and cardiovascular peptides that play roles in regulating both physiological and pathological conditions (Ferro et al., 2020; Liu et al., 2021). This enzyme was first detected in the bovine anterior pituitary in 1980 and was shown to be effective at cleaving Gnrh (Horsthemke & Bauer, 1980). It is reported to degrade several bioactive peptides apart from Gnrh and has a potential function of the metalloendopeptidase in neuropeptide metabolism in rat brain and testis (Liu et al., 2021; Orlowski et al., 1983, Orlowski et al., 1989). Upregulated Thop1 in the *scg2a-/- ; scg2b-/-* DKO pituitary could indicate a compensatory mechanism to maintain neuropeptide homeostasis in the absence of *scg2* genes. Given its role in degrading Gnrh and other bioactive peptides, increased Thop1 may reflect an adaptive response to altered peptide production or disrupted pituitary communication.

Cerebellin 13 (Protein ID: B1H1I1, gene: *cbln13*) is upregulated in the DKO pituitaries. Even though there is limited information regarding Clbn13, other family members of the Clb family, particularly cerebellin-1, function in synapse formation by binding to the presynaptic cell-adhesion neurexin molecules, and some suggest that other cerebellin isoforms may also have a similar function (Ghai et al., 2011). While some forms of cerebellin have been reported in the human pituitary (Satoh et al., 1997), its function there is unknown. In zebrafish larvae, serine/threonine kinase Akt/PKB (Akt*2*) KO was reported to have significantly lower *clbn13* mRNA, as a significant downregulation of *clbn13* in a transcriptome analysis (Zhang et al., 2017).

Double-stranded RNA-binding protein Staufen homolog 2 (Protein ID: F1QJT6, gene: *stau2*) is upregulated in the DKO pituitary. Staufen homolog 2 is a member of the family of double-stranded RNA (dsRNA)-binding proteins involved in the transport and/or localization of mRNAs to different subcellular compartments and/or organelles, so it could be involved in numerous critical processes. Zebrafish Staufen1 and Staufen2 are required for the survival and migration of

primordial germ cells, and Stau2 is important for the survival of neurons in the central nervous system (Ramasamy et al., 2006). When Stau1 and Stau2 functions are compromised in embryos injected with antisense morpholino-modified oligonucleotides, it alters the migration of primordial germ cells (PGCs) in zebrafish, and improperly migrated PGCs fail to survive in embryos with Stau deficiency (Ramasamy et al., 2006). In early zebrafish embryos, *stau2* expression is observed in periventricular neurons of the diencephalon and midbrain regions and auditory vesicles and is required for the survival of neurons in the central nervous system (Ramasamy et al., 2006).

Zebrafish oxysterol-binding protein (Protein ID: F6P8R2, gene: *osbp*) is orthologous to human OSBP and upregulated in the DKO pituitaries. In humans, it mediates lipid exchange between organelles at membrane contact sites, thereby regulating lipid dynamics and homeostasis (Lin et al., 2023). Some studies in mice demonstrate a significantly high expression of OSBP in liver triglycerides and show that it regulates hepatic triglyceride metabolism. They also suggest the involvement of OSBP in the insulin signalling pathways that control hepatic lipogenesis (Yan et al., 2007). Another upregulated protein is protein-L-isoaspartate O-methyltransferase (Protein ID: Q6PBS7, gene: *pcmtl*). It is regarded as a repair enzyme that begins the process of converting abnormal l-isoaspartyl residues back to normal l-aspartyl residues in proteins. Zebrafish homologous genes for PCMT are *pcmt* and *pcmtl*, found in the brain and testis tissues. Knockdown of both the *pcmt* and *pcmtl* genes reported morphological abnormalities, decreased survival, and altered brain calcium homeostasis in zebrafish (Soliman et al., 2021).

In conclusion, based on our data of the significantly dysregulated proteins in the *scg2a-/-; scg2b-/-* DKO female pituitary, we could predict a suppressed pituitary function, altered cellular reprogramming and a compensatory response activation. The *scg2* deletion appears to alter key proteins involved in hormone biosynthesis, peptide processing, and signalling, downregulate oxidative stress-related enzymes, and reduce the expression of proteins involved in ECM stability and structural integrity, shifting away from hormone production toward survival or structural adaptation.

Chapter 6: General discussion and conclusion

6.1 Overview of the thesis

Secretoneurin is a neuropeptide derived from the selective processing of the Scg2 precursor protein. It has been studied for over 20 years, and there is evidence for its reproductive role, particularly in Lh release (Chapter 1). However, there was a clear research gap regarding its role in spawning and ovulation. To address this and investigate further, we developed and extensively validated CRISPR-Cas9 KO models that completely lack both the *scg2a* and *scg2b* genes. In this thesis, we present evidence supporting the hypothesis that complete deletion of the *scg2* genes results in severe reproductive deficits because Scg2/SN is critical for normal pituitary and gonadal function in zebrafish.

6.2 Establishment of the *scg2* full gene KO

As the first objective, we developed *scg2a-/-, scg2b-/-* single KO lines and a *scg2a-/-; scg2b-/-* complete DKO line. The CRISPR-Cas9 gene editing technology successfully enabled the precise mutations and excision of the *scg2a* and *scg2b* genes from the zebrafish genome, which were validated at both the DNA and protein levels. By incorporating mass spectrometry into the validation process, we confirmed the absence of SN peptides in these KO lines. This extra validation step was crucial, as not all knockout lines passed the mass spectrometry assessment (Appendix A- Figure A1), despite some evidence for gene deletion at the DNA level. Furthermore, we developed a specific monoclonal antibody for SNb (Appendix A- Figure A3), and the immunohistochemistry visualization indicates that both SNa and SNb are located in key hypophysiotropic areas of the zebrafish pre optic area and pituitary (PN and PI) are co-expressed with Oxt.

6.3 The *scg2* full gene KO reduces spawning and affects reproduction.

We evaluated the morphological and reproductive phenotypes resulting from the complete loss of *scg2a* and *scg2b*. Sexually mature fish at 6 to 8 months of age were tested for their reproductive performance by allowing them to spawn over a 90-minute period in within-line pairwise matings. The spawning success rates for all *scg2a* and *scg2b* single KO and *scg2a-/-; scg2b-/-* DKO fish were reduced to 28%, 24%, and 16.6%, respectively, compared to the 64.5% rate recorded in WT siblings.

Detailed video analysis revealed that both *scg2a-/-* and *scg2b-/-* single KO males displayed a reduced number of quivers with their female counterparts, while the DKO fish exhibited an intermediate response. The time taken for the first spawning event (Time to first oviposition) was calculated from the side views of the video, and WT couples were spawning within a median time of 1.25 minutes. The *scg2b-/-* KO and DKO fish exhibited significant delay by media time of 45.96 minutes and 41.18 minutes, respectively. In contrast, *scg2a-/-* KO fish showed an intermediate effect, not significantly different from the WT.

The observed differences in the *scg2a-/-* and *scg2b-/-* single KO indicate a possible differential role between the *scg2a* and *scg2b* paralogues. Phylogenetic analysis reveals that in the common ancestor of teleost fishes, the duplication of the *scg2a* locus led to the formation of the *scg2b* locus, suggesting that SNa is the ancient, conserved peptide (Peng et al., 2025). The *in vivo* evidence in *scg2* TALEN mutants shows that *scg2b* plays a critical role in neurovascular modelling of the hindbrain in zebrafish (Tao et al., 2018). In the orange spotted grouper, they report that both SN peptides could stimulate *gnrh1, gnrh3, fshb and lhb*, but the *in vivo* effects of SNa were long-lasting compared to the SNb. There were some differences between *scg2a* and *scg2b* mRNA expression in different tissues, where only *scg2b* was detected in tissues such as liver, heart, and ovary (Shu et al., 2018). Also, we observe a differential distribution of SNa and SNb immunoreactivity in the zebrafish pituitary, where it partially co-localizes only in some cell populations and nerve terminals. The possibility of a neofunctionalization in the *scg2b* paralogue is worth exploring in the future.

Further analysis revealed that all the single KO and DKO fish have low fecundity, but embryo survival after 24 hours remained unchanged. In a subsequent breeding trial, when unspawned DKO females were paired with naïve WT males, they were not able to spawn at all. Thus, we investigated ovarian morphology in the *scg2a-/-; scg2b-/-* DKO females and tried to rescue the reproductive deficits. Histological analysis of the ovaries indicated a maturation defect in later-stage oocytes of DKO females, along with a significantly increased count of late-stage atresia, which explained the low fecundity levels. Moreover, *in vivo* injections of synthetic SNa and SNb peptides or hCG could not restore spawning. In the previous TALEN *scg2* mutants, Mitchell et al., (2020) reported that the intraperitoneal injection of SNa and hCG partially restored the spawning defects, but neither the SNa nor hCG injection altered the latency to quiver or rescue the quiver behaviour itself (Kimberly, 2018). This partial responsiveness in the TALEN mutants

was completely absent in the *scg2* DKO females, and they were less responsive to exogenous SN peptides and hCG. From this data, we speculate that there could be developmental level defects and other factors, resulting in reproductive dysfunction of the *scg2a-/-; scg2b-/-* DKO zebrafish.

To uncover the impact of the *scg2* deletion in the HPG axis, we measured mRNA levels of key neuropeptides and gonadotropins in *scg2a-/-; scg2b-/-* DKO zebrafish females using digital PCR across four different tissues. In the hypothalamus, *gnrh3* was significantly downregulated in DKO females before ovulation, and *gnrh2* was downregulated after ovulation. Expression of *oxt* was downregulated in DKO females at ovulation in both the telencephalon and the hypothalamus, and *avp* was time-dependent and fluctuated, where it was significantly high before ovulation and at ovulation, but significantly low at a basal level. Therefore, in the hypothalamus, reproductive genes were mostly downregulated in the absence of *scg2a* and *scg2b*.

The levels of *gnrhr2* were significantly downregulated in the *scg2a-/-; scg2b-/-* DKO pituitary before ovulation and at ovulation. The reduced *gnrhr2* levels in the pituitary correspond with the decreased expression of *gnrh2 and gnrh3* in the hypothalamus, suggesting that the *scg2* deletion has significantly influenced Gnrh signals at the hypothalamic and pituitary levels. Surprisingly, the gonadotrophin beta subunits (*lhb* and *fshb*) were upregulated before ovulation and at ovulation in the DKO pituitary, and the alpha subunit (*cga*) was downregulated at the times of ovulation and post-ovulation. This result was unexpected, especially given the *gnrh2/3* downregulations in the hypothalamus. Since *cga* was downregulated, we expected that the Lh and Fsh proteins would be significantly downregulated as well, but from the proteomics analysis at a different basal time point in the pituitary, Lh and Fsh and Cga proteins were not significantly altered in the DKO females. A speculation is that the negative feedback at the pituitary level, from the gonadal steroids, could be dysregulated or reduced, and that can cause an elevated Lh and Fsh. Another possibility is that since the Scg2 is part of the chromogranin/secretogranin family, this deletion could affect the peptide hormone processing and secretory granule formation/exocytosis, causing hormones to be accumulated internally (Courel et al., 2010). In contrast to this, one study of *scg2a* KO reports no overt changes in secretory granule packaging in a female-specific, sex steroid-responsive peptidergic (FeSP) neurons in medaka (Fleming et al., 2023).

Ovarian *lhcgr* and *star1* remained significantly downregulated in DKO females at all sampling timepoints. Despite the high *lhb* and *fshb* at the pituitary, this *lhcgr* downregulation was significant, and supports the speculation of gonadotrophin accumulation and reduced release in the

pituitary. Also, since *star1* is significantly reduced in the DKO animals, the steroidogenesis pathways could be affected, supporting the speculation of negative feedback disruption. Ovarian histology data from Chapter 3 support this gene expression data, which showed low oocyte maturation and high levels of late-stage atresia. However, *npr* and *pgrmc1* mRNA were not altered in the ovary. The *pgrmc2* and other downstream mRNA were not investigated, thus it needs to be explored in the future.

Another surprising observation is that pituitary morphology was abnormal in the *scg2a-/-; scg2b-/-* DKO females, having an elongated shape and a bump-like outgrowth in the rostral pars distalis from the sagittal view of the pituitary. To examine the pituitary at the protein level, we conducted a mass spectroscopy-based proteomics analysis using single pituitaries of the DKO females and compared them with WT at a basal timepoint at 2.00 p.m., outside the expected times of ovulatory hormone fluctuations. We were able to identify 3674 proteins and 51 were significantly dysregulated in the pituitary. As expected, Scg2a and Scg2b were absent in the DKO pituitaries, and this deregulation impacted key cellular functions such as protein maturation, mitochondrial respiratory chain and several other key pathways. Moreover, compensatory pathways were activated, and the extracellular matrix proteins were altered, indicating a pituitary level disruption.

6.4 Future directions

The findings presented in this thesis indicate that the *scg2a* and *scg2b* genes play a stimulatory role in regulating reproductive processes, but significant research gaps remain to be addressed. Some of these possible future directions include characterization of the *scg2a* and *scg2b* in the gonads. In this thesis, our focus was mainly on the female zebrafish and determining the role of *scg2* in the ovarian tissue. Thus, male gonadal development or other possible functions in male zebrafish should be explored in the future. Moreover, local immunoreactivity and expression of the SNa and SNb have not yet been characterized in ovary and testis, so characterization of the SN peptide distribution may provide some insight into their functions and sites of action. Despite extensive research, the SN receptor remains unidentified (Mitchell et al., 2020; Trudeau et al., 2012). Discovering the SN receptor would open new avenues of research, reveal all SN targets, their associated tissues, and functions.

Analysis of ovarian gene expression (Chapter 4) indicates that *lhcgr* and *star1* are downregulated in the *scg2a-/-; scg2b-/-* DKO ovaries. Since in zebrafish both Lh and Fsh can bind

to both *fshr* and *lhcgr*, expression of the *fshr* should be measured in the future. Downregulation of *star1* implies that steroidogenesis could be affected in these KO animals. However, the impact of full *scg2a/scg2b* gene deletion on steroidogenesis is still unknown. Future studies should focus on measuring steroids in the *scg2a-/-; scg2b-/-* DKO gonads and comparing them with WT. For this purpose, ovarian samples have been collected, and our laboratory is in the process of developing a new highly sensitive quantitative mass spectroscopy method to profile steroids in these KO fish. Analyzing steroid levels in the *scg2a-/-; scg2b-/-* DKO may reveal the impact of *scg2* deletion on steroidogenesis in zebrafish and potential disruption of feedback mechanisms at the hypothalamus and pituitary levels. It is noteworthy that SNa inhibits aromatase in the goldfish brain (Fonte et al., 2018). Surprisingly, *scg2a-/-; scg2b-/-* DKO females could not be rescued with SNa, SNb or hCG injections (Chapter 3). To investigate the effect of SNa and SNb synthetic peptides on final oocyte maturation *in vitro*, we conducted some promising preliminary experiments revealing modest stimulatory effects of SNa and SNb on germinal vesicle breakdown (Appendix B). However, the effect of the SNa or DHP on *scg2a-/-; scg2b-/-* DKO ovary has not yet been observed; thus, downstream of *lhcgr*, the effect of DHP should be explored.

We observed that the *scg2a-/-; scg2b-/-* DKO female pituitaries were histologically abnormal. In the future, abnormal growth of the *scg2* KO pituitaries should be investigated by whole pituitary observation methodologies and by evaluating the area/volume of each pituitary region over the developmental period. The proteomic analysis of *scg2a-/-; scg2b-/-* DKO female pituitaries (Chapter 5) indicates that only 51/3674 (~1.4%) identified proteins were altered. While several critical processes appear to be deregulated, rigorous testing is required to link them to the morphological and functional changes observed. To investigate further, a peptidomics/proteomics and transcriptomic analysis on both the pituitary and the ovary would provide the necessary details of the protein and peptide content in these KO fish and their impact on reproduction-related peptides. Also, it is worth exploring whether these KO fish have disrupted lipid metabolism that is associated with reproductive failure. Even though gene deletions were not lethal, the proteomics analysis shows that the full gene excision of the *scg2a* and *scg2b* had impacted several core cellular processes in the pituitary and possible compensation mechanisms and immune-related pathways are activated. Compensatory mechanisms could be masking the true impact of the role of SN in the reproduction-specific pathways. Thus, conditional, tissue-specific KO would be beneficial to further investigate the connection between SN and ovulation/spawning.

6.5 Concluding remarks

We completely deleted both paralogues of *scg2* from the zebrafish genome, creating a *scg2a-/-; scg2b-/-* complete DKO line. Based on the data presented in this thesis, we demonstrated that the complete deletion of *scg2* reduced reproductive success, reduced fecundity, decreased oocyte maturation (Chapter 3), and altered reproductive-related gene expression in the HPG axis (Chapter 4). Further investigation through proteomics (Chapter 5) revealed structural adaptations in the pituitary and key cellular pathways that are affected due to the gene deletions. The data presented provide evidence that *scg2* has a fundamental role in zebrafish and that its deletion alters the HPG axis, reduces reproduction, and impacts other cellular and molecular pathways. A new model is presented for the roles of Scg2/SN in reproduction (Figure 31). It is hoped that this can be the foundation for future investigation of the secretogranins and their derived peptides.

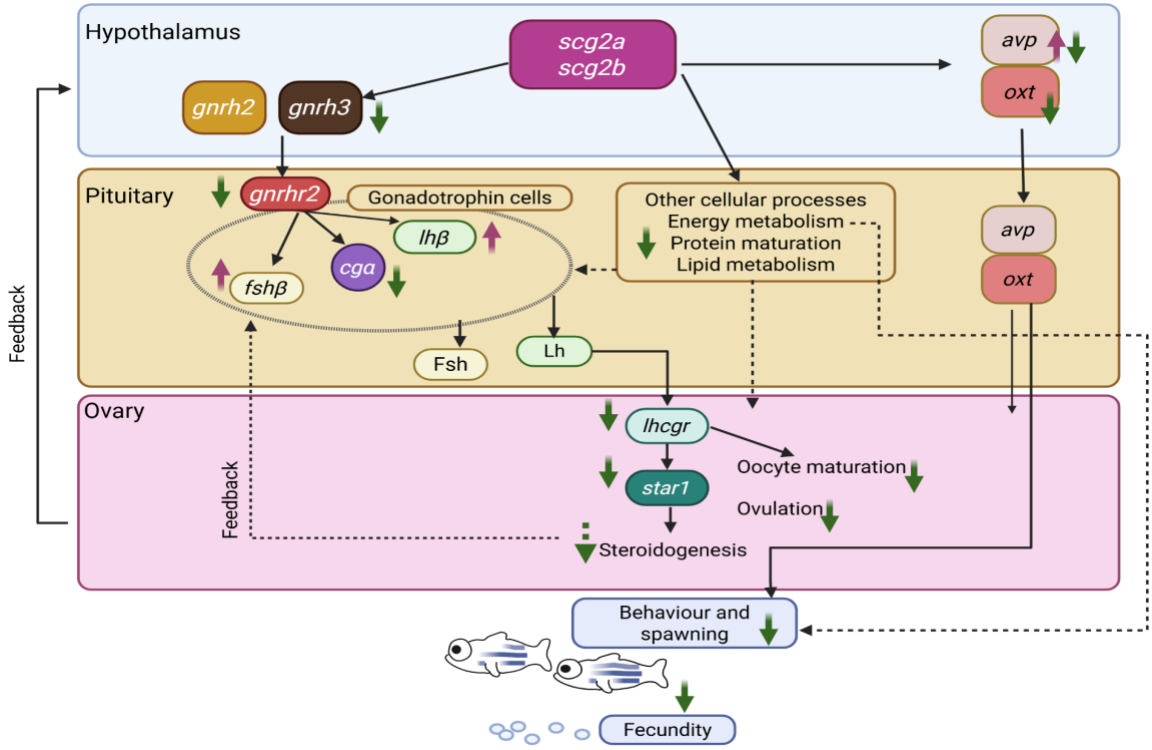

Figure 31. Neuroendocrine model of *scg2a* and *scg2b* action in the regulation of reproductive processes in the adult female zebrafish. Solid lines represent tested results, while dashed lines are speculations. Green arrows are downregulations, and red arrows are upregulations in *scg2a-/-; scg2b-/-* complete DKO females. Note that the gonadotroph is shown as a single cell for convenience, but Lh and Fsh would be secreted from separate specific cell types in the pituitary.

Appendix A: Method validations

W.K.C.U. Erandani[1] , Chunyu Lu[2], Vance L. Trudeau[3]

A1. Introduction

Mass spectroscopy validation failure of the *scg2a-/-*(16A), *scg2a-/-*(4A), and *scg2b-/-*(6 B) lines is described in detail here. This failure, despite validation through several DNA-based methods, underscores the importance of verifying KO models at the genomic DNA level and for the absence of target proteins to avoid misinterpretations from residual expression or off-target effects. In this study, we utilized genotyping using PCR and Sanger sequencing for DNA-level validation, which are clearly defined as standard validation methods for CRISPR-edited animals, especially in knockout models. (Bunton-Stasyshyn et al., 2022). Beyond the standard validations, several studies have emphasized the need for protein-level confirmation. Although DNA sequencing can verify mutations induced by CRISPR-Cas9, research indicates that residual protein expression may remain in many knockout lines, due to processes such as translation reinitiation or exon skipping. (Smits et al., 2019). Therefore, validating knockouts at the protein level is essential to assess gene disruption and avoid misinterpretation of phenotypes accurately.

Protein level validations could be done using immunohistochemistry, by the absence of the immunoreactivity of a specific protein. We only had a SNa antibody until now, but we developed a mouse monoclonal anti-zebrafish SNb antibody during this study. The validation of the newly developed SNb antibody and its partial co-localization with SNa-immunoreactivity is presented in this appendix. Antibody validation, particularly specificity testing, is critical to avoid cross-reactivity and false positives. Pre-absorption assays (pre-adsorbing antibodies with target antigens to confirm binding loss) are traditionally used to demonstrate specificity (Burry, 2000).

A.2 Materials and methods

A.2. 1 Experimental animals

Wildtype (WT) zebrafish were sourced from an in-house stock at the University of Ottawa (uOttawa Wild Type), bred and raised according to standard husbandry procedures. Fish were maintained in 10-L tanks of dechlorinated City of Ottawa tap water at a density of 5fish/L in a recirculating system (Techniplast, Montréal, QC, Canada) at a temperature of 28°C on a 14:10 light-dark cycle. Fish were fed once or twice daily with GEMMA zebrafish diets (Skretting,

Vancouver, BC, Canada) according to embryonic larval and adult life stages. (Created in Biorender.com)

A2.2 Mass spectroscopy assessment

Brain and pituitary samples were dissected from F2 generation of *scg2a-/-* (4 A) and *scg2b-/-* (6 B) homozygous female zebrafish and their sibling WT. Peptide extraction and LC-MS/MS analysis methods (Lu et al., 2023) with modifications were described in Chapter 2.

A2.3 Validation of SNb antibody

The fish head samples of WT, *scg2b-/-* 4B KO and *scg2a-/-*, *scg2b-/-* DKO were paraffin fixed, sectioned and rehydrated following the methods and steps explained in Chapter 2. For the SNb pre-adsorption assay, WT brain pituitary sections were used, and the SNb mouse monoclonal anti-zebrafish antibody in 1:300 dilution was pre-adsorbed with 10 µM synthetic SNb peptide (ABclonal Inc., Woburn, MA, USA) at 4°C, 24 hours before the primary antibody incubation. SNa rabbit-anti-goldfish SNa antiserum (1:600) was used as a positive control to confirm the specificity of the SNb immunoreactivity.

Further antibody assessments were performed with the *scg2b-/-* 4B KO, and WT brain/pituitary sections were incubated with SNa (1:600) and SNb (1:200) primary antibodies without antigen pre-adsorption. For the observation of SNb-ir and co-localization with SNa-ir, WT sections were separately incubated with SNa rabbit-anti-goldfish SNa antiserum (1:600) and SNb mouse monoclonal anti-zebrafish antibody (1:200). For SNa and SNb co-localizations, we respectively used goat anti-rabbit IgG (H+L) secondary antibody, Alexa Fluor™ Plus 488 (ThermoFisher Scientific, San Jose, CA, cat#A32731) and goat anti-mouse IgG1 Cross-Adsorbed Secondary Antibody, Alexa Fluor™ 594 (ThermoFisher Scientific, San Jose, CA, cat # A-21125) diluted to 1:500.

A.3 Results

A.3.1 Three KO lines failed to pass the mass spectroscopy assay

According to the results of the mass spectroscopy validation (Figure A1), the *scg2a -/-* (16 A) and *scg2a-/-* (4 A) (Not shown) still presented with the SNa peptide in their brain and pituitary, despite being a presumptive knockout by the genotyping and sequencing. Similarly, *scg2b-/-* (6 B) fish (Figure A2), SNb was still intact and similar to their WT siblings.

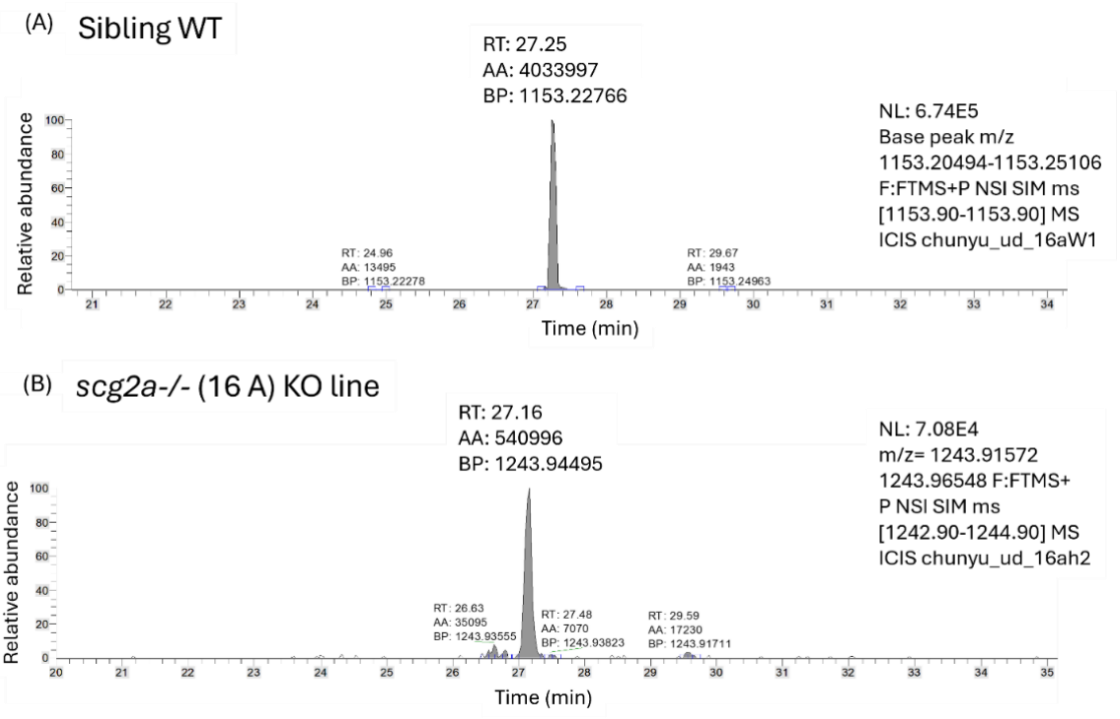

Figure A1. Chromatograms showing the detection of SNa in sibling WT and the *scg2a-/-* (16 A) line zebrafish brain and pituitary extracts. (A) The chromatograms for sibling WT, presence of the SNa peptides by distinct retention times (RT) and peak intensities. (B) Shows chromatograms of *scg2a-/-* (16 A) line fish, where SNa remains intact and the relative abundance is high (N=3). RT: retention time, BP: base peak, AA: apex area

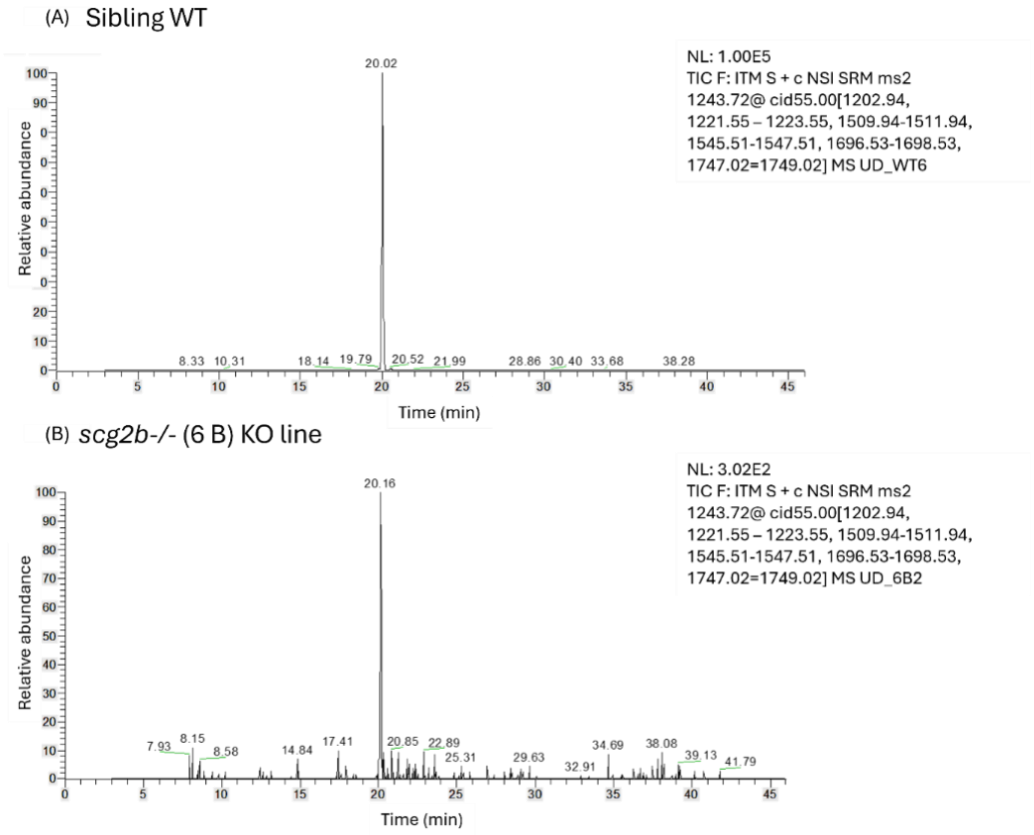

Figure A2. Chromatograms showing the detection of SNb in sibling WT and the *scg2b-/-* (6 B) line (Failed at the mass spectroscopy) zebrafish brain and pituitary explants. (A) The chromatograms for sibling WT show the presence of the SNb peptides by distinct retention times (RT) and peak intensities. (B) Chromatograms of *scg2b-/-* (6 B) line fish, where SNb remains intact and the relative abundance is high (N=3).

Name of the KO fish line	**Mass spectroscopy**
scg2a -/- 4 A KO	Failed
scg2a -/- 7 A KO	Confirmed
scg2a -/- 13 A KO	Confirmed
scg2a-/- 16 A KO	Failed
scg2a -/- 18 A KO	Confirmed

scg2b -/- 4 A KO	Confirmed
scg2b -/- 6 B KO	Failed
scg2b -/- 12 B KO	Confirmed
scg2b -/- 20 B KO	Confirmed
scg2a -/-; scg2b -/- (7A x 4B)	Confirmed

Table A1: Details of the validated and failed *scg2a-/-* and *scg2b-/-* KO line at the mass spectroscopy assessment.

Three KO lines failed at the mass spectroscopy assessment, due to the presence of SNa and SNb peptides despite being validated by DNA-based methods. These failed lines and all the related fish were immediately removed; thus, they were not further tested by the immuno-histochemistry assays.

A.3.2 SNb antibody immunoreactivity is specific and partially co-localized with SNa-ir

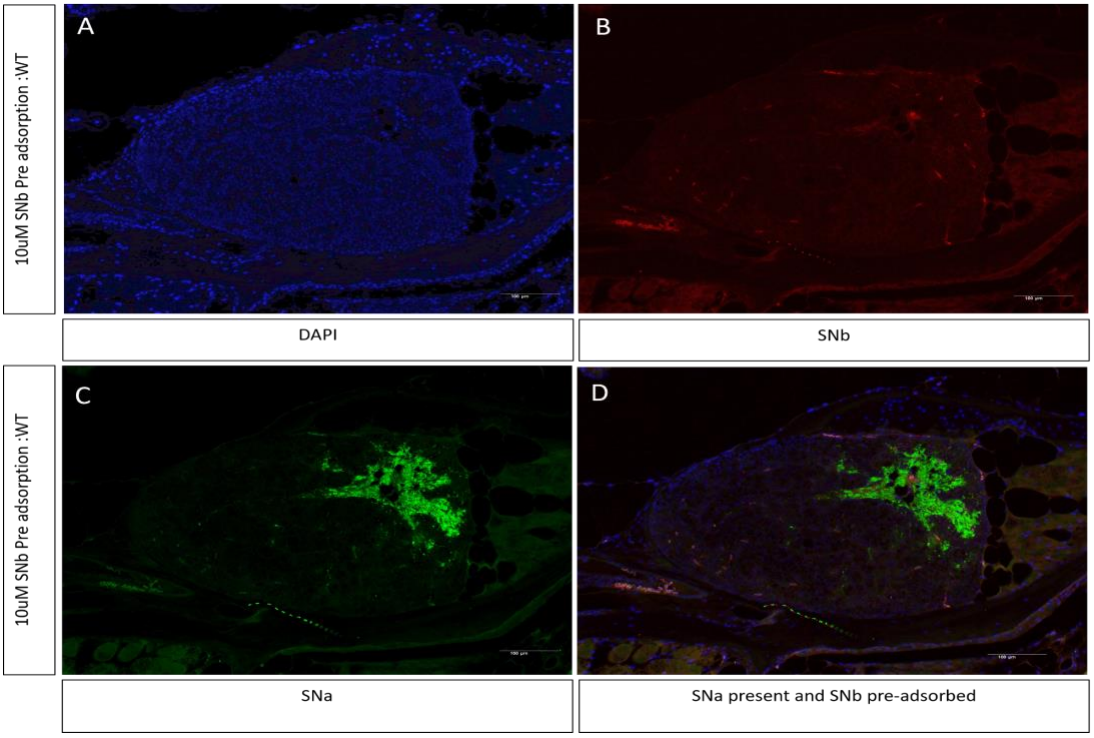

Figure A3. Confirmation of the specificity of SNb immunoreactivity (ir) in the pituitary of wild-type (WT) zebrafish through pre-adsorption of the SNb antibody, with 10 µM SNb synthetic

peptide. (A-D) WT Pituitary, DAPI nuclear staining, (A), SNb-ir pre-adsorbed (B) SNa-ir intact (C), and SNb-ir absent with SNa-ir (D) (scale bar: 100 µm).

The newly developed monoclonal SNb antibody was tested through each development stage (described in Chapter 2), and finally, two specific clones were selected (CMC0539-02-A) and (CMC0532-02-A), purified as the final SNb antibody. The clone CMC0539-02-A was validated for its specificity using the pre-absorption assay, when incubated with synthetic SNb (10 µM), the SNb-ir was specifically pre-absorbed without affecting the SNa-ir.

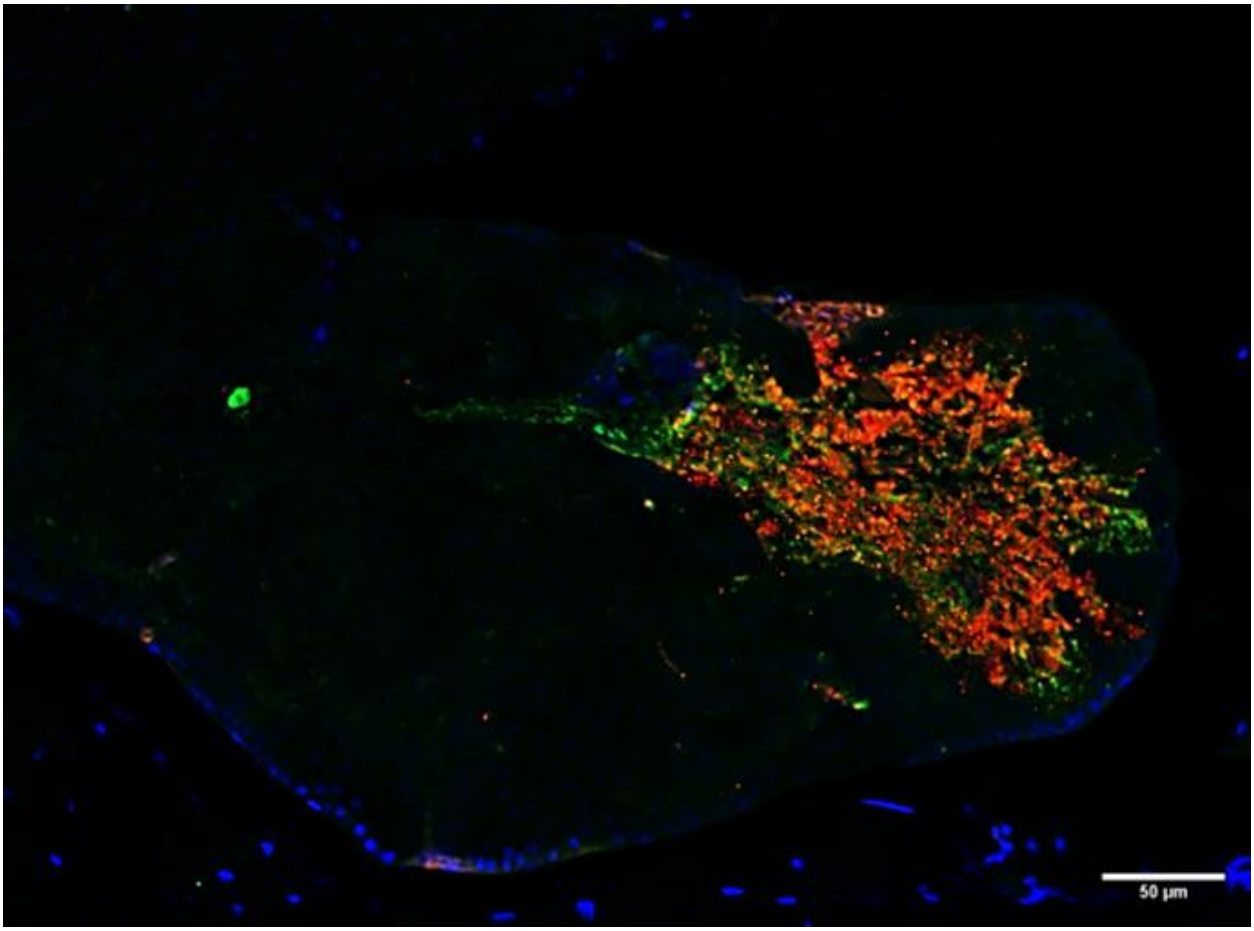

Figure A4. Colocalization of the SNa and SNb immunoreactivity (ir) in the pituitary of wild-type (WT) zebrafish. Green fluorescence labels the SNa-ir, red fluorescence labels the SNb-ir, and blue is the DAPI nuclear staining. Yellow colour shows the areas where SNa and SNb are co-localized (scale bar: 50µm).

In WT zebrafish pituitaries, SNb-ir was mainly observed in nerve fibers of the PN, nerve terminals of the PI and PPD, where it co-localized with SNa-ir only in some areas (Figure A4). Fibers and

nerve terminals that are only SNa-positive are in green, while those that are only SNb-positive without co-localization are in red. Colocalization of both SNa and SNb-ir is shown in yellow and can be noted throughout the PI.

A4. Discussion

The *scg2a* and *scg2b* DKO lines were created and validated at both DNA and protein levels, and 3/8 lines failed at the protein level assessment. As part of the extensive validation protocol, we developed a new monoclonal mouse anti-zebrafish SNb antibody and validated its specificity. The partial co-localization of SNb-ir with SNa-ir is reported for the first time.

For the *scg2a-/-* KO line development, initially five (4A, 7A, 13A, 16A, 18A) were identified as founder fish, and for the *scg2b-/-* KO line development, four (4B, 6B, 12B, 20B) founder fish were identified (See also Chapter 2). After confirming at the genomic DNA level by gel electrophoresis, these fish were crossed with WT to generate the heterozygous F1 generation. Selected heterozygous fish were in-crossed within the line to generate the F2 generation, where the population consisted of 25% of homozygous KO fish. Each fish line generated from each founder fish was maintained separately and named after the main founder fish number, and each line was validated at the protein level. As we described in Chapter 2, the *scg2a-/-*, *scg2b-/-* and sibling WT fish were tested for the presence and absence of SNa and SNb peptide in their brain and pituitary. Two out of five *scg2a* KO lines failed, and one out of four *scg2b* KO lines failed to pass the mass spectroscopy analysis (Table A1), still having corresponding SNa and SNb peptides. Since these lines were carefully housed separately, we eliminated these failed lines from the study and continued with the multi-step validated single and DKO fish.

These findings highlight the significance of using several validation strategies, which include both genomic and proteomic assessments, in the process of establishing a genetically modified knockout line. Some DNA level validation methods, like PCR, sequencing, or restriction digest, can miss the existence of alternative transcripts or leftover protein products due to translation or compensatory splicing events. Also, until complete validation, the independent maintenance of founder-derived lines was important to selectively eliminate the failed lines, thereby ensuring the integrity of the validated *scg2a-/-, scg2b-/-,* and subsequent DKO populations for further experiments.

The specificity of the developed SNb antibody was confirmed through a pre-absorption assay, where it was completely absorbed by SNb peptide incubation. The pre-absorption did not affect the SNa-ir in the zebrafish pituitary, indicating the specificity of the SNb antibody. The expression of SNb was observed mainly in the neural (PN) and intermediate lobe (PI) of the pituitary, where it partially co-localized with SNa. The SNb-ir in a few neural fibers in PPD suggests a neuroendocrine role for SNb, and the partial co-localization at the pituitary could be due to different timing of release or independent roles, which need to be investigated in the future.

Appendix B: *In vitro* effects of SNa and SNb peptides on germinal vesicle breakdown in zebrafish oocytes

W.K.C.U. Erandani[1] , Majd Sabbagh[1], Vance L. Trudeau[2]

B1. Introduction

Oocyte maturation, the meiotic development of ovarian follicles, represents the final stage of oogenesis, preparing the immature oocyte for fertilization (Masui & Clarke, 1979). Germinal Vesicle Breakdown (GVBD) is a crucial step in oocyte maturation, marking the progression from the arrested phase of prophase I to metaphase II of meiosis, a process vital for successful ovulation (Tokumoto et al, 2011). Mature oocytes that are ready to ovulate disassemble the germinal vesicle, and the appearance changes from opaque to transparent due to the reorganization of yolk granules and oocyte hydration (Tokumoto et al.,2005). The GVBD assay is a key experimental tool to study oocyte maturation, where it revealed factors influencing maturation, such as membrane progestin receptor deficiencies and environmental contaminants (Tang et al., 2016; Tokumoto et al., 2005).

In zebrafish, GVBD is induced by maturation-promoting factor (MPF) activation, which is triggered by hormonal signals, particularly 17α,20β-dihydroxy-4-pregnen-3-one (DHP). The pituitary Lh surge is critical for initiating GVBD, as it lowers intracellular cyclic AMP (cAMP) levels in the oocyte, allowing meiosis to resume. Although not directly initiating GVBD, Fsh prepares the follicle by enhancing its responsiveness to LH (Arroyo et al., 2020). The data from this thesis and the accumulating literature indicate that *scg2* genes play a stimulatory role in zebrafish reproduction. In the *scg2a-/-; scg2b-/-* DKO line, oocyte maturation and overall reproduction output are reduced. As a modulator, SN directly and indirectly impacts reproductive hormonal pathways, thus affecting oocyte ovulation (Zhao et al., 2010; Zhao et al.,2011). Thus, we hypothesized that *in vitro* incubation of SNa and SNb directly enhances GVBD in wild-type zebrafish oocytes, thereby inducing final oocyte maturation.

B.2 Materials and methods

B.2.1 Experimental animals

Mature WT female zebrafish aged between 8 to 11 months were housed in 3-L tanks with a density of 3 fish /L. The temperature was maintained at 28°C with a photoperiod of 14-hour light, 10-hour dark. Fish were fed once daily with GEMMA zebrafish diets (Skretting, Vancouver, BC, Canada), and the diet was supplemented with brine shrimp twice a week to ensure optimal health and nutritional status conducive to reproductive readiness. One week before the experiments, females were separated from their male counterparts to eliminate any male influence on oocyte maturation.

B.2.2 The GVBD assay protocol

This assay was performed according to procedures highlighted in a previous study (Pang & Thomas, 2009). Before the assay, 5-8 zebrafish were acclimated to laboratory conditions by incubating them in a laboratory fish incubator at 28°C for 2-3 hours. This acclimation period allowed the fish to adjust to minor variations between the tank and experimental conditions, minimizing stress. Fish were then anesthetized in ice water for 2 minutes and dissected at 7.30 p.m. on ice using a fine scalpel blade. Afterwards, ovaries were carefully extracted, placed in a 100 mm petri dish, and washed several times in 60% Leibovitz's L-15 growth medium to remove any debris and extraneous tissue. The follicles were then carefully isolated using fine forceps, ensuring the ovarian membrane remained intact, under a dissecting microscope. Fully grown Stage 4 oocytes (0.50–0.55 mm in diameter) were then selected, pooled and distributed into multiple 6-well plates containing 4 ml of 60% L-15 medium per well. Around 30-35 oocytes were present in each well. The *in vitro* incubation started at 8.00 p.m.

The experiment consisted of a positive control group treated with 10 nM DHP and it was only soluble in ethanol (EtOH). Therefore, DHP positive control contained 0.1% EtOH in the media, and to replicate this, all the peptide treatment groups and the negative control group had 0.1% ethanol. This was done by removing 4 µL of incubation medium from the negative control and treatment group plates, followed by adding back 4 µL 99.9% EtOH. Three treatment groups were tested for each SNa and SNb peptides, at concentrations of 0.1 nM, 1 nM, and 10 nM to examine dose-dependent effects. Another subsequent set of experiments was conducted without adding ethanol in the treatment and negative control groups, to exclude any effect generated by adding ethanol. Following treatment application, plates were incubated at 25°C to facilitate the

maturation process and prepare for subsequent analysis of GVBD.

B.2.3 Assessment of GVBD and data collection

The final oocyte maturation was assessed by observing the oocytes for signs of ovulation under a microscope 12-14 hours post-incubation (hpi). The 12 hpi was selected to represent data, as oocytes would begin to degrade afterwards, giving a "false ovulation" appearance, which would alter results at the 14 hpi. For this same reason, the treatment and positive control groups mentioned above were chosen, as any higher doses would take longer than 12 hours to fully take effect. The percentage of GVBD was calculated by counting the number of transparent oocytes and expressing it as a percentage of the total number of oocytes per well. Experiments were repeated at least 6 times to confirm the results.

B.2.4 Statistical Analysis

Statistical analysis was performed using the Shapiro-Wilk Test to assess normality in data, followed by the One-Way ANOVA test to compare the rates of GVBD across different treatment and control groups at 12 hpi. The Tukey Honest Significant Difference (HSD) test was applied post-hoc to determine significant differences between individual groups.

B.3 Results

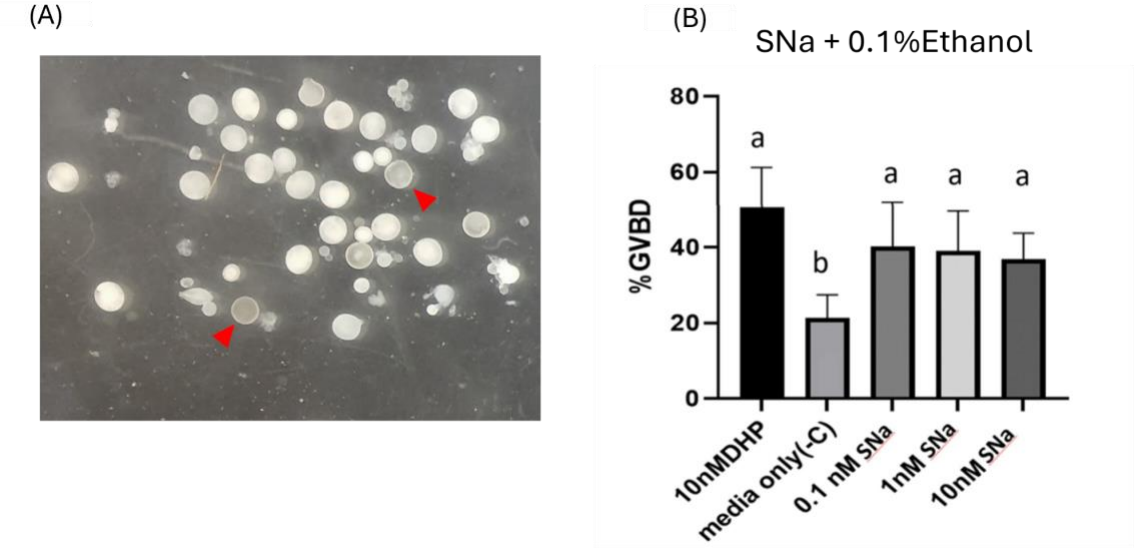

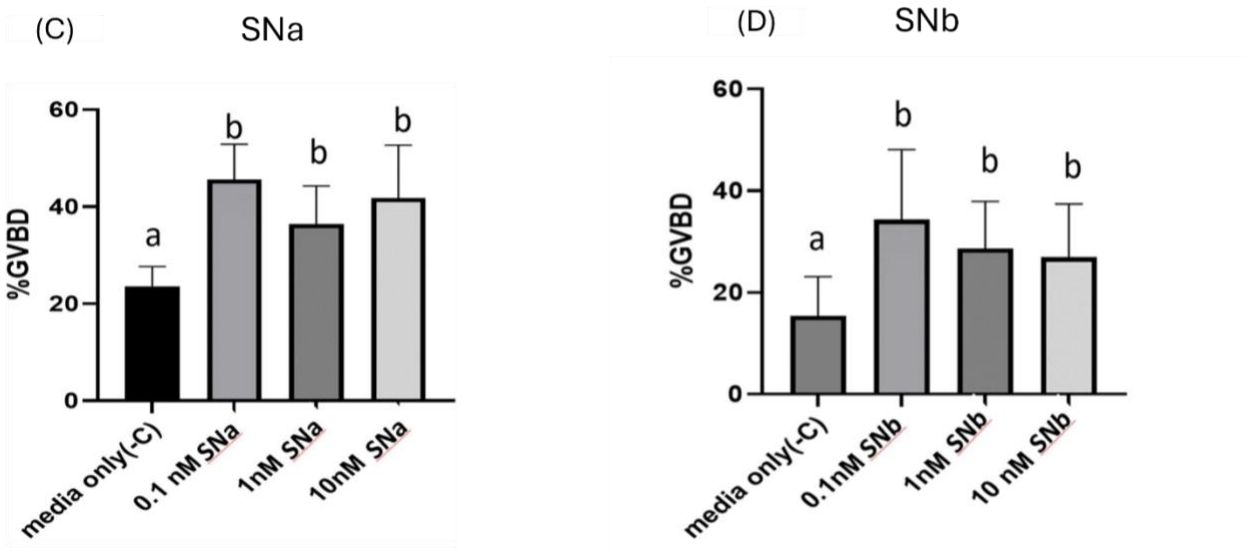

Figure B1. The percentage of GVBD in WT zebrafish oocytes with *in vitro* incubation of SNa, SNb and DHP, at 12 hours post-incubation (hpi). (A) An image of mature zebrafish oocytes at 12 hpi, and the red arrowheads indicate the successful GVBD oocytes that became transparent. (B) Effect of DHP (Positive control) and SNa +0.1% ethanol on the percentage of GVBD. (C) Effect of SNa, without ethanol, on the percentage of GVBD. (D) Effect of SNb, without ethanol, on the percentage of GVBD. Groups labelled with the same letter (a or b) are similar according to the Tukey HSD test and are not similar when they are labelled with different letters ($P<0.05$). All data groups were found to be normally distributed ($p>0.05$). The experiments were repeated 6 times, and similar results were obtained every time. Each data point is from a well plate containing roughly 30-35 oocytes. % GVBD results are expressed as Mean ± SD (N = 12).

The positive control DHP (10 nM) significantly increased GVBD to 50.54 ± 10.68% compared to the negative control group, which had 21.37 ± 6.09 % GVBD (Figure B1 -B) at 12 hpi. All the SNa treatment groups with 0.1% EtOH also significantly increased GVBD, similar to the DHP effect (0.1 nM SNa 40.23 ± 11.78, 1 nM SNa 39.12 ± 10.52%, and 10 nM SNa 36.81 ± 6.95%).

When incubated without EtOH in the media (Figure B1- C), all the SNa treatment groups were still able to significantly increase the GVBD rate (0.1 nM SNa; 45.64 ± 7.24%, 1 nM SNa; 36.42 ± 7.83%, 10 nM SNa; 41.80 ± 10.87%) compared to the media-only group (negative control 23.64 ± 4.02%). Similarly, *in vitro* SNb incubation (Figure B1-D) significantly increased the % GVBD in zebrafish oocytes at 12 hpi, with 0.1 nm SNb (31.32 ± 8.82%), 1 nM SNb (28.70 ± 9.25%), and 10 nm SNb (27.00 ± 10.45%) compared to the negative control (15.40 ± 7.71%, $p<0.001$).

B.4 Discussion

Our findings indicate that the *in vitro* incubation of stage 4 oocytes with either SNa or SNb synthetic peptides enhanced GVBD in WT zebrafish. The use of EtOH as a medium to dissolve DHP positive control did not compromise the validity of the results, with similar trends noted in the absence of EtOH. These results support the hypothesis that SN plays an active role in the regulation of oocyte maturation.

This aligns closely with another study examining how LH initiates meiotic resumption in mouse oocytes (Mehlmann et al., 2006). It notably demonstrates that LH treatment universally leads to a significant increase in GVBD compared to no treatment, showing a two-fold increase at 0.01 μg/ml LH and nearly a four-fold increase at 1 μg/ml LH (Mehlmann et al., 2006). Similarly, 0.1 nM SNa or 0.1 nM SNb, respectively, induced a 1.9-fold and 2-fold increase in GVBD compared to the negative control in each experiment. Our findings highlight the novel aspect of SNa and SNb involvement in the final oocyte maturation and support the phenotypic observations of the number of mature oocytes, reduced fecundity and low spawning rates observed in the *scg2a-/-; scg2b-/-* DKO zebrafish females (Chapter 3). For future experiments, exploring the combinatory effects of both SNa and SNb on GVBD could further reveal whether these molecules act additively or synergistically, potentially optimizing SN-based interventions to enhance fertility. Additionally, the *in vitro* effect of SNa, SNb, and DHP on *scg2a-/-; scg2b-/-* DKO oocytes and their GVBD needs to be examined in the future to determine the hormone responsiveness of the DKO fish.

References

Abdollahpour, H., Falahatkar, B., & Lawrence, C. (2020). The effect of photoperiod on growth and spawning performance of zebrafish, Danio rerio. *Aquaculture Reports*, 17, 100295. https://doi.org/10.1016/J.AQREP.2020.100295

Abraham, E., Palevitch, O., Gothilf, Y., & Zohar, Y. (2010). Targeted gonadotropin-releasing hormone-3 neuron ablation in zebrafish: Effects on neurogenesis, neuronal migration, and reproduction. *Endocrinology*, 151(1), 332–340. https://pubmed.ncbi.nlm.nih.gov/19861502/

Anouar, Y., Benie, T., De Monti, M., Counis, R., & Duval, J. (1991). Estradiol negatively regulates secretogranin II and chromogranin A messenger ribonucleic acid levels in the female rat pituitary but not in the adrenal. *Endocrinology*, 129(5), 2393–2399. https://doi.org/10.1210/ENDO-129-5-2393

Anouar, Y., de Monti, M., Galindo, E., Benié, T., Aunis, D., & Duval, J. (1991). Regulatory Effects of Estrogens on the Pituitary Content of Secretogranin II and Chromogranin A. *Journal of Neuroendocrinology*, 3(3), 233–235. https://doi.org/10.1111/J.1365-2826.1991.TB00269.X

Anouar, Y., & Duval, J. (1991). Differential expression of secretogranin II and chromogranin A genes in the female rat pituitary through sexual maturation and estrous cycle. *Endocrinology*, 128(3), 1374–1380. https://doi.org/10.1210/ENDO-128-3-1374

Anouar, Y., & Duval, J. (1992). Direct estradiol down-regulation of secretogranin II and chromogranin A mRNA levels in rat pituitary cells. *Molecular and Cellular Endocrinology*, 88(1–3), 97–104. https://doi.org/10.1016/0303-7207(92)90013-V

Arroyo, A., Kim, B., & Yeh, J. (2020). Luteinizing Hormone Action in Human Oocyte Maturation and Quality: Signaling Pathways, Regulation, and Clinical Impact. *Reproductive Sciences*, 27(6), 1223–1252. https://doi.org/10.1007/S43032-019-00137-X

Banerjee, A., Biswas, D., Barpanda, A., Halder, A., Sibal, S., Kattimani, R., Shah, A., Mahadevan, A., Goel, A., & Srivastava, S. (2022). The First Pituitary Proteome Landscape From Matched Anterior and Posterior Lobes for a Better Understanding of the Pituitary Gland. *Molecular & Cellular Proteomics:* MCP, 22(1), 100478. https://doi.org/10.1016/J.MCPRO.2022.100478

Banerjee, P., Joy, K. P., & Chaube, R. (2017). Structural and functional diversity of nonapeptide hormones from an evolutionary perspective: A review. *General and Comparative Endocrinology*, 241, 4–23. https://doi.org/10.1016/J.YGCEN.2016.04.025

Baroiller, J. F., D'Cotta, H., & Saillant, E. (2009). Environmental effects on fish sex determination and differentiation. *Sexual Development*, 3(2–3), 118–135. https://pubmed.ncbi.nlm.nih.gov/19684457/

Bartolomucci, A., Possenti, R., Mahata, S. K., Fischer-Colbrie, R., Loh, Y. P., & Salton, S. R. J. (2011). The extended granin family: Structure, function, and biomedical implications. *Endocrine Reviews*, 32(6), 755–797. https://doi.org/10.1210/er.2010-0027

Bassetti, M., Huttner, W. B., Zanini, A., & Rosa, P. (1990). Co-localization of secretogranins/chromogranins with thyrotropin and luteinizing hormone in secretory granules of cow anterior pituitary. *Journal of Histochemistry and Cytochemistry*, 38(9), 1353–1363. https://doi.org/10.1177/38.9.2387987

Benarafa, C., LeCuyer, T. E., Baumann, M., Stolley, J. M., Cremona, T. P., & Remold-O′Donnell, E. (2011). SerpinB1 protects the mature neutrophil reserve in the bone marrow. *Journal of Leukocyte Biology*, 90(1), 21–29. https://doi.org/10.1189/JLB.0810461

Bertilsson, L., Dahl, M. L., Dalén, P., & Al-Shurbaji, A. (2002). Molecular genetics of CYP2D6: Clinical relevance with focus on psychotropic drugs. *British Journal of Clinical Pharmacology*, 53(2), 111. https://doi.org/10.1046/J.0306-5251.2001.01548.X

Blázquez, M., Bosma, P. T., Chang, J. P., Docherty, K., & Trudeau, V. L. (1998). γ-Aminobutyric Acid Up-Regulates the Expression of a Novel Secretogranin-II Messenger Ribonucleic Acid in the Goldfish Pituitary. *Endocrinology*, 139(12), 4870–4880. https://doi.org/10.1210/ENDO.139.12.6339

Bose, A., Teh, M. T., Mackenzie, I. C., & Waseem, A. (2013). Keratin K15 as a Biomarker of Epidermal Stem Cells. *International Journal of Molecular Sciences*, 14(10), 19385. https://doi.org/10.3390/IJMS141019385

Bouligand, J., Ghervan, C., Tello, J. A., Brailly-Tabard, S., Salenave, S., Chanson, P., Lombès, M., Millar, R. P., Guiochon-Mantel, A., & Young, J. (2009). Isolated Familial Hypogonadotropic Hypogonadism and a GNRH1 Mutation. *New England Journal of Medicine*, 360(26), 2742–2748. https://doi.org/10.1056/NEJMOA0900136,

Boutahricht, M., Guillemot, J., Montero-Hadjadje, M., Barakat, Y., El Ouezzani, S., Alaoui, A., Yon, L., Vaudry, H., Anouar, Y., & Magoul, R. (2007). Immunohistochemical distribution of the secretogranin II-derived peptide EM66 in the rat hypothalamus: A comparative study with jerboa. Volume 414, Issue 3, Pages 268 - 272, 414(3), 268–272. https://doi.org/10.1016/j.neulet.2006.12.033

Breen, K. M., Billings, H. J., Wagenmaker, E. R., Wessinger, E. W., & Karsch, F. J. (2005). Endocrine Basis for Disruptive Effects of Cortisol on Preovulatory Events. *Endocrinology*, 146(4), 2107–2115. https://doi.org/10.1210/EN.2004-1457

Breton, B., Mikolajczyk, T., Popek, W., Bieniarz, K., & Epler, P. (1991). Neuropeptide Y stimulates in vivo gonadotropin secretion in teleost fish. *General and Comparative Endocrinology*, 84(2), 277–283. https://doi.org/10.1016/0016-6480(91)90050-G

Bunton-Stasyshyn, R. K., Codner, G. F., & Teboul, L. (2022). Screening and validation of genome-edited animals. *Laboratory Animals*, 56(1), 69–82. https://pmc.ncbi.nlm.nih.gov/articles/PMC9008557/

Canosa, L. F., Chang, J. P., & Peter, R. E. (2007). Neuroendocrine control of growth hormone in fish. *General and Comparative Endocrinology*, 151(1), 1–26. https://doi.org/10.1016/J.YGCEN.2006.12.010

Canosa, L. F., Lopez, G. C., Scharrig, E., Lesaux-Farmer, K., Somoza, G. M., Kah, O., & Trudeau, V. L. (2011). Forebrain mapping of secretoneurin-like immunoreactivity and its colocalization with isotocin in the preoptic nucleus and pituitary gland of goldfish. *Journal of Comparative Neurology*, 519(18), 3748–3765. https://doi.org/10.1002/cne.22688

Carolsfeld, J., Powell, J. F. F., Park, M., Fischer, W. H., Craig, A. G., Chang, J. P., Rivier, J. E., & Sherwood, N. M. (2000). Primary Structure and Function of Three Gonadotropin-Releasing Hormones, Including a Novel Form, from an Ancient Teleost, Herring. *Endocrinology*, 141(2), 505–512. https://doi.org/10.1210/ENDO.141.2.7300

Casteel, C. O., & Singh, G. (2023). Physiology, Gonadotropin-Releasing Hormone. *StatPearls*. https://www.ncbi.nlm.nih.gov/books/NBK558992/

Cattanach, B. M., Iddon, C. A., Charlton, H. M., Chiappa, S. A., & Fink, G. (1977). Gonadotrophin-releasing hormone deficiency in a mutant mouse with hypogonadism. *Nature*, 269(5626), 338–340.https://www.nature.com/articles/269338a0

Cerdá-Reverter, J. M., Sorbera, L. A., Carrillo, M., & Zanuy, S. (1999). Energetic dependence of NPY-induced LH secretion in a teleost fish (Dicentrarchus labrax). *American Journal of Physiology* Regulatory Integrative and Comparative Physiology, 277(6 46-6). https://pubmed.ncbi.nlm.nih.gov/10600908/

Cha, K. B., Douglas, K. R., Potok, M. A., Liang, H., Jones, S. N., & Camper, S. A. (2004). WNT5A signaling affects pituitary gland shape. *Mechanisms of Development*, 121(2), 183–194. https://doi.org/10.1016/J.MOD.2003.12.002

Chakraborty, S., Pramanik, J., & Mahata, B. (2021). Revisiting steroidogenesis and its role in immune regulation with the advanced tools and technologies. *Genes & Immunity* 2021 22:3, 22(3), 125–140. https://doi.org/10.1038/s41435-021-00139-3

Chang, J. P., & Pemberton, J. G. (2018). Comparative aspects of GnRH-Stimulated signal transduction in the vertebrate pituitary – Contributions from teleost model systems. *Molecular and Cellular Endocrinology*, 463, 142–167. https://www.sciencedirect.com/science/article/abs/pii/S0303720717303222?via%3Dihub

Chapman, S. C., Sawitzke, A. L., Campbell, D. S., & Schoenwolf, G. C. (2005). A three-dimensional atlas of pituitary gland development in the zebrafish. *Journal of Comparative Neurology*, 487(4), 428–440. https://onlinelibrary.wiley.com/doi/10.1002/cne.20568

Chen, L., Huang, R., Zhu, D., Wang, Y., Mehjabin, R., Li, Y., Liao, L., He, L., Zhu, Z., & Wang, Y. (2019). Cloning of six serpin genes and their responses to GCRV infection in grass carp (Ctenopharyngodon idella). *Fish & Shellfish Immunology*, 86, 93–100. https://doi.org/10.1016/J.FSI.2018.11.008

Chen, L., Jiang, Z. G., Khan, A. A., Chishti, A. H., & McKnight, C. J. (2009). Dematin exhibits a natively unfolded core domain and an independently folded headpiece domain. Protein Science : *Protein Society*, 18(3), 629. https://doi.org/10.1002/PRO.59

Chen, Y., Tang, H., Wang, L., He, J., Guo, Y., Liu, Y., Liu, X., & Lin, H. (2018). Fertility enhancement but premature ovarian failure in esr1-deficient female zebrafish. *Frontiers in Endocrinology*, 9(SEP), 405380. https://pubmed.ncbi.nlm.nih.gov/30319547/

Chu, L., Li, J., Liu, Y., Hu, W., & Cheng, C. H. K. (2014). Targeted gene disruption in zebrafish reveals noncanonical functions of lh signaling in reproduction. *Molecular Endocrinology*, 28(11), 1785–1795. https://pubmed.ncbi.nlm.nih.gov/25238195/

Clark, T. S., Pandolfo, L. M., Marshall, C. M., Mitra, A. K., & Schech, J. M. (2018). Body Condition Scoring for Adult Zebrafish (Danio rerio). *Journal of the American Association for Laboratory Animal Science* : JAALAS, 57(6), 698. https://doi.org/10.30802/AALAS-JAALAS-18-000045

Clarkson, J., d'Anglemont de Tassigny, X., Colledge, W. H., Caraty, A., & Herbison, A. E. (2009). Distribution of kisspeptin neurones in the adult female mouse brain. *Journal of Neuroendocrinology*, 21(8), 673–682. https://pubmed.ncbi.nlm.nih.gov/19515163/

Clarkson, J., & Herbison, A. E. (2006). Postnatal development of kisspeptin neurons in mouse hypothalamus; sexual dimorphism and projections to gonadotropin-releasing hormone neurons. *Endocrinology*, 147(12), 5817–5825. https://pubmed.ncbi.nlm.nih.gov/16959837/

Clelland, E., & Peng, C. (2009). Endocrine/paracrine control of zebrafish ovarian development. *Molecular and Cellular Endocrinology*, 312(1–2), 42–52. https://doi.org/10.1016/J.MCE.2009.04.009

Conlon, J. M., Collin, F., Chiang, Y. C., Sower, S. A., & Vaudry, H. (1993). Two molecular forms of gonadotropin-releasing hormone from the brain of the frog, Rana ridibunda: Purification, characterization, and distribution. *Endocrinology*, 132(5), 2117–2123. https://doi.org/10.1210/ENDO.132.5.8477660,

Connahs, H., Tlili, S., van Creij, J., Loo, T. Y. J., Banerjee, T. Das, Saunders, T. E., & Monteiro, A. (2019). Activation of butterfly eyespots by Distal-less is consistent with a reaction-diffusion process. *Development (Cambridge)*, 146(9). https://journals.biologists.com/dev/article/146/9/dev169367/49252/Activation-of-butterfly-eyespots-by-Distal-less-is

Conneely, O. M., Mulac-Jericevic, B., Lydon, J. P., & De Mayo, F. J. (2001). Reproductive functions of the progesterone receptor isoforms: lessons from knock-out mice. *Molecular and Cellular Endocrinology*, 179(1–2), 97–103. https://doi.org/10.1016/S0303-7207(01)00465-8

Corriero, A., Zupa, R., Mylonas, C. C., & Passantino, L. (2021). Atresia of ovarian follicles in fishes, and implications and uses in aquaculture and fisheries. *Journal of Fish Diseases*, 44(9), 1271. https://doi.org/10.1111/JFD.13469

Courel, M., Soler-Jover, A., Rodriguez-Flores, J. L., Mahata, S. K., Elias, S., Montero-Hadjadje, M., Anouar, Y., Giuly, R. J., O'Connor, D. T., & Taupenot, L. (2010). Pro-hormone secretogranin II regulates dense core secretory granule biogenesis in catecholaminergic cells. *The Journal of Biological Chemistry*, 285(13), 10030–10043. https://doi.org/10.1074/JBC.M109.064196

Crawford, J. L., & McNeilly, A. S. (2002). Co-localisation of gonadotrophins and granins in gonadotrophs at different stages of the oestrous cycle in sheep. *The Journal of Endocrinology*, 174(2), 179–194. https://doi.org/10.1677/JOE.0.1740179

Da Fonte, D. F., Xing, L., Mikwar, M., & Trudeau, V. L. (2018). Secretoneurin-A inhibits aromatase B (cyp19a1b) expression in female goldfish (Carassius auratus) radial glial cells. *General and Comparative Endocrinology*, 257, 106–112. https://doi.org/10.1016/J.YGCEN.2017.04.014

Dalvie, N. C., Lorgeree, T., Biedermann, A. M., Love, K. R., & Love, J. C. (2022). Simplified Gene Knockout by CRISPR-Cas9-Induced Homologous Recombination. *ACS Synthetic Biology*, 11(1), 497–501. https://pubs.acs.org/doi/10.1021/acssynbio.1c00194

Darrow, K. O., & Harris, W. A. (2004). Characterization and Development of Courtship in Zebrafish, Danio rerio. *Zebrafish*, 1(1), 40–45. https://doi.org/10.1089/154585404774101662
de Roux, N. (2006). GnRH receptor and GPR54 inactivation in isolated gonadotropic deficiency. Best Practice and Research: *Clinical Endocrinology and Metabolism*, 20(4), 515–528. https://doi.org/10.1016/j.beem.2006.10.005

De Roux, N., Genin, E., Carel, J. C., Matsuda, F., Chaussain, J. L., & Milgrom, E. (2003). Hypogonadotropic hypogonadism due to loss of function of the KiSS1-derived peptide receptor GPR54. *Proceedings of the National Academy of Sciences of the United States of America*, 100(19), 10972–10976. https://pubmed.ncbi.nlm.nih.gov/12944565/

De Vriendt, S., Laporte, E., Abaylı, B., Hoekx, J., Hermans, F., Lambrechts, D., & Vankelecom, H. (2025). Single-cell transcriptome atlas of male mouse pituitary across postnatal life highlighting its stem cell landscape. *IScience*, 28(2). https://doi.org/10.1016/J.ISCI.2024.111708

Deniz Koç, N., Aytekin, Y., & Yüce, R. (2008). Ovary Maturatıon Stages and Histological Investigation of Ovary of the Zebrafish (Danio rerio). *Braz. Arch. Biol. Technol*. v, 51(3), 513-522.https://www.scienceopen.com/document?vid=c700ffad-a914-4e41-9a17-e046f8fb7a8c

Desaulniers, A. T., Cederberg, R. A., Lents, C. A., & White, B. R. (2017). Expression and Role of Gonadotropin-Releasing Hormone 2 and Its Receptor in Mammals. *Frontiers in Endocrinology*, 8(DEC), 269. https://doi.org/10.3389/FENDO.2017.00269

Di, P. (2022). Characterization and Role of Secretoneurin in the Ovulatory Cycle of Zebrafish [University of Ottawa]. https://ruor.uottawa.ca/items/0bb4ff3a-aef2-40c2-a84c-58b4a64c8070
Eaton, R. C., & Farley, R. D. (1974). Spawning Cycle and Egg Production of Zebrafish, Brachydanio rerio, in the Laboratory. *Behaviour*, 1974(1), 195. https://doi.org/10.2307/1443023

El Yamani, F. Z., Yon, L., Guérin, M., El Ouezzani, S., Alaoui, A., Chartrel, N., Anouar, Y., & Magoul, R. (2013). Immunocytochemical distribution of EM66 within the hypothalamic parvocellular paraventricular nucleus: Colocalization with CRH and TRH but no plasticity related to acute stress and thyroidectomy in the rat. *Regulatory Peptides*, 182(1), 28–34. https://doi.org/10.1016/J.REGPEP.2012.12.008

El Yamani, F.-Z., Yon, L., Guérin, M., El Ouezzani, S., Alaoui, A., Chartrel, N., Anouar, Y., & Magoul, R. (2010). EM66-containing neurones in the hypothalamic parvicellular paraventricular nucleus of the rat: No plasticity related to acute immune stress. *Neuroendocrinol* Lett, 31(5), 21173750–21310510. https://www.frontiersin.org/10.3389/conf.fnins.2010.12.00028/event_abstract

Evans, J. J., Reid, R. A., Wakeman, S. A., Croft, L. B., & Benny, P. S. (2003). Evidence that oxytocin is a physiological component of LH regulation in non-pregnant women. *Human Reproduction* (Oxford, England), 18(7), 1428–1431. https://doi.org/10.1093/HUMREP/DEG291

Fabre-Nys, C., Cognie, J., Dufourny, L., Ghenim, M., Martinet, S., Lasserre, O., Lomet, D., Millar, R. P., Ohkura, S., & Suetomi, Y. (2017). The Two Populations of Kisspeptin Neurons Are Involved in the Ram-Induced LH Pulsatile Secretion and LH Surge in Anestrous Ewes. *Endocrinology*, 158(11), 3914–3928. https://doi.org/10.1210/EN.2017-00429

Farley, K., Stolley, J. M., Zhao, P., Cooley, J., & Remold-O'Donnell, E. (2012). A SerpinB1 Regulatory Mechanism Is Essential for Restricting Neutrophil Extracellular Trap Generation. *The Journal of Immunology*, 189(9), 4574–4581. https://doi.org/10.4049/JIMMUNOL.1201167

Faught, E., Santos, H. B., & Vijayan, M. M. (2020). Loss of the glucocorticoid receptor causes accelerated ovarian ageing in zebrafish. Proceedings. *Biological Sciences*, 287(1940). https://doi.org/10.1098/RSPB.2020.2190

Feng, K., Cui, X., Song, Y., Tao, B., Chen, J., Wang, J., Liu, S., Sun, Y., Zhu, Z., Trudeau, V. L., & Hu, W. (2020). Gnrh3 Regulates PGC Proliferation and Sex Differentiation in Developing Zebrafish. *Endocrinology*, 161(1). https://doi.org/10.1210/ENDOCR/BQZ024

Fernald, R. D., & White, R. B. (1999). Gonadotropin-releasing hormone genes: Phylogeny, structure, and functions. *Frontiers in Neuroendocrinology*, 20(3), 224–240. https://doi.org/10.1006/frne.1999.0181

Fernandes, A., Alvarenga, É., Oliveira, D., Aleixo, C., Prado, S., Luz, R., Sarmento, N., Teixeira, E., Luz, M., & Turra, E. (2013). Production of oocytes of Nile tilapia (Oreochromis niloticus) for in vitro fertilization via hormonal treatments. *Reproduction in Domestic Animals*, 48(6), 1049–1055. https://doi.org/10.1111/RDA.12212

Ferro, E. S., Gewehr, M. C. F., & Navon, A. (2020). Thimet Oligopeptidase Biochemical and Biological Significances: Past, Present, and Future Directions. *Biomolecules*, 10(9), 1229. https://doi.org/10.3390/BIOM10091229

Fischer-Colbrie, R., Laslop, A., & Kirchmair, R. (1995). Secretogranin II: Molecular properties, regulation of biosynthesis and processing to the neuropeptide secretoneurin. Progress in Neurobiology, 46(1), 49–70. https://doi.org/10.1016/0301-0082(94)00060-U

Fleming, T., Tachizawa, M., Nishiike, Y., Koiwa, A., Homan, Y., & Okubo, K. (2023). Estrogen-dependent expression and function of secretogranin 2a in female-specific peptidergic neurons. *PNAS Nexus*, 2(12), pgad413. https://doi.org/10.1093/pnasnexus/pgad413

Fontaine, R., Ciani, E., Haug, T. M., Hodne, K., Ager-Wick, E., Baker, D. M., & Weltzien, F. A. (2020). Gonadotrope plasticity at cellular, population and structural levels: A comparison between fishes and mammals. *General and Comparative Endocrinology*, 287. https://doi.org/10.1016/J.YGCEN.2019.113344

Frasor, J., Danes, J. M., Komm, B., Chang, K. C. N., Richard Lyttle, C., & Katzenellenbogen, B. S. (2003). Profiling of estrogen up- and down-regulated gene expression in human breast cancer cells: insights into gene networks and pathways underlying estrogenic control of proliferation and cell phenotype. *Endocrinology*, 144(10), 4562–4574. https://doi.org/10.1210/EN.2003-0567

Frasor, J., Weaver, A. E., Pradhan, M., & Mehta, K. (2008). Synergistic up-regulation of prostaglandin E synthase expression in breast cancer cells by 17beta-estradiol and proinflammatory cytokines. *Endocrinology*, 149(12), 6272–6279. https://doi.org/10.1210/EN.2008-0352

Froese, R. (2006). Cube law, condition factor and weight–length relationships: history, meta-analysis and recommendations. *Journal of Applied Ichthyology*, 22(4), 241–253. https://doi.org/10.1111/J.1439-0426.2006.00805.X

Ghai, R., Waters, P., Roumenina, L. T., Gadjeva, M., Kojouharova, M. S., Reid, K. B., Sim, R. B., Kishore, U., Hirai, H., Pang, Z., Bao, D., Miyazaki, T., Li, L., Miura, E., Parris, J., Rong, Y., Watanabe, M., Yuzaki, M., Morgan, J. I., … Malenka, R. C. (2011). Cerebellins meet neurexins (Commentary on Matsuda & Yuzaki). *European Journal of Neuroscience*, 33(8), 1445–1446. https://doi.org/10.1111/J.1460-9568.2011.07665.X

Gharib, S. D., Wierman, M. E., Shupnik, M. A., & Chin, W. W. (1990). Molecular biology of the pituitary gonadotropins. *Endocrine Reviews*, 11(1), 177–199. https://doi.org/10.1210/EDRV-11-1-177

Godwin, J., & Thompson, R. (2012). Nonapeptides and Social Behavior in Fishes. *Hormones and Behavior*, 61(3), 230–238. https://doi.org/10.1016/J.YHBEH.2011.12.016

Grigg, A. G., Lowi-Merri, T. M., Hutchings, J. A., & Massey, M. D. (2023). Thermal variability induces sex-specific morphometric changes in zebrafish (Danio rerio). *Journal of Fish Biology*, 103(4), 839–850. https://doi.org/10.1111/JFB.15551

Gross, T., Jeney, C., Halm, D., Finkenzeller, G., Stark, G. B., Zengerle, R., Koltay, P., & Zimmermann, S. (2021). Characterization of CRISPR/Cas9 RANKL knockout mesenchymal stem cell clones based on single-cell printing technology and Emulsion Coupling assay as a low-cellularity

workflow for single-cell cloning. *PLOS ONE*, 16(3), e0238330. https://doi.org/10.1371/JOURNAL.PONE.0238330

Helle, K. B. (2004). The granin family of uniquely acidic proteins of the diffuse neuroendocrine system: Comparative and functional aspects. *Biological Reviews of the Cambridge Philosophical Society*, 79(4), 769–794. https://doi.org/10.1017/S146479310400644X,

Hill, R. M., Coates, L. C., Parmar, P. K., Mezey, E. V. A., Pearson, J. F., & Birch, N. P. (2002). Expression and functional characterization of the serine protease inhibitor neuroserpin in endocrine cells. *Annals of the New York Academy of Sciences*, 971, 406–415. https://doi.org/10.1111/J.1749-6632.2002.TB04503.X,

Hirshfield, A. N. (1991). Development of Follicles in the Mammalian Ovary. *International Review of Cytology*, 124(C), 43–101. https://doi.org/10.1016/S0074-7696(08)61524-7

Ho, Y., Hu, P., Peel, M. T., Chen, S., Camara, P. G., Epstein, D. J., Wu, H., & Liebhaber, S. A. (2020). Single-cell transcriptomic analysis of adult mouse pituitary reveals sexual dimorphism and physiologic demand-induced cellular plasticity. *Protein & Cell*, 11(8), 565–583. https://doi.org/10.1007/S13238-020-00705-X

Hofmann, H. A. (2006). Gonadotropin-releasing hormone signaling in behavioral plasticity. *Current Opinion in Neurobiology*, 16(3), 343–350. https://doi.org/10.1016/J.CONB.2006.05.005

Hollander-Cohen, L., Cohen, O., Shulman, M., Aiznkot, T., Fontanaud, P., Revah, O., Mollard, P., Golan, M., & Levavi-Sivan, B. (2024). The satiety hormone cholecystokinin gates reproduction in fish by controlling gonadotropin secretion. *ELife*, 13, RP96344. https://doi.org/10.7554/ELIFE.96344

Hook, V., Funkelstein, L., Lu, D., Bark, S., Wegrzyn, J., & Hwang, S. R. (2008). Proteases for Processing Proneuropeptides into Peptide Neurotransmitters and Hormones. Annual *Review of Pharmacology and Toxicology*, 48, 393. https://doi.org/10.1146/ANNUREV.PHARMTOX.48.113006.094812

Horsthemke, B., & Bauer, K. (1980). Characterization of a nonchymotrypsin-like endopeptidase from anterior pituitary that hydrolyzes luteining hormone-releasing hormone at the tyrosyl-glycine and histidyl-tryptophan bonds. Biochemistry, 19(13), 2867–2873. https://doi.org/10.1021/BI00554A008
Hotta, K., Hosaka, M., Tanabe, A., & Takeuchi, T. (2009). Secretogranin II binds to secretogranin III and forms secretory granules with orexin, neuropeptide Y, and POMC. Journal of Endocrinology, 202(1), 111–121. https://doi.org/10.1677/JOE-08-0531

Hou, L., Farley, K., & Remold-O'Donnell, E. (2015). SerpinB1: A Global Regulator of Neutrophil Homeostasis. The Serpin Family: *Proteins with Multiple Functions in Health and Disease*, 77–91. https://doi.org/10.1007/978-3-319-22711-5_6

Hutter S., Penn D.J, Magee S., & Zala S.M. (2010). Reproductive behaviour of wild zebrafish (Danio rerio) in large tanks. *Behaviour*, 641–660.https://brill.com/view/journals/beh/147/5-6/article-p641_5.xml?language=en

Huttner, W. B., Gerdes, H. H., & Rosa, P. (1991). The granin-(chromogranin/secretogranin) family. *Trends in Biochemical Sciences*, 16(C), 27–30. https://pubmed.ncbi.nlm.nih.gov/2053134/

Huttner, W. B., & Natori, S. (1995). Regulated Secretion: Helper proteins for neuroendocrine secretion. *Current Biology*, 5(3), 242–245. https://doi.org/10.1016/S0960-9822(95)00049-2

Hwang, W. Y., Fu, Y., Reyon, D., Maeder, M. L., Tsai, S. Q., Sander, J. D., Peterson, R. T., Yeh, J.-R. J., & Joung, J. K. (2013). Efficient genome editing in zebrafish using a CRISPR-Cas system. *Nature Biotechnology*, 31(3), 227–229. https://doi.org/10.1038/nbt.2501

Ida-Eto, M., Oyabu, A., Ohkawara, T., Tashiro, Y., Narita, N., & Narita, M. (2012). Existence of Manserin, a Secretogranin II–Derived Neuropeptide, in the Rat Inner Ear: Relevance to Modulation of Auditory and Vestibular System. *Journal of Histochemistry and Cytochemistry*, 60(1), 69. https://doi.org/10.1369/0022155411425688

Ings, J. S., & Van Der Kraak, G. J. (2006). Characterization of the mRNA expression of StAR and steroidogenic enzymes in zebrafish ovarian follicles. *Molecular Reproduction and Development*, 73(8), 943–954. https://doi.org/10.1002/MRD.20490

Irwig, M. S., Fraley, G. S., Smith, J. T., Acohido, B. V., Popa, S. M., Cunningham, M. J., Gottsch, M. L., Clifton, D. K., & Steiner, R. A. (2004). Kisspeptin activation of gonadotropin releasing hormone neurons and regulation of KiSS-1 mRNA in the male rat. *Neuroendocrinology*, 80(4), 264–272.https://pubmed.ncbi.nlm.nih.gov/15665556/

Jéhannet, P., Palstra, A. P., Meijerhof, M., Schipper, H., Giménez, I. N., Dirks, R. P., Swinkels, W., Heinsbroek, L. T. N., & Komen, H. (2023). The induction of oocyte maturation and ovulation in the European eel (Anguilla anguilla): in vitro and in vivo comparison of progesterone with 17α,20β-dihydroxy-4-pregnen-3-one. *Frontiers in Physiology*, 14, 1207542. https://pubmed.ncbi.nlm.nih.gov/37614755/

Jin, S., Yan, X., Zhang, H., & Fan, W. (2015). Weight-length relationships and Fulton's condition factors of skipjack tuna (Katsuwonus pelamis) in the western and central Pacific Ocean. *PeerJ*, 2015(2), e758. https://pubmed.ncbi.nlm.nih.gov/25699207/

Kakar, S. S., Malik, M. T., Winters, S. J., & Mazhawidza, W. (2004). Gonadotropin-Releasing Hormone Receptors: Structure, Expression, and Signaling Transduction. *Vitamins and Hormones*, 69, 151–207. https://doi.org/10.1016/S0083-6729(04)69006-6

Kalueff, A. V., Gebhardt, M., Stewart, A. M., Cachat, J. M., Brimmer, M., Chawla, J. S., Craddock, C., Kyzar, E. J., Roth, A., Landsman, S., Gaikwad, S., Robinson, K., Baatrup, E., Tierney, K., Shamchuk, A., Norton, W., Miller, N., Nicolson, T., Braubach, O., … Schneider, H. (2013). Towards a Comprehensive Catalog of Zebrafish Behavior 1.0 and Beyond.*Zebrafish*, 10(1), 70–86. https://doi.org/10.1089/ZEB.2012.0861

Kapahnke, M., Banning, A., & Tikkanen, R. (2016). Random Splicing of Several Exons Caused by a Single Base Change in the Target Exon of CRISPR/Cas9 Mediated Gene Knockout. *Cells*, 5(4). https://doi.org/10.3390/CELLS5040045

Kaprara, A., & Huhtaniemi, I. T. (2018). The hypothalamus-pituitary-gonad axis: Tales of mice and men. Metabolism: Clinical and Experimental, 86, 3–17. https://doi.org/10.1016/J.METABOL.2017.11.018

Kasten, T. L., White, S. A., Norton, T. T., Bond, C. T., Adelman, J. P., & Fernald, R. D. (1996). Characterization of two new preproGnRH mRNAs in the tree shrew: First direct evidence for mesencephalic GnRH gene expression in a placental mammal. *General and Comparative Endocrinology*, 104(1), 7–19. https://doi.org/10.1006/gcen.1996.0135

Kimberly, M. (2018). Characterization and Role of Secretogranin-II/Secretoneurin in Zebrafish Reproduction [university of Ottawa]. https://ruor.uottawa.ca/items/00a37aa0-6c18-4b1a-a4b0-cd0a60f06c3a

Komori, T., Hata, S., Mabuchi, A., Genova, M., Harada, T., Fukuyama, M., Chinen, T., & Kitagawa, D. (2023). A CRISPR-del-based pipeline for complete gene knockout in human diploid cells. *Journal of Cell Science*, 136(6). https://doi.org/10.1242/jcs.260000

Kornbluth, S., & Fissore, R. (2015). Vertebrate Reproduction. *Cold Spring Harbor Perspectives in Biology*, 7(10), a006064.https://doi.org/10.1101/CSHPERSPECT.A006064

Ku, N. O., Strnad, P., Bantel, H., & Omary, M. B. (2016). Keratins: Biomarkers and Modulators of Apoptotic and Necrotic Cell Death in the Liver. *Hepatology* (Baltimore, Md.), 64(3), 966. https://doi.org/10.1002/HEP.28493

Kwok, H. F., So, W. K., Wang, Y., & Ge, W. (2005). Zebrafish Gonadotropins and Their Receptors: I. Cloning and Characterization of Zebrafish Follicle-Stimulating Hormone and Luteinizing Hormone Receptors— Evidence for Their Distinct Functions in Follicle Development. *Biology of Reproduction*, 72(6), 1370–1381. https://pubmed.ncbi.nlm.nih.gov/15728795/

Labrou, N. E., & Clonis, Y. D. (1997). L-Malate Dehydrogenase fromPseudomonas stutzeri:Purification and Characterization. *Archives of Biochemistry and Biophysics*, 337(1), 103–114. https://doi.org/10.1006/ABBI.1996.9748

Lakshminarasimha, A. B., Puvvada, M., Hammerschmidt, M., & Michel, M. (2022). Leptin modulates oocyte maturation by a central and a direct pathway in zebrafish. *Journal of Endocrinology*, 254(1), 1–12. https://doi.org/10.1530/JOE-22-0026

Lee, S. L. J., Horsfield, J. A., Black, M. A., Rutherford, K., & Gemmell, N. J. (2018). Identification of sex differences in zebrafish (Danio rerio) brains during early sexual differentiation and masculinization using 17α-methyltestoterone. *Biology of Reproduction*, 99(2), 446–460. https://doi.org/10.1093/BIOLRE/IOX175

Lethimonier, C., Madigou, T., Muñoz-Cueto, J. A., Lareyre, J. J., & Kah, O. (2004). Evolutionary aspects of GnRHs, GnRH neuronal systems and GnRH receptors in teleost fish. *General and Comparative Endocrinology*, 135(1), 1–16. https://doi.org/10.1016/j.ygcen.2003.10.007

Li, H., Liang, H., Gao, X., Zeng, X., Zheng, S., Wang, L., Yuan, F., Xu, S., Yin, Z., & Hu, G. (2025). Cholecystokinin (CCK) Is a Mediator Between Nutritional Intake and Gonadal Development in Teleosts. Cells, 14(2), 78. https://pubmed.ncbi.nlm.nih.gov/39851506/

Li, H., Yang, Y., Hong, W., Huang, M., Wu, M., & Zhao, X. (2020). Applications of genome editing technology in the targeted therapy of human diseases: mechanisms, advances and prospects. *Signal Transduction and Targeted Therapy*, 5(1), 1. https://doi.org/10.1038/s41392-019-0089-y

Li, J., & Ge, W. (2020). Zebrafish as a model for studying ovarian development: Recent advances from targeted gene knockout studies. *Molecular and Cellular Endocrinology*, 507. https://doi.org/10.1016/J.MCE.2020.110778
Li, N., & Zhan, X. (2019). Mitochondrial Dysfunction Pathway Networks and Mitochondrial Dynamics in the Pathogenesis of Pituitary Adenomas. *Frontiers in Endocrinology*, 10, 427526. https://pubmed.ncbi.nlm.nih.gov/31649621/

Li, S., Zhang, Y., Liu, Y., Huang, X., Huang, W., Lu, D., Zhu, P., Shi, Y., Cheng, C. H. K., Liu, X., & Lin, H. (2009). Structural and functional multiplicity of the kisspeptin/GPR54 system in goldfish (Carassius auratus). *Journal of Endocrinology*, 201(3), 407–418. https://doi.org/10.1677/JOE-09-0016,
Li, Y., Jia, Z., Zhang, S., & He, X. (2021). Progress in Gene-Editing Technology of Zebrafish. *Biomolecules*, 11(9), 1300. https://doi.org/10.3390/biom11091300

Liang, F., Li, J. Y., Lovisetti-Scamihorn, P., Coen, E., Depreitere, J., Claeys, M., Wechsung, E., Dahlström, A., Winkler, H., & De Potter, W. P. (1999). The processing of secretogranin II in the peripheral nervous system: release of secretoneurin from porcine sympathetic nerve terminals. *Brain Research*, 818(2), 459–467. https://doi.org/10.1016/S0006-8993(98)01327-4

Lin, Q., Low, L. W. L., Lau, A., Chua, E. W. L., Matsuoka, Y., Lian, Y., Monteiro, A., Tate, S., Gunaratne, J., & Carney, T. J. (2019). Tracking genome-editing and associated molecular perturbations by SWATH mass spectrometry. *Scientific Reports*, 9(1). https://doi.org/10.1038/S41598-019-51612-Z

Lin, Y., Ran, L., Du, X., Yang, H., & Wu, Y. (2023). Oxysterol-Binding Protein: new insights into lipid transport functions and human diseases. Biochimica et Biophysica Acta (BBA) - *Molecular and Cell Biology of Lipids*, 1868(9), 159365. https://doi.org/10.1016/J.BBALIP.2023.159365

Liu, D. T., Carter, N. J., Wu, X. J., Hong, W. S., Chen, S. X., & Zhu, Y. (2018). Progestin and nuclear progestin receptor are essential for upregulation of metalloproteinase in zebrafish preovulatory follicles. *Frontiers in Endocrinology, 9*, Article 517. https://doi.org/10.3389/fendo.2018.00517

Liu, Y., Tang, H., Xie, R., Li, S., Liu, X., Lin, H., Zhang, Y., & Cheng, C. H. K. (2017). Genetic evidence for multifactorial control of the reproductive axis in zebrafish. *Endocrinology, 158*(3), 604–611. https://doi.org/10.1210/en.2016-1540

Liu, Z., Niu, C., & Li, J. (2021). Pyroptosis is involved in ovulation of zebrafish. *Cell Discovery, 7*, Article 4. https://doi.org/10.1038/s41421-021-00263-4

Lord, M. S., Melrose, J., Day, A. J., & Whitelock, J. M. (2020). The inter-α-trypsin inhibitor family: Versatile molecules in biology and pathology. *Journal of Histochemistry & Cytochemistry, 68*(12), 907–927. https://doi.org/10.1369/0022155420940067

Lu, C., Peng, D., Erandani, W. C. K. U., Mitchell, K., Martyniuk, C. J., & Trudeau, V. L. (2023). Simultaneous extraction and detection of peptides, steroids, and proteins in small tissue samples. *Frontiers in Endocrinology, 14*, Article 1266985. https://doi.org/10.3389/fendo.2023.1266985

Lydon, J. P., DeMayo, F. J., Funk, C. R., Mani, S. K., Hughes, A. R., Montgomery, C. A., Shyamala, G., Conneely, O. M., & O'Malley, B. W. (1995). Mice lacking progesterone receptor exhibit pleiotropic reproductive abnormalities. *Genes & Development, 9*(18), 2266–2278. https://doi.org/10.1101/gad.9.18.2266

Ma, A. C. H., Chen, Y., Blackburn, P. R., & Ekker, S. C. (2016). TALEN-mediated mutagenesis and genome editing. In M. J. Stewart (Ed.), *Methods in Molecular Biology* (Vol. 1451, pp. 17–30). Springer. https://doi.org/10.1007/978-1-4939-3771-4_2

Mahata, M., Mahata, S. K., Fischer-Colbrie, R., & Winkler, H. (1993). Ontogenic development and distribution of mRNAs of chromogranin A and B, secretogranin II, p65 and synaptin/synaptophysin in rat brain. *Developmental Brain Research, 76*(1), 43–58. https://doi.org/10.1016/0165-3806(93)90121-P

Mank, J. E., Promislow, D. E. L., & Avise, J. C. (2006). Evolution of alternative sex-determining mechanisms in teleost fishes. *Biological Journal of the Linnean Society, 87*(1), 83–93. https://doi.org/10.1111/j.1095-8312.2006.00558.x

Martinez-Mayer, J., Brinkmeier, M. L., O'Connell, S. P., Ukagwu, A., Marti, M. A., Miras, M., Forclaz, M. V., Benzrihen, M. G., Cheung, L. Y. M., Camper, S. A., Ellsworth, B. S., Raetzman, L. T., Pérez-Millán, M. I., & Davis, S. W. (2024). Knockout mice with pituitary malformations help identify human cases of hypopituitarism. *Genome Medicine, 16*(1), Article 75. https://doi.org/10.1186/s13073-024-01347-y

Marvel, M., Levavi-Sivan, B., Wong, T. T., Zmora, N., & Zohar, Y. (2021). Gnrh2 maintains reproduction in fasting zebrafish through dynamic neuronal projection changes and regulation of gonadotropin synthesis, oogenesis, and reproductive behaviors. *Scientific Reports, 11*, Article 6657. https://doi.org/10.1038/s41598-021-86018-3

Marvel, M., Spicer, O. S., Wong, T. T., Zmora, N., & Zohar, Y. (2018). Knockout of the Gnrh genes in zebrafish: Effects on reproduction and potential compensation by reproductive and feeding-related neuropeptides. *Biology of Reproduction, 99*(3), 565–577. https://doi.org/10.1093/biolre/ioy078

Masui, Y., & Clarke, H. J. (1979). Oocyte maturation. *International Review of Cytology, 57*, 185–282. https://doi.org/10.1016/S0074-7696(08)61464-3

Mayer, I. (2019). The role of reproductive sciences in the preservation and breeding of commercial and threatened teleost fishes. In C. Yoshizaki & N. Yoshikuni (Eds.), *Reproductive Biology and Phylogeny of Fishes (Agnathans and Bony Fishes)* (Vol. 1200, pp. 187–224). Springer. https://doi.org/10.1007/978-3-030-23633-5_7

Mehlmann, L. M., Kalinowski, R. R., Ross, L. F., Parlow, A. F., Hewlett, E. L., & Jaffe, L. A. (2006). Meiotic resumption in response to luteinizing hormone is independent of a Gi family G protein or calcium in the mouse oocyte. *Developmental Biology, 299*(2), 345–355. https://doi.org/10.1016/j.ydbio.2006.07.039

Messager, S., Chatzidaki, E. E., Ma, D., Hendrick, A. G., Zahn, D., Dixon, J., Thresher, R. R., Malinge, I., Lomet, D., Carlton, M. B. L., Colledge, W. H., Caraty, A., & Aparicio, S. A. J. R. (2005). Kisspeptin directly stimulates gonadotropin-releasing hormone release via G protein-coupled receptor 54. *Proceedings of the National Academy of Sciences, 102*(5), 1761–1766. https://doi.org/10.1073/pnas.0409330102

Migliaccio, M., Chioccarelli, T., Ambrosino, C., Suglia, A., Manfrevola, F., Carnevali, O., Fasano, S., Pierantoni, R., & Cobellis, G. (2018). Characterization of follicular atresia responsive to BPA in zebrafish by morphometric analysis of follicular stage progression. *International Journal of Endocrinology, 2018*, Article 4298195. https://doi.org/10.1155/2018/4298195

Millar, R. P. (2003). GnRH II and type II GnRH receptors. *Trends in Endocrinology & Metabolism, 14*(1), 35–43. https://doi.org/10.1016/S1043-2760(02)00016-4

Mitchell, K., Zhang, W. S., Lu, C., Tao, B., Chen, L., Hu, W., & Trudeau, V. L. (2020). Targeted mutation of secretogranin-2 disrupts sexual behavior and reproduction in zebrafish. *Proceedings of the National Academy of Sciences, 117*(23), 12958–12966. https://doi.org/10.1073/pnas.2002004117

Miyamoto, K., Hasegawa, Y., Minegishi, T., Nomura, M., Takahashi, Y., Igarashi, M., Kangawa, K., & Matsuo, H. (1982). Isolation and characterization of chicken hypothalamic luteinizing hormone-releasing hormone. *Biochemical and Biophysical Research Communications, 107*(3), 820–827. https://doi.org/10.1016/0006-291x(82)90596-4

Mohamedien, D., Mokhtar, D. M., Abdellah, N., Awad, M., Albano, M., & Sayed, R. K. A. (2023). Ovary of zebrafish during spawning season: Ultrastructure and immunohistochemical profiles of Sox9 and myostatin. *Animals, 13*(21), Article 3362. https://doi.org/10.3390/ani13213362

Mohseni, M., & Chishti, A. H. (2008). The headpiece domain of dematin regulates cell shape, motility, and wound healing by modulating RhoA activation. *Molecular and Cellular Biology, 28*(15), 4712–4725. https://doi.org/10.1128/MCB.00237-08

Mollah, M. F. A., & Tan, E. S. P. (1983). HCG-induced spawning of the catfish, Clarias macrocephalus (Günther). *Aquaculture, 35*(1), 239–247. https://doi.org/10.1016/0044-8486(83)90094-7

Montero-Hadjadje, M., Pelletier, G., Yon, L., Li, S., Guillemot, J., Magoul, R., Tillet, Y., Vaudry, H., & Anouar, Y. (2003). Biochemical characterization and immunocytochemical localization of EM66, a novel peptide derived from secretogranin II, in the rat pituitary and adrenal glands. *Journal of Histochemistry & Cytochemistry, 51*(8), 1083–1095. https://doi.org/10.1177/002215540305100812

Mou, H., Smith, J. L., Peng, L., Yin, H., Moore, J., Zhang, X. O., Song, C. Q., Sheel, A., Wu, Q., Ozata, D. M., Li, Y., Anderson, D. G., Emerson, C. P., Sontheimer, E. J., Moore, M. J., Weng, Z., & Xue, W. (2017). CRISPR/Cas9-mediated genome editing induces exon skipping by alternative splicing or exon deletion. *Genome Biology, 18*(1), Article 108. https://doi.org/10.1186/s13059-017-1237-8

Murphy, D., Si-Hoe, S.-L., Brenner, S., & Venkatesh, B. (1998). Something fishy in the rat brain: Molecular genetics of the hypothalamo-neurohypophysial system. *BioEssays, 20*(9), 741–749. https://doi.org/10.1002/(SICI)1521-1878(199809)20:9<741::AID-BIES7>3.0.CO;2-J

Nagahama, Y., & Yamashita, M. (2008). Regulation of oocyte maturation in fish. *Development, Growth & Differentiation, 50*(Suppl. 1), S195–S219. https://doi.org/10.1111/j.1440-169X.2008.01019.x

Nagahama, Y., Yoshikuni, M., Yamashita, M., Tokumoto, T., & Katsu, Y. (1995). Regulation of oocyte growth and maturation in fish. *Current Topics in Developmental Biology, 30*, 103–145. https://doi.org/10.1016/S0070-2153(08)60565-7

Nakajo, M., Kanda, S., Karigo, T., Takahashi, A., Akazome, Y., Uenoyama, Y., Kobayashi, M., & Oka, Y. (2018). Evolutionally conserved function of kisspeptin neuronal system is nonreproductive regulation as revealed by nonmammalian study. *Endocrinology, 159*(1), 163–183. https://doi.org/10.1210/en.2017-00808

Nasiadka, A., & Clark, M. D. (2012). Zebrafish breeding in the laboratory environment. *ILAR Journal, 53*(2), 161–168. https://doi.org/10.1093/ilar.53.2.161

Neill, J. D. (2002). Minireview: GnRH and GnRH receptor genes in the human genome. *Endocrinology, 143*(3), 737–743. https://doi.org/10.1210/endo.143.3.8705

Nejad, S. Z., Tehrani, F. R., & Zadeh-Vakili, A. (2017). The role of kisspeptin in female reproduction. *International Journal of Endocrinology and Metabolism, 15*(3), e44337. https://doi.org/10.5812/ijem.44337

Newman, M., & Ausubel, F. M. (2016). Introduction to gene editing and manipulation using CRISPR/Cas9 technology. *Current Protocols in Molecular Biology, 115*(1), 31.1.1–31.1.11. https://doi.org/10.1002/cpmb.14

Nicol, L., McNeilly, J. R., Stridsberg, M., Crawford, J. L., & McNeilly, A. S. (2002). Influence of steroids and GnRH on biosynthesis and secretion of secretogranin II and chromogranin A in relation to LH release in LβT2 gonadotroph cells. *Journal of Endocrinology, 174*(3), 473–483. https://doi.org/10.1677/joe.0.1740473

Nishiguchi, R., Azuma, M., Yokobori, E., Uchiyama, M., & Matsuda, K. (2012). Gonadotropin-releasing hormone 2 suppresses food intake in the zebrafish, *Danio rerio*. *Frontiers in Endocrinology, 3*, Article 122. https://doi.org/10.3389/fendo.2012.00122

Oduwole, O. O., Peltoketo, H., & Huhtaniemi, I. T. (2018). Role of follicle-stimulating hormone in spermatogenesis. *Frontiers in Endocrinology, 9*, Article 763. https://doi.org/10.3389/fendo.2018.00763

Ogawa, S., & Parhar, I. S. (2018). Biological significance of kisspeptin–Kiss1 receptor signaling in the habenula of teleost species. *Frontiers in Endocrinology, 9*, Article 222. https://doi.org/10.3389/fendo.2018.00222

Ogawa, S., Yamamoto, N., Hagio, H., Oka, Y., & Parhar, I. S. (2022). Multiple gonadotropin-releasing hormone systems in non-mammalian vertebrates: Ontogeny, anatomy, and physiology. *Journal of Neuroendocrinology, 34*(5), e13068. https://doi.org/10.1111/jne.13068

Orlowski, M., Michaud, C., & Chu, T. G. (1983). A soluble metalloendopeptidase from rat brain. Purification of the enzyme and determination of specificity with synthetic and natural peptides. *European Journal of Biochemistry, 135*(1), 81–88. https://doi.org/10.1111/j.1432-1033.1983.tb07620.x

Orlowski, M., Reznik, S., Ayala, J., & Pierotti, A. R. (1989). Endopeptidase 24.15 from rat testes: Isolation of the enzyme and its specificity toward synthetic and natural peptides, including enkephalin-containing peptides. *Biochemical Journal, 261*(3), 951–958. https://doi.org/10.1042/bj2610951

Ottesen, A. H., Louch, W. E., Carlson, C. R., Landsverk, O. J. B., Kurola, J., Johansen, R. F., Moe, M. K., Aronsen, J. M., Høiseth, A. D., Jarstadmarken, H., Nygård, S., Bjørås, M., Sjaastad, I., Pettilä, V., Stridsberg, M., Omland, T., Christensen, G., & Røsjø, H. (2015). Secretoneurin is a novel prognostic cardiovascular biomarker associated with cardiomyocyte calcium handling. *Journal of the American College of Cardiology, 65*(4), 339–351. https://doi.org/10.1016/j.jacc.2014.10.065

Ozawa, H., & Takata, K. (1995). The granin family: Its role in sorting and secretory granule formation. *Cell Structure and Function, 20*(6), 415–420. https://doi.org/10.1247/csf.20.415

Ozdemir, V., Bertilsson, L., Miura, J., Carpenter, E., Reist, C., Harper, P., Widén, J., Svensson, J. O., Albers, L. J., Kennedy, J. L., Endrenyi, L., & Kalow, W. (2007). CYP2D6 genotype in relation to perphenazine concentration and pituitary pharmacodynamic tissue sensitivity in Asians: CYP2D6-serotonin-dopamine crosstalk revisited. *Pharmacogenetics and Genomics, 17*(5), 339–347. https://doi.org/10.1097/fpc.0b013e32801a3c10

Palstra, A. P., van de Ven, I., Jéhannet, P., Kruijt, L., Schipper, H., Swinkels, W., & Heinsbroek, L. T. N. (2023). Human chorionic gonadotropin enhancement of early maturation and consequences for reproductive success of feminized European eel (*Anguilla anguilla*). *Fishes, 8*(6), 281. https://doi.org/10.3390/fishes8060281

Pang, Y., & Thomas, P. (2009). Involvement of estradiol-17β and its membrane receptor, G protein coupled receptor 30 (GPR30), in regulation of oocyte maturation in zebrafish, *Danio rerio*. *General and Comparative Endocrinology, 161*(1), 58–61. https://doi.org/10.1016/j.ygcen.2008.10.003

Patiño, R., Yoshizaki, G., Thomas, P., & Kagawa, H. (2001). Gonadotropic control of ovarian follicle maturation: The two-stage concept and its mechanisms. *Comparative Biochemistry and Physiology Part B: Biochemistry and Molecular Biology, 129*(2–3), 427–439. https://doi.org/10.1016/s1096-4959(01)00344-x

Peñas-Lledó, E. M., & Llerena, A. (2014). CYP2D6 variation, behaviour and psychopathology: Implications for pharmacogenomics-guided clinical trials. *British Journal of Clinical Pharmacology, 77*(4), 673–683. https://doi.org/10.1111/bcp.12227

Peng, C., Humphries, S., Peter, R. E., Rivier, J. E., Blomqvist, A. G., & Larhammar, D. (1993). Actions of goldfish neuropeptide Y on the secretion of growth hormone and gonadotropin-II in female goldfish. *General and Comparative Endocrinology, 90*(3), 306–317. https://doi.org/10.1006/gcen.1993.1086

Peng, D., Lu, C., Spadacini, V., Mitchell, K., Tan, Y., Zhang, D., Levavi-Sivan, B., Hu, W., & Trudeau, V. L. (2025). Hormonal dynamics reveal a stimulatory role for secretoneurin in zebrafish ovulation. *PNAS Nexus, 4*(4), pgaf097. https://doi.org/10.1093/pnasnexus/pgaf097

Pertl, C., Kaufmann, W., Amann, R., Heinemann, A., Ebeleseder, K., Polansky, R., Saria, A., & Kim, S. (1998). Secretoneurin, a novel neuropeptide, in the human dental pulp. *Archives of Oral Biology, 43*(5), 361–365. https://doi.org/10.1016/s0003-9969(98)00016-8

Plášek, J., Lazárová, M., Dodulík, J., Šulc, P., Stejskal, D., Švagera, Z., Všianský, F., & Václavík, J. (2022). Secretoneurin as a novel biomarker of cardiovascular episodes: Are we there yet? A narrative review. *Journal of Clinical Medicine, 11*(23), 7191. https://doi.org/10.3390/jcm11237191

Pogoda, H. M., & Hammerschmidt, M. (2007). Molecular genetics of pituitary development in zebrafish. *Seminars in Cell & Developmental Biology, 18*(4), 543–558. https://doi.org/10.1016/j.semcdb.2007.04.004

Pouso, P., Quintana, L., López, G. C., Somoza, G. M., Silva, A. C., & Trudeau, V. L. (2015). The secretogranin-II derived peptide secretoneurin modulates electric behavior in the weakly pulse type electric fish, *Brachyhypopomus gauderio*. *General and Comparative Endocrinology, 222*, 158–166. https://doi.org/10.1016/j.ygcen.2015.06.015

Prykhozhij, S. V., Steele, S. L., Razaghi, B., & Berman, J. N. (2017). A rapid and effective method for screening, sequencing and reporter verification of engineered frameshift mutations in zebrafish. *Disease Models & Mechanisms, 10*(6), 811–822. https://doi.org/10.1242/dmm.026765

Royan, M. R., Siddique, K., Csucs, G., Puchades, M. A., Nourizadeh-Lillabadi, R., Bjaalie, J. G., Henkel, C. V., Weltzien, F.-A., Fontaine, R., Parhar, I., & Somoza, G. M. (2021). 3D atlas of the pituitary gland of the model fish medaka (*Oryzias latipes*). *Frontiers in Endocrinology, 12*, 719843. https://doi.org/10.3389/fendo.2021.719843

Rajendiran, P., Jaafar, F., Kar, S., Sudhakumari, C., Senthilkumaran, B., & Parhar, I. S. (2021). Sex determination and differentiation in teleost: Roles of genetics, environment, and brain. *Biology, 10*(10), 973. https://doi.org/10.3390/biology10100973

Ramachandran, D., Sharma, K., Saxena, V., Nipu, N., Rajapaksha, D. C., Mennigen, J. A., Bertucci, J. I., & Rajeswari, J. J. (2023). Knock-out of vasotocin reduces reproductive success in female zebrafish, *Danio rerio*. *Frontiers in Endocrinology, 14*, 1151299. https://doi.org/10.3389/fendo.2023.1151299

Ramasamy, S., Wang, H., Quach, H. N. B., & Sampath, K. (2006). Zebrafish Staufen1 and Staufen2 are required for the survival and migration of primordial germ cells. *Developmental Biology, 292*(2), 393–406. https://doi.org/10.1016/j.ydbio.2006.01.014

Reyes, R., Cardeñes, B., Machado-Pineda, Y., & Cabañas, C. (2018). Tetraspanin CD9: A key regulator of cell adhesion in the immune system. *Frontiers in Immunology, 9*, 863. https://doi.org/10.3389/fimmu.2018.00863

Rideout, R. M., & Tomkiewicz, J. (2011). Skipped spawning in fishes: More common than you might think. *Marine and Coastal Fisheries, 3*(1), 176–189. https://doi.org/10.1080/19425120.2011.556943

Roch, G. J., Tello, J. A., & Sherwood, N. M. (2014). At the transition from invertebrates to vertebrates, a novel GnRH-like peptide emerges in amphioxus. *Molecular Biology and Evolution, 31*(4), 765–778. https://doi.org/10.1093/molbev/mst269

Rosa, P., & Zanini, A. (1981). Characterization of adenohypophysial polypeptides by two-dimensional gel electrophoresis. II. Sulfated and glycosylated polypeptides. *Molecular and Cellular Endocrinology, 24*(2), 181–193. https://doi.org/10.1016/0303-7207(81)90058-7

Sage, M., & Bern, H. A. (1971). Cytophysiology of the teleost pituitary. *International Review of Cytology*, *31*, 339–376. https://doi.org/10.1016/S0074-7696(08)60062-5

Saito, D., Hasegawa, Y., & Urano, A. (2003). Gonadotropin-releasing hormones modulate electrical activity of vasotocin and isotocin neurons in the brain of rainbow trout. *Neuroscience Letters*, *351*(2), 107–110. https://doi.org/10.1016/j.neulet.2003.08.017

Sales, C. F., Melo, R. M. C., Pinheiro, A. P. B., Luz, R. K., Bazzoli, N., & Rizzo, E. (2019). Autophagy and cathepsin D mediated apoptosis contributing to ovarian follicular atresia in the Nile tilapia. *Molecular Reproduction and Development*, *86*(11), 1592–1602. https://doi.org/10.1002/mrd.23245

Samia, M., Larivière, K. E., Rochon, M. H., Hibbert, B. M., Basak, A., & Trudeau, V. L. (2004). Seasonal cyclicity of secretogranin-II expression and its modulation by sex steroids and GnRH in the female goldfish pituitary. *General and Comparative Endocrinology*, *139*(3), 198–205. https://doi.org/10.1016/j.ygcen.2004.09.004

Santos, H. B., Thomé, R. G., Arantes, F. P., Sato, Y., Bazzoli, N., & Rizzo, E. (2008). Ovarian follicular atresia is mediated by heterophagy, autophagy, and apoptosis in *Prochilodus argenteus* and *Leporinus taeniatus* (Teleostei: Characiformes). *Theriogenology*, *70*(9), 1449–1460. https://doi.org/10.1016/j.theriogenology.2008.06.091

Satoh, F., Takahashi, K., Murakami, O., Totsune, K., Ohneda, M., Mizuno, Y., Sone, M., Miura, Y., Takase, S., Hayashi, Y., Sasano, H., & Mouri, T. (1997). Cerebellin and cerebellin mRNA in the human brain, adrenal glands and the tumour tissues of adrenal tumour, ganglioneuroblastoma and neuroblastoma. *Journal of Endocrinology*, *154*(1), 27–34. https://doi.org/10.1677/joe.0.1540027

Schmidt, F., & Braunbeck, T. (2011). Alterations along the hypothalamic-pituitary-thyroid axis of the zebrafish (*Danio rerio*) after exposure to propylthiouracil. *Journal of Thyroid Research*, *2011*, Article 376243. https://doi.org/10.4061/2011/376243

Selman, K., Wallace, R. A., Sarka, A., & Qi, X. (1993). Stages of oocyte development in the zebrafish, *Brachydanio rerio*. *Journal of Morphology*, *218*(2), 203–224. https://doi.org/10.1002/jmor.1052180209

Seminara, S. B., Messager, S., Chatzidaki, E. E., Thresher, R. R., Acierno, J. S., Shagoury, J. K., Bo-Abbas, Y., Kuohung, W., Schwinof, K. M., Hendrick, A. G., Zahn, D., Dixon, J., Kaiser, U. B., Slaugenhaupt, S. A., Gusella, J. F., O'Rahilly, S., Carlton, M. B. L., Crowley, W. F., Aparicio, S. A. J. R., & Colledge, W. H. (2003). The GPR54 gene as a regulator of puberty. *New England Journal of Medicine*, *349*(17), 1614–1627. https://doi.org/10.1056/nejmoa035322

Shang, G., Peng, X., Ji, C., Zhai, G., Ruan, Y., Lou, Q., Jin, X., He, J., Wang, H., & Yin, Z. (2019). Steroidogenic acute regulatory protein and luteinizing hormone are required for normal ovarian steroidogenesis and oocyte maturation in zebrafish. *Biology of Reproduction*, *101*(4), 760–770. https://doi.org/10.1093/biolre/ioz132

Sharma, L., Lu, J., & Bai, Y. (2009). Mitochondrial respiratory complex I: Structure, function and implication in human diseases. *Current Medicinal Chemistry*, *16*(10), 1266–1277. https://doi.org/10.2174/092986709787846578

Shaw, K., Lu, C., Liu, X., & Trudeau, V. L. (2023). Arginine vasopressin injection rescues delayed oviposition in *cyp19a1b* -/- mutant female zebrafish. *Frontiers in Endocrinology*, *14*, Article 1308675. https://doi.org/10.3389/fendo.2023.1308675

Shaw, K., Therrien, M., Lu, C., Liu, X., & Trudeau, V. L. (2023). Mutation of brain aromatase disrupts spawning behavior and reproductive health in female zebrafish. *Frontiers in Endocrinology*, *14*, Article 1225199. https://doi.org/10.3389/fendo.2023.1225199

Sherwood, N. M., Lovejoy, D. A., & Coe, I. R. (1993). Origin of mammalian gonadotropin-releasing hormones. *Endocrine Reviews*, *14*(2), 241–254. https://doi.org/10.1210/edrv-14-2-241

Shewchuk, B. M. (2014). Prostaglandins and n-3 polyunsaturated fatty acids in the regulation of the hypothalamic–pituitary axis. *Prostaglandins, Leukotrienes and Essential Fatty Acids*, *91*(6), 277–287. https://doi.org/10.1016/j.plefa.2014.09.005

Shi, S., Zhang, Y., Huang, J., Lou, Q., Jin, X., He, J., Zhai, G., & Yin, Z. (2024). Effective "off-on" switch for fertility control in female zebrafish. *Frontiers in Marine Science*, *11*, Article 1381305. https://doi.org/10.3389/fmars.2024.1381305

Shu, H., Yang, L., Zhang, Y., Liu, X., Lin, H., & Li, S. (2018). Identification and functional characterization of two secretogranin II genes in orange-spotted grouper (*Epinephelus coioides*). *General and Comparative Endocrinology*, *261*, 115–126. https://doi.org/10.1016/j.ygcen.2018.02.010

Siddique, K., Ager-Wick, E., Fontaine, R., Weltzien, F. A., & Henkel, C. V. (2021). Characterization of hormone-producing cell types in the teleost pituitary gland using single-cell RNA-seq. *Scientific Data*, *8*(1), Article 279. https://doi.org/10.1038/s41597-021-01058-8

Smits, A. H., Ziebell, F., Joberty, G., Zinn, N., Mueller, W. F., Clauder-Münster, S., Eberhard, D., Fälth Savitski, M., Grandi, P., Jakob, P., Michon, A. M., Sun, H., Tessmer, K., Bürckstümmer, T., Bantscheff, M., Steinmetz, L. M., Drewes, G., & Huber, W. (2019). Biological plasticity rescues target activity in CRISPR knock outs. *Nature Methods*, *16*(11), 1087–1093. https://doi.org/10.1038/s41592-019-0614-5

So, W. K., Kwok, H. F., & Ge, W. (2005). Zebrafish gonadotropins and their receptors: II. Cloning and characterization of zebrafish follicle-stimulating hormone and luteinizing hormone subunits—their spatial-temporal expression patterns and receptor specificity. *Biology of Reproduction*, *72*(6), 1382–1396. https://doi.org/10.1095/biolreprod.104.038216

Soliman, R., Cordero-Maldonado, M. L., Martins, T. G., Moein, M., Conrotte, J. F., Warmack, R. A., Skupin, A., Crawford, A. D., Clarke, S. G., & Linster, C. L. (2021). *L-Isoaspartyl methyltransferase deficiency in zebrafish leads to impaired calcium signaling in the brain*. *Frontiers in Genetics, 11*, 612343. https://doi.org/10.3389/fgene.2020.612343

Somoza, G. M., Miranda, L. A., Strobl-Mazzulla, P., & Guilgur, L. G. (2002). Gonadotropin-releasing hormone (GnRH): From fish to mammalian brains. *Cellular and Molecular Neurobiology, 22*(5–6), 589–609. https://doi.org/10.1023/A:1021888420271

Spadacini, V. (2024). *Activation of novel secretoneurin circuits in ovulating zebrafish* [Master's thesis, University of Ottawa]. uO Research. https://doi.org/10.20381/ruor-30299

Spence, R., Gerlach, G., Lawrence, C., & Smith, C. (2008). The behaviour and ecology of the zebrafish, *Danio rerio*. *Biological Reviews, 83*(1), 13–34. https://doi.org/10.1111/j.1469-185x.2007.00030.x

Spicer, O. S., Wong, T. T., Zmora, N., & Zohar, Y. (2016). Targeted mutagenesis of the hypophysiotropic *gnrh3* in zebrafish (*Danio rerio*) reveals no effects on reproductive performance. *PLOS ONE, 11*(6), e0158141. https://doi.org/10.1371/journal.pone.0158141

Stacey, N. E., & Peter, R. E. (1979). Central action of prostaglandins in spawning behaviour of female goldfish. *Physiology & Behavior, 22*(6), 1191–1196. https://doi.org/10.1016/0031-9384(79)90275-0

Takahashi, A., Kanda, S., Abe, T., & Oka, Y. (2016). Evolution of the hypothalamic-pituitary-gonadal axis regulation in vertebrates revealed by knockout medaka. *Endocrinology, 157*(10), 3994–4002. https://doi.org/10.1210/en.2016-1356

Takahashi-Íñiguez, T., Aburto-Rodríguez, N., Vilchis-González, A. L., & Flores, M. E. (2016). Function, kinetic properties, crystallization, and regulation of microbial malate dehydrogenase. *Journal of Zhejiang University - Science B, 17*(4), 247–266. https://doi.org/10.1631/jzus.B1500219

Tanaka, S., Yu, Y., Levavi-Sivan, B., Zmora, N., & Zohar, Y. (2024). GnRH–gonadotropes interactions revealed by pituitary single-cell transcriptomics in zebrafish. *Endocrinology, 165*(12), bqae151. https://doi.org/10.1210/endocr/bqae151

Tang, H., Liu, Y., Li, J., Yin, Y., Li, G., Chen, Y., Li, S., Zhang, Y., Lin, H., Liu, X., & Cheng, C. H. K. (2016). Gene knockout of nuclear progesterone receptor provides insights into the regulation of ovulation by LH signaling in zebrafish. *Scientific Reports, 6*, 28545. https://doi.org/10.1038/srep28545

Tang, H., Liu, Y., Luo, D., Ogawa, S., Yin, Y., Li, S., Zhang, Y., Hu, W., Parhar, I. S., Lin, H., Liu, X., & Cheng, C. H. K. (2015). The kiss/kissr systems are dispensable for zebrafish reproduction: Evidence from gene knockout studies. *Endocrinology, 156*(2), 589–599. https://doi.org/10.1210/en.2014-1204

Tao, B., Hu, H., Mitchell, K., Chen, J., Jia, H., Zhu, Z., Trudeau, V. L., & Hu, W. (2018). Secretogranin-II plays a critical role in zebrafish neurovascular modeling. *Journal of Molecular Cell Biology, 10*(5), 388–401. https://doi.org/10.1093/jmcb/mjy027

Teixeira, C. M. M., Correa, C. N., Iwai, L. K., Ferro, E. S., & Castro, L. M. de. (2019). Characterization of intracellular peptides from zebrafish (*Danio rerio*) brain. *Zebrafish, 16*(3), 240–251. https://doi.org/10.1089/zeb.2018.1718

Tello, J. A., Wu, S., Rivier, J. E., & Sherwood, N. M. (2008). Four functional GnRH receptors in zebrafish: Analysis of structure, signaling, synteny and phylogeny. *Integrative and Comparative Biology, 48*(5), 570–587. https://doi.org/10.1093/icb/icn070

Tokumoto, T., Tokumoto, M., & Nagahama, Y. (2005). Induction and inhibition of oocyte maturation by EDCs in zebrafish. *Reproductive Biology and Endocrinology, 3*, 69. https://doi.org/10.1186/1477-7827-3-69

Tokumoto, T., Yamaguchi, T., Ii, S., & Tokumoto, M. (2011). In vivo induction of oocyte maturation and ovulation in zebrafish. *PLOS ONE, 6*(9), e25206. https://doi.org/10.1371/journal.pone.0025206

Tong, C., Liang, Y., Zhang, Z., Wang, S., Zheng, X., Liu, Q., & Song, B. (2023). Review of knockout technology approaches in bacterial drug resistance research. *PeerJ, 11*, e15790. https://doi.org/10.7717/peerj.15790

Trebak, F., Dubuc, I., Arabo, A., Alaoui, A., Boukhzar, L., Maucotel, J., Picot, M., Cherifi, S., Duparc, C., Leprince, J., Prévost, G., Anouar, Y., Magoul, R., & Chartrel, N. (2017). A potential role for the secretogranin II-derived peptide EM66 in the hypothalamic regulation of feeding behaviour. *Journal of Neuroendocrinology, 29*(3), e12459. https://doi.org/10.1111/jne.12459

Troger, J., Theurl, M., Kirchmair, R., Pasqua, T., Tota, B., Angelone, T., Cerra, M. C., Nowosielski, Y., Mätzler, R., Troger, J., Gayen, J. R., Trudeau, V., Corti, A., & Helle, K. B. (2017). Granin-derived peptides. *Progress in Neurobiology, 154*, 37–61. https://doi.org/10.1016/j.pneurobio.2017.04.003

Trudeau, V. L. (2018). Facing the challenges of neuropeptide gene knockouts: Why do they not inhibit reproduction in adult teleost fish? *Frontiers in Neuroscience, 12*, 302. https://doi.org/10.3389/fnins.2018.00302

Trudeau, V. L. (2022). Neuroendocrine control of reproduction in teleost fish: Concepts and controversies. *Annual Review of Animal Biosciences, 10*(1), 107–130. https://doi.org/10.1146/annurev-animal-020420-042015

Trudeau, V. L., Martyniuk, C. J., Zhao, E., Hu, H., Volkoff, H., Decatur, W. A., & Basak, A. (2012). Is secretoneurin a new hormone? In *General and Comparative Endocrinology, 175*(1), 10–18. Academic Press Inc. https://doi.org/10.1016/j.ygcen.2011.10.008

Trudeau, V. L., Shaw, K., Spadacini, V., & Hu, W. (2023). Reproductive neuroendocrinology in teleost fishes. *SSRN Electronic Journal*. https://doi.org/10.2139/ssrn.4661396

Trudeau, V. L., & Somoza, G. M. (2020). Multimodal hypothalamo-hypophysial communication in the vertebrates. *General and Comparative Endocrinology, 293*, 113475. https://doi.org/10.1016/j.ygcen.2020.113475

Tsakoumis, E., Ahi, E. P., & Schmitz, M. (2022). Impaired leptin signaling causes subfertility in female zebrafish. *Molecular and Cellular Endocrinology, 546*, 111595. https://doi.org/10.1016/j.mce.2022.111595

Tsukada, T., Isowa, Y., Kito, K., Yoshida, S., Toneri, S., Horiguchi, K., Fujiwara, K., Yashiro, T., Kato, T., & Kato, Y. (2019). Identification of TGFβ-induced proteins in non-endocrine mouse pituitary cell line TtT/GF by SILAC-assisted quantitative mass spectrometry. *Cell and Tissue Research, 376*(2), 281–293. https://doi.org/10.1007/s00441-018-02989-2

Unlu, E., Unlu, B. S., Turamanlar, O., Acay, M. B., Kacar, E., Yıldız, Y., Verim, O., Okur, N., Balcik, C., Tasgetiren, S., & Yucel, A. (2015). Alterations in pituitary gland volume in polycystic ovary syndrome: A structural magnetic resonance imaging study. *Clinical Imaging, 39*(3), 449–453. https://doi.org/10.1016/j.clinimag.2014.10.002

Wang, J., Lu, T., Gui, Y., Zhang, X., Cao, X., Li, Y., Li, C., Liu, L., & Ding, Z. (2023). HSPA12A controls cerebral lactate homeostasis to maintain hippocampal neurogenesis and mood stabilization. *Translational Psychiatry, 13*(1). https://doi.org/10.1038/s41398-023-02573-5

Wang, X., Yin, G., Zhang, W., Song, K., Zhang, L., & Guo, Z. (2021). Prostaglandin reductase 1 as a potential therapeutic target for cancer therapy. *Frontiers in Pharmacology, 12*, 717730. https://doi.org/10.3389/fphar.2021.717730

Watanabe, T., Uchiyama, Y., & Grube, D. (1991). Topology of chromogranin A and secretogranin II in the rat anterior pituitary: Potential marker proteins for distinct secretory pathways in gonadotrophs. *Histochemistry, 96*(4), 285–293. https://doi.org/10.1007/bf00271348

White, R. B., Eisen, J. A., Kasten, T. L., & Fernald, R. D. (1998). Second gene for gonadotropin-releasing hormone in humans. *Proceedings of the National Academy of Sciences of the United States of America, 95*(1), 305–309. https://doi.org/10.1073/pnas.95.1.305

White, S. A., & Fernald, R. D. (1993). Gonadotropin-releasing hormone-containing neurons change size with reproductive state in female *Haplochromis burtoni*. *Journal of Neuroscience, 13*(2), 434–441. https://doi.org/10.1523/jneurosci.13-02-00434.1993

Wiedermann, C. J. (2000). Secretoneurin: A functional neuropeptide in health and disease. *Peptides, 21*(8), 1289–1298. https://doi.org/10.1016/s0196-9781(00)00271-0

Wong, A. P. Y., Pipitone, J., Park, M. T. M., Dickie, E. W., Leonard, G., Perron, M., Pike, B. G., Richer, L., Veillette, S., Chakravarty, M. M., Pausova, Z., & Paus, T. (2014). Estimating volumes of the pituitary gland from T1-weighted magnetic-resonance images: Effects of age, puberty, testosterone, and estradiol. *NeuroImage, 94*, 216–221. https://doi.org/10.1016/j.neuroimage.2014.02.030

Wood, A. W., & Van Der Kraak, G. (2002). Inhibition of apoptosis in vitellogenic ovarian follicles of rainbow trout (*Oncorhynchus mykiss*) by salmon gonadotropin, epidermal growth factor, and 17beta-estradiol. *Molecular Reproduction and Development, 61*(4), 511–518. https://doi.org/10.1002/mrd.10108

Wootton, R. J. (1993). The evolution of life histories: Theory and analysis. *Reviews in Fish Biology and Fisheries, 3*(4), 384–385. https://doi.org/10.1007/bf00043394

Wootton, R. J., & Smith, C. (2014). *Reproductive biology of teleost fishes* (pp. 1–472). https://doi.org/10.1002/9781118891360

Wu, X. J., Liu, D. T., Chen, S., Hong, W., & Zhu, Y. (2020). Impaired oocyte maturation and ovulation in membrane progestin receptor (mPR) knockouts in zebrafish. *Molecular and Cellular Endocrinology, 511*, 110856. https://doi.org/10.1016/j.mce.2020.110856

Wu, X. J., Thomas, P., & Zhu, Y. (2018). Pgrmc1 knockout impairs oocyte maturation in zebrafish. *Frontiers in Endocrinology, 9*(SEP), 400527. https://doi.org/10.3389/fendo.2018.00560

Wu, X. J., & Zhu, Y. (2021). Downregulation of nuclear progestin receptor (Pgr) and subfertility in double knockouts of progestin receptor membrane component 1 (pgrmc1) and pgrmc2 in zebrafish. *General and Comparative Endocrinology, 285*, 113275. https://doi.org/10.1016/j.ygcen.2019.113275

Xie, Y., & Dorsky, R. I. (2017). Development of the hypothalamus: Conservation, modification and innovation. *Development (Cambridge, England), 144*(9), 1588–1599. https://doi.org/10.1242/dev.139055

Yajima, A., Ikeda, M., Miyazaki, K., Maeshima, T., Narita, N., & Narita, M. (2004). Manserin, a novel peptide from secretogranin II in the neuroendocrine system. *Neuroreport, 15*(11), 1755–1759. https://doi.org/10.1097/01.wnr.0000127634.38052.84

Yajima, A., Narita, N., & Narita, M. (2008). Recently identified a novel neuropeptide manserin colocalize with the TUNEL-positive cells in the top villi of the rat duodenum. *Journal of Peptide Science, 14*(6), 773–776. https://doi.org/10.1002/psc.991

Yan, D., Lehto, M., Rasilainen, L., Metso, J., Ehnholm, C., Ylä-Herttuala, S., Jauhiainen, M., & Olkkonen, V. M. (2007). Oxysterol binding protein induces upregulation of SREBP-1c and enhances hepatic lipogenesis. *Arteriosclerosis, Thrombosis, and Vascular Biology, 27*(5), 1108–1114. https://doi.org/10.1161/atvbaha.106.138545

Yang, M. J., Xu, D., Yang, D. X., Li, L., Peng, X. X., Chen, Z. gui, & Li, H. (2020). Malate enhances survival of zebrafish against *Vibrio alginolyticus* infection in the same manner as taurine. *Virulence, 11*(1), 349. https://doi.org/10.1080/21505594.2020.1750123

Yang, Q., Liu, C., Qi, K., Xiong, Y., Pan, Y., & Tian, C. (2024). Imaging and quantification of neuropeptides in mouse pituitary tissue by atmospheric pressure matrix-assisted laser desorption/ionization mass spectrometry. *Rapid Communications in Mass Spectrometry: RCM, 38*(12). https://doi.org/10.1002/rcm.9755

Yang, W., Zhang, N., Wu, Y., Zhang, L., Zhang, L., & Zhang, W. (2021). Oxytocin-like signal regulates Lh cells directly but not Fsh cells in the ricefield eel *Monopterus albus*. *Biology of Reproduction, 104*(2), 399–409. https://doi.org/10.1093/biolre/ioaa202

Yang, Y., Wang, G., Li, Y., Hu, J., Wang, Y., & Tao, Z. (2022). Oocytes skipped spawning through atresia is regulated by somatic cells revealed by transcriptome analysis in *Pampus argenteus*. *Frontiers in Marine Science, 9*, 927548. https://doi.org/10.3389/fmars.2022.927548

Yang, Z., Sun, J., Ji, H., Shi, X. C., Li, Y., Du, Z. Y., & Chen, L. Q. (2017). Pigment epithelium-derived factor improves TNFα-induced hepatic steatosis in grass carp (*Ctenopharyngodon idella*). *Developmental & Comparative Immunology, 71*, 8–17. https://doi.org/10.1016/j.dci.2017.01.016

Yeh, Y.-C., Kinoshita, M., Hann Ng, T., Chang, Y.-H., Maekawa, S., Chiang, Y.-A., Aoki, T., & Wang, H.-C. (2017). Using CRISPR/Cas9-mediated gene editing to further explore growth and trade-off effects in myostatin-mutated F4 medaka (*Oryzias latipes*). *Scientific Reports, 7*(1), 11435. https://doi.org/10.1038/s41598-017-09966-9

Yokoi, S., Naruse, K., Kamei, Y., Ansai, S., Kinoshita, M., Mito, M., Iwasaki, S., Inoue, S., Okuyama, T., Nakagawa, S., Young, L. J., & Takeuchi, H. (2020). Sexually dimorphic role of oxytocin in medaka mate choice. *Proceedings of the National Academy of Sciences of the United States of America, 117*(9), 4802–4808. https://doi.org/10.1073/pnas.1921446117

Yong, L., Thet, Z., & Zhu, Y. (2017). Genetic editing of the androgen receptor contributes to impaired male courtship behavior in zebrafish. *Journal of Experimental Biology, 220*(17), 3017–3021. https://doi.org/10.1242/jeb.161596

Zempo, B., Tanaka, N., Daikoku, E., & Ono, F. (2021). High-speed camera recordings uncover previously unidentified elements of zebrafish mating behaviors integral to successful fertilization. *Scientific Reports, 11*(1), 1–9. https://doi.org/10.1038/s41598-021-99638-6

ZFIN: Zebrafish Book: Contents. (n.d.). Retrieved April 27, 2025, from https://zfin.org/zf_info/zfbook/cont.html

Zhang, D., Wang, J., Zhou, C., & Xiao, W. (2017). Zebrafish akt2 is essential for survival, growth, bone development, and glucose homeostasis. *Mechanisms of Development, 143*, 42–52. https://doi.org/10.1016/j.mod.2017.01.004

Zhang, X., Chen, X., Qi, T., Kong, Q., Cheng, H., Cao, X., Li, Y., Li, C., Liu, L., & Ding, Z. (2019). HSPA12A is required for adipocyte differentiation and diet-induced obesity through a positive feedback regulation with PPARγ. *Cell Death & Differentiation, 26*(11), 2253–2267. https://doi.org/10.1038/s41418-019-0300-2

Zhang, X. F., Zhang, X. L., Guo, L., Bai, Y. P., Tian, Y., & Luo, H. Y. (2024). The function of the inter-alpha-trypsin inhibitors in the development of disease. *Frontiers in Medicine, 11*, 1432224. https://doi.org/10.3389/fmed.2024.1432224

Zhang, Y., Liu, Y., Sun, J., Zhang, W., Guo, Z., & Ma, Q. (2023). Arachidonic acid metabolism in health and disease. *MedComm, 4*(5), e363. https://doi.org/10.1002/mco2.363

Zhang, Z., Lau, S. W., Zhang, L., & Ge, W. (2015). Disruption of zebrafish follicle-stimulating hormone receptor (fshr) but not luteinizing hormone receptor (lhcgr) gene by TALEN leads to failed follicle activation in females followed by sexual reversal to males. *Endocrinology, 156*(10), 3747–3762. https://doi.org/10.1210/en.2015-1039

Zhang, Z., Zhu, B., & Ge, W. (2014). Genetic analysis of zebrafish gonadotropin (FSH and LH) functions by TALEN-mediated gene disruption. *Molecular Endocrinology, 29*(1), 76. https://doi.org/10.1210/me.2014-1256

Zhao, E., Basak, A., Crump, K., & Trudeau, V. L. (2006). Proteolytic processing and differential distribution of secretogranin-II in goldfish. *General and Comparative Endocrinology, 146*(2), 100–107. https://doi.org/10.1016/j.ygcen.2005.10.007

Zhao, E., Basak, A., Wong, A. O. L., Ko, W., Chen, A., Lopez, G. C., Grey, C. L., Canosa, L. F., Somoza, G. M., Chang, J. P., & Trudeau, V. L. (2009). The secretogranin II-derived peptide secretoneurin stimulates luteinizing hormone secretion from gonadotrophs. *Endocrinology, 150*(5), 2273–2282. https://doi.org/10.1210/en.2008-1060

Zhao, E., Grey, C. L., Zhang, D., Mennigen, J. A., Basak, A., Chang, J. P., & Trudeau, V. L. (2010). Secretoneurin is a potential paracrine factor from lactotrophs stimulating gonadotropin release in the

goldfish pituitary. *American Journal of Physiology - Regulatory Integrative and Comparative Physiology, 299*(5). https://doi.org/10.1152/ajpregu.00407.2010

Zhao, E., Hu, H., & Trudeau, V. L. (2010). Secretoneurin as a hormone regulator in the pituitary. *Regulatory Peptides, 165*(1), 117–122. https://doi.org/10.1016/j.regpep.2009.11.019

Zhao, E., McNeilly, J. R., McNeilly, A. S., Fischer-Colbrie, R., Basak, A., Seong, J. Y., & Trudeau, V. L. (2011). Secretoneurin stimulates the production and release of luteinizing hormone in mouse LβT2 gonadotropin cells. *American Journal of Physiology. Endocrinology and Metabolism, 301*(2). https://doi.org/10.1152/ajpendo.00070.2011

Zhou, R., Tsang, A. H. K., Lau, S. W., & Ge, W. (2011). Pituitary adenylate cyclase-activating polypeptide (PACAP) and its receptors in the zebrafish ovary: Evidence for potentially dual roles of PACAP in controlling final oocyte maturation. *Biology of Reproduction, 85*(3), 615–625. https://doi.org/10.1095/biolreprod.111.091884

Zhu, Y., Liu, D., Shaner, Z. C., Chen, S., Hong, W., & Stellwag, E. J. (2015). Nuclear progestin receptor (Pgr) knockouts in zebrafish demonstrate role for Pgr in ovulation but not in rapid non-genomic steroid mediated meiosis resumption. *Frontiers in Endocrinology, 6*(MAR). https://doi.org/10.3389/fendo.2015.00037

Zidan, S. R. S., Saleh, H. H. E., Semaida, A. I., Abou-Zied, R. M., & Allam, S. M. (2020). Effect of different doses of human chorionic gonadotropin (HCG) hormone on stripping response and reproductive performance of the African catfish (Clarias gariepinus). *Egyptian Journal of Aquatic Biology and Fisheries, 24*(6), 225–242. https://doi.org/10.21608/ejabf.2020.111531